Kingston University London

Oleic acid induced alterations in pancreatic cancer cell proliferation, a consequence of a pre-programmed dependence on lipid synthesis.

A thesis submitted in partial fulfilment for the degree of

Doctor of Philosophy

By Nico LAMBRI

Faculty of Science, Engineering and Computing

September 2018

Declaration

This thesis entitled ‘Oleic acid induced alterations in pancreatic cancer cell proliferation, a consequence of a pre-programmed dependence on lipid synthesis’ is based upon the work conducted in the Faculty of Science, Engineering and Computing at Kingston University London. All the work described here is the candidate’s own original work unless otherwise acknowledged in the text or by references. None of the work presented here has been submitted for another degree at this or any other university.

Acknowledgements

The completion of this project would have not been possible without the support and assistance of many people. Firstly, I would like to thank and express my sincere gratitude towards my primary supervisor Dr Michael Stolinski. His passion, knowledge, dedication and commitment towards the project contributed greatly towards the completion of this thesis. I would further like to highlight the endless meetings we had discussing and arguing about numerous hypotheses which made my PhD experience both academically challenging and fun. In addition, I would like to thank the other members of my supervisory team, Professor Helmout Modjtahedi who also donated several of his pancreatic cancer cell lines towards this project and Dr Andrew Snabaitis with his wealth of knowledge regarding Western blotting. They were both a valuable resource and provided solid feedback when required.

I would like to extend my gratitude towards other academics that supported me throughout my PhD, Dr Adam Le Gresley, Dr Jean-Marie Peron, Dr Gordon Hunter, and Dr Natasha Hill. They are true experts of their respective field's chemistry, mathematics and molecular biology, offering a broad wealth of knowledge.

A special acknowledgement must go to the people who I worked alongside at the IRTL, which made it a great and fun working environment. Sinead, Loryn, Sharan, Tasha, Jon, Olga, Alex and Brian, their help and friendship made this experience so much better.

I would also like to thank some of the people who were behind the scenes but were always there and extremely supportive. My friends from Cyprus, George and Charalambos along with their lovely parents Marios and Anthi Soteriou, who have been a massive support not only through my PhD but since I was 15 years old. My friends from the University of Huddersfield Joe and Jimmy and finally Nick who I met as a post-doctoral researcher and later became flat mates with and share some awesome memories.

Finally, a massive thank you goes to my parents, their patience, understanding and constant belief in me along with the endless and never-ending support, which without I would not have been able to complete my thesis.

Publications

Lambri N, Snabaitis A, Le Gresley A, Modjtahedi H, Stolinski M. (2016). A preliminary characterization of *de novo* lipogenesis in pancreatic (Capan-1) and liver (HepG2) cancer cell lines. *European Journal of Cancer,* Vol. 61, S106. Conference abstract.

List of Acronyms

3-MA: 3-Methyl Adenine

6PG: 6-Phosphogluconate

6PGD: 6-Phosphogluconate Dehydrogenase

ACADM: Acyl-Coenzyme A Dehydrogenase

ACADVL: Very Long-chain Specific Acyl-CoA Dehydrogenase

ACC: Acetyl CoA Carboxylase

Acetyl CoA: Acetyl Coenzyme A

ACL: ATP Citrate Lyase

ACSL1: Acyl-CoA synthetase long-chain family member 1

ACSL4: Acyl-CoA synthetase long-chain family member 4

AMPK: AMPK-activated Protein Kinase

ATG7: Autophagy Related 7

ATP: Adenine triphosphate

AUC: Area Under the Curve

Bcl-2: B-cell lymphoma 2

bHLHZ: basis helix loop helix zipper

BRCA: Breast Cancer gene

CFSE: Carboxyfluorescein succinimidyl ester

ChERBP: Carbohydrate-response Element-Binding Protein

DAG: Diacylglycerol

DNL: *de novo* lipogenesis

ECM: Extracellular Matrix

EMT: Epithelial Mesenchymal Transition

ETC: Electron Transport Chain

FAO: Fatty Acid Oxidation

FAS: Fatty Acid Synthase

FBP1: Fructose-1,6-bisphosphatase

FAME: Fatty acid Methyl Esters

FFA: Free Fatty Acid

G6P: Glucose-6-Phosphate

G6PD: Glucose 6-Phosphate Dehydrogenase

GC-MS: Gas Chromatography Mass Spectrometry

GDP: Guanosine diphosphate

GLUD1: Glutamate Dehydrogenase 1

Glut-1: Glucose Transporter-1

GOT1: Aspartate aminotransferase 1

GTP: Guanosine-5'-triphosphate

HIF1: Hypoxia Inducible Factor 1

ChIP: Chromatin ImmunoPrecipitation

CPT1: Carnitine Palmitoyl transferase 1

LC3: Light chain 3

LD: Lipid Droplet

LDH: Lactate Dehydrogenase

LKB1: Liver Kinase B1

MAPK: Mitogen Activated Protein Kinase

Mcl-1: Myeloid leukemia cell differentiation protein

MCN: Mucinous Cystic Neoplasm

ME1: Malic Enzyme

mTOR: mammalian Target of Rapamycin

MUFAs: Monounsaturated Fatty Acids

OA: Oleic Acid

Oxphos: Oxidative Phosphorylation

PA: Palmitic Acid

PanINs: Pancreatic Intraepithelial Lesions

PC: Pancreatic Cancer

PDAC: Pancreatic Ductal Adeno Carcinoma

PDH: Pyruvate Dehydrogenase

PI3K: Phosphoinosite 3 Kinase

PIP3: Phosphatidyl Inositol Tri Phosphate

IDH1: Isocitrate dehydrogenase

IPMN: Intraductal Papillary Mucinous Neoplasm

PPAR: Peroxisome Proliferator-Activated Receptor 1

PPP: Pentose Phosphate Pathway

PTEN: Phosphate and Tensin homolog

ROS: Reactive Oxygen Species

RT-PCR: real time Polymerase Chain Reaction

Ru5D: Ribulose-5 Dehydrogenase

SAM: S - adenosyl Methionine

SCD: Sterol CoA Desaturase

SREBP-1: Sterol Response Element Binding Protein 1

TCA: Tri Carboxylic Acid

TF: Transcription Factor

TG: Triglyceride

THF: Tetra Hydro Folate

TSG: Tumour Suppressor Gene

ULK1: Unc-51 like autophagy activating kinase 1

VHL: Von Hippel-Lindau

VPS34: Vacuolar protein sorting 34

WT: Wild Type

Table of Contents

List of Figures

List of Tables

Abstract

Cancer cells demonstrate elevated levels of *de novo* lipogenesis (DNL), which represent a component of the reprogramming of tumour metabolism, driving uncontrolled cell growth. *In vitro* inhibition of this pathway results in reduced cell proliferation, viability and tumour size, however therapeutic attempts at successfully targeting this pathway are limited.

Following an initial phenotypic characterization of a panel of pancreatic cell lines (BxPC-3, AsPC-1, Capan-1 and MiaPaca-2), along with a well characterized hepatic cell line (HepG2), cells were exposed to long term incubation (120 hours) with 300µM oleic acid (OA) and effects on cell proliferation were determined. BxPC-3 cells demonstrated a significant reduction of 16% in cell proliferation ($p<0.05$) as demonstrated by a live cell analysis system. These results were confirmed using an independent cell tracking staining assay which showed a 14% decrease in proliferation at 48 hours. Several approaches were utilised to determine the mechanisms responsible for this reduced proliferation.

On supplementation with OA, all pancreatic cancer cell lines showed a reduction in glucose derived carbon contribution towards palmitate enrichment, however only BxPC-3 cells showed an increase in labelled glutamine derived palmitic acid enrichment when compared to MiaPaca-2. Extensive comparative studies were performed between MiaPaca-2 and BxPC-3 cells, since MiaPaca-2 cells are Kras positive, whereas BxPC-3 are Kras negative, which consequently results to distinct

metabolic phenotypes between the two cell lines. Crosstalk between DNL and the pentose phosphate pathway (PPP) was investigated by measuring glucose-6-phosphate dehydrogenase activity and shown to be reduced in BxPC-3 cells (~50%) following the addition of OA, thus perturbing a major NADPH generating pathway for this cell line. However, although NADPH/NADP ratios did not seem to be affected by the addition of OA for the pancreatic cancer cell lines, NADPH labelling by [3-2H] glucose and its utilization by DNL through the measurement of labelled palmitate showed reduced levels (-20%) of labeled palmitate following the addition of OA in BxPC-3 and MiaPaca-2 cells. The dependency of the pancreatic cell lines to β-oxidation was indirectly measured by incorporating the carnitine palmitoyltransferase 1 (CPT1) inhibitor etomoxir with the OA supplementation experiments. Results showed growth arrest could be rescued with the addition of OA to all cell lines although levels of the β-oxidation enzymes ACADVL and ACADM were expressed at much lower levels in BxPC-3 compared to MiaPAca-2 cells (2-3 fold lower), possibly indicating less reliance on the β-oxidation pathway in this cell line.

This study has potentially identified a metabolic weakness of BxPC-3 cells based on their metabolic phenotype. The data reveals the interdependency of DNL on the PPP pathway and the key role of maintaining a homeostatic balance regarding NADP+/NADPH levels. Further understanding and exploitation of these metabolic weakness may provide novel therapeutic strategies that can be developed for targeting cell survival.

Chapter 1 – Introduction

1.1 The Hallmarks of Cancer

Cancer is a complex polygenic disease which breaks some of the most basic and fundamental biological rules evolution has established to foster life (Coleman and Tsongalis, 2009). The human body consists of 10^{14} cells, and when present in a healthy/homeostatic environment, cells behave as social entities communicating via complex signaling pathways (Alberts, 2008). In addition, mitotic divisions and apoptosis are two tightly regulated pathways which replenish and maintain healthy cell populations. However, during carcinogenesis, opposite phenomena are observed. Cells become antisocial entities, ignoring signals from surrounding cells, conforming to a new state of homeostasis. This transformation is characterized by lack of cell cycle restraints leading to uncontrollable cell proliferation and tissue invasion, forming metastasis (Weinberg, 2007).

A review of the ten biological transformative features of cancer cells (hallmarks) has been provided by (Hanahan and Weinberg, 2011). These include sustaining proliferative signals, evasion of growth suppressors, resisting cell death, enabling replicative immortality, inducing angiogenesis, evading immune destruction and activating invasion and metastasis. The underlying cause for developing these characteristics is genomic instability, which results in the polygenicity and complexity of carcinogenesis. Furthermore, due to increased biosynthetic and energy requirements, metabolic reprogramming is fundamental to ensuring cancer cell growth. Finally, the tumour microenvironment, which consists of various cell types (cancerous

and non-cancerous) which participate in heterotypic interactions influencing cell signaling and metabolism, provides a deeper level of complexity. Further investigation and understanding of these concepts will increasingly support the development of novel therapeutic strategies against cancer (Figure 1.1)

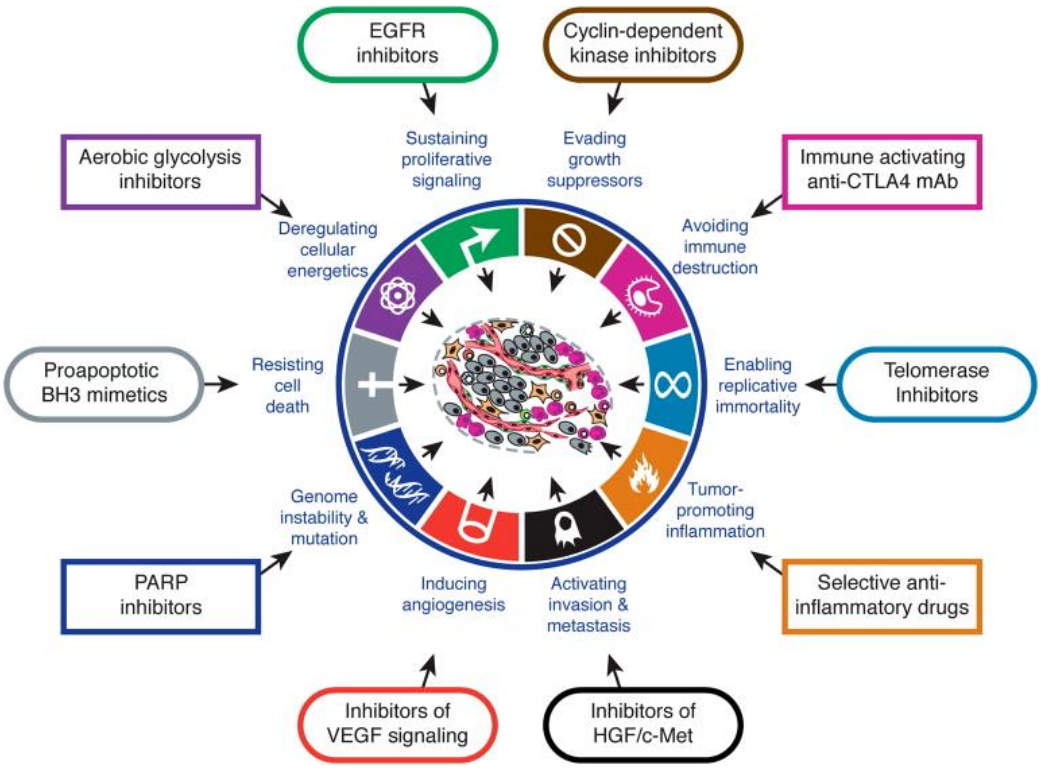

Figure 1.1 - The 10 hallmarks of cancer and therapeutic targets.
A schematic representation of the biological hallmarks and potential therapeutic targets (Image taken from Hanahan and Weinberg, 2011).

Characterising the mechanisms of carcinogenesis, cancer cell growth and survival has proved to be one of the greatest scientific challenges. The acquisition of DNA mutations, later termed ‘genomic instability’, is now widely accepted to be the underlying factor for the initiation of cancer. Genomic instability may cause mutations in proto-oncogenes and tumour suppressor genes (TSGs), which are then unable to

control cell cycle progression. In addition, the rate of mutagenesis is time dependent, therefore, when few mutations are present, the cell may be able to compensate by using other restriction points, cell cycle repressors or undergo apoptosis. However, accumulation of such mutations and the loss of multiple gene functions, inevitably results in tumour development (Strachan *et al*., 2011).

Cell division is tightly regulated by the cell cycle, which is controlled by cyclins and cyclin dependent kinases. Fluctuating levels of cyclins activate specific cyclin dependent kinases, which then regulate cell cycle progression to the next phase (Deshpande et al., 2005). During tumourigenesis, agents which alter signal transduction pathways and promote cell cycle progression are characterized as oncogenes. Oncogenes operate in a dominant, gain of function manner and are activated in four ways: point mutation, amplification, chromosomal rearrangement or translocation (Strachan *et al*., 2011). An example of a point mutation is K-ras^{G12D} (which results to glycine a neutral amino acid at position 12 being substituted by aspartate, a negatively charged amino acid, resulting to a conformational change) which occurs frequently in pancreatic cancer (PC) causing increased cell proliferation and tissue invasion (Rachagani *et al*., 2011).

In comparison to oncogenes, TSGs operate by inhibiting cell cycle progression, thus preventing tumourigenesis. In contrast to the dominant effect of oncogenes, TSGs lose their function in a recessive manner, i.e. when both alleles are affected by mutations. Individuals which carry germline TSG mutations, are genetically predisposed to develop cancer due to loss of heterozygosity. This phenomenon led to Knudson (1993) developing the two-hit hypothesis theory; that it is unlikely for two somatic mutations to

occur sporadically in the same cell. However, in familial cases where one allele is already mutated, given the number of cells, it is probable that one or more cells will suffer another hit (Knudson, 1993). Indeed, nearly all the familial genes which predispose to cancer such as *BRACA1*, *BRACA2*, *TP53*, *VHL* and *PTEN* are TSGs (Weinberg, 2007).

1.2 Cancer cell metabolism: A rewiring of metabolic pathways

All cells fundamentally require energy to function, as well as to fuel their proliferative and biosynthetic demands. Therefore, they have developed a set of finely tuned pathways, which produce energy in the form of adenosine triphosphate (ATP). The initial phase of carbohydrate metabolism is glycolysis, which begins by utilizing glucose to produce pyruvate, whilst generating a net yield of two ATP molecules. Under normoxic conditions, pyruvate enters the mitochondria where it is metabolized to acetyl-coenzyme A (acetyl-CoA) via pyruvate dehydrogenase (PDH). Acetyl-CoA condenses with oxaloacetate to generate citrate, which enters the Krebs cycle (also known as the tricarboxylic cycle (TCA) or citric acid cycle). Once a full cycle is completed, reducing power in the form of NADH and $FADH_2$ as well as two molecules of ATP are produced. NADH and $FADH_2$ are used to fuel oxidative phosphorylation (OxPhos), which requires oxygen, in order to receive the high-energy electrons. Finally, OxPhos produces a net yield of 36 ATP molecules (Berg *et al*., 2007; Anastasiou and Cantley, 2012).

Under hypoxic conditions, pyruvate does not enter the mitochondria, but is reductively metabolized to lactate, by lactate dehydrogenase (LDH) in a process known as fermentation (Hatzivassiliou *et al*., 2005b). Since fermentation is anaerobic, the conversion of glucose to lactate can occur independently of oxygen availability. This maintains a high glycolytic flux providing sufficient levels of glucose are present. Despite the poor yield of two ATP molecules, fermentation is capable of rapidly producing sufficient amounts of ATP to fuel numerous eukaryotic organisms (Rolland *et al*., 2002). In addition, a process known as aerobic fermentation has been noted to occur in numerous healthy (non-cancerous) rapidly proliferating mammalian cells such as: fibroblasts, lymphocytes and thymocytes (Munyon and Merchant, 1959; Hedeskov, 1968).

Otto Warburg in the 1920s, discovered that glucose consumption in cancer cells was much higher compared to healthy, non-cancerous cells. Furthermore, Warburg demonstrated that cancer cells predominantly metabolised glucose using glycolysis, generating high levels of lactate under normoxic conditions (Warburg, 1956). Warburg hypothesized that cancer cells underwent high levels of aerobic fermentation due to faulty mitochondria, thus compensating for the loss of OxPhos. However, this hypothesis was later found to be inaccurate by several studies demonstrating that the mitochondrial respiration chain was fully intact and functional (Moreno-Sanchez et al., 2007; Zu and Guppy, 2004; Ju et al., 2014; Xu et al., 2015). Although glycolysis remains a fundamental pathway in cancer cell metabolism, increased glycolytic flux is not a result of faulty mitochondria.

Considering the above statement, the underlying reason as to why cancer cells would rewire their metabolism to synthesise ATP via glycolysis instead of OxPhos, which is extremely inefficient, remained unclear. In addition, cancer cells have been shown to reprogram metabolic pathways by upregulating glycolytic enzymes and inhibiting feedback mechanisms, which would normally downregulate glycolysis (Altenberg and Greulich, 2004; Zu and Guppy, 2004). However, Zu and Guppy (2004) presented data from 31 cancer cell lines/tissues which demonstrated that only 17% of the total ATP produced was derived from glycolysis (Zu and Guppy, 2004). Thus, most of the cells' ATP is derived from the mitochondria through OxPhos and only drops by 33% when oxygen concentration is as low as 25μM (Chandel *et al*., 1997).

Evidently, rapidly proliferating cells are heavily dependent on glycolysis, but ATP production may not be the only underlying factor for this metabolic phenotype. Proliferating cells have high biosynthetic demands, as they require rapid amplification of their DNA, RNA, proteins and lipids. A hypothesis initially proposed by (Potter, 1958) and recently revisited by (Vander Heiden *et al*., 2009) suggests that intermediary products of glycolysis may be utilized to fuel biosynthetic pathways, thus enhancing the production of nucleotides, proteins and lipids. The numerous associations of glycolytic intermediates to produce macromolecular biosynthetic precursors are highlighted in Figure 1.2.

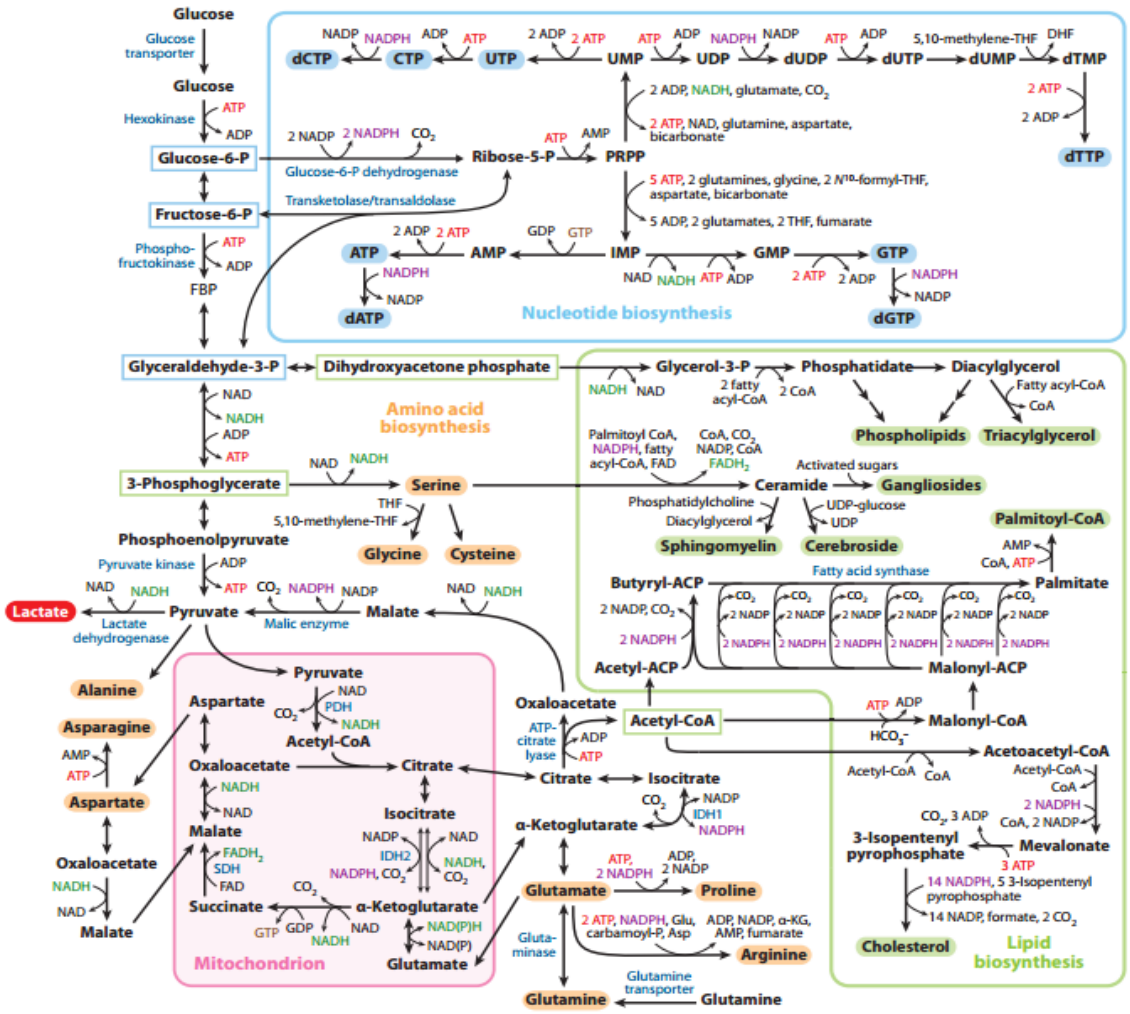

ABBREVIATIONS:

ACP	Acyl carrier protein	**dUTP**	Deoxyuridine triphosphate	**PDH**	Pyruvate dehydrogenase
ADP	Adenosine diphosphate	**FAD**	Flavin adenine dinucleotide	**PRPP**	Phosphoribosyl pyrophosphate
Asp	Aspartate	**$FADH_2$**	Flavin adenine dinucleotide, reduced	**SDH**	Succinate dehydrogenase
ATP	Adenosine triphosphate	**Glu**	Glutamate	**THF**	Tetrahydrofolate
CoA	Coenzyme A	**GMP**	Guanosine monophosphate	**UDP**	Uridine diphosphate
CTP	Cytidine triphosphate	**GTP**	Guanosine triphosphate	**UMP**	Uridine monophosphate
dATP	Deoxyadenosine triphosphate	**IDH1**	Isocitrate dehydrogenase 1	**UTP**	Uridine triphosphate
dCTP	Deoxycytidine triphosphate	**IDH2**	Isocitrate dehydrogenase 2	**α-KG**	α-Ketoglutarate
dGTP	Deoxyguanosine triphosphate	**IMP**	Inosine monophosphate		
DHF	Dihydrofolate	**NAD**	Nicotinamide adenine dinucleotide		
dTMP	Deoxythymidine monophosphate	**NADH**	Nicotinamide adenine dinucleotide, reduced		
dTTP	Deoxythymidine triphosphate	**NADP**	Nicotinamide adenine dinucleotide phosphate		
dUDP	Deoxyuridine diphosphate	**NADPH**	Nicotinamide adenine dinucleotide phosphate, reduced		
dUMP	Deoxyuridine monophosphate	**P**	Phosphate		

Figure 1.2 – The contribution of glycolytic intermediates in biosynthetic processes.
A schematic representation of the link between glycolysis, oxidative phosphorylation, glutamine metabolism, lipid biosynthesis and the pentose phosphate pathway are shown. Metabolites involved in nucleotide biosynthesis are shown in blue, metabolites contributing towards lipogenesis are shown in green and non-essential amino acids are shown in orange (Lunt and Vander Heiden, 2011).

Glucose-6-phosphate dehydrogenase converts glucose-6-phosphate to ribose-5-phosphate which is utilized by the pentose phosphate pathway (PPP), to allow nucleotide biosynthesis. Glyceraldehyde-3-phosphate can be converted to glycerol which supports *de novo* lipogenesis (DNL). In order for cells to undergo DNL, citrate exits the Krebs cycle and is converted to acetyl-CoA (Lunt and Vander Heiden, 2011). The process where citrate exits the Krebs cycle to fuel a different pathway is known as cataplerosis. Consequently, the opposite phenomenon must occur, in order to restore the lost metabolite. This is known as anaplerosis. Anaplerosis, occurs via glutamine metabolism, where glutamine is converted to glutamate, and subsequently to α-ketoglutarate, thus allowing it to enter the Krebs and continue towards OxPhos (DeBerardinis *et al*., 2007). Finally, 3-phophoglycerate and oxaloacetate may contribute towards amino acid synthesis (Lunt and Vander Heiden, 2011).

1.3 The hallmarks of cancer metabolism

Tumourigenesis requires cellular metabolism to be reprogrammed, as both a direct and indirect consequence of oncogenic mutations. A common characteristic, and challenge for cancer cells, is the ability to acquire nutrients in usually nutrient poor environments to fuel their bioenergetic and biosynthetic demands. Furthermore, changes in intracellular and extracellular metabolite concentrations have been shown to alter gene expression patterns, cellular differentiation and the tumour microenvironment. Pavlova and Thomson (2016), have further categorized six additional sub hallmarks as the metabolic changes which occur in cancer cells: deregulated glucose and amino acid uptake, use of opportunistic modes of nutrient acquisition, use of glycolytic and TCA

intermediates for NADP(H) production and biosynthesis, increased demand for nitrogen, changes in metabolite driven gene expression, and metabolic interactions with the microenvironment.

As mentioned in the previous section, cancer cells increase nutrient uptake to support their bioenergetic and biosynthetic demands. The two main nutrients that cells heavily depend on are glucose and glutamine. By catabolizing these two nutrients into a diverse pool of carbon intermediates, the cell can assemble various macro-molecules. Moreover, glutamine not only contributes carbon, but also provides the cell with reduced nitrogen which is required for synthesizing purine and pyrimidine nucleotides, glucose-6-phophate and non-essential amino acids (Bhutia *et al*., 2015). The high dependency of cancer cells for glutamine was initially described by (Eagle, 1955), who demonstrated that HeLa cells required 10- to 100-fold molar excess glutamine relative to other amino acids to achieve optimal growth. In addition, genetic alterations affecting *PI-3 kinase*, *PTEN*, *INPP4B* and *Ras* lead to increased glucose uptake, whereas *c-myc* is the principal driver for glutamine uptake (Wang *et al*., 2011).

Despite rapid nutrient uptake mechanisms, cancer cells must often survive under low nutrient conditions. However, mutant *Ras* or *c-Src* alleles have been shown to enable processes such as macropinocytosis, a process by which cells can catabolise extracellular nutrients, such as protein through lysosomal degradation and recover amino acids (Commisso *et al*., 2013). In addition to macropinocytosis, amino acids can also be recovered through phagocytosis, which is the engulfment and breakdown of entire cells via entosis (Krajcovic *et al*., 2013). Moreover, due to poor vasculature cancer cells may grow under hypoxic conditions, which suppresses numerous

biosynthetic reactions that require oxygen as an electron acceptor. For example, Stearoyl-CoA desaturase 1 function is compromised in hypoxic conditions, thus leading to a reduction in the production of unsaturated fatty acids. Therefore, cancer cells are required to import 'ready-made' unsaturated fatty acids to supplement their intracellular fatty acid pool (Kamphorst *et al*., 2013). Finally, even in the absence of extracellular nutrients, cells can survive prolonged periods through a self-catabolic process termed autophagy. During autophagy, intracellular macromolecules and organelles are enveloped and fused with lysosomes which leads to the recovery of amino acids and fatty acids. However, the autophagic process does not supply the cell with new biomass, and therefore only promotes cell survival under low nutrient conditions and not proliferation (Boya *et al*., 2013).

A novel lipid degradation pathway using the autophagic machinery has recently been described, termed lipophagy (Singh *et al*., 2009). Triglycerides (TG) and cholesterol, are stored as neutral lipids in the form of lipid droplets (LD) (Kuerschner *et al*., 2008). Until recently, it was thought that LD were metabolised exclusively by cytosolic hydrolytic enzymes or lipases. However, the involvement of lysosomes in autophagic LD breakdown provides a new understanding of fat metabolism in response to cellular requirements and external stimuli (Zechner and Madeo, 2009). Studies have shown that through genetic or pharmacological inhibition of autophagy, cellular TG concentration and LD numbers increase in cultured hepatocytes. Moreover, β-oxidation was shown to be impaired, due to the decrease in free fatty acid (FFA) generation from LD breakdown (Singh *et al*., 2009). It has also been demonstrated that defects in autophagy promote hepatic steatosis (Czaja, 2016). Therefore, lipophagy can regulate

lipid catabolism in situations of nutrient scarcity by providing FFA substrates for β-oxidation, and maintain homeostatic levels of intracellular lipid concentrations, thus preventing lipotoxicity (Liu and Czaja, 2013).

Fatty acids, cholesterol, glycerol, nucleotide and non-essential amino acid synthesis greatly depend on the availability of reduced carbon. For example, palmitic acid synthesis requires 14 reducing equivalents, while synthesizing cholesterol requires 26. The assigned donor for reducing equivalents is NADPH, which is synthesized from $NADP^+$ through the oxidation of carbon substrates (Lunt and Vander Heiden, 2011). As described earlier, the Warburg effect, is characterized by the rapid and continuous conversion of glucose to lactate. However, proliferating cells show minor increases in ATP consumption relatively to their need for biosynthetic precursors and NADPH. Therefore, by decoupling glycolysis from the TCA cycle and OxPhos, the accumulation of ATP and NADH which act as repressive feedback mechanisms towards glycolysis is prevented (Lunt and Vander Heiden, 2011).

Several intracellular metabolic pathways have been shown to support cell proliferation by producing NADPH. It is widely assumed that the oxidative PPP is the major source of NADPH through the oxidation of glucose-6-phosphate to ribose 5-phosphate (Lehninger *et al*., 1993). However, this notion has been challenged through labeling experiments using 1,2-^{13}C-labelled glucose in several cancer cell types, indicating that the PPP cannot account for the NADPH requirements in all cancer cells (Boros *et al*., 1998, Boros *et al*., 2000). In addition, patients deficient of glucose-6-phosphate dehydrogenase, appear to be asymptomatic without showing any reduced risk in developing cancer (Cocco *et al*., 1987). An additional source of NADPH occurs via the

metabolism of glutamine through the malic enzyme. Oxidative metabolism of glutamine to malate, which is subsequently converted to pyruvate (which may be excreted as lactate or reenter the TCA cycle) by the malic enzyme, generates one molecule of NADPH (DeBerardinis *et al*., 2007). Use of isotopically labeled precursors for estimating glutamine contribution to NADPH is challenging, due to the recycling of TCA metabolites. However, glioblastomas have been shown to convert over 50% of their glutamine uptake to lactate, which suggests a high dependency on glutamine for NADPH production, although not all cells demonstrate a high glutamine uptake (Dang *et al*., 2010). Furthermore, the conversion of citrate to α-ketoglutarate by cytosolic isocitrate dehydrogenase can also produce one molecule of NADPH (Thompson, 2009).

Recent work examining the role of serine metabolism has surprisingly presented another major source for NADPH production. Serine plays a key metabolic role as a major substrate for the one-carbon folate cycle. The β-carbon of serine is taken by tetrahydrofolate (THF), catalysed by the enzyme hydroxymethyltransferase 2 in the mitochondria and hydroxymethyltransferase 1 in the cytosol, producing 5, 10-methylene-THF and glycine. The 5, 10-methylene-THF undergoes various oxidative and reductive transformations, producing a variety of one-carbon THF molecules (Tibbetts and Appling, 2010). One-carbon THF species can then be further metabolised to produce purines, thymidine and S-adenosylmethionine. This recent work demonstrates that further oxidation of one-carbon THF species may generate up to 50% of cellular NADPH (Fan *et al*., 2014). Therefore, according to the cell's metabolic

phenotype, cells may utilise different sources of nutrients for NADPH synthesis as to fuel their biosynthetic demands (Figure 1.3).

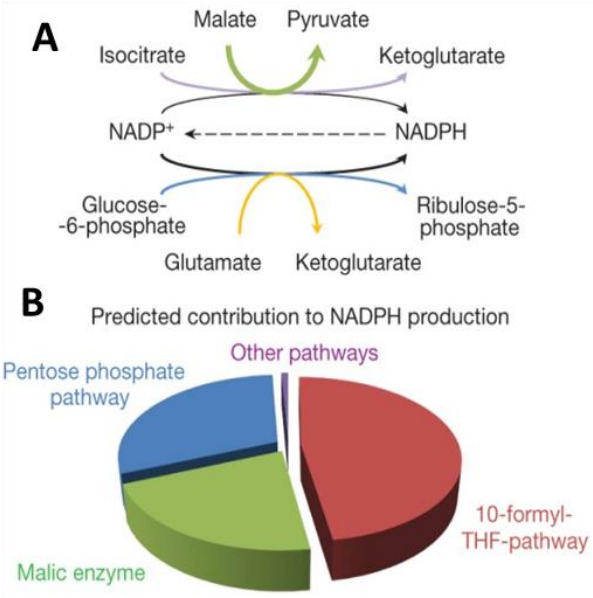

Figure 1.3 – Pathways contributing to NADPH production.
(A) Demonstrates canonical NADPH production pathways. **(B)** NADPH production routes calculated by experimentally constrained genome-scale flux analysis (Fan, 2014).

Excess pyruvate is converted into lactate and excreted into the extracellular environment, therefore allowing the increased glycolytic flux under normoxic conditions. Moreover, through the cataplerotic process, pyruvate can be converted in to citrate and secreted into the cytosol where it is broken down to acetyl-CoA and oxaloacetate. Oxaloacetate is converted into malate and reimported into the mitochondria to maintain anaplerosis, whereas the acetyl-CoA is utilised by DNL. Several oncogenes have been shown to orchestrate these metabolic processes. For example, *c-myc* upregulates the expression of lactate dehydrogenase and the

monocarboxylate transporter 1, which converts pyruvate to lactate and excretes it into the extracellular environment (Wahlstrom and Henriksson, 2015).

However, even with the above protective adaptations, cancer cells often accumulate increased levels of electron transport flux which surpasses ATP synthases capacity, leading to the formation of reactive oxygen species (ROS). Accumulation of ROS may have detrimental effects to the cell as they cause DNA, lipid and protein damage, which eventually results in cell death (Morry *et al*., 2017). Therefore, cells have adapted to having both fast-acting and long-term regulation mechanisms to control increased cellular redox levels. In addition to having a critical role in producing reduced carbon for biosynthesis, NADPH also maintains reduced glutathione levels, a key antioxidant which mitigates cellular damage from ROS (Metallo and Vander Heiden, 2013).

Although in healthy adults, DNL is only primarily active in lipogenic tissues such as liver, adipose and mammary cells, tumour cells demonstrate dramatic increases in DNL (Menendez and Lupu, 2007). The ability to produce lipids *de novo* not only aids the formation of new lipid bilayers, but enhances alterations in lipid bilayer composition, incorporating newly synthesized saturated oxidative damage resistant fatty acids.

The initial step for fatty acid synthesis is the conversion of citrate to acetyl-CoA by ATP-citrate lyase (ACL). Carboxylation of cytosolic acetyl-CoA by acetyl-CoA carboxylase (ACC) produces malonyl-CoA. Fatty acid synthase (FAS) then uses malonyl-CoA to produce long chain fatty acids (Chajes *et al*., 2006). Malonyl-CoA is also utilised for the *de novo* synthesis of cholesterol, which plays a key role in membrane composition, fluidity, tissue architecture and anchorage-independent growth (Freed-Pastor *et al*., 2012). In addition, ACL prevents the cytosolic accumulation of citrate, which would

result in the downregulation of glycolysis (Hatzivassiliou *et al*., 2005b). Oncogenic mutations particularly in the phosphatidyl inositol 3'kinase pathways/Akt/mTOR have been shown to drive lipogenesis (Samuels and Ericson, 2006). Upregulation of these pathways leads to expression of the sterol response element binding protein-1 (SREBP-1) which subsequently localises in the nucleus. SREBP-1 is a transcription factor which targets ACL, ACC and FAS (Porstmann *et al*., 2005). Furthermore, mTOR has been shown to increase expression of glucose transporter 1 (GLUT1), therefore increasing cellular intake of glucose, which is a major lipogenic precursor (Wieman *et al*., 2007).

The reprogramming of cellular metabolism to meet the biosynthetic demands of tumourigenesis, is directly linked to gene expression patterns, mediated by changes in the epigenome of the cell (Katada *et al*., 2012). Increased glucose metabolism results in elevated levels of acetyl-CoA, the necessary substrate for histone acetylation and subsequently gene activation. Increased acetylation causes the unwiring of chromatin; thus, transcription start sites become more accessible to transcription factors leading to aberrant gene expression patterns. Changes in histone acetylation patterns can be directly associated with nutrient and signaling status (Cai *et al*., 2011). Moreover, histone and DNA methylation patterns which are associated with gene silencing, utilize S-adenosylmethionine (SAM) as a methyl donor. SAM is produced through serine metabolism via the one-carbon pathway. Additionally, recent work reveals that methylation patterns are sensitive to SAM concentration (Shyh-Chang *et al*., 2013; Towbin *et al*., 2012).

The metabolic changes and adaptations which occur within a cancer cell to support growth, may also have profound effects on the tumour microenvironment. These have also been shown to affect mechanisms by which immune cell can detect, infiltrate and eradicate tumours. Hanahan and Coussens demonstrate how a group of genetically stable cell lines undergo phenotypic changes by residing in the vicinity of tumour cells (Hanahan and Coussens, 2012). For example, increased glucose and glutamine consumption, which results in extracellular lactate accumulation, has been shown to impair T-cell activation and monocyte migration (Gottfried *et al*., 2006). Furthermore, macrophages can adopt multiple functional programs from signals exerted by the microenvironment as part of the innate immune response. The macrophage phenotype for simplicity can be separated between the M1 and M2 state (classical and alternatively activated macrophages respectively). In the M1 state macrophages are typically characterised as the pro-inflammatory type, secreting inflammatory cytokines and provide defence against pathogens. In the M2 state macrophages are known to exert opposite functions such as regulation of inflammation and repair of damaged tissue. In addition to impairing T cell activation, lactate causes polarisation of the surrounding macrophages to an M2 state, which further enhances immune suppression (Carmona-Fontaine *et al*., 2013).

In summary, due to oncogene mediated metabolic rewiring, cancer cells can adopt numerous metabolic phenotypes, thus being able to sustain a high proliferative phenotype, overcome metabolic stresses such as hypoxia, oxidative stress and nutrient scarcity, whilst also hijacking the tumour microenvironment to facilitate growth and dissemination. Although, glucose and glutamine are the main metabolites of focus,

little is known about the role of fatty acids, sulphur containing amino acids (cysteine and methionine), choline, trace metals and vitamins as influencers of metabolism (Pavlova and Thompson, 2016). Furthermore, the gut microbiota produce a broad spectrum of metabolites, whose effect on tumour initiation and growth are still unclear (Garrett, 2015). Besides having a crucial role in biosynthesis, fatty acids are an extremely efficient energy source providing double the amount of ATP compared to carbohydrates. Acquisition of fatty acids can occur via DNL, the extracellular environment, cytoplasmic triglyceride hydrolysis through neutral hydrolases, or triglyceride hydrolases via lipophagy (Singh and Cuervo, 2012).

Fatty acids can be catabolised through fatty acid oxidation (FAO) also known as β-oxidation in order to generate ATP. FAO is a mitochondrial process, which consists of a series of cyclical reactions, that results in the shortening of the fatty acid carbon chain, generating acetyl-CoA, NADH and $FADH_2$ (Figure 1.4).

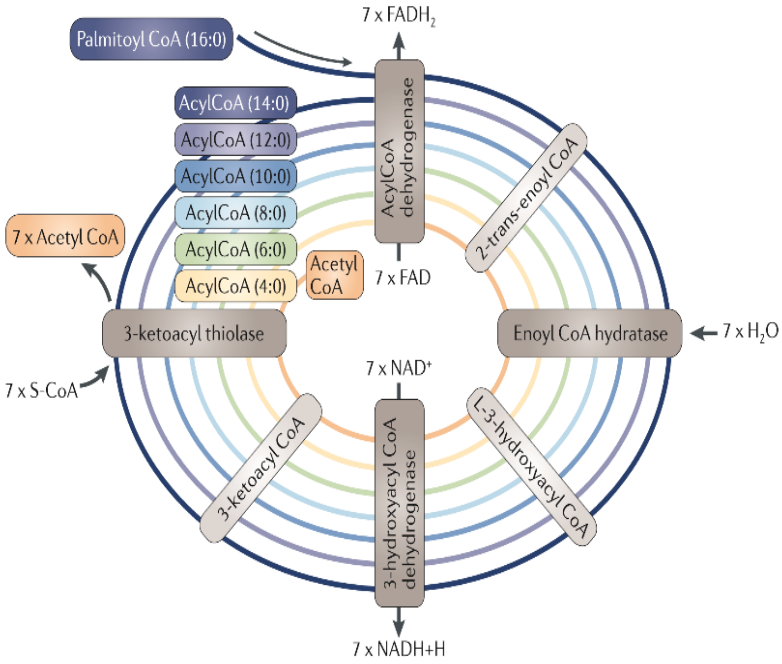

Figure 1.4 – A schematic representation of β-oxidation.
Palmitic acid enters the FAO pathway where it is dehydrogenated, hydrated and decarboxylated cyclically. Each cycle generates acetyl-CoA, NADH and FADH2 (Image adapted by Carracedo *et al*., 2013).

The generated redox cofactors NADH and $FADH_2$, contribute to the electron transport chain (ETC) for ATP synthesis, whilst also maintaining a reduced mitochondrial environment (Carracedo *et al*., 2013, Rustin, 2002).

As previously mentioned, the metabolic reprograming which occurs in cancer cells, prevails ATP production. However, in certain situations it has been shown that cancer cells rely on increased levels of ATP. Cells which become detached from solid tumours through a process termed “loss of attachment”, demonstrate reduced glucose uptake, resulting in a decrease in NADPH and ATP as well as an increase in ROS leading to anoikis mediated cell death. The promyelocytic leukaemia protein which is peroxisome proliferator-activated receptors (PPAR) dependent, has recently been shown to

stimulate β-oxidation, and rescue cells from loss of adhesion mediated anoikis (Carracedo *et al*., 2013). Moreover, a recently discovered isoform of carnitine palmitoyltransferase 1 (CPT1) CPT1C rescues cancer cells from metabolic stress and mTOR complex 1 inhibitors. This is mediated by conjugating fatty acids with carnitine and trans-locating them to the mitochondria to enhance β-oxidation and ATP production (Zaugg *et al*., 2011). CPT1 facilitates β-oxidation which has also been shown to have antiapoptotic effects, by inhibiting BAK and BAX mitochondrial pore formation (Samudio *et al*., 2010). In addition, β-oxidation maintains homeostatic lipid levels and prevents lipid mediated cytotoxicity (Vickers, 2009).

In addition, β-oxidation has been shown to exert a crucial role indirectly towards the production of NADPH, mainly when the cell accumulates high levels of ROS. Each cycle of β-oxidation produces one molecule of acetyl-CoA (besides the final cycle, which produces two molecules of acetyl-CoA) which then enters the TCA cycle. The increased fuelling of the TCA cycle gives rise to citrate, which when exported to the cytosol has two metabolic fates that produce NADPH either through ME1 or IDH1 metabolism (Figure 1.5) (Pike *et al*., 2011). Furthermore, when the cell is under metabolic stress, AMP-activated protein kinase (AMPK) regulates NADPH consumption and NADPH production through FAS and β-oxidation respectively. AMPK enhances β-oxidation, by phosphorylation mediated inhibition of ACC. Thus, AMPK is a crucial sensor of metabolic stress and can regulate catabolic pathways to provide the cell with the necessary ATP and NADPH levels (Zaugg *et al*., 2011; Mihaylova and Shaw, 2011; Diradourian *et al*., 2005).

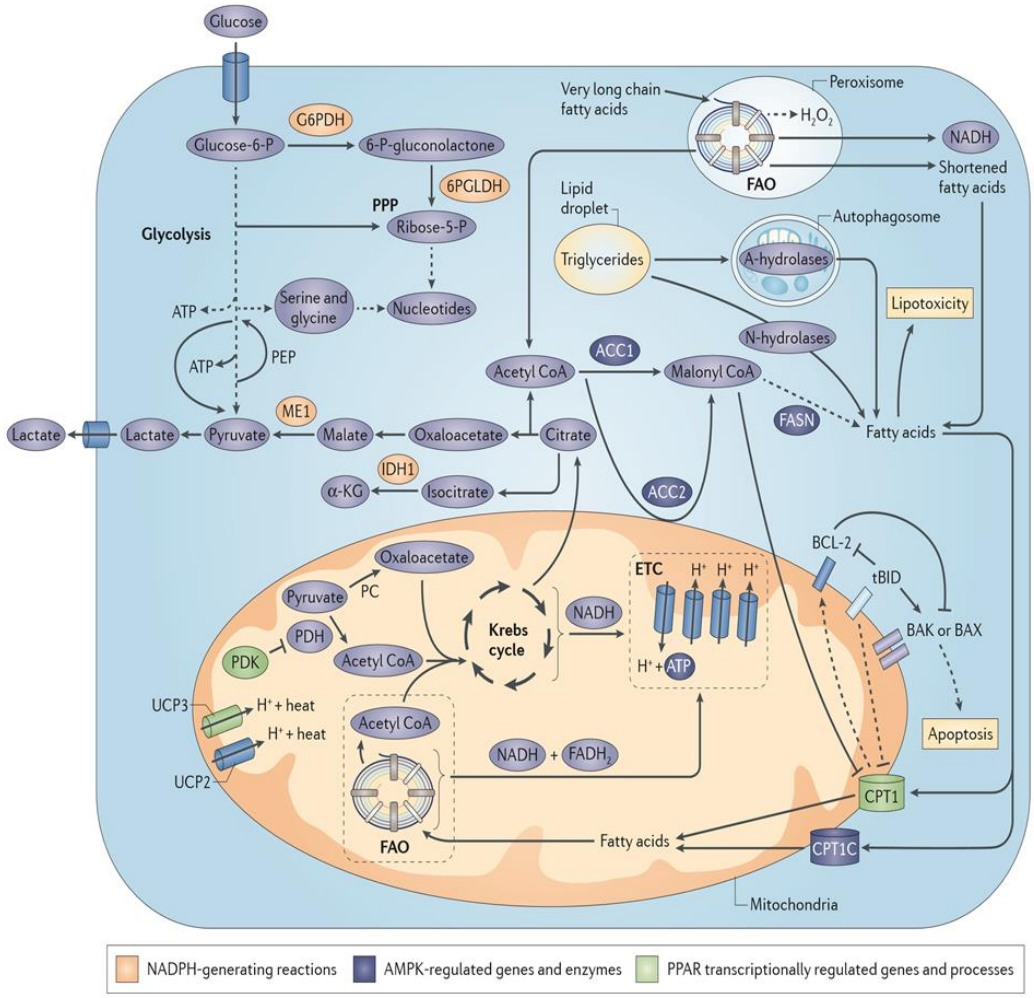

Figure 1.5 – Linking β-oxidation to NADPH production.
A schematic representation of the interconnection between metabolic pathways such as glycolysis, PPP, ETC and β-oxidation. Furthermore, linkage between NADPH producing reactions, AMPK regulated genes and PPAR regulated genes is also highlighted (Image adapted by Carracedo *et al*., 2013).

AMPK is a heterotrimeric protein consisting of a catalytic subunit and two regulatory subunits (α, β, γ) able to sense decreases in ATP, relative to increases in AMP and ADP levels (Mihaylova and Shaw, 2011). Liver Kinase B1 (LKB1) is the main kinase responsible for AMPK activation by phosphorylating Thr172 (subunit α). Increased expression levels of AMPK have been shown to stop cell proliferation which suggest a TSG role, however loss of AMPK is insufficient to cause a tumourigenic transformation

(Hardie *et al*., 2012). Furthermore, lack of AMPK renders cells resistant to oncogene driven carcinogenesis. Germline *LKB1* mutations cause Peutz-Jegher syndrome, an inherited syndrome which causes benign intestinal polyps. Somatic *LKB1* mutations also occur and have been found in lung and cervical cancers, therefore *LKB1* can be confidently described as a TSG (Ollila and Makela, 2011). In contrast, *AMPK* is frequently found to be amplified in cancers instead of being mutated and provides the cell with metabolic flexibility promoting cell survival under conditions of metabolic stress, thus having oncogene like properties (Jiyong *et al*., 2013; Jeon *et al*., 2012). Moreover, inactivation of the catalytic α1 subunit of AMPK enhances Myc driven lymphoblastogenesis in mice, however deletion of the α2 subunit increases H-RasV12 mediated transformation in mice fibroblasts (Faubert *et al*., 2013). Further work demonstrates that the α2 subunit may control p53, mitosis, chromosome segregations and cell division symmetry (Banko *et al*., 2011). Therefore, it is suggested that AMPK subunits can promote tumour suppression independent or in addition to the tumour promoting function of AMPK in terms of energy sensing. Current data is conflicting regarding the role of AMPK; however, emphasis may be required into which cellular and genetic context AMPK function is being deciphered (Jiyong *et al*., 2013)

1.4 Oncogene mediated metabolic adaptations

The carcinogenic transformations that occur in cancer require intimately interconnected and interdependent processes such genetic and epigenetic alterations, changes in cell signaling and metabolic reprogramming. Due to the high biosynthetic demands of proliferating cells, and recent advancements in the understanding of cancer cell

metabolism, it is widely accepted that increased glucose and glutamine metabolism fuel anabolic pathways. Furthermore, by understanding the role of key oncogenes such as *AMPK, KRAS* and *MYC* in the production of NADPH, focus has been taken away from ATP, as the rate limiting metabolite. Moreover, NADPH has a dual role for cellular homeostasis, as it is required for lipid and deoxynucleotide triphosphate synthesis, as well as maintaining a reduced intracellular environment by neutralizing ROS.

A major oncogenic driver found to be active in approximately 30% of all neoplasms and reaching a frequency close to 100% in pancreatic ductal adenocarcinoma (PDAC) is *KRAS* (Hezel *et al*., 2017). The *RAS* family of genes encodes four proteins, KRAS4A, KRAS4B, Harvey rat sarcoma (HRAS) and the neuroblastoma RAS (NRAS). These proteins mediate regulation of the mitogen-activated protein kinase (MAPK), phosphoinositide-3-kinase (PI3K) and ral guanine nucleotide dissociation stimulator (RalGDS) pathway, thus regulating a diverse array of complex signal transduction pathways, which control cell proliferation, differentiation, angiogenesis and cell survival (Figure 1.6) (Campbell *et al*., 1998).

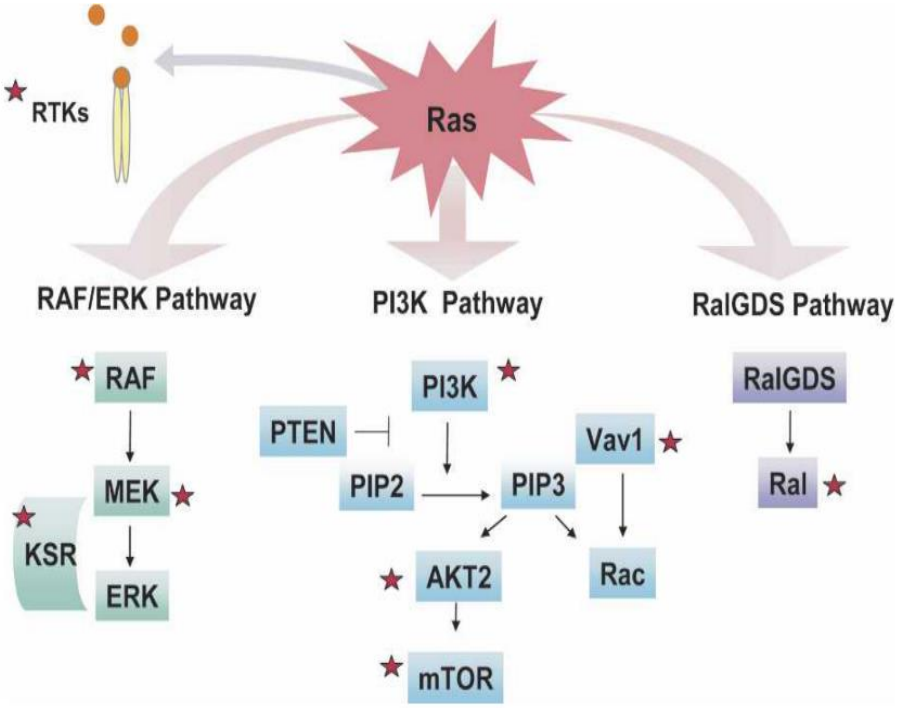

Figure 1.6 – The Ras signaling network.
Depicted above are the three main signalling cascades associated with PDAC development. *In vitro* and *in vivo* studies demonstrate that inhibition of these cascades at various levels (indicated by the red stars), inhibits pancreatic cancer. (Image adapted from Hezel *et al*., 2017).

KRAS activation occurs through guanine triphosphate (GTP) binding, and inactivation occurs by guanine diphosphate (GDP) binding, thus KRAS is GTP/GDP ratio dependent (Satoh *et al*., 1992). The most common activating mutation in KRAS is a substitution of glycine at position 12, by aspartate, valine, or arginine (Klimstra and Longnecker, 1994).

Recently, it has been demonstrated that pancreatic tumours depend on KRAS activation for regulating anabolic glucose metabolism (Ying *et al*., 2012). Furthermore,

mutant *KRAS* was shown to drive glucose metabolism through the non-oxidative phase of the PPP to produce ribose 5-phosphate for nucleic acid synthesis (Figure 1.7).

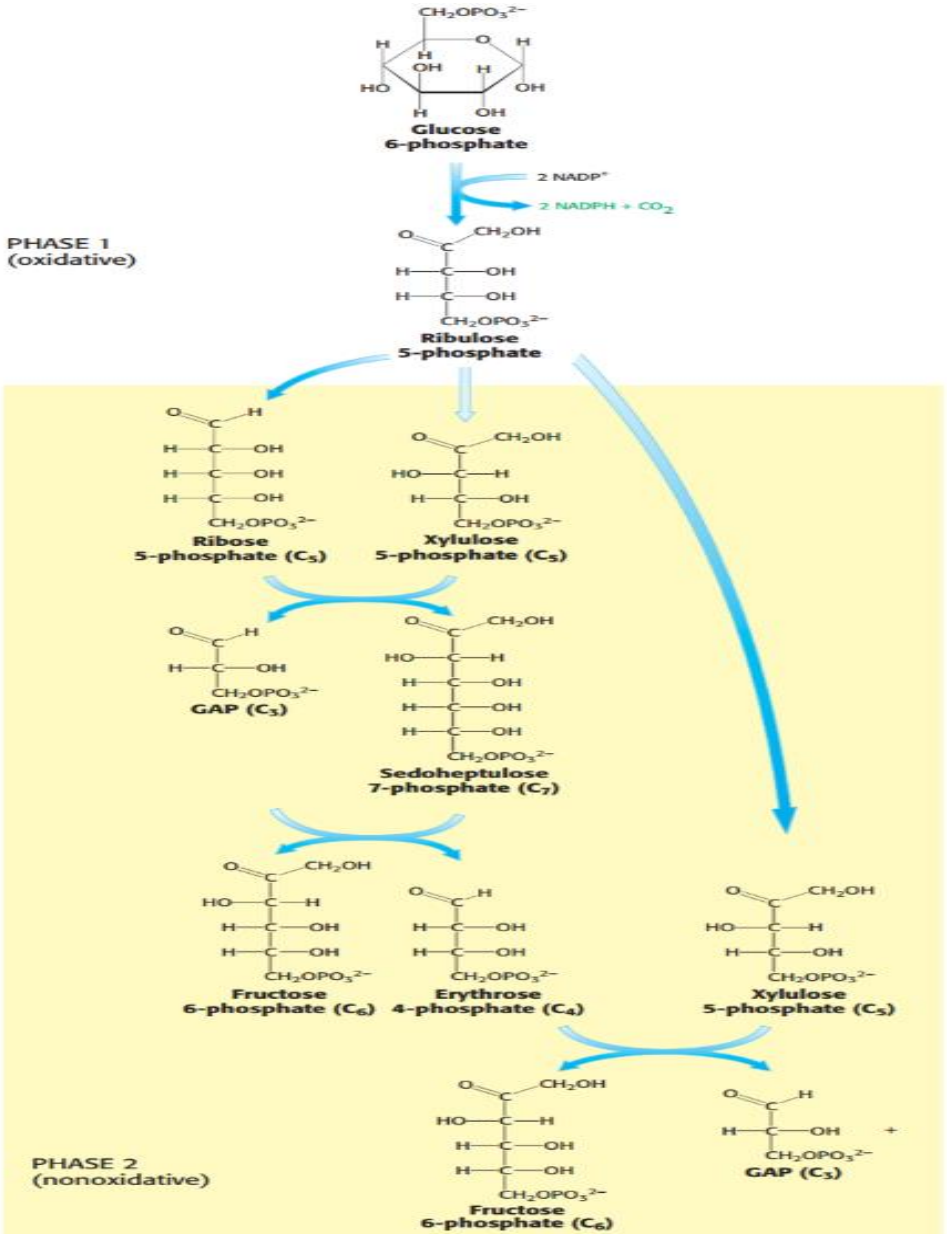

Figure 1.7 – The pentose phosphate pathway.
The PPP consist of two phases, (1) the oxidative phase where NADPH is produced, and (2) the non-oxidative phase where phosphorylated sugars become interconverted. Both phases are utilized for the production of nucleotides (Image adapted from Berg *et al*., 2007).

In addition, the TSG p53 has been shown to inhibit the oxidative phase by binding directly to glucose 6 phosphate dehydrogenase. Thus, it is likely that the oxidative phase will occur when cells are p53 deficient, whereas KRAS activation will lead to nucleotide biosynthesis through the non-oxidative phase, regardless of p53 status (Ying *et al*., 2012). However, the non-oxidative phase produces no NADPH, and therefore an alternative NADPH producing pathway must be present in *KRAS* mutant cells.

A recent study which assessed the role of the two main anabolic substrates, glucose and glutamine on cellular redox state, demonstrated that although both are required for cellular proliferation, only glutamine deprivation caused a dramatic increase in ROS in PDAC. Supplementing pancreatic cancer cells with the carbon skeleton of glutamine, α-ketoglutarate, was insufficient to rescue growth, unless also supplied with a cocktail of non-essential amino acids (Son *et al*., 2013). This in turn suggested that KRAS mutant pancreatic cancer cells metabolise glutamine differently, compared to the typical α-ketoglutarate generating pathway, which occurs through glutamine dehydrogenase (GLUD1) (Lyssiotis *et al*., 2013) (Figure 1.8A). The role of transaminases was then examined, and indeed aspartate aminotransferase 1 (GOT1) played a key role in redox control and pancreatic cancer cell proliferation. Moreover, it was shown that GOT1 functioned upstream ME1, thus through the rewired metabolism of glutamine, cells could maintain high NADPH levels (Figure 1.8B). Therefore, KRAS driven pancreatic cancer, alters glutamine metabolism by increasing GOT1 and decreasing GLUD1 expression, thus fluxing glutamine carbon towards ME1 and increasing NADPH levels, to combat ROS and sustain growth (Son *et al*., 2013).

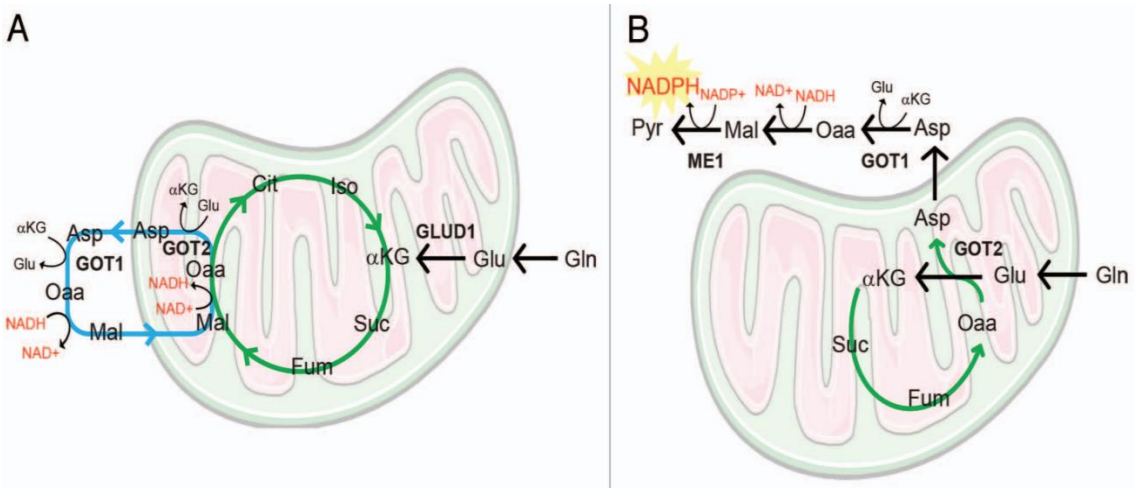

Figure 1.8 – Rewiring glutamine metabolism.
(A) The canonical anaplerotic pathway where glutamine is metabolised to α-ketoglutarate through mitochondrial GLUD1, to restore the TCA cycle when citrate is exported for DNL. **(B)** Mutant *KRAS* causes rewiring of glutamine metabolism in pancreatic cancer by increasing GOT1 and repressing GLUD1 expression, resulting in increased malate production, which is metabolised by ME1 to pyruvate giving rise to NADPH (Image adapted from Lyssiotis *et al*., 2013).

As previously described, despite glutamine being a non-essential amino acid and able to be synthesized from glucose, some cancer cells display a high rate of glutamine consumption which exceeds its biosynthetic properties (Wise and Thompson, 2010), but has anaplerotic and NADPH producing functions. The oncogene *c-Myc*, a basic helix-loop-helix zipper (bHLHZ) protein which binds and heterodimerizes with the small bHLHZ protein MAX, has been shown to alter cell proliferation, differentiation, metabolism and senescence (Eilers and Eisenman, 2008). Moreover, it is a major driver for increased glutamine consumption in PDAC (Guillaumond *et al*., 2013), and is the third most commonly found amplified gene in human neoplasms (Table 1.1) (Zack *et al*., 2013). Chromatin immunoprecipitation (ChIP) as well as quantitative RT-PCR studies, have indicated that *c-Myc* transcriptionally activates SLC38A5 and SLC1A5, which are two high affinity glutamine transporters (Nicklin *et al*., 2009). Furthermore, c-

Myc facilitates the conversion of glutamine to glutamate, by increasing glutaminase expression, and subsequently in to lactic acid, giving rise to NADPH through ME1 (Wise *et al*., 2008). However, whether a direct synergistic effect exists by c-Myc increasing glutamine consumption, and KRAS rewiring glutamine metabolism, remains unclear. It is evident that oncogenes play a direct role on cancer cell metabolism. As genomic instability is necessary for carcinogenesis (Hanahan and Weinberg, 2011), it also provides cancer cells with metabolic flexibility. Thus, when examining cellular energetics, a non-dogmatic approach must be taken, taking into consideration the cellular, genetic and microenvironmental state of which a tumour is presented with. Since different cell types are exposed to different levels of nutrients, ROS and oxygen levels, a diverse array of metabolic functional networks exists which can also vary depending on changes of different metabolic stresses. Therefore, a comprehensive approach must be taken when interrogating cancer cell metabolism (Figure 1.9) (Metallo and Vander Heiden, 2013).

Table 1.1 – Glutamine metabolism

Changes in glutamine metabolism due to oncogenic changes (Table adapted from Altman *et al*., 2016).

Oncogene and TSG mediated effects on glutamine metabolism	
Oncogenic change	**Effect on glutamine metabolism**
MYC upregulation	Upregulates glutamine metabolism enzymes and transporters
KRAS mutations	Drives dependence on glutamine metabolism, suppresses GLUD and drives NADPH generation via ME1
HIF1α or HIF2α stabilization	Drives reductive carboxylation of glutamine to citrate for lipid production
HER2 upregulation	Activates glutamine metabolism through MYC and NF-κB
p53, p63 or p73 activity	Activates GLS expression
JAK2-V617F mutation	Activates GLS and increases glutamine metabolism
mTOR upregulation	Promotes glutamine metabolism via induction of MYC and GLUD or aminotransferases
NRF2 activation	Promotes production of glutathione from glutamine
TGFβ-WNT upregulation	Promotes SNAIL and DLX2 activation, which upregulate GLS and activates epithelial to mesenchymal transition
PKCζ loss	Stimulates glutamine metabolism through serine synthesis
PTEN loss	Decreased GLS ubiquitylation
RB1 loss	Upregulates GLS and SLC1A5 expression

GLUD, glutamate dehydrogenase; GLS, kidney-type glutaminase; GLS2, liver-type glutaminase; HIF, hypoxia-inducible factor; JAK2, Janus kinase 2; ME1, malic enzyme 1; NF-κB, nuclear factor-κB; NRF2, nuclear factor, erythroid derived 2, like 2; PKCζ, protein kinase Cζ; RB1, retinoblastoma 1; TGFβ, transforming growth factor-β

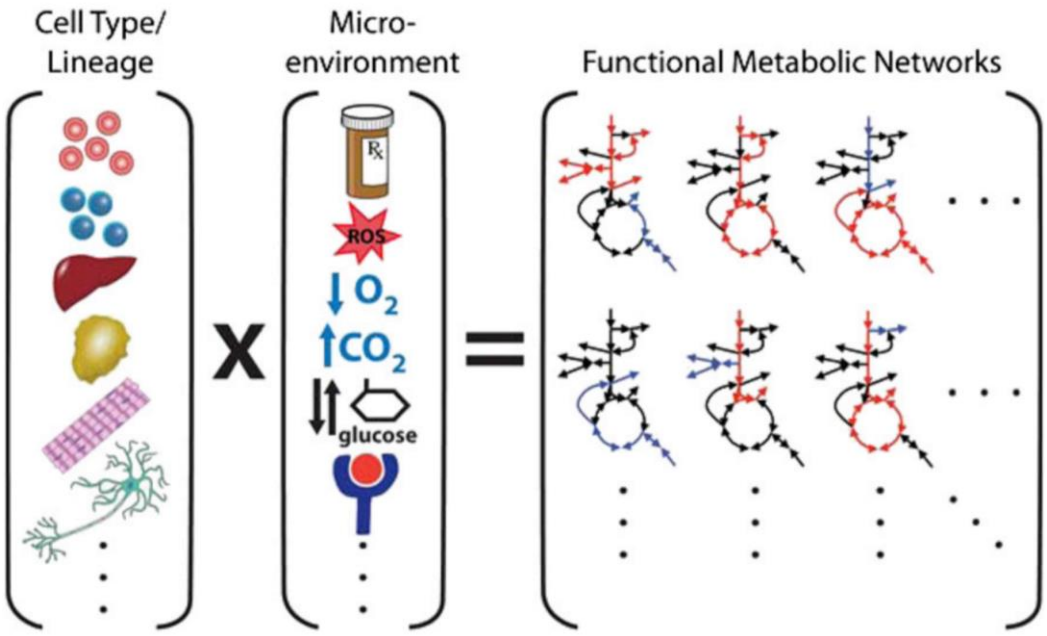

Figure 1.9 – Cellular and environmental mediated metabolic diversity.
Depending on the cell lineage and the exposure to various environmental cues such as drugs, oxygen levels, nutrient availability and hormonal signals, it results to a diverse array of functional metabolic networks (Image adapted from Metallo and Vander Heiden, 2013).

1.5 Pancreatic cancer biology and physiology

The pancreas is responsible for regulating blood glucose homeostasis, as well as lipid, protein and carbohydrate digestion. Approximately 80% of the pancreas exerts exocrine functions, being composed of acinar and ductal cells which produce gastrointestinal zymogens used in digestion. The remaining 20% of the pancreas, which accounts for the endocrine part, regulates glucose homeostasis through the production of hormones (such as insulin and glucagon) into the bloodstream. Four specialized clusters of endocrine cells are grouped together termed the Islets of Langerhans (Figure 1.10) (Hezel *et al*., 2006).

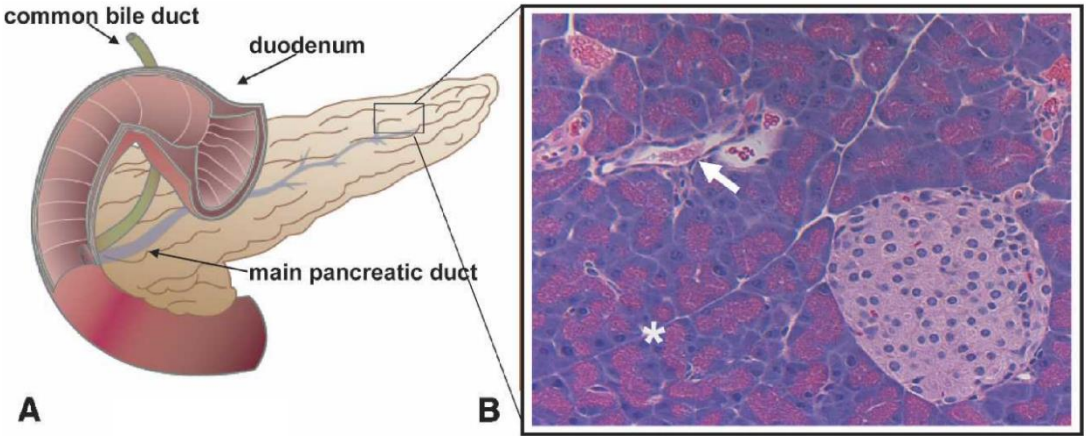

Figure 1.10 – Pancreatic anatomy.
(A) The structure of the pancreas and its anatomical positioning with the duodenum and common bile duct. **(B)** A histological representation of the pancreatic parenchyma. A pancreatic islet of Langerhans is shown at the lower right, which is the endocrine part of the pancreas regulating glucose homeostasis. The asterisk is placed among acini, which produce zymogens in order to aid digestion are secreted into the ducts shown by the arrow. (Image adapted from Hezel *et al*., 2006).

More than 85% of pancreatic cancer cases resemble ductal cells and thus are characterized as pancreatic ductal adenocarcinoma (PDAC). PDAC is the 11th most commonly occurring cancer in men and 9th in women (GLOBOCAN, 2018). The median survival rate is typically less than 1 year, and a 5-year survival rate remains less than 10% (O'Reilly et al., 2020). Advanced age, smoking, chronic pancreatitis, diabetes and obesity are some of the environmental risk factors that have been suggested to cause PDAC. Moreover, 10% of PDAC cases are associated with germline mutations in TSGs such as *INK4A, BRCA1,2* and *LKB1,* the DNA mismatch repair gene *MLH1* and the cationic trypsinogen gene *PRSS1* (Becker *et al.*, 2014).

PDAC usually presents in the head of the pancreas, with a high infiltrating potential into the lymph nodes, spleen and peritoneal cavity, as well as metastasizing to the liver and

lungs. Furthermore, a dense stroma of fibroblasts and inflammatory cells, known as desmoplasia, typically characterizes the disease. PDAC commonly exhibits a glandular like phenotype with duct like structures and demonstrates various levels of cellular atypia and differentiation, whereas colloid, adenosquamous and sarcomatoid histology is less commonly found. Histopathological studies demonstrate three precursor lesions: pancreatic intraepithelial lesions (PanINs), mucinous cystic neoplasm (MCN) and intraductal papillary mucinous neoplasm (IPMN) (Figure 1.11) (Hezel *et al*., 2006).

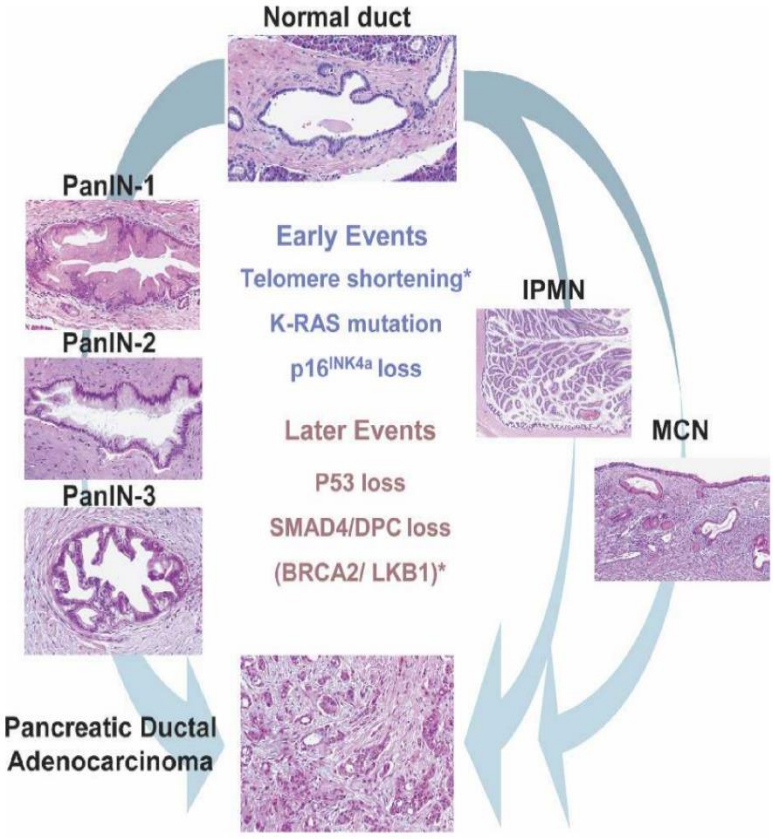

Figure 1.11 – Pancreatic pre-invasive neoplasms.
The three grades of PanIN, as well as IPMN and MCN leading to PDAC are pictured. In addition, the genetic alterations which most often occur in PanIN are shown and are grouped into early and later events towards the progression of PDAC (Image adapted from Hezel *et al*., 2006).

The most commonly found precursor lesion is PanIN located in the small caliber pancreatic ducts. PanINs demonstrate various morphological characteristics and are characterized by a columnar, mucinous epithelium. PanINs are split into three groups depending on their levels of cytological atypia and dysplasia (PanIN-1 – low grade dysplasia, PanIN-2 – moderate dysplasia, PanIN-3 – high grade dysplasia) (Figure 1.12) (Makohon-Moore and Iacobuzio-Donahue, 2016). MCN and IPMNs are large mucin-producing epithelial cystic neoplasms, which are characterized by an ovarian-type stroma and varying levels of cellular dysplasia (Hezel *et al*., 2006).

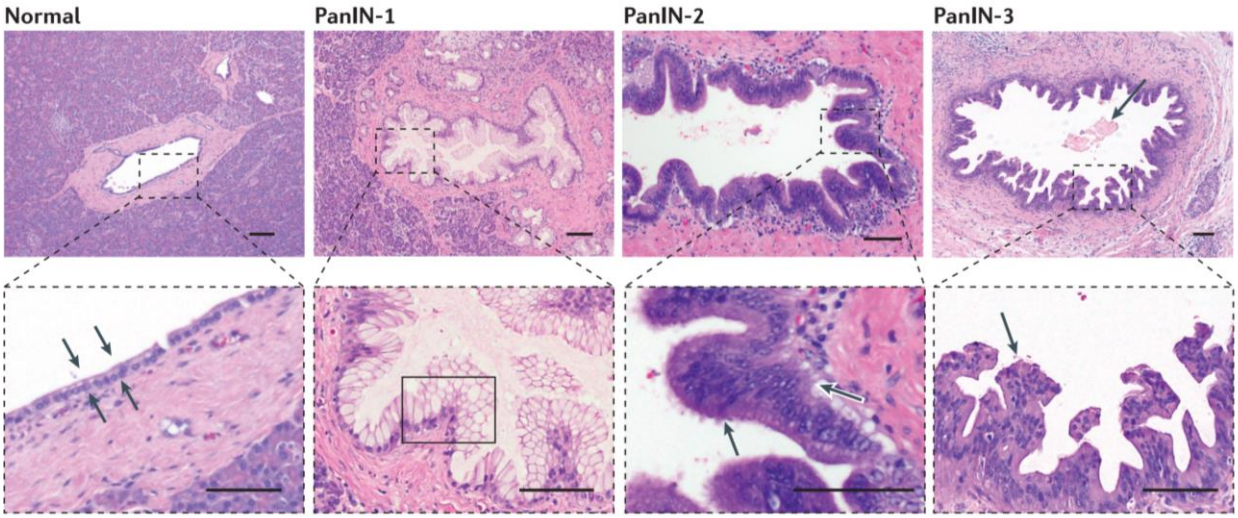

Figure 1.12 – Histopathological features of PanIN.
Pancreatic ductal epithelial cells are shown to have a simple cuboidal phenotype, shown by the arrows in the first panel. PanIN-1 is characterized by a mucinous differentiation and elongation of the ductal cells whilst having minimal cell atypia. PanIN-2 demonstrate loss of mucinous epithelium as well as nuclear pleomorphism and mitotic figures. PanIN-3 corresponds to frank carcinoma *in situ,* with pseudopapillary lesions, high levels of nuclear atypia, intraluminal apoptotic debris, and frequent mitotic figures (Image adapted from Makohon-Moore and Iacobuzio-Donahue, 2016).

Unlike skin, liver and colorectal cells, the pancreas is not a rapidly proliferative tissue, thus the probability of a sporadic driver gene mutation occurring is low. It is estimated that in patients who present with sporadic pancreatic cancer, the mutation occurred 20 years before diagnosis (Yachida *et al*., 2010). Moreover, a sporadic mutation does not guarantee cancer development, since the mutation must be fixed in the epithelial cell population (Figure 1.13). Therefore, when a healthy pancreatic cell acquires a somatic mutation due to environmental factors or a fault in DNA repair mechanisms, the cell will usually undergo apoptosis or senescence, or will be lost due to genetic drift, or immune detection. However, if these mechanisms fail, and the cell due to the driver mutation acquires survival or proliferative advantages, it will proceed to epithelial fixation. The cell will then continue to proliferate producing a clonal population defined by the driver gene mutation. The descendant progeny (which has a proliferative advantage) will then develop further driver gene mutations as well as acquiring passenger mutations, thus increasing genetic heterogeneity of the emerging neoplasm (characterized as stepwise evolution). In addition, the punctuated evolution model may take place, where a single mutation has genome wide catastrophic consequences through the acquisition of multiple driver gene mutations. Following increased cell proliferation, the neoplasm can break through the basement membrane and enter the surrounding stroma. Further genetic mutations, stromal signals, deposition of the extracellular matrix and immune infiltrates provide the selective forces for adapting the subclonal populations overall fitness. Although dissemination is likely to be an ongoing process in tumour development, it is unknown whether cells from the entire neoplasm uniformly enter the bloodstream or dissemination is constrained to a specific subpopulation. Nevertheless,

the disseminated cells had achieved high fitness levels when located in the primary site and are most likely to colonize new microenvironments successfully (Makohon-Moore and Iacobuzio-Donahue, 2016).

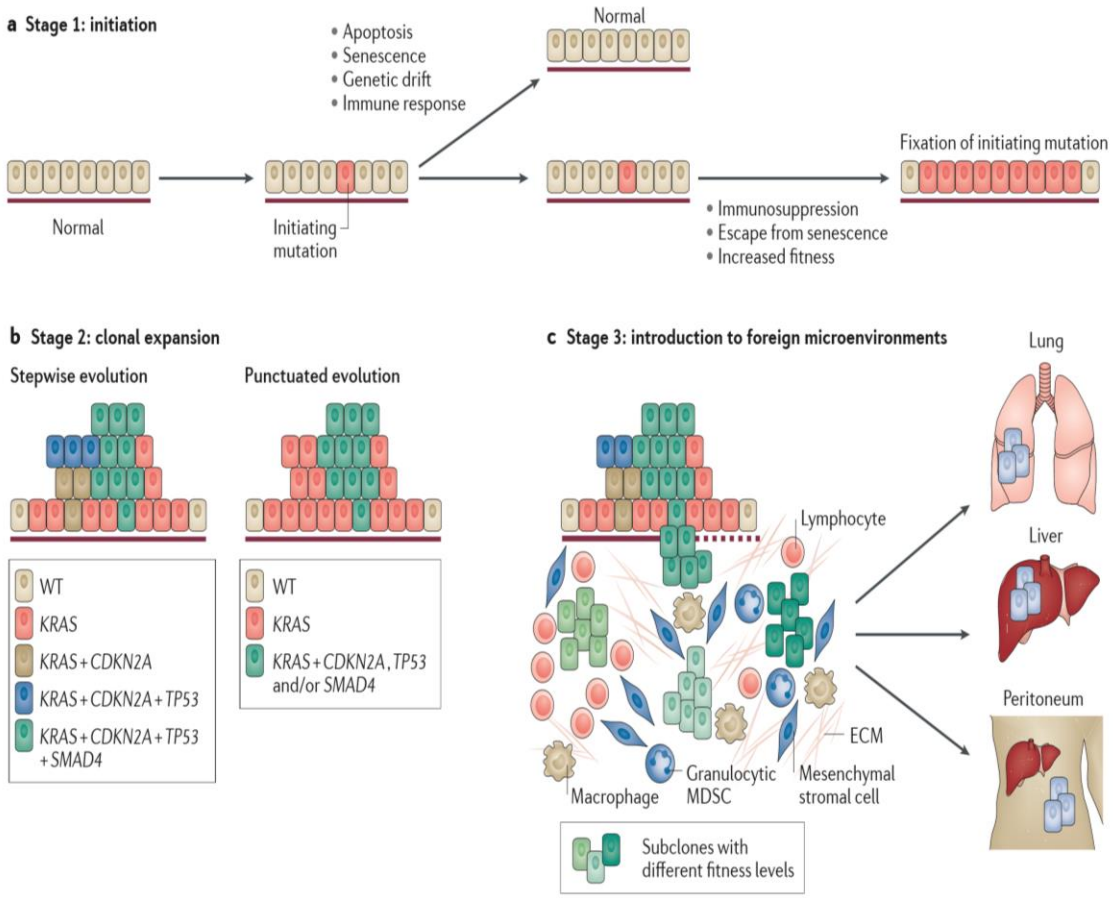

Figure 1.13 – The evolutionary stages of pancreatic cancer development.
A schematic representation of **(a)** the initiation stage where a driver mutation occurs and undergoes epithelial fixation. **(b)** clonal expansion either through stepwise or punctuated evolution. **(c)** Further expansion into the stromal region, where cells interact with the microenvironment and develop into various subclones which eventually results in dissemination and successful metastasis forming in other tissues such as the lung, liver and peritoneum (Image adapted from Makohon-Moore and Iacobuzio-Donahue, 2016).

In addition, the genetic profile of pancreatic tumours is dominated by *KRAS*, *CDKN2A*, *SMAD4* and *TP53* mutations (Waddell *et al*., 2015; Biankin *et al*., 2012).

1.6 Hypothesis and aims

Tumour cells, share a common proliferative phenotype due to a lack of cell cycle restraints and oncogenic signaling. Metabolic reprogramming is firmly accepted as an established hallmark of carcinogenesis, which provides the cell with energy and biosynthetic material in order to proliferate. Due to the various oncogenic profiles which drive cancer initiation and progression, as well as the challenges imposed by the tumour microenvironment, such as nutrient scarcity and poor oxygenation, cancer cells have developed a diverse repertoire of metabolic phenotypes. Although the adaptation of cancer cells to increase glucose metabolism (Warburg effect) was identified in the 1920s, the true nature of this metabolic switch has only recently begun to be understood. An increased glycolytic flux not only provides the cell with increased levels of ATP to fuel its bioenergetic demands, but also provides carbon for the biosynthesis of lipids, nucleotides and non-essential amino acids.

Most cancer cells commonly show a high dependence on lipids. In addition to having a crucial role as an energy source, they are precursors for the biosynthesis of cell membranes and mediators of signalling processes (Beloribi-Djefaflia *et al*., 2016). These demands are predominantly met by increased levels of DNL where lipogenic enzymes are overexpressed in cells which are still able to take up exogenous lipids (Menendez and Lupu, 2007). Moreover, numerous tumours grow near adipose tissue, or form metastasis in adipose rich environments, which are an important source of fatty acids. Fatty acids are then oxidised within the tumour cells and used as an energy source through FAO (Carracedo *et al*., 2013). The ability to utilize exogenous lipids appears to be contrary to the high rates of DNL in cancer cells, for example, data from

Ehrlich ascites suggests that cancer cells synthesize >93% of their TG *de novo*, irrespective of being able to utilize FAs that can be obtained exogenously (Ookhtens *et al*., 1984; Menendez and Lupu, 2007). Indeed, it is the ability of cells to import and utilise various intermediates to produce lipids that has compromised the various classes of lipid synthesis inhibitors which were thought to provide cytotoxicity against cancer cells known to be highly dependent on lipid synthesis.

Recent studies have attempted to gain an insight into the relationship between exogenous lipid availability and DNL by examining lipid deprivation on cell proliferation. Long term (72hr) experimental studies have shown that lipid reduced environments differentially affect cell growth rates with some cancer cell lines showing that a lack of exogenous lipids can influence DNL by switching it on. This has been observed in cell lines considered to be non-lipogenic, enabling the cells to cope better under lipid reduced conditions (Daemen *et al*., 2015), also providing evidence for the importance of extracellular conditions in regulating cancer cell growth. However, what the implications of the long-term effects of a fatty acid rich environment on cell proliferation has not been reported, especially in cells that show a reliance on DNL. In the same way that DNL can be upregulated in a lipid (fatty acid) poor environment, can it also be reduced in a lipid (fatty acid) rich environment and what would the implications of this be in relation to cancer cells that are reliant on high levels of DNL?

The focus of this study will be to examine how manipulating the environment through the addition of the fatty acid oleic acid affects proliferation in a panel of pancreatic cancer cell lines, which demonstrate different levels of metastatic potential as well as differentiation. Microarray analysis has already shown lipid metabolism to be most

altered set of metabolic pathways in pancreatic cancer cells (Guillaumond *et al*., 2013). Furthermore, metabolic pathways are highly interconnected with metabolic products being used as anabolic precursors or for subsequent pathways or for the generation of redox coenzymes. By perturbing intracellular lipid levels and examining the effects on lipid synthesis, the subsequent effect on interconnected pathways such as the Pentose Phosphate Pathway (PPP) and the redox cofactor NADPH will be examined. Given the difficulties in treating PC and the importance of lipid metabolism in this cancer, providing an approach which may sensitize cells by altering DNL may result to alternative therapeutic strategies to cancer therapy.

Aims:

1) To determine the effect of exogenously supplied oleic acid on pancreatic cancer cell growth.
2) To characterize changes associated with the uptake of fat by examining DNL using isotopically labeled biosynthetic substrates, such as glucose and glutamine.
3) Examine the interconnection between lipid synthesis and associated pathways such as the pentose phosphate pathway and NADPH generation to provide a new direction for susceptibility.

Chapter 2 – Material and Methods

2.1 Cell culture

The cell lines shown in Table 2.1 were purchased from ATCC and were maintained in the relevant media which was supplemented with 10% (v/v) foetal calf serum and 1% (v/v) antibiotics (penicillin, streptomycin and neomycin) (Sigma-Aldrich, UK) under normoxic conditions. All remaining constituents, (glucose and glutamine were present in the media). Cells were cultured in T-75 flasks and were trypsinised (Sigma-Aldrich, UK) once achieving 80-90% confluency. Cells were seeded in both T-75 and 6-well plates at densities of 2×10^6 and 0.3×10^6 respectively.

The cell lines BxPC-3, HepG2 and SH-SY5Y were new purchases from ATCC (passage 1) for the completion of this project. The additional cell lines (AsPC-1, Capan-1, MiaPaca-2 and HeLa) had been recently authenticated and were shown to be suitable for experimental use. All cell lines were used up to 10 passages from the day of thaw from liquid nitrogen.

Table 2.1 – Cell culture media
The following table describes the cell culture media used for culturing each cell line.

Cell Culture						
Cell line	**Source**	**Vendor**	**Passage**	**Catalog number**	**Culture media**	**Vendor**
AsPC-1	Pancreas	ATCC	20	CRL-1682	RPMI	Sigma-Aldrich
BxPC-3	Pancreas	ATCC	1	CRL-1687	RPMI	Sigma-Aldrich
Capan-1	Pancreas	ATCC	35	HTB-79	RPMI	Sigma-Aldrich
MiaPaca-2	Pancreas	ATCC	40	CRL-1420	DMEM	Sigma-Aldrich
HepG2	Liver	ATCC	1	HB-8065	DMEM	Sigma-Aldrich
HeLa	Cervix	ATCC	7	CCL-2	RPMI	Sigma-Aldrich
SH-SY5Y	Nerve	ATCC	1	CRL-2266	1:1 Ham's F12/DMEM	Thermo Fisher

2.2 Epithelial mesenchymal transition screening via Western blotting

The panel of cancer cell lines shown in Table 2.1 were cultured in 6-well plates and were harvested once achieving 70-80% confluency. Cells were lysed using 200µL of RadioImmunoprecipitation assay (RIPA) buffer (ThermoFisher, UK) which was supplemented with (1:100) protease inhibitors (P8340, Sigma-Aldrich, UK). Samples were sonicated, to ensure cell lysis and to reduce DNA viscosity. Protein concentration was determined using a Bradford assay (Bio-Rad, UK). Samples were calculated to contain 20µg/µL of protein in a total volume of 13µL (distilled water would be added to bring the volume to 13µL) and 5µL of the lithium dodecyl sulphate (LDS) sample buffer along with 2µL of reducing agent (ThermoFisher, UK) were added bring the sample volume to 20µL. Reducing agent containing 500mM dithiothreitol was added to maintain protein samples in a reduced state during gel electrophoresis. Subsequently,

samples were heated at 95^{o}C for 5 minutes and 20µL were loaded on to a Bis-Tris NuPAGE 4-12% 1mm thick gradient gel and ran using MES running buffer for 40 minutes at 200V (ThermoFisher, UK). Additionally, 5µL of the chameleon duo (LI-COR, UK) protein ladder were added in the first lane. The chameleon duo protein ladder allows detection of bands in both the 700 and 800nm channel. The proteins were then transferred onto an Immobilon-P Polyvinylidene fluoride (PVDF, Merck Millipore, UK) membrane using premade transfer buffer (ThermoFisher, UK) for 2.5hr at 30V. Both PVDF and Nitrocellulose (Bio-Rad, UK) membranes were trialed. Results were in agreement with LI-COR Biosciences recommendation, demonstrating high background levels when using a nitrocellulose membrane on the Odyssey Infra-red imaging system. The membrane was then blocked using 5% Bovine Serum Albumin (BSA) for two hours and incubated over night with the primary antibody. Milk and BSA (5%) blocking buffers had been trialed, with BSA demonstrating the best signal to background blots. Following overnight incubation with the primary antibody, three 5-minute washes with Tween Tris buffer saline (TTBS) were performed. The membrane was then incubated for 1 hour secondary antibody. The membrane was then subjected to three 5-minute washes with TTBS before being scanned on the Odyssey Li-Cor Infra-red imaging system (Li-Cor Biotechnology, UK). During all incubation steps and washes the membrane was placed on an orbital shaker at 80rpm.

2.3 IncuCyte growth curves

The IncuCyte real-time imaging system automatically acquires and analyses images, providing an information-rich analysis (Essenbioscience, UK). The technology became

available in 2007 and to date 2291 peer reviewed publications have produced data using this method. This system automatically scans cells every two hours, therefore enabling users to obtain measurements without causing any disruption to the cells. The IncuCyte can provide numerous biological measurements such as: changes in cell confluency, migration, invasion, cell death, and immune cell killing. Publications to be referred to for demonstrating the use of the IncuCyte Imaging system to monitor proliferation in terms of confluency (Falcon et al., 2013; Daniels et al., 2014) whereas to monitor cell death and apoptosis (Artymovich and Appledorn, 2015; Aftab et al., 2014; Zweemer et al., 2017). A limitation of using a confluency-based system to determine cell proliferation is the reduced sensitivity in terms of differences in cell size, and cell densities. However, it is an efficient and low cost method to provide cell growth patterns with and without treatment. The data provided by the IncuCyte real-time imaging system can then be validated using independent molecular techniques such as cell cycle analysis and CFSE staining.

BxPC-3, HeLa, Capan-1, MiaPaca-2 and HepG2 cells were seeded in 6-well plates and were incubated overnight. Following treatment, cells were placed in the IncuCyte ZOOM real time imaging system and were incubated for 120 hours.

Upon collection of all images, a confluency mask was set specific to each cell line in order to exclude signal from isolated dead cells and debris. Growth curves based on cell confluency were produced using the IncuCyte software.

2.4 Lipid extraction and preparation of fatty acid methyl esters

Lipids were extracted using the Folch procedure (Folch *et al*., 1957). Cells were trypsinised in 0.5ml of PBS and lipids were extracted overnight with a 4-fold volume of ice-cold chloroform-methanol 2:1 (v/v) at 4^{o}C. Following overnight extraction, samples were centrifuged at 2500rpm 4^{o}C for 30 minutes to separate the solvent from the aqueous layer. The lower layer contains the high concentration lipid fraction whereas the upper layer is the low concentration fraction. The infranatant (i.e. the upper layer of the two-layer solution), was re-extracted to ensure maximal lipid extraction and was transferred into a clean glass tube using a glass Pasteur pipette. The supernatant was re-extracted with a further 2-fold volume of ice-cold chloroform-methanol 2:1 (v/v) at 4^{o}C for 1 hour and again was centrifuged at 2500rpm for 30 minutes at 4^{o}C. The solvent extracts were combined and a quarter of the volume of all the solvent extracts used to extract the lipids of KCl (0.88% w/v) was added. Samples were centrifuged at 2500rpm for 30 minutes at 4^{o}C. The aqueous layer was then discarded and 100µL of ethanol was added to the solvent phase. Fatty acid methyl esters (FAME) were prepared. Samples were placed under nitrogen gas in order to evaporate and were resuspended in 0.2mL toluene, 1.5mL of methanol and 0.3mL of 8% HCl. Samples were placed in a water bath at 80^{o}C for 3 hours. Finally, 1mL of 5% NaCl along with 0.5mL of hexane was added to the samples, and the hexane layer was pipetted into gas chromatography mass spectrometry (GC/MS) vials using a Pasteur pipette. The addition of NaCl causes polar material to be retained in the aqueous phase, whereas the hexane layer contains molecules of low polarity (such as FAME) which will be analysed via GC-MS.

2.5 Gas Chromatography Mass Spectrometry

A standardized protocol for measuring levels of enrichment in FAME provided by Rosenblatt *et al,* 1992, was applied and optimized per the following conditions. Fatty acid methyl esters were analysed by electron impact ionisation using an Agilent 5975C coupled to a 7890A GC system (Agilent Technologies, UK). Samples were run on a HP 5 MS capillary column 30m x 0.25mm i.d x 0.25µm film thickness (Agilent Technologies, UK). Two microliters of each sample were injected by splitless injection with the temperature of the injector at 270^{o}C. The GC oven temperature was held at 60^{o}C for 2 minutes and the increased at 10^{o}C/minute to 220^{o}C and then increased at 5^{o}C/min to 280^{o}C where temperature was held for 1 minute. The ion source temperature was held at 230^{o}C and the quadrupole temperature held at 150^{O}C. Enrichment of palmitic acid was determined by measuring the mass to charge ratios of 270, 271, 272, 273 and 274amu, representing the molecular ion for unlabeled and labelled palmitate methyl ester (the mass-to-charge ratio of unlabeled palmitate is 270, whether 1,2,3 or 4 13C labelled units were added it would result to a 271, 272 273 and 274 mass-to-charge ratio being produced). Artefacts resulting from concentration-dependent self-chemical ionization of methyl palmitate were minimized by ensuring that similar peak areas were obtained for all samples measured within a single analysis (Rosenblatt *et al*., 1992). Since enrichment was measured by the change in ratio between m+1 and m, ionization in the ion source can be concentration dependent. Therefore, in order to prevent concentration dependent effects altering the distribution of molecular fragments, samples were run at similar concentrations.

2.6 Statistical analysis

Statistical analysis was conducted using GraphPad Prism version 7.0 (GraphPad software). A Two way ANOVA test was used to determine any significant differences between test samples. *P* values were computed, and graphs were compiled using the software. In addition, changes in cell proliferation were also characterised by measuring changes in area under the curve (AUC).

Chapter 3 – Initial characterization; Epithelial Mesnchymal Transistion status, glucose dependency and *de novo lipogenesis* from glucose in a panel of pancreatic cancer cells

3.1 Introduction

The divergence between epithelial and mesenchymal cells is a crucial and tightly regulated developmental process. The epithelial phenotype consists of well differentiated adherent cells, whereas mesenchymal cells demonstrate an undifferentiated phenotype which is highly motile, fibroblastic and tissue invasive (Micalizzi *et al*., 2010). Mesenchymal epithelial transition takes place in embryogenesis during gastrulation, neural crest formation and heart morphogenesis. However, the opposite phenomenon termed epithelial mesenchymal transition (EMT) may also occur. In cancer EMT results in accelerated proliferation, resistance to apoptotic signals, evasion of senescence and metastasis Figure 3.1) (Kalluri and Weinberg, 2009).

In this chapter the expression levels of the cell adhesion protein E-cadherin, the cytoskeletal protein Vimentin and the transcription factor (TF) Twist which are markers of EMT will be examined in a panel of cancer cell lines (AsPC-1, BxPC-3, Capan-1, MiaPaca-2 HepG2, HeLa and SH-SY5Y).

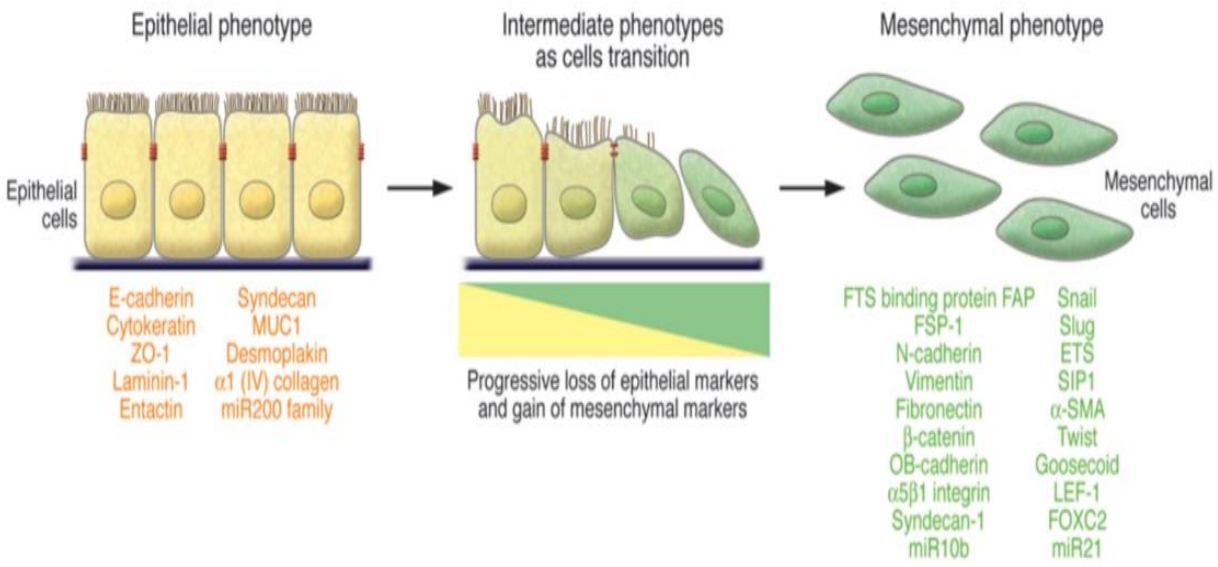

Figure 3.1 – Molecular and morphological changes in EMT.
During EMT, epithelial cells lose apical cell polarity followed by loss of cell adhesion proteins such E-cadherin. Cytoskeletal proteins are rearranged with cytokeratin intermediate filaments being replaced by Vimentin. Epigenetic regulators such as Zeb 1, Zeb 2, Twist, Snail and Slug have been shown to induce EMT. Image adapted by Kalluri and Weinberg, 2009).

As described previously, cancer cells maintain a high glycolytic flux in both normoxic and hypoxic conditions, which enables them to fuel their bioenergetic and anabolic requirements (Vander Heiden *et al*., 2009). In addition, cancer cells also demonstrate elevated levels of *de* novo fatty acid synthesis, used for lipogenesis (DNL) and membrane synthesis.

Therefore, as a way of metabolically profiling the cells in addition to EMT status, this chapter will also examine glucose dependency in relation to cell growth in BxPC-3, Capan-1, MiaPaca-2, HepG2 and HeLa cells (a well characterised cell line). AsPC-1 cells were omitted from the growth experiment as their morphological phenotype was difficult to capture through the IncuCyte imaging system. The effect on DNL from glucose in cells cultured under high, medium and low glucose concentrations will also

be investigated using [U-^{13}C-Glucose] to characterise the influence of different media glucose concentrations on the incorporation of glucose carbon into palmitic acid in BxPC-3, AsPC-1, Capan-1, MiaPaca-2 and HepG2 cells. The focus of this study is to examine pancreatic cancer metabolism, HeLa (cervical) and SH-SY5Y (neuronal) cells were omitted from DNL investigation. HepG2 (hepatic) cells were included due to their well characterised metabolically flexible phenotype which would help in the interpretation of the pancreatic data (Rui, 2014). Furthermore, standardising the media in which cells were maintained during flux experiments (i.e. determination of [U-^{13}C] glucose contribution to palmitate) proved challenging. BxPC-3, AsPC-1, Capan-1 cells were maintained in RPMI media which contained 11mM glucose and 2mM glutamine. In comparison, MiaPaca-2 and HepG2 cells were cultured using DMEM media, containing 25mM glucose and 4mM glutamine, according to the manufacturer's instructions. Culturing of cells in identical media was trialled; however, cells demonstrated atypical morphological patterns and growth profiles. In order to remain consistent with the manufacturer's recommendations and to obtain comparative data with scientific community, it was decided to culture cell lines in the recommended media.

Increased rates of DNL are key to defining the lipogenic phenotype in malignant cells. A lipogenic phenotype is associated with poor prognosis of many human carcinomas. Lipidomic profiling and the modulation of multiple lipogenic enzymes have been shown to correlate with cell proliferation and metastatic ability (Daemen *et al*., 2015; Lupu and Menendez, 2006).

3.2 Materials and Methods

3.2.1 Epithelial Mesenchymal Transition - Western blotting

BxPC-3, AsPC-1, Capan-1, MiaPaca-2, HepG2, HeLa (positive control for Vimentin) and SH-SY5Y (positive control for Twist) cells were seeded in 6-well plates and cultured under standard conditions until achieving ~80% confluency (see section 2.1). Cells were collected and prepared for Western blotting analysis (see section 2.2). Table 3.2 provides information regarding the antibodies used for examining EMT status. The primary antibody concentration (1:1000) and secondary antibody concentration (1:10000) were used based on the manufacturer's recommendation.

Table 3.1 – Western blotting
Antibodies used for EMT status examination

EMT Western blot antibodies			
Cell line	**Vendor**	**Catalog number**	**Concentration**
E-Cadherin	Cell Signaling	144725	1:1000
Twist	Santa Cruz	sc-81417	1:1000
Vimentin	Santa Cruz	sc-32322	1:1000
beta-actin	Santa Cruz	sc-376421	1:1000
Anti-mouse	Li-cor	926-68072	1:10000
Anti-Rabbit	Li-cor	926-32213	1:10000

3.2.2 Glucose dependant growth curves

BxPC-3, Capan-1, MiaPaca-2, HeLa and HepG2 cells were seeded in 6-well plates at ~20% confluency. Cells were grown over a 5-day period without changing media. BxPC-3, Capan-1 and HeLa cells were grown in RPMI media containing 11, 5.5 and 2.75mM glucose. MiaPaca-2 and HepG2 cells were grown in DMEM media containing 25, 5.5 and 2.75mM glucose. Cell growth in terms of confluency was determined using

the IncuCyte ZOOM imaging system (Essenbioscience, UK; see section 2.3). Changes in the area under the curve (AUC) in order to demonstrate changes in cell growth, along with a 2-way ANOVA was used to assess the statistical significance between the different glucose concentrations.

3.2.3 Contribution of labelled glucose to palmitic acid

BxPC-3, AsPC-1, Capan-1, MiaPaca-2 and HepG2 cells were seeded in 6-well plates at ~20% confluency for a 48hr period. BxPC-3, AsPC-1 and Capan-1 cells were grown in RPMI media containing 11, 5.5 and 2.75mM glucose. MiaPaca-2 and HepG2 cells were grown in DMEM media contacting 25, 5.5 and 2.75mM glucose. In all treatments 50% of the total glucose concentration had been replaced with [U-^{13}C] glucose. Samples were collected at 48 hours to compare levels of palmitate enrichment based on glucose concentration.

In addition, Capan-1 and HepG2 cells were seeded in T-25 flasks at ~20% confluency and were treated with 11, 5.5 and 2.75 RPMI media and 25, 5.5 and 2.75mM DMEM respectively, over a 5-day period (50% of glucose had also been replaced with [U-^{13}C] glucose) with samples being collected every 24 hour period. See section 2.4 for details regarding GC-MS methodology and experimental parameters.

3.3 Results

3.3.1 Epithelial Mesenchymal Transition status

AsPC-1 cells were positive for E-cadherin (an epithelial cell marker) and Vimentin (a mesenchymal cell marker). BxPC-3 and Capan-1 cells were also positive for E-cadherin but negative for Vimentin, indicating an epithelial cell phenotype. MiaPaca-2, HeLa and SH-SY5Y were all negative for E-cadherin and positive for Vimentin with SH-SY5Y cells also being positive for Twist, suggesting a mesenchymal cell phenotype. Finally, HepG2 cells were negative for all three markers (Figure 3.2).

A representative image of the Western blot shown in Figure 3.2 demonstrating the protein ladder along with molecular weights is shown in Appendix 1, Figure 1.1. AsPC-1 cells demonstrate statistically significantly ($p<0.001$) lower levels of E-cadherin compared to Capan-1 cells only. MiaPaca-2 and HeLa cells express Vimentin at statistically significant levels compared to AsPC-1, BxPC-3, Capan-1, HepG2 and SH-SY5Y cells ($p<0.0001$). However, no statistical significance is shown between MiaPaca-2 and HeLa cells. Although minor levels of Vimentin were detected in AsPC-1 and SH-SY5Y cells, no statistical difference is shown when compared against BxPC-3, Capan-1 and HepG2 cells. Finally, Twist demonstrated statistically significant expression only in SH-SY5Y cells ($p<0.0001$), whereas all other cells demonstrated negligible amounts.

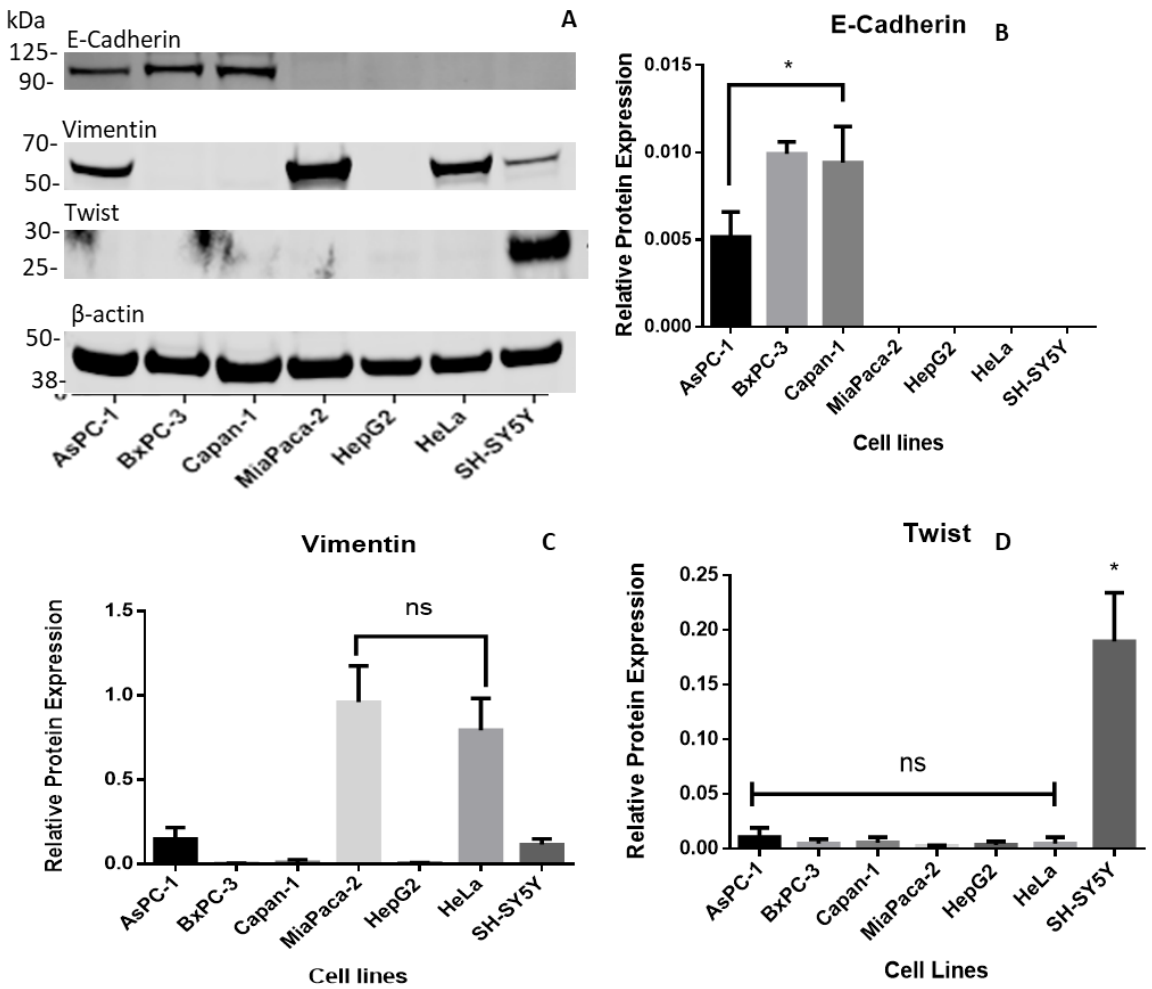

Figure 3.2 – Examination of EMT status
Expression of EMT markers by Western blotting **(A)** Levels of E-cadherin, Vimentin and Twist from cultured AsPC-1, BxPC-3, Capan-1, MiaPaca-2, HepG2, HeLa and SH-SY5Y cells (See Appendix 1, Figure 1). Data was quantified by densitometry analysis and normalised to β-actin **(B-D)** and represented as mean +/- SD, (n=3). Not significant (ns), Statistically significant (*).

3.3.2 Glucose dependence

Cell proliferation under the different glucose concentrations was determined by measuring levels of confluency using the IncuCyte ZOOM imaging system. BxPC-3 cells demonstrated the highest level of growth arrest ($p<0.0002$, 11 vs 5.5mM).

However, HeLa and MiaPaca-2 cells showed three separate growth curves dependent on glucose concentration. The Capan-1 cell line was the least affected pancreatic cell line but showed a decrease in growth at later time points (>72hr). HepG2 cells only showed a decrease in growth when cultured with 2.75mM glucose media over the five-day period (Figure 3.3).

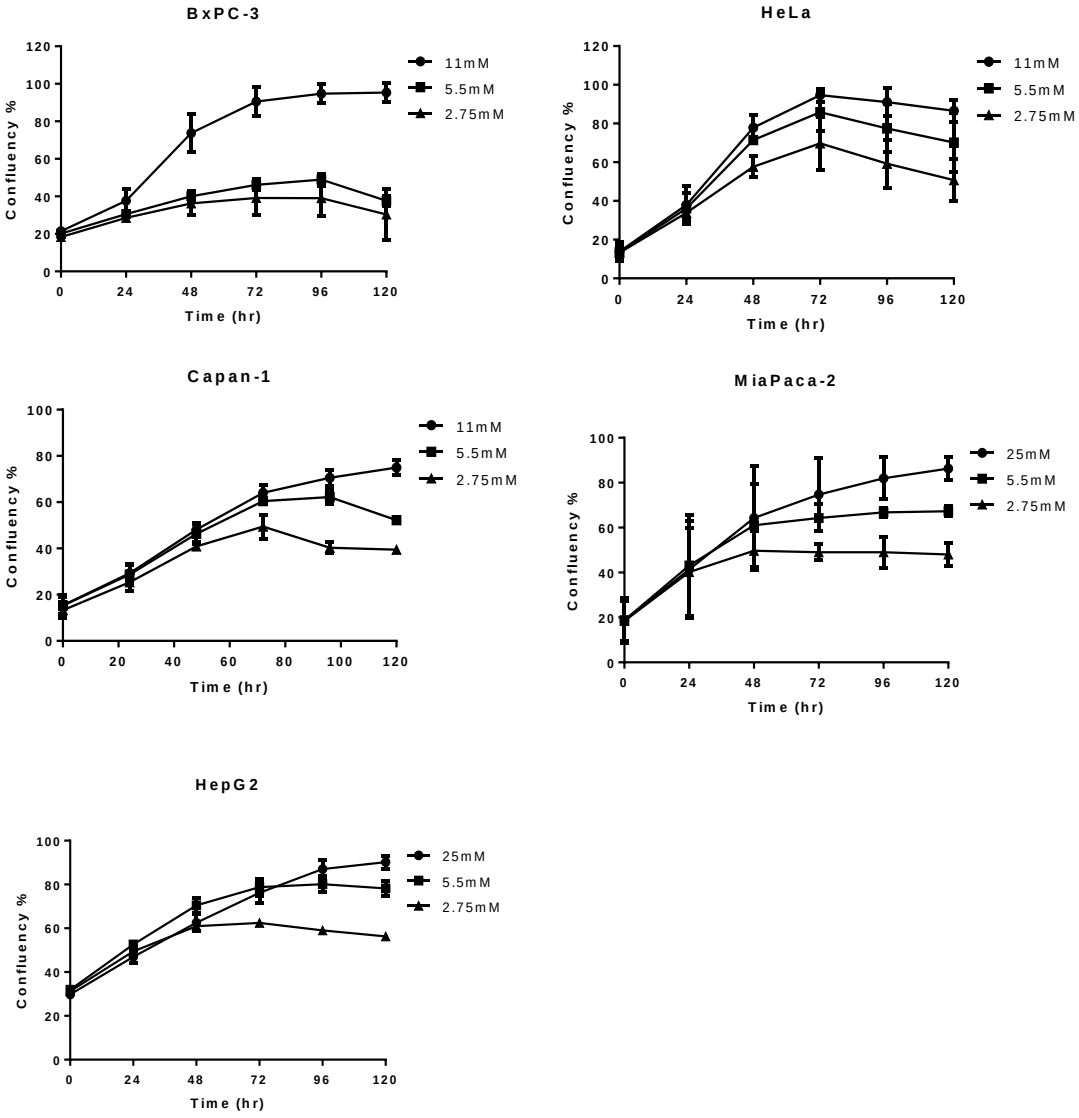

Figure 3.3 – Glucose dependent growth curves.
The above panel of cancer cell lines were cultured under three different glucose concentrations, with the data suggesting that BxPC-3 cells were the most affected and HepG2 cells the least affected in terms of growth when cultured under 5.5mM glucose (mean +/- SD, n=3).

The percentage difference in area under the curve (AUC) was calculated in order to demonstrate changes in growth when cells were cultured under high medium and low glucose concentrations (Table 3.2).

Table 3.2 – Percentage change in AUC
Percentage change AUC with cells cultured under high, medium and low glucose concentrations.

Percentage change in AUC					
Glucose conc	**BxPC-3**	**Capan-1**	**MiaPaca-2**	**HepG2**	**HeLa**
High*	100	100	100	100	100
Medium	55	90	88	101	89
Low	47	71	70	83	72

*Percentage area was calculated by standardizing to the high glucose concentration values.

In addition to AUC, a two way ANOVA was used to assess the statistical significance when comparing high vs medium, high vs low and medium vs low glucose concentration (Table 3.3).

Table 3.3 – Statistical analysis two-tailed t-test
Statistical analysis using a two way ANOVA when culturing cells under high, medium and low glucose concentrations.

Statistical analysis		
Glucose concentration (mM)	**Significance**	**P values**
BxPC-3		
5.5 vs 11	Yes	0.0002
2.75 vs 11	Yes	0.0002
5.5 vs 2.75	No	ns
Capan-1		
5.5 vs 11	Yes	0.0001
2.75 vs 11	Yes	0.0001
5.5 vs 2.75	Yes	0.0001
HeLa		
5.5 vs 11	Yes	0.04
2.75 vs 11	Yes	0.0001
5.5 vs 2.75	Yes	0.0001
HepG2		
5.5 vs 25	No	ns
2.75 vs 25	Yes	0.0001
5.5 vs 2.75	Yes	0.0001
MiaPaca-2		
5.5 vs 25	No	ns
2.75 vs 25	Yes	0.0001
5.5 vs 2.75	Yes	0.0006

The data in Tables 3.2 and 3.3 demonstrate that BxPC-3 and HeLa cells show significant reduction in cell proliferation when cultured under 5.5 and 2.75mM glucose concentration. Furthermore, cell growth between 5.5 and 2.75mM varies significantly

in Capan-1, HeLa, MiaPaca-2 and HepG2 cells. However, BxPC-3 cells, only show differences in growth between 11mM glucose with 5.5 and 2.75mM glucose.

3.3.3 De novo Lipogenesis - Incorporation of labelled glucose into palmitic acid

HepG2 and MiaPaca-2 cells demonstrated media glucose concentration dependent enrichment levels of palmitic acid, whereas Capan-1, BxPC-3 and AsPC-1 cells showed the incorporation of glucose from the media into palmitic acid was independent of glucose concentration, even at the higher concentrations of glucose media (Figure 3.4). No statistically significant difference was shown in palmitate enrichment between Capan-1 cells compared to BxPC-3 and AsPC-1 cells. Additionally, no differences were shown between HepG2 and MiaPaca-2 cells. However, significant differences ($p<0.001$) were shown between BxPC-3 and AsPC-1 cells, as well as HepG2 and MiaPaca-2 cells when compared against Capan-1, BxPC-3 and AsPC-1 cells ($p<0.0001$) when using a 2-way ANOVA.

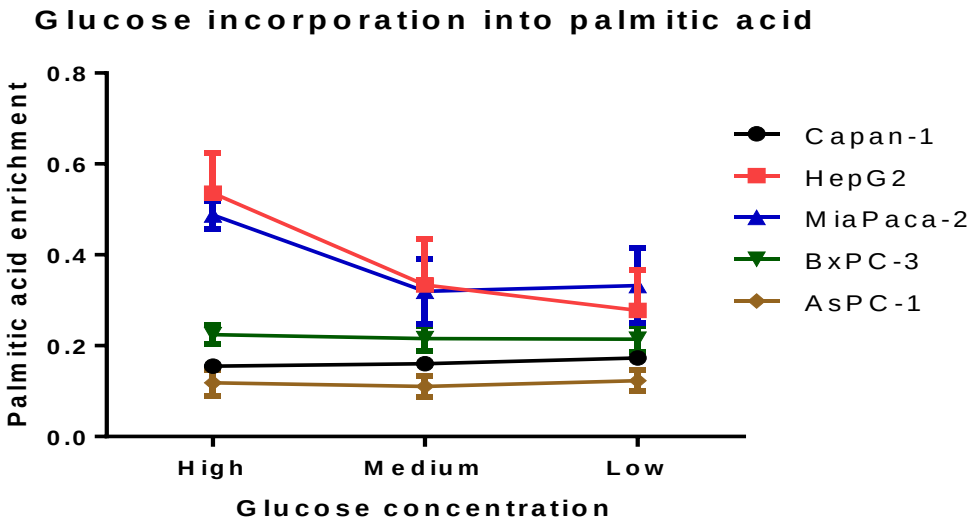

Figure 3.4 – Palmitic acid enrichment following 48 hour incubation with 50% U-13C glucose.
HepG2 and MiaPaca-2 cells were cultured under DMEM media containing 25mM, 5.5mM, 2.75mM glucose, whilst Capan-1, BxPC-3 and AsPC-1 cells were cultured under RPMI media containing 11mM, 5.5mM and 2.75mM glucose. HepG2 and MiaPaca-2 cells demonstrate glucose dependent palmitic acid enrichment levels, whereas Capan-1 cells demonstrate enrichment values independent of glucose concentration. Palmitic acid enrichment represents a ratio of labelled to unlabelled palmitate as measured by following the enrichment of m+2/m in palmitate (mean +/- SD, n=3).

To confirm these findings, the dependence of media glucose concentration on its incorporation into palmitate was further investigated by following the enrichment of palmitate in a representative dependent and non-dependent cell line. HepG2 and Capan-1 cells were cultured over a 5-day period under high, medium and low glucose concentrations with samples collected every 24 hours (Figure 3.5). The two data sets showed similar trends to the data described in Figure 3.4 and showed the dependent and non-dependent relationship was maintained. HepG2 cells displayed steady levels of palmitate enrichment over the 5-day period, being dependent of glucose

concentration. However, Capan-1 cells demonstrate similar levels of palmitate enrichment during the initial 24-72hr incubation period, followed by a decrease in enrichment in cells cultured with 5.5 and 2.75mM glucose (Figure 3.5).

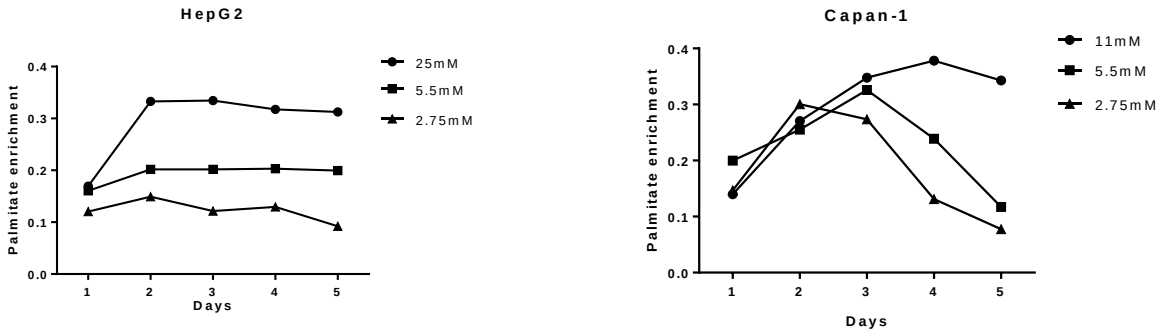

Figure 3.5 – Five-day profile of ^{13}C labelled glucose incorporation into palmitic acid.
Enrichment of palmitic acid in HepG2 and Capan-1 cells when cultured under high (25 and 11), medium 5.5 and low 2.75mM glucose concentrations respectively. Results showed steady levels of palmitate enrichment over the 5-day period for HepG2 cells at each of the glucose concentrations. However, Capan-1 cells demonstrated similar enrichment values for the first 48hr followed by a decrease in enrichment in cells cultured with 5.5 and 2.75mM glucose (n=1).

Table 3.4 summarises both glucose dependent growth and DNL as well as indicating whether the cell lines used tested positive or negative for EMT markers. In addition, due to its wide array of oncogenic effects including metabolic reprogramming (see chapter 1.4), KRAS status is also included.

Table 3.4 – Summary
Summarising both glucose dependent growth and palmitic acid synthesis, as well as the expression profile of EMT markers and KRAS mutant status (Deer *et al*., 2010).

Summary						
Cell lines	**Glucose dependent growth**	**Glucose dependent DNL**	**E-cadherin**	**Vimentin**	**Twist**	**KRAS mutant**
BxPC-3*	High	No	+	-	-	-
ASPC-1*	Not determined	No	+	+	-	+
Capan-1*	Medium	No	+	-	-	+
MiaPaca-2*	Medium	Yes	-	+	-	+
HepG2	Low	Yes	-	-	-	-
HeLa	High	Not determined	-	+	-	-
SH-SY5Y	Not determined	Not determined	-	+	+	-

*Pancreatic cancer cell lines

3.4 Discussion

3.4.1 Epithelial Mesenchymal Tranisition status

E-cadherin is a transmembrane glycoprotein which spans the cell membrane and forms homophilic interactions with adjacent E-cadherin molecules, thus ensuring epithelial cell adhesion. Loss of E-cadherin expression not only results in cells gaining motility but induces signal transduction pathways. Dissemination of cells from the extracellular matrix (ECM) may result in cell death via anoikis, however, cells which detach from the ECM due to loss of E-cadherin demonstrate resistance to death signals and have increased motility and tissue invasiveness. E-cadherin sequesters β-catenin from the nucleus, however loss of E-cadherin enables β-catenin to enter the nucleus and bind to the lymphoid-binding factor/T-cell factor 4 promoting the Wnt signalling pathway, resulting in a neoplastic transformation (Onder *et al*., 2008; Stadler and Allis, 2012).

Vimentin is a type 3 intermediate filament protein which replaces cytokeratin intermediate filaments during EMT and promotes changes in cell shape and motility (Micalizzi *et al*., 2010). In addition to E-cadherin, cell adhesion is also maintained through desmosomes which bind to cytokeratin intermediate filaments through the adaptor protein desmoplakin. However, expression of Vimentin reduces levels of desmoplakin in the cell periphery, thus preventing cell adhesion and inducing cell motility (Mendez *et al*., 2010). Twist is a TF found to be present in high grade and advanced staged malignant cells (Yu *et al*., 2010). It is a helix loop helix TF which can homodimerize or heterodimerize with other helix loop helix proteins and regulate diverse downstream targets. Twist has been shown to inhibit cell death when cells detach from the ECM due to loss of E-cadherin (Krause *et al*., 1997).

The results from this study show BxPC-3 and Capan-1 cells are positive for E-cadherin and negative for Vimentin and Twist indicating an epithelial cell phenotype. MiaPaca-2, HeLa and SH-SY5Y cells appear to be undergoing EMT with SH-SY5Y cells being the only cell line in the present study to express Twist, under normoxic conditions, indicating a strong mesenchymal phenotype. The data also shows that HepG2 cells are negative for E-cadherin, Vimentin and Twist. However, published data demonstrate that HepG2 cells are positive for E-cadherin and Vimentin and are negative for Twist (Matsuo *et al*., 2009). In addition, SH-SY5Y have been shown to be negative for E-cadherin and positive for Vimentin and Twist. Others have shown that SH-SY5Y cells are positive for E-cadherin, expressing low levels of Vimentin and negative for Twist (Debruyne *et al*., 2016).

Interestingly, AsPC-1 cells co-express E-cadherin and Vimentin. Although E-cadherin has been characterized as a tumour suppressor gene (TSG) and its downregulation is associated with EMT (as well as Vimentin upregulation), the role of E-cadherin may be more complex. Yamashita *et al.,* (2015) investigated the clinical significance of co-expression of E-cadherin and Vimentin in invasive breast cancer, concluding that co-expression was associated with the most aggressive phenotype and poor prognosis (Yamashita *et al*., 2015). The results from this study also showed that HeLa cells were negative for E-cadherin expression, but positive for Vimentin and negative for Twist which is in agreement with (Li and Zhou, 2011).

Li and Zhou (2011), also investigated the effects of Twist upregulation in HeLa cell transfectants. Their findings showed HeLa cells were positive for E-cadherin and Vimentin and are negative for Twist. However, when inducing Twist expression, E-

cadherin expression was reduced, and Vimentin expression increased, resulting in a stronger mesenchymal phenotype, thereby demonstrating the potential crosstalk these biomarkers have once upregulated (Li and Zhou, 2011).

Hotz and colleagues studied the expression of Twist in 36 tissue samples of pancreatic ductal adenocarcinoma and 5 pancreatic cancer cell lines (AsPC-1, Capan-1, HPAF-2, MiaPaca-2 and Panc-1) with 97% of the tissue samples and all the cell lines being negative for Twist expression (Hotz et al., 2007). Their data agrees with this study's findings; however, this was reported as an unexpected result as the overexpression of Twist has been published in several studies, showing to promote EMT and metastasis in several types of cancer (Karreth and Tuveson, 2004; Yang *et al*., 2015; Kwok *et al*., 2005). Further investigation of Twist by (Hotz *et al*., 2007) demonstrated that a 48hr incubation of pancreatic cancer cells under hypoxic conditions led to an upregulation of Twist.

It is known that pancreatic tumours grow under hypoxic conditions which promote cell proliferation and metastasis (Harris, 2002). This suggests that Twist may play a crucial role in pancreatic cancer development during hypoxia and that environmental conditions play a role in regulating these markers (Hotz *et al*., 2007). Although this study only examined EMT status under normoxic, basal conditions, understanding the consequences of changes in metabolism on EMT status may provide the identification of novel targets for treating metastatic cancer. This also suggests that changes in metabolism and the cellular environment may influence EMT status and could provide an explanation for the discrepancy in the data between a lot of the studies.

Dong *et al*. (2013) have provided data which demonstrate that loss of fructose-1,6-bisphosphatase (FBP1) triggers metabolic reprogramming, providing basal like breast cancer with metabolic advantages such as: increased glucose uptake, elevated levels of glycolytic intermediates for biosynthesis, maintenance of ATP under hypoxic conditions and reducing oxygen dependency and ROS generation. Fructose-1,6-bisphosphatase is a rate limiting enzyme in gluconeogenesis. In addition, the *FBP1* gene is shown to be a downstream target of the TF Snail (Dong *et al*., 2013). The Snail-G9a-Dnmt1 complex, which mediates silencing of E-cadherin, is also responsible for repressing FBP1 in basal like breast cancer. Thus, a synergistic effect between loss of E-cadherin and FBP1 to increase basal like breast cancer malignancy may exist (Dong *et al*., 2013). Moreover, disruption of mitochondrial bioenergetics via citrate synthetase downregulation promotes tumour malignancy. Loss of citrate synthetase causes cells to switch from aerobic respiration to glycolytic metabolism whilst inducing EMT in cervical cancer cell lines (Lin et al., 2012). Finally, Sanchez-Martinez *et al*. (2015) discuss how FA metabolism can induce EMT. Acyl-CoA synthetases (ACSL) converts long FA chains to acyl-CoA which is used for phospholipid and TG synthesis, lipid modification of proteins and β-oxidation (Sánchez-Martínez *et al*., 2015). Steraoyl-CoA desaturase (SCD) is the rate limiting marker converting saturated fatty acids to monounsaturated fatty acids (MUFAs), with several cancers exhibiting elevated levels of MUFAs (Patra, 2008). Overexpression of ACSL1, ACSL4 and SCD, has been shown to provide a cooperative effect in inducing EMT in colorectal cancer. It was the first study to demonstrate that genes involved in lipid metabolism can induce EMT(Sánchez-Martínez *et al*., 2015).

3.4.2 Glucose and lipid dependency

KRAS driven mutations in pancreatic tumours have been shown to induce aerobic glycolysis through multiple changes in nutrient driven pathways. These have been shown to enhance glucose uptake through upregulation of the *GLUT1* and regulate glucose rate limiting enzymes at the transcriptional level, thereby directing glucose metabolism into biosynthetic pathways (Ying *et al*., 2012). Studies in KRAS mutated colorectal cancer cells show that these cells were able to survive at very low glucose conditions (Yun *et al*., 2009). The studies showed only those cells with KRAS genes vs wild type clones were able to survive for 2-4 days at 0.5mM glucose and that this growth was dependent on *GLUT1* conferring a selective growth advantage. Similar reduction of approximately 50% in proliferation rate found in the current study when BxPC-3 cells were grown in 25 vs 5.5mM glucose at 48hr have also been reported by (Karnevi *et al*., 2013; Han *et al*., 2011) who investigated the proliferation of a panel of pancreatic cell lines including BxPC-3 and MiaPaca-2 cells grown in normal or high (25mM) glucose for 72hr with proliferation assessed by 3-(4,5-Dimethylthiazol-2-yl)-2,5-diphenyltetrazolium bromidefor (MTT) assay.

HepG2 cells appeared to be the least affected when maintained under 5mM glucose as compared to the other cell lines. This may be due to the metabolic plasticity hepatic cells inherently retain (Rui, 2014). They were also cultured in media containing 4mM glutamine (a standard nutrient component of cell culture media) where glutamine could have been catalyzed by glutaminase, glutamine dehydrogenase and/or aminotransferase to produce α-ketoacids. α-ketoacids can then be further metabolised to TCA metabolites such as: pyruvate, oxaloacetate, fumarate, succinyl-CoA and α-

ketoglutarate. These metabolites may then serve as substrates for gluconeogenesis or fuel the anaplerotic pathway of the TCA cycle during DNL (Rui, 2014). MiaPaca-2, Capan-1, HeLa and BxPC-3 were shown to be more sensitive to 5.5 and 2.75mM glucose concentrations, with BxPC-3 cells being the most sensitive (Tables 3.2 and 3.3). This data suggests that pancreatic and cervical cancer cells do not have the same degree of metabolic plasticity in relation to a reliance on glucose metabolism in comparison to HepG2 cells. They are therefore more dependent on glucose supply for growth.

Although, BxPC-3 and Capan-1 cells are both positive for E-cadherin and negative for Vimentin, indicating an epithelial cell phenotype, their site of origin as cancer cells differs. Capan-1 cells were originally collected from a liver metastasis, with the patient also demonstrating regional lymph node metastases (Deer *et al*., 2010). BxPC-3 cells however, were collected from the primary tumour site, and showed no metastasis or metastatic potential when cultured in mice (Deer *et al*., 2010). This suggests that BxPC-3 cells would be more likely to demonstrate epithelial characteristics and would therefore be potentially less metabolically flexible than Capan-1 cells. MiaPaca-2 and HeLa cells which tested negative for E-cadherin and positive for Vimentin, indicating EMT produced three distinct growth curves dependent on glucose concentration, potentially being more metabolically flexible than BxPC-3 cells.

This study also seeks to investigate the lipogenic phenotype of the liver and pancreatic cancerous cell lines in relation to DNL. Data suggests that in both MiaPaca-2 and HepG2 cells, growth and DNL can be regulated by glucose concentration. This is indicated by steady growth and palmitate enrichment profiles dependent on glucose

concentration. However, Capan-1, BxPC-3 and AsPC-1 cells showed similar growth and enrichment profiles, independent of glucose concentration (Figure 3.4). Moreover, the 5-day profiling experiment with HepG2 and Capan-1 (Figure 3.5) showed Capan-1 cells presented with similar levels of palmitic acid enrichment under the 3-different glucose concentrations for the initial 48-hour incubation. However, when glucose availability becomes limited, a rapid decline in growth and palmitic acid enrichment was observed. The incorporation of glucose into palmitic acid also shows that palmitate obtained from glucose as measured at 48 hours is already under steady state conditions, plateau enrichment has been rapidly reached. This can be used to provide indirect information related to the rate of synthesis or turnover of the lipid pool. However, with Capan-1 cells, enrichment plateau was much later (96hr) and only occurred under conditions of high glucose media. This shows the glucose isotope takes longer to mix with palmitate production pathways in Capan-1 cells than it does in HepG2 cells.

Cells undergoing aerobic glycolysis, donate a significant fraction of glucose carbon towards anabolic processes such as lipid and nucleotide synthesis (Tong *et al*., 2009). The carbohydrate responsive element binding protein (ChREBP) has been shown to be a master regulator of glycolytic and lipogenic enzymes (Hatzivassiliou *et al*., 2005b). ChREBP expression and activity have been shown to be influenced by cellular levels of nutrients. In healthy individuals, ChREBP can be detected in most tissues; however, it is highly expressed in the liver, thus providing the metabolic flexibility required. Further studies suggest that ChREBP may be associated with cancer development. A link between loss of p53-induced cell cycle arrest and ChREBP expression has been

made, which is thought to promote aerobic glycolysis, one of the major hallmarks of cancer. Moreover, it has been suggested that cross-talk between ChERBP, SREBP and HIF-1 upregulate DNL and aerobic glycolysis respectively (Airley *et al*., 2014). Therefore, different metabolic phenotypes may be a result of the default expression level of ChREBP. Further work will be required in order to examine the expression levels of ChREBP within liver and pancreatic cancerous cell lines, as well as how the expression of ChREBP may be altered, when cells are incubated with different levels of nutrients.

The purpose of this chapter has been to provide an initial profile of a panel of pancreatic cancer cell lines in relation to glucose dependent growth, DNL and EMT. In addition, HepG2, HeLa and SH-SY5Y cells lines derived from different tissues were used to provide comparative data. As summarized in Table 3.4, BxPC-3 cells appear to be the most epithelial like pancreatic cancer cell line in the panel selected, whilst MiaPaca-2 appeared to be the most mesenchymal. Moreover, MiaPaca-2 cells demonstrate glucose concentration dependent DNL whilst also being KRAS positive, whereas BxPC-3 cells undergo glucose concentration independent DNL and are KRAS negative. Therefore, in the following chapters, BxPC-3 and MiaPaca-2 cells will be selected to study the effects of the addition of a lipid nutrient (oleic acid). In addition, due to their metabolically flexible phenotype, HepG2 cells will be used as a comparative cell line.

Chapter 4 – The effects of oleic acid supplementation on pancreatic cancer cell growth

4.1 Introduction

Lipids are a diverse group of hydrophobic biomolecules which include sterols, isoprenoids, acylglycerols and phospholipids. They are the main components of biological membranes and can also be used for energy production, storage and as signaling molecules. Most lipids are synthesized from fatty acids (FAs), a broad class of molecules consisting of hydrocarbon chains of varying lengths and degrees of desaturation. The long hydrocarbon chains of FAs form the hydrophobic tails of phospholipids and glycolipids, which along with cholesterol, represent the main components of cell membranes. Moreover, membrane lipids give rise to secondary messengers which form in response to extracellular stimuli such as diacylglycerol (DAG) and phosphatidylinositol-3,4,5-triphosphate (PIP3). In addition, FAs can be esterified to triacylglycerides (TGs) which are nonpolar lipids, that are produced and stored during periods of high nutrient availability and when broken down, produce large amounts of energy (Rohrig and Schulze, 2016).

In healthy adults, rates of *de novo* lipogenesis (DNL) are low and occur mainly in the liver, adipose and lactating breast tissue. Cells tend to obtain lipids through receptor/transporter proteins associated with the plasma membrane. Under physiological conditions, cellular lipid homeostasis is maintained by regulating lipid uptake, DNL and utilization to provide energy and storage. Excess lipids in the form of

TAGs are stored in organelles termed lipid droplets (LDs) (Baenke *et al*., 2013). In contrast to normal cells, cancer cells demonstrate high rates of DNL which may be in response to the high biosynthetic demands and/or due to the reduced availability of lipids in the tumour microenvironment (Menendez and Lupu, 2007). In addition to increased DNL, recent studies indicate that some cancer cells may also have a high lipid content, and that the catabolism of LDs maintains their high proliferation rate (Nieman *et al*., 2011; Schlaepfer *et al*., 2014).

The tumour microenvironment in pancreatic cancer is often hypoxic, due to poor vascularization. Therefore, entry of glucose derived pyruvate into the TCA cycle is inhibited under hypoxic conditions and consequently, cancer cells undergo DNL through reductive glutamine metabolism (Wise *et al*., 2011; Metallo, 2012). Accumulating evidence suggests that cancer cells can increase exogenous lipid uptake, to compensate for reduced rates of DNL under hypoxic conditions (Kamphorst *et al*., 2013). Furthermore, several studies indicate DNL and exogenous lipid uptake result in cancer cells being rich in LDs, the presence of which is also viewed as a hallmark of aggressive cancers (Koizume and Miyagi, 2016). However, when cells become re-oxygenated, catabolism of LDs occurs for both energy production and antioxidant defense (Bensaad *et al*., 2014).

Transformed KRAS positive cells (kidney iBMK and pancreatic HPNE cells), have been shown to increase exogenous lipid uptake, whereas cells transformed by constitutively active Akt (protein kinase B) demonstrate increased rates of DNL. The PI3K-Akt and Ras pathways are two of the most commonly activated pathways in cancer (Kamphorst *et al*., 2013). Poor perfusion will lead to reduced availability of serum derived lipids,

exposing cells to similar lipid gradients as glucose and oxygen. Therefore, the cells genetic milieu along with the tumour microenvironment require the cells to maintain metabolic plasticity in order to overcome challenges such as oxygen and nutrient (lipid) scarcity. In addition, exogenous lipid uptake is still necessary for essential FAs such α-linoneic acid and linoleic acid which carry double bonds beyond position 9, that cannot be synthesised by human cells and must be provided through the consumption of dietary fat (Rohrig and Schulze, 2016).

The two most common fatty acids found in plasma are oleic acid (OA), an 18-carbon, neutral, unsaturated FA with a double bond at position 9 (C:18:1). It is one of the most widely abundant FAs in nature and ranges between 0.03 to 3.2mM concentration in blood. Palmitic acid (PA) is a common 16-carbon (C:16), saturated FA ranging between 0.3 to 4.1mM in blood plasma (Abdelmagid *et al*., 2015).

Hardy and colleagues (2000) investigated the effects of supplementing exogenous OA and PA, to a panel of breast cancer cell lines over a period of 24 hours. The cells were cultured up to concentrations of 0.5mM OA and 0.4mM PA. Results showed increased proliferation of most cells when cultured with OA. However, PA decreased proliferation. Furthermore, PA treated cells demonstrated morphological changes consistent with apoptosis, such as cell blebbing, rounding and detachment. This proapoptotic effect of PA was also shown to be inhibited by OA (Hardy *et al*., 2000). The study clearly demonstrates that the two major circulating FAs have opposite effects in breast cancer. These acute effects with OA and PA have also been demonstrated in other cancer and normal healthy cells (Hardy *et al*., 2000).

A large number of studies have clearly demonstrated the importance of cancer cells maintaining lipid homeostasis to fuel their proliferative requirements (Santos and Schulze, 2012; Baenke et al., 2013; Agmon and Stockwell, 2017). Therefore, it is crucial for cancer cells to regulate exogenous lipid uptake, DNL and LD formation. The choice of fatty acid used for studies also being of vital importance.

This chapter will examine the effects of an exogenous supply of OA on pancreatic cancer cells. Following cell line characterization (Chapter 3), the focus of Chapter 4 will investigate differences between BxPC-3 (epithelial phenotype, KRAS negative) and MiaPaca-2 cells (mesenchymal phenotype, KRAS positive). However, additional cell lines will be included when necessary to differentiate cell line specific trends or widescale biological phenomena. Previous studies suggest that OA does not cause cytotoxic effects in pancreatic cancer cell lines (AR42J and 1.1B4) such as those seen with PA (Ahn et al., 2013; Nemecz et al., 2018). Furthermore, OA demonstrates protective effects against palmitic acid induced apoptosis. However, OA has been shown to induce apoptosis in SH-SY5Y cells (Zhu et al., 2005). Therefore, a range of physiological measures will be used to assess differences between cell lines when exposed to OA, these include measures of proliferation, regulation of the cell cycle, determination of the presence of lipophagy and the capacity of the cells to store lipid as triglycerides.

4.2 Materials and Methods

4.2.1 The effect of oleic acid on cell growth

An initial dose response experiment was performed using BxPC-3, MiaPaca-2 and HepG2 cells (in 6-well plates) when cultured with 0, 37.5, 75, 150, 300 and 600μM OA over a 5-day period. Following, BxPC-3, AsPC-1, Capan-1, MiaPaca-2 and HepG2 cells were cultured with 300μM OA over a 5-day period. Cell growth in terms of confluency was determined using the IncuCyte ZOOM imaging system (Essenbioscience, UK). The AUC along with a two-way ANOVA were used to assess the statistical significance when comparing 0, 37.5, 75, 150, 300 and 600μM OA concentration at individual timepoints. It is noteworthy that the initial percentage of confluency must be identical between replicates, in order to produce reproducible data. Furthermore, the initial percentage of confluency was cell line dependent in order to achieve >90% confluency over the 5-day period but preventing the cells from becoming overconfluent and inducing cell death. This was particularly important for MiaPaca-2 cells which had the highest doubling rate compared to BxPC-3 and HepG2 cells. Therefore, an initial confluency of 15-20% before treatment for MiaPaca-2 cells was applied, whereas BxPC-3 and HepG2 cells were treated at 20-30 and 30-40% confluency respectively.

4.2.2 Oleic acid mediated effects on cell proliferation

BxPC-3, MiaPaca-2 and HepG2 cells at $1x10^6$/mL concentration were resuspended in PBS and stained with 1μM carboxyfluorescein succinimidyl ester (CFSE)

(ThermoFisher, UK) stain for 10 minutes at room temperature in the dark. Cells were centrifuged at 1200rpm for 4 minutes. The supernatant was discarded, and cells were resuspended in media and seeded onto 6-well plates. Following a 24 hour incubation period, the media was replaced, and cells were treated with and without 300μM OA over a 48 hour period. Cells were then trypsinised, centrifuged and resuspended in fresh media. Cell proliferation was then determined using the Canto II flow cytometer (BD Bioscience, UK) at 494/521nm. Statistical analysis was performed using a Two-way ANOVA. It is noteworthy that the experiment was initially trialed over a 96 hour period; however, due to multiple cell divisions, the CFSE stain was not detectable. Therefore, the experiment was repeated over a 48 hour period. The .fcs files were then analyzed using the FlowJo software to determine cell proliferation.

4.2.3 Triglyceride quantification assay

BxPC-3, MiaPaca-2 and HepG2 cells were cultured in 6-well plates until achieving ~30% confluency. Cells were treated with fresh media containing 300μM OA. Samples were analysed at 48 and 96 hours. Due to the 48 and 96 hour timepoints, cells were initially treated at 30% confluency to ensure adequate cell numbers for running the assay as well as reducing the risk of cells becoming overconfluent. Triglyceride concentrations in cells per mg of protein were quantified using the TG quantification kit (AbCam, UK), following the manufacturers protocol. Triglycerides were converted to FFAs and glycerol. Glycerol was then oxidized to generate a product which reacts with a probe to generate colour (λ=570nm). Statistical analysis was performed using a Two-way ANOVA.

4.2.4 Oleic acid mediated effects on cell cycle

BxPC-3, MiaPaca-2 and HepG2 cells were cultured in 6-well plates, with and without 300μM OA over a 96 hour period with samples taken every 24 hours. Cells were trypsinised and centrifuged at 1200rpm for 4 minutes. Cells were re-suspended in 200μL of cold PBS and fixed by adding 1mL of ice cold 70% ethanol (in PBS) and kept at -20^{o}C overnight. Cells were then stained with Propidium Iodide and RNase (PI/RNase) staining buffer for 15 minutes at room temperature. Propidium iodide intercalates with both DNA and RNA, therefore RNase is added to destroy RNA and allow detection of DNA only. Cell cycle status was then determined using a FL3/PI detector, 620nm (FACS Calibur, BD Biosciences, UK) with at least 10,000 events counted. The .fcs files were the analyzed using the FlowJo software to determine cell cycle status.

4.2.5 Oleic acid induced apoptosis detection via Annexin V

The IncuCyte Annexin V reagent was used to assess OA mediated apoptosis. Annexin V is commonly used to detect apoptotic cells by its ability to bind to phosphatidylserine. Phosphatidylserine is a phospholipid which is externalized during apoptosis and provide's a signal to phagocytes for clearing. BxPC-3, MiaPaca-2 and HepG2 cells were seeded in 6-well plates until achieving ~20% confluency. The IncuCyte Annexin V reagent was solubilized in 100μL of PBS and then diluted in full media containing 1mM $CaCl_2$ at a concentration of 1:200. Cells were then treated with and without 300μM of OA and images were collected every 2 hours over a 5-day period. One hundred

micromolar of H_2O_2 was added to the cells as a positive control for detecting apoptosis. The IncuCyte live-cell analysis system was used for the collection and analysis of the data according to the manufacturer's instructions (EssenBioscience, UK). Statistical analysis was performed using a Two-way ANOVA.

4.2.6 Oleic acid mediated effects on autophagy

BxPC-3, MiaPaca-2 and HepG2 cells were cultured in 6-well plates until achieving ~40% confluency. Cells were then treated with 300μM OA, 150μM Torin 1 (Tocris Bioscience, UK), 300μM OA + 150μM Torin 1, 2mM 3-methyladenine (3-MA) (Tocris Bioscience, UK) and 300μM OA + 2mM 3-MA over a 24 hour period. Cells were then collected and changes in microtubule-associated protein 1A/1B-light chain 3 (LC3) LC3-I and LC3-II expression were examined by Western blotting as described in section 2.2. Torin-1 and 3-MA were shown to exert toxic effects to the cells. Therefore, cells were cultured for a 24 hour period and were treated at 40% confluency to ensure sufficient lysate for use in Western blotting. Table 4.1 provides further details regarding the antibodies used for this experiment.

Table 4.1 – Autophagy related antibodies
Antibodies used for autophagy western blotting

Antibodies used for examining autophagy					
Antibody	**Species**	**Concentration**	**Product code**	**Vendor**	**Application**
LC3-II	Mouse	1:1000	83506	Cell Signaling	Primary
β-actin	Mouse	1:1000	sc-517582	Santacruz	Primary
IRDye 680	Goat	1:10000	925-68070	Li-Cor	Secondary

4.3 Results

4.3.1 Oleic acid mediated effects on cell proliferation

In order to determine whether OA influences cell growth, BxPC-3, MiaPaca-2 and HepG2 cells were first cultured with 0, 37.5, 75, 150, 300 and 600μM OA over a 5-day period and monitored by the IncuCyte Zoom system. Unexpectedly, BxPC-3 cells demonstrated a reduction in growth which was OA concentration dependent. MiaPaca-2 cells showed a non-significant minor decline in growth only at 600μM OA, whereas HepG2 cells showed OA concentration dependent increases in proliferation (Figure 4.1).

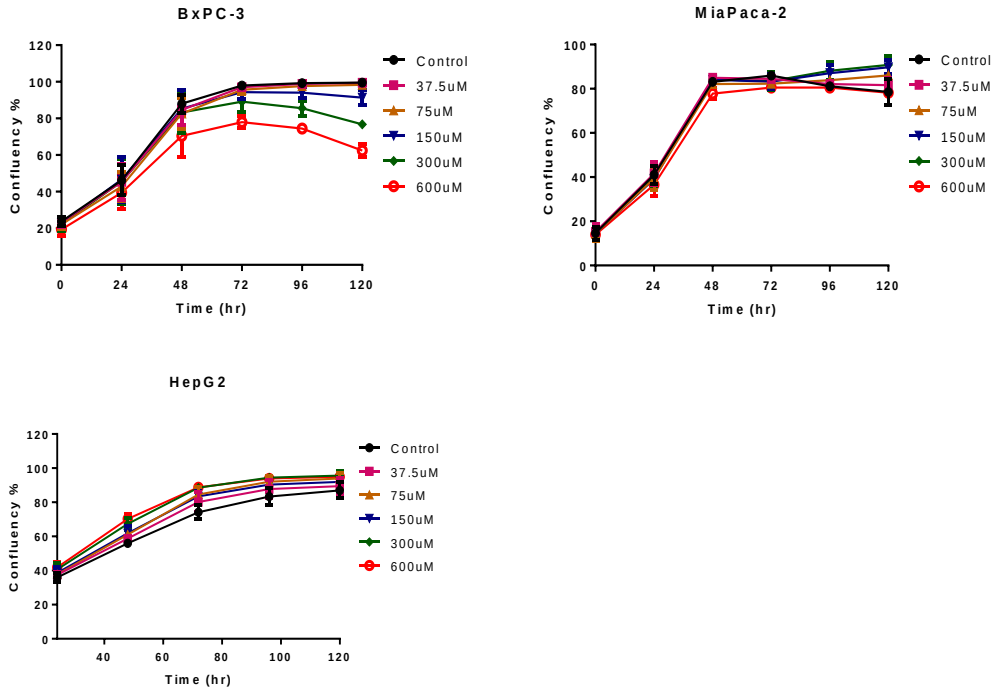

Figure 4.1 – The effect of OA on cell growth.
Cell lines were cultured under 0, 37.5, 75, 150, 300 and 600μM, with the data showing growth inhibition in BxPC-3 cells at 48 hours at concentrations >300μM. MiaPaca-2 show a reduction in growth when supplemented with 600μM OA, whereas HepG2 cells show OA concentration dependent increases in proliferation (mean +/- SD, n=3).

The percentage difference in AUC (0-120 hours) was calculated in order to demonstrate changes in growth, when cells were cultured with 0, 37.5, 75, 150, 300 and 600μM OA concentrations (Table 4.2). By establishing the AUC in control samples for each of the cell lines as 100% growth, the percentage change in area dependent to each OA concentration was determined.

Table 4.2 – Percentage change in AUC when cultured under multiple concentrations of OA

Percentage change in AUC when cells were cultured with 0, 37.5, 75, 150, 300 and 600μM OA

Percentage change in AUC			
	BxPC-3	**MiaPaca-2**	**HepG2**
Control	100	100	100
37.5μM	99	101	105
75μM	96	100	110
150μM	96	102	109
300μM	86	103	115
600μM	77	95	116

In addition to AUC, a two-way ANOVA was used to assess the statistical significance when comparing 0, 37.5, 75, 150, 300 and 600μM OA concentration at individual time points (see Appendix 1, Tables 1.1, 1.2 and 1.3). BxPC-3 cells showed a statistically significant deviation within a 24 hour period when cultured with 600μM OA ($p<0.0001$). Overall, the data demonstrates a significant dose response inhibition of BxPC-3 cell growth over time (48, 72, 96 and 120 hours), when cultured with increasing concentrations of OA ($p<0.0001$). MiaPaca-2 cells begin to show differences only at 96 hours ($p<0.0001$). Fewer differences in growth were noted for HepG2 cells, However, an initial increase in proliferation with cells cultured with 300 and 600μM OA was noted ($p<0.05$).

Although a larger decrease in proliferation was noted in BxPC-3 cells with 600μM OA (Figure 4.2, Table 4.3), all future experiments were conducted using 300μM OA, in order to provide more physiologically relevant, lower nutrient conditions and to avoid overloading with lipid. To confirm these initial findings, the above experiment was repeated and revalidated using BxPC-3, MiaPaca-2 and HepG2 cells, along with additional pancreatic cancer cell lines AsPC-1 and Capan-1 in 300μM OA. In addition, changes in cell morphology between OA treated and control cells were also noted (Figure 4.2). BxPC-3 and Capan-1 cells showed evidence of cell shrinkage, loss of epithelial monolayer morphology and loss of adhesion, whereas the morphology of AsPC-1, MiaPaca-2 and HepG2 cells remained unchanged.

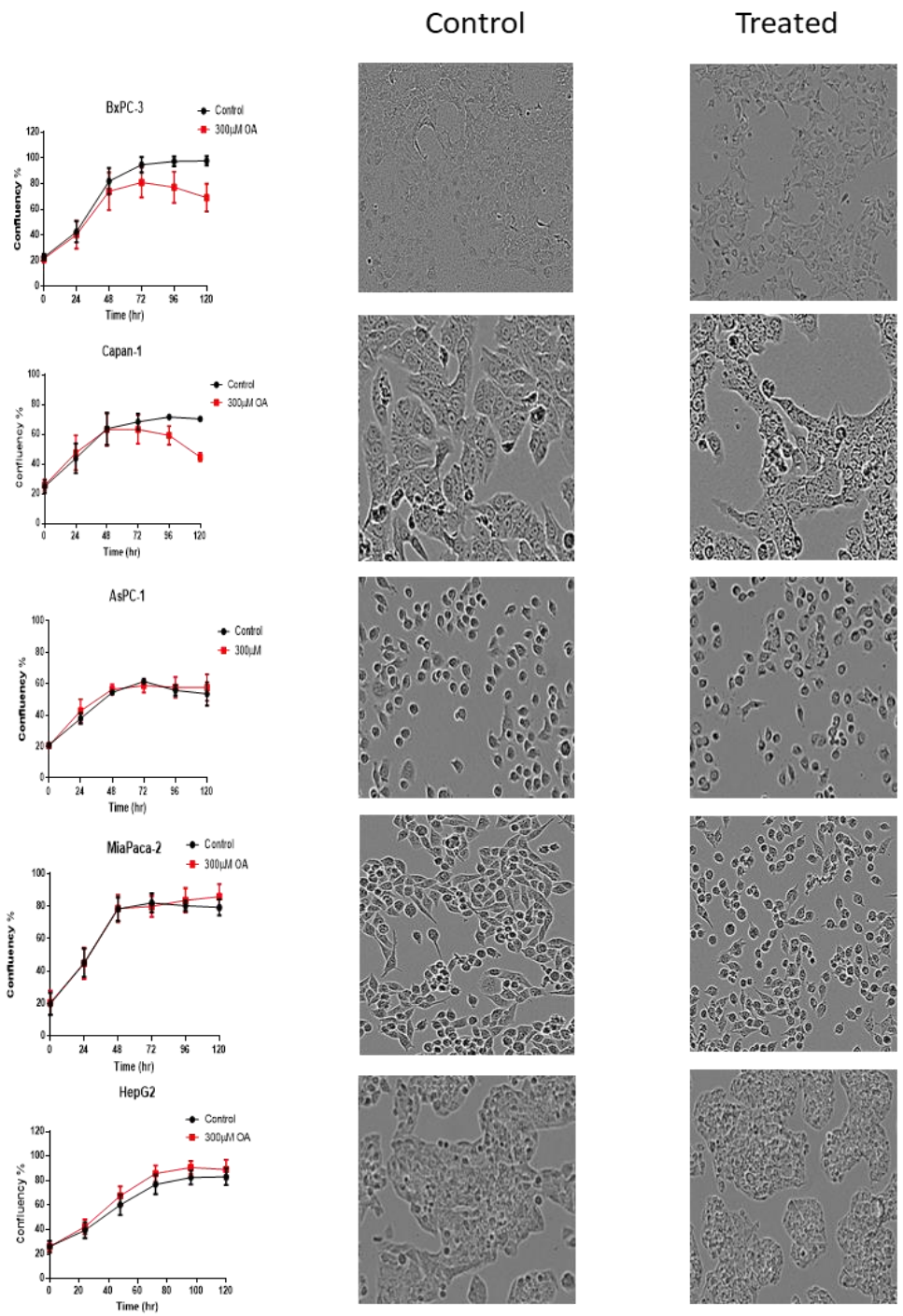

Figure 4.2 – The effect of 300μM OA on pancreatic cancer cell growth.
The above panel of cancer cell lines were cultured with and without 300μM OA. BxPC-3 and Capan-1 cells show a decrease in cell proliferation following 48 hours of incubation. AsPC-1 and MiaPaca-2 appear to be unaffected and HePG2 cells demonstrate an increase when supplemented with 300μM OA (mean +/- SD, n=7, magnification 10x).

The percentage difference in area under the curve (AUC) was calculated in order to demonstrate changes in growth (Table 4.3) and showed consistent changes with those observed in the dose response experiment (Table 4.2).

Table 4.3 – Percentage change in AUC under 300μM OA
Percentage change in AUC when cells were cultured with 300μM OA.

Percentage AUC		
Cell line	**Untreated**	**300μM OA**
BxPC-3	100	84
AsPC-1	100	103
Capan-1	100	91
MiaPaca-2	100	101
HepG2	100	110

A two-way ANOVA was used to analyse the data in Figure 4.2. BxPC-3 cells demonstrate significant changes at 72, 96 and 120hr ($p<0.05$, $p<0.001$ and $p<0.0001$ respectively). Capan-1 cells demonstrate significant differences at 96 and 120 hours ($p<0.01$ and $p<0.0001$ respectively). AsPC-1, MiaPaca-2 and HepG2 cells demonstrate no significant changes upon addition of OA over the 5 day period.

4.3.2 Oleic acid mediated effects on cell proliferation as analysed by flow cytometry

As an alternative methodology, the Cell Trace CFSE cell proliferation stain, was also used to provide a measure of cell proliferation in BxPC-3, MiaPaca-2 and HepG2 cells. Cell proliferation was determined following a 48-hour incubation with and without the addition of OA (Figure 4.3). Results demonstrated a 14% ($p<0.01$) decrease in

proliferation in BxPC-3 cells, whereas MiaPaca-2 and HepG2 cells showed a non-significant 2 and 5% decrease respectively.

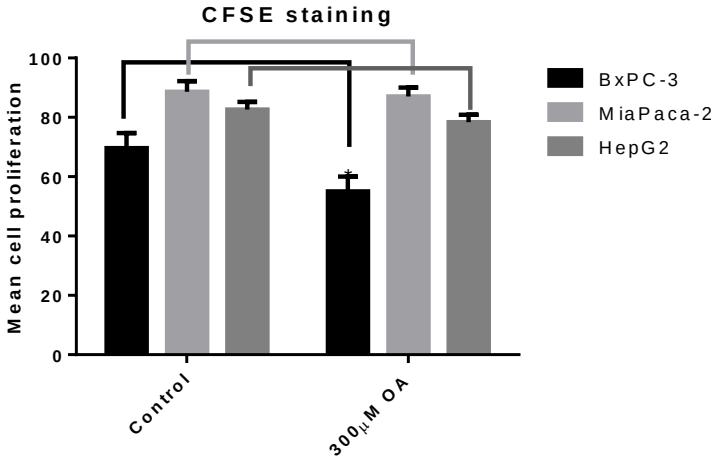

Figure 4.3 – Cell proliferation assay
BxPC-3 cells show a 14% decrease in proliferation when treated with OA over a 48hr period, (*) statistically significant ($p<0.01$), whereas MiaPaca-2 and HepG2 cells show minor differences (mean +/- SD, n=3).

Both proliferation protocols independently showed a decrease in the abundance of BxPC-3 cells when incubated with OA. Before examining OA mediated effects further, OA uptake was investigated between all the cell lines.

4.3.3 Accumulation of supplemented Oleic acid as stored triglyceride

BxPC-3, MiaPaca-2 and HepG2 cells were cultured with and without 300μM OA over a 96 hour incubation period, with samples taken at 48 and 96 hours to measure the uptake of OA through its conversion to triglyceride and storage. At 48 hours, control BxPC-3 cells showed no detectable levels of TG, MiaPaca-2 cells showed low levels of TG, 7nmol/mg protein and HepG2 cells contained the highest concentration,

86nmol/TG/mg of protein. Upon treatment with OA, BxPC-3, MiaPaca-2 and HepG2 cells showed similar additive increases in triglyceride concentration, of 78, 66 and 84nmol of TG/mg protein respectively (Figure 4.4A).

As expected, at 96 hours, control BxPC-3, MiaPaca-2 and HepG2 cells showed lower levels of TG than those present at 48 hours. TG values for BxPC-3 cells were still non-detectable. Control HepG2 cells showed a drop of TG of 70nmol/mg protein from 48 to 96 hours. At 96 hours post treatment with OA BxPC-3, MiaPaca-2 and HepG2 cells showed decreases in TG concentration (Figure 4.4B). Interestingly, at 48 hours both treated BxPC-3 and MiaPaca-2 cells demonstrate similar concentrations of TG, which were not statistically different. However, at 96 hours, treated MiaPaca-2 cells had similar TG levels to control MiaPaca-2 cells, whereas treated BxPC-3 cells were able to retain a statistically significant amount of TG (14.4ng/mg protein) compared to the control ($p<0.0001$).

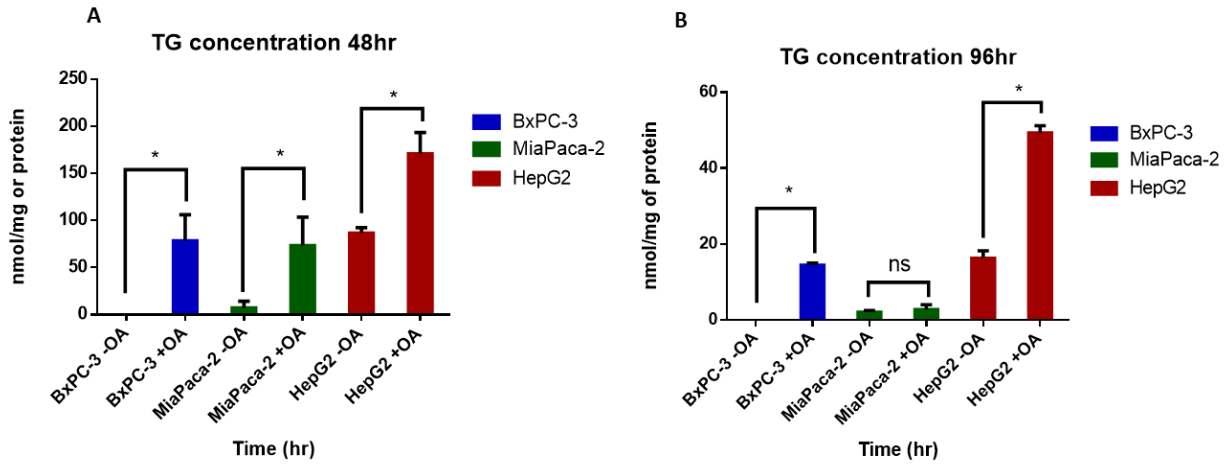

Figure 4.4 – Quantifying total TG concentration.
BxPC-3, MiaPaca-2 and HepG2 cells were cultured with and without OA and total TG concentration was measured. **(A)** Cells treated with OA showed similar and significant increases in total TG concentration at 48 hours ($p<0.0001$), however, **(B)** at 96 hours TG concentration declined at different rates amongst the three cell lines $p<0.0001$ treatment vs control BxPC-3 cells; whereas, MiaPaca-2 showed no significance (mean +/- SD, n=3), (*) indicates statistical significance, (ns) no significance.

These results indicate that the administered 300µM OA increases cellular TG levels in BxPC-3, MiaPaca-2 and HepG2 cells in a comparable manner. The results also demonstrate that exogenous OA is capable of being removed from the media by the cells and converted into TG at similar rates and then utilised by the cells. However, the degree of utilisation appears to differ between cell lines.

4.3.4 Oleic acid mediated effects on the cell cycle

Changes in phases of the cell cycle, were determined every 24 hours, in BxPC-3, MiaPaca-2 and HepG2 cells when cultured with and without 300µM OA following a total incubation period of 96 hours (Figure 4.5).

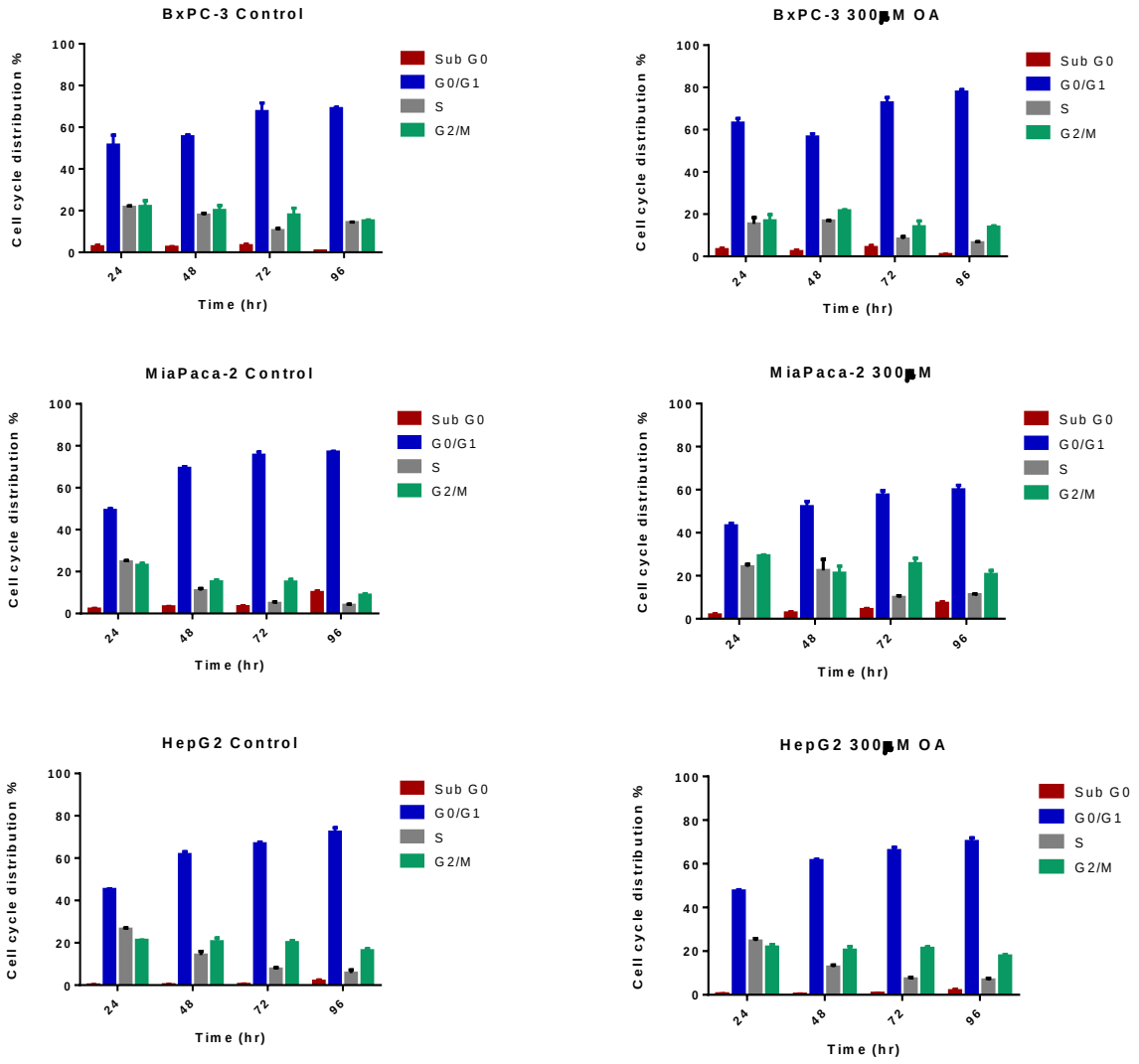

Figure 4.5 – Cell cycle distribution analysis.
BxPC-3, MiaPaca-2 and HepG2 cells were cultured with and without 300µM OA over a 96 hour incubation period. Differences were noted in BxPC-3 and MiaPaca-2 cells, whereas HepG2 cells appear to be unaffected (mean +/- SD, n=3).

BxPC-3 cells showed ~25% increase in G0/G1 phase ($p<0.001$) and a ~25% decrease in S and G2/M phase ($p<0.001$) when treated with OA at 24 hours. This effect disappeared at 48 and 72 hours, with treated cells demonstrating similar cell cycle percentage distributions to control samples. However, at 96 hours a ~5% increase in G0/G1 phase ($p<0.001$) and a 50% decrease in S phase ($p<0.001$) was shown in cells treated with OA, whilst G2/M phase remained similar to the control samples (Table 4.4)

MiaPaca-2 cells treated with OA showed a consistent decline in G0/G1 phase reaching ~25% decrease at 96 hours ($p<0.0001$). In addition, both S and G2/M phase increased over the 96 hour incubation period with almost 3 times as many cells being in S-phase and double the number of cells being in G2/M phase when treated with OA over the entire incubation period ($p<0.0001$).

Finally, HepG2 cells showed almost identical cell cycle distribution patterns in both OA treated and untreated samples (Figures 4.5 and 4.6, Table 4.4) with no statistically significant changes. The data was analysed using a Two-way ANOVA.

Table 4.4 – Mean percentage cell cycle distribution analysis.
Mean cell cycle percentage distribution in BxPC-3, MiaPaca-2 and HepG2 cells when cultured with and without OA. Data was collected every 24 hours over a 96-hour incubation period. (n=3)

	Mean cell cycle distribution %										
	Control						300µM OA				
	Time (hr)	Sub G0	G0/G1	S	G2/M		Time (hr)	Sub G0	G0/G1	S	G2/M
BxPC-3	24	2.74	51.43	21.63	22.03		24	3.20	63.13	15.40	16.87
	48	2.44	55.43	17.90	20.13		48	2.25	56.50	16.77	21.60
	72	3.19	67.53	10.46	17.93		72	4.17	72.67	8.20	14.07
	96	0.71	68.97	14.27	15.10		96	0.89	77.80	6.44	13.90
MiaPaca-2	24	2.12	49.17	24.63	23.00		24	1.75	43.23	24.13	29.33
	48	3.17	69.30	10.88	15.10		48	2.68	52.10	22.43	21.20
	72	3.26	75.50	4.89	15.03		72	4.31	57.50	9.93	25.63
	96	10.02	77.00	3.95	8.78		96	7.20	59.97	11.20	20.63
HepG2	24	0.16	45.17	26.47	21.20		24	0.42	47.53	24.60	21.90
	48	0.24	61.73	14.17	20.50		48	0.27	61.43	12.67	20.43
	72	0.39	66.80	7.59	20.13		72	0.70	66.00	7.27	21.27
	96	1.91	72.33	5.74	16.33		96	1.91	70.17	6.82	17.80

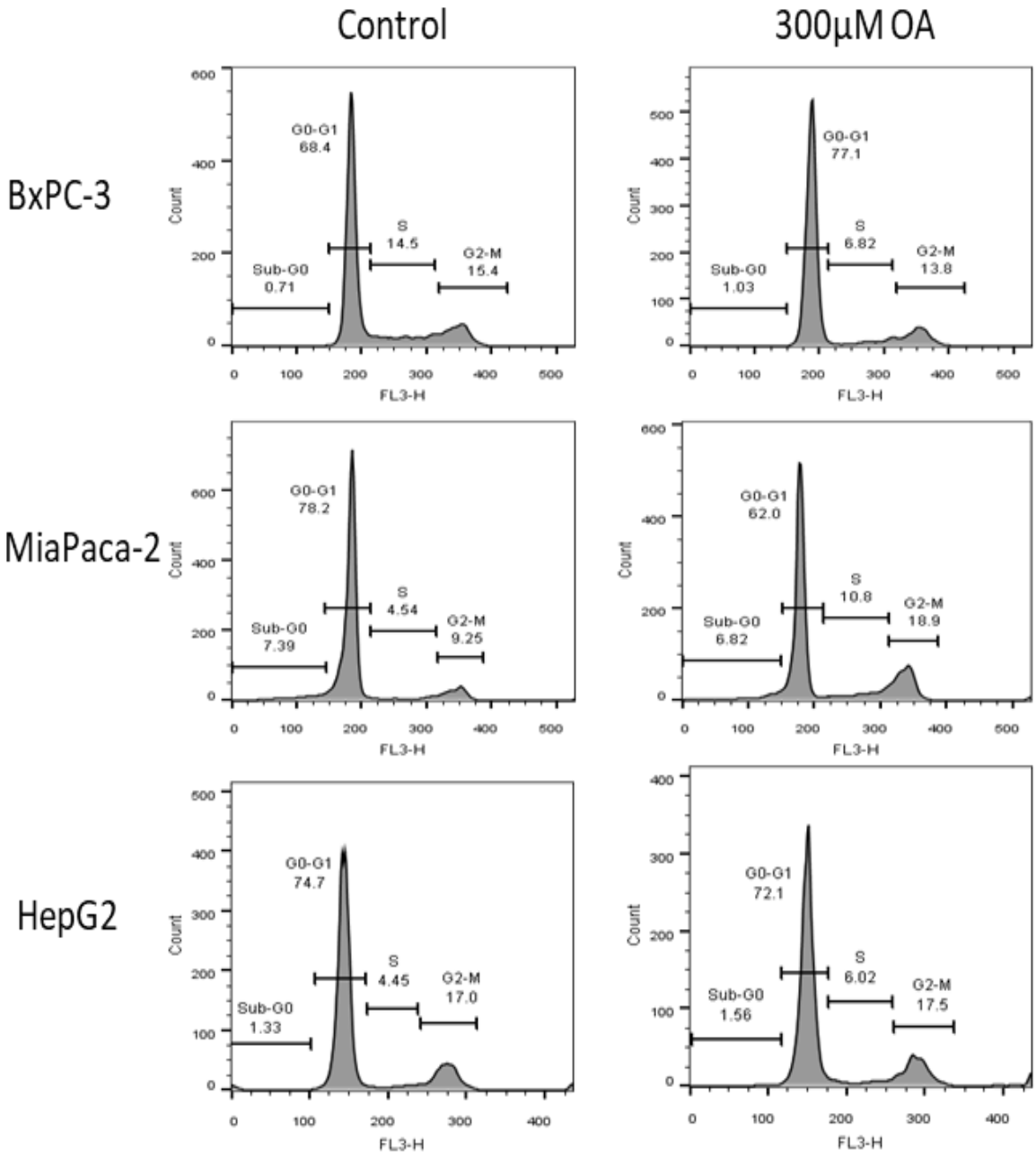

Figure 4.6 – Cell cycle analysis.
The above figure demonstrates the changes at 96 hours in BxPC-3, MiaPaca-2 and HepG2 cells when cultured with and without 300µM OA. BxPC-3 cells show a decrease in S-phase compared to untreated cells, MiaPaca-2 show an increase in S and G2/M phase, whereas HepG2 cells are unaffected. This image is a representative from 1 of 3 independent experiments and was generated using the FlowJo software.

4.3.5 Oleic acid induced apoptosis

Annexin V staining was also used to determine whether cells were becoming apoptotic. BxPC-3, MiaPaca-2 and HepG2 cells were cultured over a 5-day period with and without OA. Hydrogen peroxide was used as a positive control to induce apoptosis and apoptosis was determined in real time using the IncuCyte Zoom imaging system (see section 2.1 and 2.3). As shown in Figure 4.7, cells treated with control H_2O_2, were positive for Annexin V. MiaPaca-2 and HepG2 cells were negative for Annexin V demonstrating no statistical significance between control and OA treated cells. BxPC-3 cells however demonstrated cell shrinkage, and a significant increase in Annexin V ($p<0.0001$) indicating apoptotic cell death.

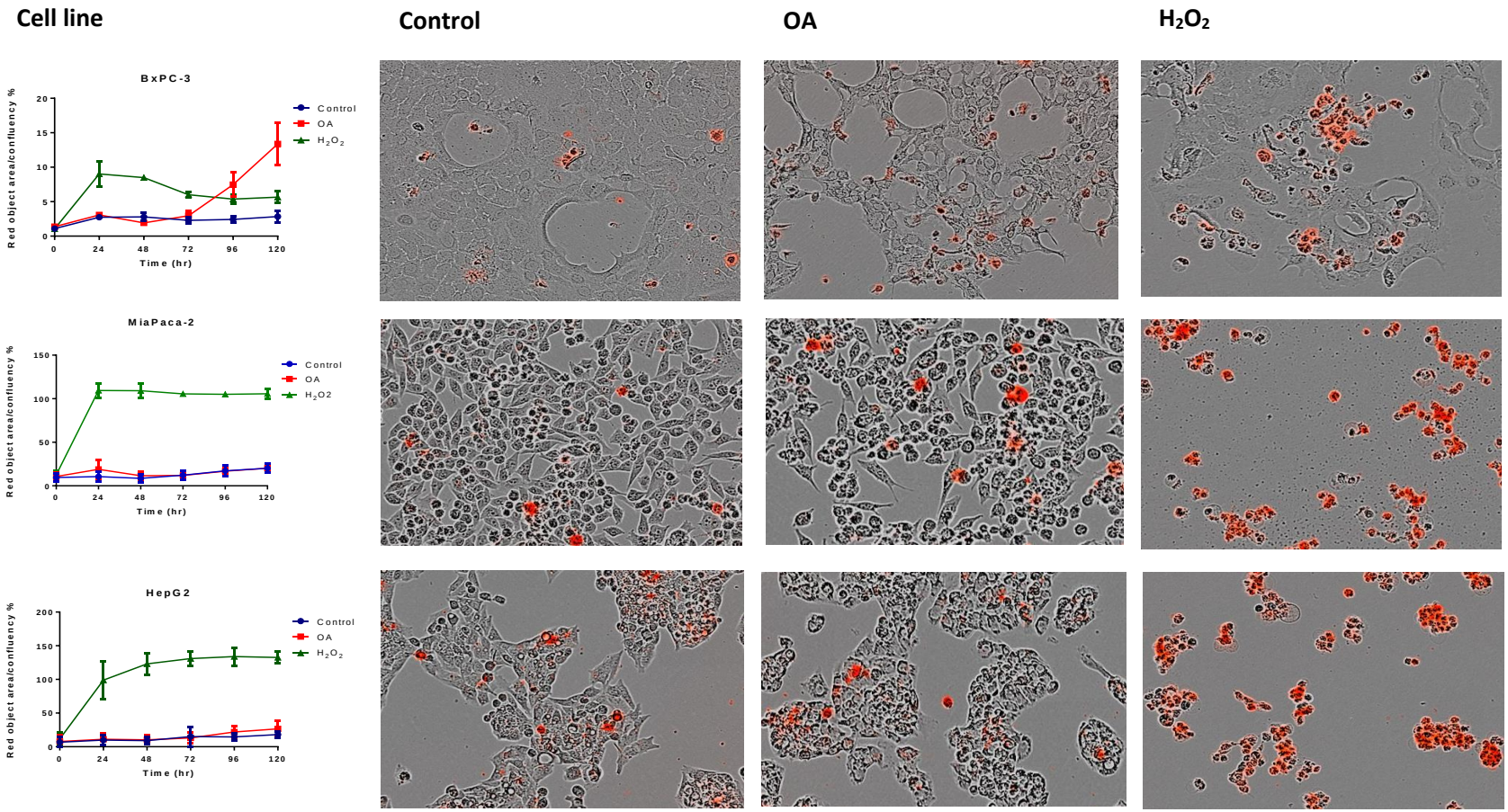

Figure 4.7 – Investigating cell death using Annexin V.
BxPC-3, MiaPaca-2 and HepG2 cells were cultured with and without OA over a 5-day period and were stained with Annexin V. MiaPaca-2 and HepG2 cells were negative for Annexin V, however BxPC-3 cells demonstrated a significant increase in Annexin V ($p<0.0001$) upon addition of OA (magnification 10x).

4.3.6 Oleic acid may mediate effects on autophagy – a pilot study

In addition to examining cell death via apoptosis, other mechanisms causing reduced proliferation and potentially cell death were explored. A preliminary characterisation of autophagic flux was determined by examining LC3-II accumulation. In addition, Torin 1 and 3-methyladenine (3-MA), a known stimulator and inhibitor respectively of autophagy were used to assist with data characterisation. BxPC-3 control cells suggests that autophagy is active whereas in both MiaPaca-2 and HepG2 cells autophagy appears to be inactive. Furthermore, addition of OA does not change autophagy status at 24 hours for the three cell lines (Figure 4.8).

Torin 1, successfully stimulates autophagic flux in BxPC-3 and MiaPaca-2 cells, but not in HepG2 cells (higher concentration may have been required). Addition of Torin 1 with OA appears to further stimulate autophagic flux in BxPC-3 and HepG2 cells, whilst downregulating autophagy in MiaPaca-2 cells. Moreover, additon of 3-MA downregulates autophagy in all three cell lines, whilst addition of 3-MA and OA appears to further downregulate autophagy in BxPC-3 cells. Finally, addition of OA with 3-MA has no effect on MiaPaca-2, whilst the combination may be upregulating autophagy in HepG2 cells when comparing HepG2 cells cultured with 3-MA only (Figure 4.8).

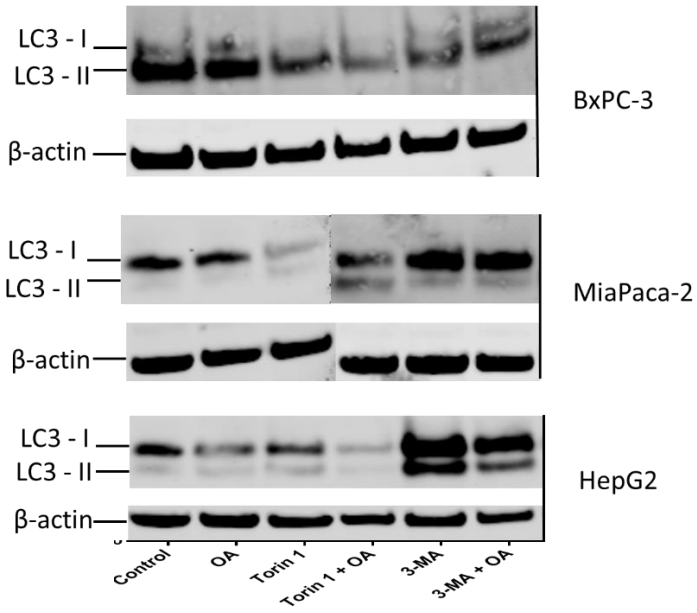

Figure 4.8 – Investigating autophagic flux using LC3-II.
BxPC-3, MiaPaca-2 and HepG2 cells were cultured with and without OA over a 24-hour period along with Torin 1 and 3-MA (n=1).

4.4 Discussion

The focus of this chapter was to identify the effects on growth of an exogenous source of lipid (OA). Initially, a dose response inhibition in growth was shown in BxPC-3 cells, whereas only minor effects on growth were shown in MiaPaca-2 and HepG2 cells (Figure 4.1). This characterization led to the selection of 300μM OA to be used in all supplementation experiments as statistically significant effects in proliferation were shown at this concentration. The same experimental system was then used to measure proliferation in a larger panel of pancreatic cell lines including Capan-1 and AsPC-1 cells (Figure 4.2). BxPC-3 and Capan-1 cells showed detrimental changes in growth as well as in morphology, when cultured with OA, whereas AsPC-1, MiaPaca-2 and HepG2 did not show any reductions in growth and remained morphologically unaffected.

An alternative proliferation assay was selected to confirm this observation. CFSE staining, a flow cytometric assay which enables the measurement of proliferation through the visualization of generations of cells demonstrated that treated BxPC-3 cells underwent a 14% reduction in proliferation compared to untreated cells. The assay could not be used beyond 48 hours because the signal became overwhelmed by cellular auto fluorescence (in MiaPaca-2 cells) but indicated BxPC-3 cells did indeed have significantly reduced proliferation when supplemented with OA. It is also interesting to note that changes were observed at 48 hours when using the CFSE proliferation assay, which was not apparent when monitoring proliferation using the IncuCyte system at such an early time point.

A TG quantification assay was used to confirm that OA was taken up by the cells. Following a 48 hour incubation period all three cell lines demonstrated a similar increase in TG concentration, indicating OA uptake and its conversion to TG. For the control samples, both pancreatic cell lines BxPC-3 and MiaPaca-2 contained low levels (undetectable and 7nmol respectively) TG/mg protein, which differed significantly to HepG2 cells which contained 86nmol of TG/mg protein. This suggests that the underlying TG storage capacity of liver cells is much higher compared to pancreatic cells. Interestingly, at 96 hours OA treated MiaPaca-2 cells demonstrated similar amounts of TG as untreated cells, suggesting that the newly formed TG presumably has been utilised, however BxPC-3 cells retained a statistically significant amount of TG 14.4nmol TG/mg protein ($p<0.0001$). This could indicate that within a 96-hour incubation period, MiaPaca-2 cells are capable of re-utilising OA derived TG either for biosynthetic or bioenergetic purposes more effectively than BxPC-3 cells which also showed reduced rates of proliferation.

Cell cycle analysis indicated significant changes in BxPC-3 cells treated with OA, indicating an inability to re-enter S-phase by having 55% less cells undergoing DNA synthesis at 96 hours (6.4 OA vs 14.3% control). Interestingly, an enhanced proliferative phenotype was shown in treated MiaPaca-2 cells, demonstrating a 2.8 and 2.3-fold increase in S and G2/M phase respectively at 96 hours compared to untreated cells. Finally, no changes in percentage cell cycle distribution were noted in HepG2 cells (Figures 4.5 and 4.6). These results correlate with the reduced rate of proliferation seen with the BxPC-3 cell line when treated with OA.

Since OA causes an inhibition in BxPC-3 cell proliferation presumably followed by cell death, the cells were monitored for apoptosis. Annexin V staining indicated significant differences between treated and untreated BxPC-3 cells, demonstrating that OA induces apoptotic cell death (Figure 4.7). The images shown in Figure 4.7 are in agreement with the quantitative measurements of Annexin V staining, demonstrating cell shrinkage. In addition, other mechanisms of cell death were also investigated. A preliminary characterisation of autophagic flux by measuring LC3-II accumulation was examined as a potential mechanism of cell death. Although, further optimisation as well as replicates need to be conducted before conclusions can be drawn. Data in Figure 4.8 indicates LC3-II accumulation in control as well as OA treated cells with the BxPC-3 cell line, whereas minor quantities are shown to be present in MiaPaca-2 and HepG2 cells. Since the amount of LC3-II is closely correlated to the number of autophagosomes this may suggest that the metabolic phenotype of BxPC-3 cells is dependent on self-catabolic processes mediated via autophagy for the acquisition of nutrients.

Cellular homeostasis is maintained by basal levels of autophagy, through the clearing of misfolded proteins or damaged organelles (Begun and Xavier, 2013; Mizushima *et al*., 2008). During periods of nutrient scarcity, autophagic flux increases beyond basal levels to supply the cell with nutrients (Komatsu *et al*., 2005). Eng and colleagues (2015) investigated the role of autophagy on growth, in a panel of KRAS mutant cell lines. Upon treatment with the chloroquine analog Lys01, which inhibits autophagy, mutant KRAS cell proliferation appeared to be less effected than in wild-type KRAS cell lines. Lysosomotropic agents such chloroquine and Lys01 may affect other pathways

as well as autophagy, therefore, shRNAs targeting ATG7, ULK1 and VPS34 which form necessary protein complexes to mediate the autophagic process, were used to uncover autophagy addicted cells in a panel of 47 cell lines. However, knockdown of ATG7, ULK2 and VPS34 did not impair cell proliferation and no significant responses had been noted between wild type (WT) or mutant KRAS cell lines. Following, zinc finger nucleases were used to knock out ATG7 in Panc 10.05 which is a KRAS mutant pancreatic cancer cell line and maintains high levels of autophagic flux. Although no visible colonies were formed when cells were deprived of serum and amino acids, under nutrient rich conditions ATG7 deficient cells demonstrated no consistent inhibition of cell proliferation. Furthermore, transcription activator-like effector nucleases (TALENs) were used to knock out ATG7 in KRAS mutant non-small cell lung cancer cell line A549. As shown in Panc 10.05 cells, ATG7 deficient A549 cells were sensitive to serum and nutrient starvation but were unaffected when cultured under standard growth conditions. In addition, cell proliferation was unaffected in both colorectal and pancreatic HCT116 and PaTu-8988T ATG knockout cancer cell lines which also harbour a KRAS mutation. Collectively, this study indicates that KRAS driven cancer cells do not depend on autophagy for growth, in nutrient replete conditions (Eng *et al*., 2016).

Therefore, since MiaPaca-2 is a KRAS mutant driven cancer cell line, autophagy is likely to be a dispensable pathway when cultured under nutrient rich conditions. However, BxPC-3 cells do not harbor a KRAS mutation, the data indicates that BxPC-3 cells require high basal levels of autophagic flux even when cultured under optimal conditions. Moreover, the autophagy stimulator Torin 1 was used to further help

interpret the data. Torin 1 stimulates autophagy by blocking phosphorylation of mTORC1 and mTORC2, thus blocking mTOR which results to mimicking cellular starvation through the blockage of signals required for cell proliferation (Jung *et al*., 2010). During starvation, LC3-I levels decrease and the amount of LC3-II increase. However, prolonged starvation may cause LC3-I and LC3-II to disappear. This occurs since LC3-II is located both on the inner and outer autophagosome membranes. Therefore, the inner LC3-II becomes degraded inside autolysosomes, and the outer LC3-II is deconjugated by ATG4 and returns to the cytosol (Tanida *et al*., 2005). Therefore, addition of Torin 1 in BxPC-3 and MiaPaca-2 cells indicates a decrease in the amount of LC3-II in BxPC-3 cells, whereas both LC3-I and II disappear in MiaPaca-2 cells. No changes were noted in HepG2 cells, this may be due to a higher concentration of Torin 1 required for this cell line. Furthermore, addition of both Torin 1 and OA, shows to further stimulate autophagy in BxPC-3 cells, whereas OA decreases autophagic flux in MiaPaca-2 cells. Interestingly, although a higher concentration of Torin 1 may have been required for HepG2 cells, a synergistic increase in autophagic flux caused by Torin 1 and OA was noted.

As described previously, the mammalian target of rapamycin (mTOR) is a key regulatory molecule influencing cell growth, proliferation, motility, survival, protein synthesis translation and autophagy (Inoki and Guan, 2006, Reiling and Sabatini, 2006). During optimal conditions mTOR will be activated and autophagy will be suppressed. Various signaling pathways regulate mTOR activation, however, phosphoinositide 3 kinase (PI3K) is the main activator in response to growth factors. PI3K is a lipid kinase which phosphorylates phosphatidylinositol (PI) and is split into

three classes. Class I PI3K typically phosphorylates PI 4,5-bisphosphate generating phosphatidylinositol 3,4,5-triphosphate (PI(3,4,5)P_3) and class III PI3K/hVps34 phosphorylates PI producing phosphatidylinositol 3-phosphate (PI3P). Currently, little is known about class II PI3K. Activation of class I PI3K via the insulin receptor, leads to activation of AKT which subsequently activates mTOR complex 1, thus leading to suppression of autophagy. However, class III PI3KhVps34 is a positive regulator of autophagy (Cantley, 2002). Autophagy Inhibitors such as 3-MA target both class I and III PI3K indiscriminately, but it is thought that autophagy becomes inhibited by suppressing class III PI3K, thus blocking PI3P formation which in turn inhibits autophagy (Corradetti and Guan, 2006). Wu and colleagues investigated the effect of 3-MA on both nutrient rich and deprived conditions. Interestingly they noted that 3-MA promotes autophagy in nutrient rich conditions, however it inhibits starvation-induced autophagy. This occurs due to 3-MA blocking class I PI3K persistently, whereas the effect on class III PI3K is transient (Wu *et al*., 2010).

Figure 4.8 shows that addition of 3-MA in BxPC-3 cells decreases LC3-II intensity, compared to the control, indicating a reduction in autophagy, however following the addition of OA, LC3-I is also present, indicating that in nutrient rich conditions 3-MA is further suppressing autophagic flux. In MiaPaca-2 cells, addition of 3-MA also indicates suppression of autophagy due to markedly increased LC3-I band intensity (compared to the control), and addition of both 3-MA and OA has no further effects. Finally, addition of 3-MA to HepG2 cells, shows an increase in LC3-I, however, LC3-II also increases when compared to the control. Furthermore, addition of 3-MA and OA shows a decrease in intensity of both bands. The effect of 3-MA on HepG2 cells requires

further investigation, however, the data suggests that 3-MA may be causing an induction of autophagy in HepG2 cells when cultured in nutrient rich conditions.

Examining TG levels showed that MiaPaca-2 cells reduced TG concentrations back to basal levels more efficiently than BxPC-3 cells. Furthermore, the data collectively indicates a reduction in cell proliferation in BxPC-3 cells when cultured with OA, whereas MiaPaca-2 cells remain unaffected. This may be due to MiaPaca-2 cells containing a mutated copy of KRAS, whereas BxPC-3 are WT KRAS. The metabolic requirements of proliferating cells in order to double their genome, proteome and lipid mass, are dependent on ATP and NADPH. Although the bioenergetic demand of proliferating cells is high, the rate limiting step is often the supply of NADPH (Lewis *et al*., 2014). It has been established that mutant KRAS is necessary for the development of most pancreatic tumours through the regulation of anabolic glucose metabolism (Ying *et al*., 2012). Mutant KRAS drives glucose uptake and its divergence to the non-oxidative arm of the PPP generating ribose 5-phosphate. This metabolic rewiring caused by KRAS bypasses the NADPH generating oxidative arm of the PPP, indicating that an alternative NADPH generating mechanism must be present in KRAS transformed pancreatic tumours. It has been demonstrated that the cytosolic malic enzyme (ME1) which converts malate to pyruvate is the main NADPH generating source in KRAS mutant pancreatic cancers. The main substrate shown to fuel the ME1 pathway is derived from anaplerotic glutamine, shuttling citrate into the cytosol which can fuel either DNL or the NADPH generating enzymes ME1 and IDH1 (Lyssiotis *et al*., 2013).

In addition to anaplerotic glutamine fueling NADPH producing pathways via ME1 and IDH1, β-oxidation also has a role in NADPH production. During each oxidative cycle, one molecule of acetyl-CoA is produced with two being produced in the last cycle. Acetyl-CoA is then able to enter the TCA cycle which along with oxaloacetate gives rise to citrate. Following export of citrate into the cytoplasm, it is able to enter to metabolic chain reactions (ME1 and IDH1) which produce cytosolic NADPH (Carracedo *et al*., 2013). Since MiaPaca-2 cells are most likely to be dependent on ME1 for NADPH production, it is suggested that they may be more efficient in undergoing β-oxidation to fuel ME1 compared to BxPC-3 cells which obtain their NADPH via the oxidative arm of the PPP. Therefore, MiaPaca-2 cells are able to reduce TG concentrations to basal levels more efficiently than BxPC-3 cells. This hypothesis will be further examined in Chapter 6.

Overall, this chapter has demonstrated that addition of OA causes a reduction in BxPC-3 cell proliferation, which has been tested with two independent methods and additionally with cell cycle analysis, showing an inability to enter S-phase. Furthermore, BxPC-3 cells were shown to be positive for Annexin V staining, indicating that cell death may be mediated via an apoptotic mechanism. This needs to be validated using an independent technique such as Flow Cytometry and DNA staining. Preliminary LC3-I and II data are provided which suggest that the self-catabolic process of autophagy may also be involved in causing cell death.

Ookhtens et al (1984) investigated the contribution of hepatic and adipose tissue (highly lipogenic tissues) synthesized FAs to newly synthesized FAs in Ehrlich ascites tumour (EAT). Mice were administered $^{3}H_2O$ subcutaneously and [^{14}C] glucose via a

test meal. Radioactivity was then measured in plasma triacylglyceride fatty acids (TGFAs), free fatty acids (FFAs) and tumour total lipid FAs (TLFAs). In addition, [^{14}C] FFA were used to selectively label epididymal TGFA in order to estimate FA uptake from the intraperitoneal adipose tissue by tumour cells. The results indicated that 93% of the tumours TLFAs had been synthesized *de novo* by the tumour cells. Liver TGFA via the plasma contributed <0.5%, adipose tissue TGFA via plasma FFAs contributed <6% and adipose tissue TGFA via direct intraperitoneal transport of FFA <1%, which in total accounted for less the 7% of the TLFA radioactivity measured in EAT. Therefore, the study concludes that all labelled esterified FAs present in EAT are produced *de novo*, instead of being imported by the tumour microenvironment (Ookhtens *et al*., 1984). Considering the above study, the following chapter will examine the effects of OA on DNL, in order to further investigate why there is a growth inhibitory effect exerted by OA on BxPC-3 and not on MiaPaca-2 and HepG2 cells.

Chapter 5 – Supplementation with oleic acid alters *de novo* lipogenesis.

5.1 Introduction

A lipogenic phenotype is associated with the poor prognosis of many human carcinomas (Daemen *et al*., 2015). The modulation of multiple lipogenic enzymes have been shown to correlate with metastatic ability. Key to defining the lipogenic phenotype in malignant cancer cells is the increased rate of DNL. Few studies have investigated how cancer cells regulate and facilitate this altered state of lipid metabolism. Identifying the mechanisms through which *de novo* lipogenesis, a highly controlled pathway, is regulated may offer potential therapeutic benefits. The cellular mechanisms by which lipogenic enzymes are up-regulated in cancer cells remains poorly understood, although the expression of major oncogenic signalling pathways such as HER2 (Menendez *et al*., 2006), PI3K and KRAS have provided evidence of DNL lipogenesis inducing mechanisms (Ricoult *et al*., 2016).

The metabolic intermediate used for DNL is cytoplasmic acetyl-CoA. Under normoxic conditions, cells metabolise glucose via glycolysis generating pyruvate. Pyruvate dehydrogenase decarboxylates pyruvate to acetyl-CoA which then feeds into the mitochondrial TCA cycle giving rise to citrate. Citrate is then shunted into the cytoplasm and ATP citrate lyase (ACL) cleaves citrate to oxaloacetate and acetyl-CoA. Malonyl-CoA is then formed by acetyl-CoA carboxylase, which following a serial condensation of 7 malonyl-CoA molecules and one priming acetyl-CoA gives rise to palmitate. This is the first product of DNL and is synthesized by the multifunctional enzyme fatty acid

synthase (FAS) (Rohrig and Schulze, 2016). During hypoxia glucose derived pyruvate entry into the mitochondria becomes inhibited. Therefore, cells switch to an alternative carbon source for acetyl-CoA synthesis. This occurs via reductive carboxylation of glutamine or the direct synthesis of acetyl-CoA from acetate by cytoplasmic acetyl-CoA synthetase (Figure 5.1) (Wise *et al*., 2011; Fan *et al*., 2014).

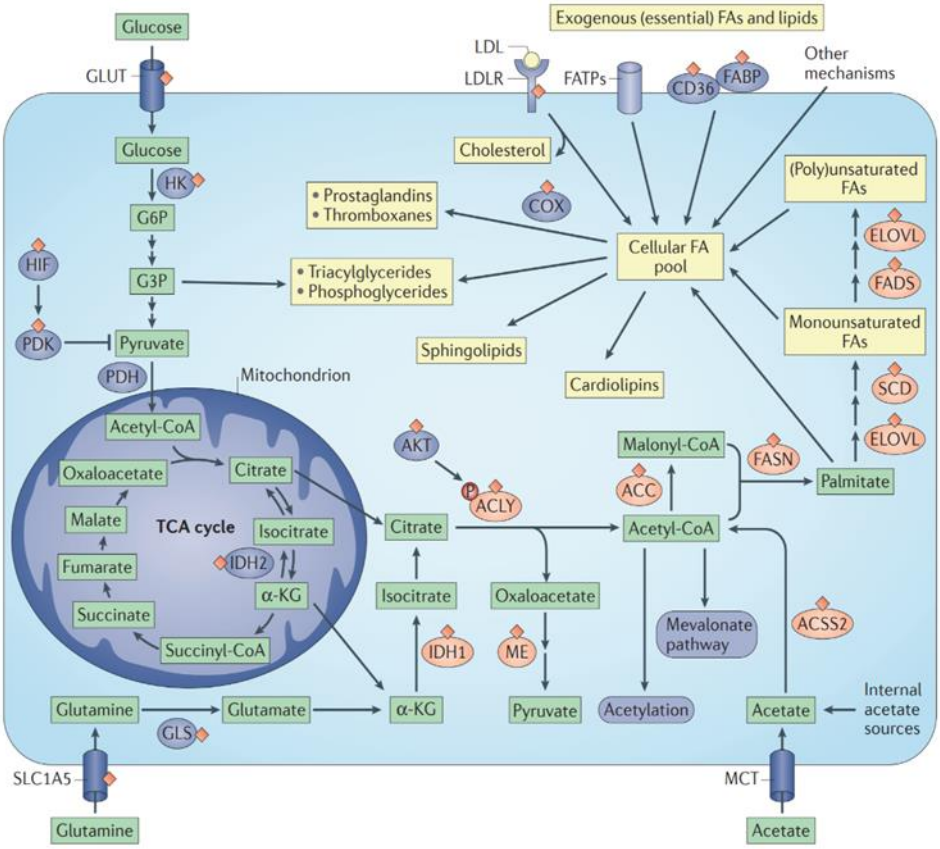

Figure 5.1 – DNL and fatty acid uptake.
Both glucose and glutamine can be used for the synthesis of citrate, which following cleavage by ACL gives rise to oxaloacetate and acetyl-CoA. Acetyl-CoA can also be synthesized from acetate which can be provided from either external or internal sources. Acetyl-CoA carboxylase will then give rise to malonyl-CoA which is then condensed by FAS to produce palmitate. Furthermore, essential FAs (which contain double bonds higher than position 9) are taken up via the bloodstream through the low-density lipoprotein receptor, FA transport proteins and FA translocase. Fatty acids are transported within the cell on FA binding proteins. Enzymes which have been shown to be regulated via the SREBP transcriptional network are shown in red, whilst proteins known to be upregulated/activated in cancer are shown with red diamonds (Image taken from Rohrig and Schulze, 2016).

The influence of the microenvironment on DNL in cancer cells is unclear. A study investigating fatty acid synthesis used lipid reduced culture media in order to limit cancer cells from accessing extracellular lipids and demonstrated that cells were able to survive and proliferate by up-regulating DNL (Ventura *et al*., 2015). Others have shown that an exogenous supply of either palmitate or oleate can fully restore cancer cell viability after FAS inhibition, showing adaptability to decreased levels of DNL (Kuhajda *et al*., 1994).

This chapter will investigate the effects of nutrient driven responses on the regulation of lipogenesis with a view to understanding the mechanisms through which *de novo* lipid synthesis may be regulated via the supplementation of exogenous lipid. The expression levels of two enzymes involved in fatty acid synthesis acetyl-CoA carboxylase (ACC) and FAS will be examined. In addition, alternative markers of DNL through the incorporation of labelled glucose and glutamine into newly synthesised PA will also be investigated.

5.2 Material and Methods

5.2.1 Examining oleic acid induced effects on Fatty Acid Synthetase and (FAS) Acetyl-CoA Carboxylase (ACC) protein quantity

BxPC-3, MiaPaca-2 and HepG2 cells were cultured in 6-well plates until achieving ~30% confluency. Cells were then treated with and without 300μM OA over a 48 hour period. Cells were then collected and changes in FAS and ACC expression were examined as described in Section 2.2. Due to the high molecular weight of FAS and ACC, 4-12% gradient NuPAGE Bis-Tris gels were used along with the MOPS running buffer to enhance the separation of high molecular weight proteins (MES has a lower pKa than MOPS, which enables gels to run faster, thus resulted to better resolution of low molecular weight proteins; whereas, MOPS is preferable for the separation of high molecular weight protein >260kDa). Samples were also run for 1 hour and 20 minutes (compared to the standard gel running lengths of 40-45 minutes) to maximize separation. Table 5.1 provides further information regarding the antibodies used for this experiment. Statistical analysis was performed using a two-way ANOVA.

Table 5.1 – FAS and ACC antibodies
Antibodies used for autophagy western blotting

Antibodies used for FAS and ACC detection					
Antibody	**Species**	**Concentration***	**Product code**	**Vendor**	**Application**
ACC	Rabbit	1:1000	3676S	Cell signaling	Primary
FAS	Rabbit	1:1000	3189S	Cell signaling	Primary
B-actin	Mouse	1:1000	sc-517582	Santacruz	Primary
IRDye 680 anti-rabbit	Donkey	1:10000	926-68073	LI-Cor	Secondary
IRDye 680 anti-mouse	Goat	1:10000	925-68070	Li-Cor	Secondary

* Antibody concentrations were selected by using the lowest concentration from the range suggested by the manufacturer.

5.2.2 [U13C] glucose derived DNL

BxPC-3, AsPC-1, Capan-1, MiaPaca-2 and HepG2 cells were cultured in 6-well plates until achieving ~30% confluency. Cells were then cultured with media containing 50% [U-13C] glucose (Goss Scientific Instruments Ltd, UK) and treated with and without 300μM OA for a 48 hour period. The labelling of the end-product (PA) reflects how much of the tracer administered is incorporated into fatty acids, the turnover of the palmitate pool and the rate of DNL. Cells were then washed twice with PBS and were collected by trypsinisation. The Folch lipid extraction procedure as described in Section 2.4 was then applied to extract lipids. It is noteworthy, that although FBS is expected to contain lipids, no lipid free FBS was used during this study. Lipid free serum is not commercially available and although methods using charcoal to extract lipids from

serum are available, it is unclear as to which other serum components would be removed. Additionally, this would create batch to batch variability, as serum components are not standardized and would result to data interpretation becoming more challenging. Therefore, it was decided to consider media supplemented with 10% FBS (without OA) to be labelled “lipid free” media.

The amount of tracer administered in the form of [U-13C] glucose was 50% of the total available glucose concentration supplied to each cell line. This was prepared by taking 0mM glucose DMEM and RPMI media and adding [U-13C] glucose to generate 25 and 11mM glucose media respectively. Labelled media was diluted with non-labelled media in a 1:1 ratio. Therefore, the amount of tracer administered was 50% of the total available glucose (Figure 5.2). The end-product enrichment of palmitate for BxPC3 cells, assuming identical metabolism between cell lines, would therefore be expected to be half that obtained for HepG2 and MiaPaca-2 cells. However, because enrichments are expressed as % change from control, this would not affect the findings. The use of high initial doses of label also ensured sufficient enrichment to permit detection, ensuring sensitivity would not be an issue. Statistical analysis was performed using a two-way ANOVA.

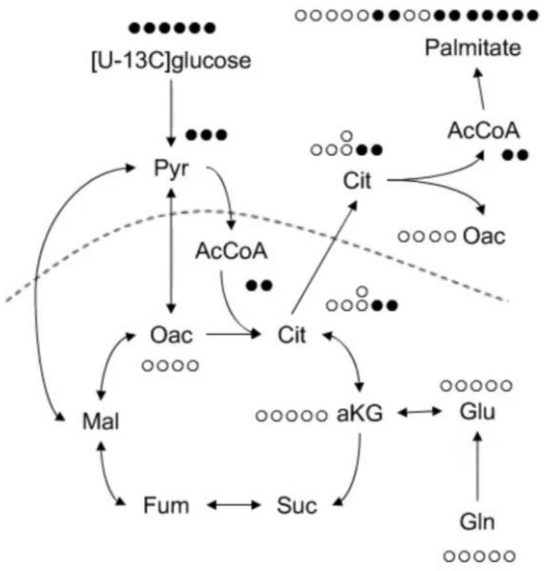

Figure 5.2 – [U-13C] glucose mediated DNL
The above schematic demonstrates the catabolism of uniformly labelled glucose, and its incorporation into PA. Thus, based on the amount of incorporated label detected in PA, the rate of DNL from glucose derived carbon can be determined (Image adapted from Vacanti *et al*., 2014).

In relation to preparing the glutamine label, as palmitate enrichment was not expected to be as high as that when adding labelled glucose, 100% [5-13C] glutamine media was prepared. DMEM and RPMI media containing 0mM glutamine were supplemented with [5-13C] glutamine, resulting in a total concentration of 4 and 2mM glutamine respectively. This matched the concentration of glutamine in the control media samples (Figure 5.3). Statistical analysis was performed using a two-way ANOVA.

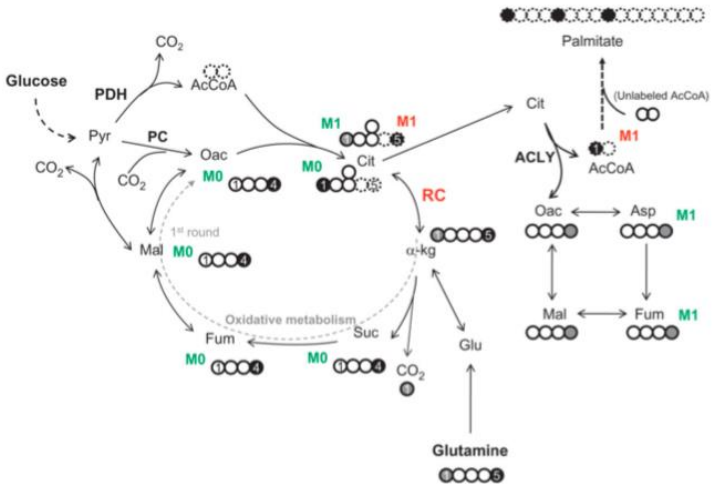

Figure 5.3 – [1,5-13C] glutamine mediated DNL
The above schematic demonstrates the catabolism of uniformly labelled glutamine, and its incorporation into PA. The amount of incorporated label detected in PA, using [5-13C] glutamine can be used to determine the rate of DNL from glutamine which feeds into the TCA cycle giving rise to labelled citrate which is converted to Acetyl-CoA and subsequently enters PA (Image taken from Metallo *et al*., 2011).

The entry of non-labelled fatty acids (palmitic acid) into the PA pool, would be expected to be minimal. The availability of exogenously derived palmitate would be very low and only that found in the 10% FBS as added to the media. Although exogenous lipid was added to the media, this was in the form of OA. Unless this was metabolized (partial oxidation) to produce palmitate the OA would not be expected to contribute to the PA pool directly. One source of ready-made palmitate that could have contributed to the PA pool would have been PA obtained from the turnover or breakdown of membrane phospholipids. In the case of proliferating cells, this would be expected to be minimal. Although proliferation was shown to decrease in BxPC-3 cells, isotopic data was obtained at 24 and 48 hours when proliferation rates were still high. Turnover of PA is therefore assumed to be similar between the cell lines.

It is known that most fatty acids in cancer cells are incorporated into phospholipids and that the cellular pool of free fatty acids is low. Under standard media conditions (low lipids) the palmitate pool measured mostly reflects the incorporation of the precursors (glucose and glutamine) in PA phospholipids. Although the fatty acid profile of cellular TG was not measured, total TG concentrations in the control pancreatic cell lines were low (Chapter 3). This would be expected to considerably change following the addition of OA.

It is the influence of the formation of OA rich lipid droplet pools on the synthesis of palmitate (DNL) which is being assessed. The utilization of OA in relation to its conversion into TG biomass was very similar between cells lines (Chapter 4, Section 4.3.3). The results showed that all cell lines had the same capacity to store lipid and therefore dilution of labelled palmitate within the TG pool would have been comparable between MiaPaca-2 and BxPC-3 cells, as they initially had similar concentration of TG. Because HepG2 cells had an initial greater biomass of TG, its palmitate enrichment would be expected to be lower as higher intracellular quantities of PA were already present.

This model describes the influence of an accumulation of OA and the resultant increase in LD formation (a pathway utilized to prevent the uncontrolled accumulation of fatty acids) on the conversion of acetyl-CoA into palmitic acid (DNL – which is strongly upregulated in cancer). In this study the monitoring of acetyl-CoA derived from either glucose or glutamine and its incorporation into palmitate will be used to provide information related to the contribution of these nutrients in relation to the formation of newly synthesized lipid.

5.3 Results

5.3.1 FAS and ACC expression

In order to determine whether OA influences the expression levels of lipogenic enzymes as well as examining baseline expression levels between cell lines, Western blot analysis was used to measure the amount of ACC and FAS. BxPC-3 cells express ACC at significantly lower levels (approximately 5-fold less) than MiaPaca-2 and HepG2 cells ($p<0.0001$) (Figure 5.4). MiaPaca-2 cells express the highest amount of ACC, with a significant decrease in ACC expression with the addition of OA. Although HepG2 cells express lower amounts of ACC than MiaPaca-2 cells, no changes were observed with the addition of OA. BxPC-3 and MiaPaca-2 cells express similar levels of FAS in contrast to HepG2 cells which produce significantly higher quantities ($p<0.001$ and $p<0.05$ respectively), however all three cell lines showed no changes in FAS expression following the addition of OA (Figure 5.4).

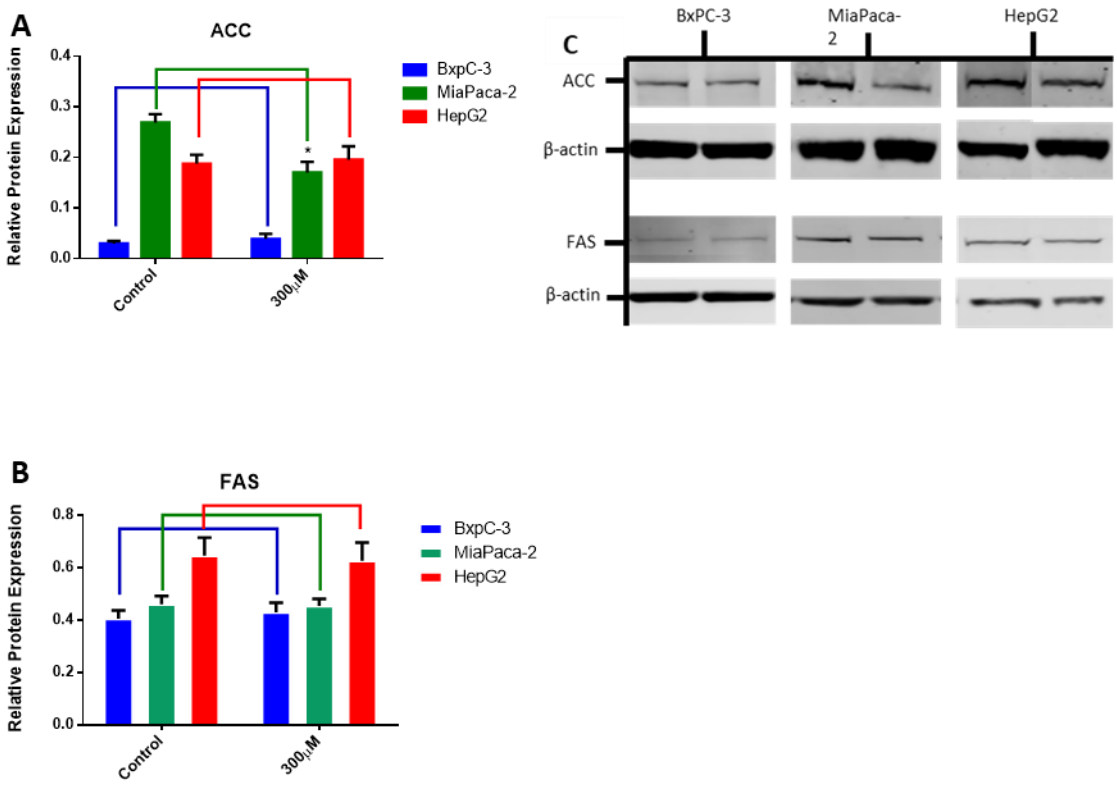

Figure 5.4 – ACC and FAS expression levels of lipogenic regulators.
Graphs **(A)** and **(B)** demonstrate the baseline levels of ACC and FAS and the changes that occur within a 48 hour period when cultured with an exogenous supply of 300μM OA. In addition, **(C)** is a representative image of the western blot data collected for this experiment (n=3). (*) Statistical analysis indicates that addition of 300μM OA causes a significant drop in ACC expression in MiaPaca-2 cells ($p<0.001$).

Except for MiaPaca-2 cells, these results indicate there are minimal changes in DNL assuming changes in lipogenesis are proportional to protein levels of the lipid synthesizing enzyme FAS and ACC.

5.3.2 Glucose derived *de novo* lipogenesis

By examining changes in key metabolic enzymes (FAS and ACC) or metabolites only partial information can be obtained regarding the cell's metabolic status. As demonstrated in Figure 5.4, no significant changes were shown in FAS expression with or without the addition of OA, with only MiaPaca-2 cells demonstrating a significant difference in ACC expression upon addition of OA. In order to obtain a comprehensive understanding of metabolic changes, the carbon contribution of key biosynthetic substrates was measured into the first product of the lipogenic pathway palmitate. Furthermore, since the interrogation of glucose derived lipogenesis was a critical element of this investigation, AsPC-1 and Capan-1 as test pancreatic cell lines were also included in addition to BxPC-3 and MiaPaca-2 cells.

DNL carbon fluxes from the two major biosynthetic substrates (glucose and glutamine) were determined using GC-MS. The panel of graphs shown in Figure 5.5, demonstrates the percentage change of M+2 label derived from [U-13C] glucose being incorporated into palmitate, from samples which were collected at 24 and at 48 hours. All 4 pancreatic cell lines demonstrated significant decreases of 13C glucose incorporation into PA when cultured with OA. AsPC-1, BxPC-3, Capan-1 and MiaPaca-2 cells demonstrated decreases in isotopic ratio of approximately 60, 50, 40 and 40% respectively for both 24 and 48 hours ($p<0.0001$). The hepatic cell line HepG2 did not show any significant changes at 24 hours but ~15% drop ($p<0.0001$) was noted at 48 hours. Of importance is that the changes in isotopic enrichment between 24 and 48 hours for all cell lines were very similar. This indicates the results were obtained at a steady state (input=output) where the enrichment of the pool being measured was

constant over a period of time. For these isotopic studies change of media or supplementation with additional glucose was therefore not required.

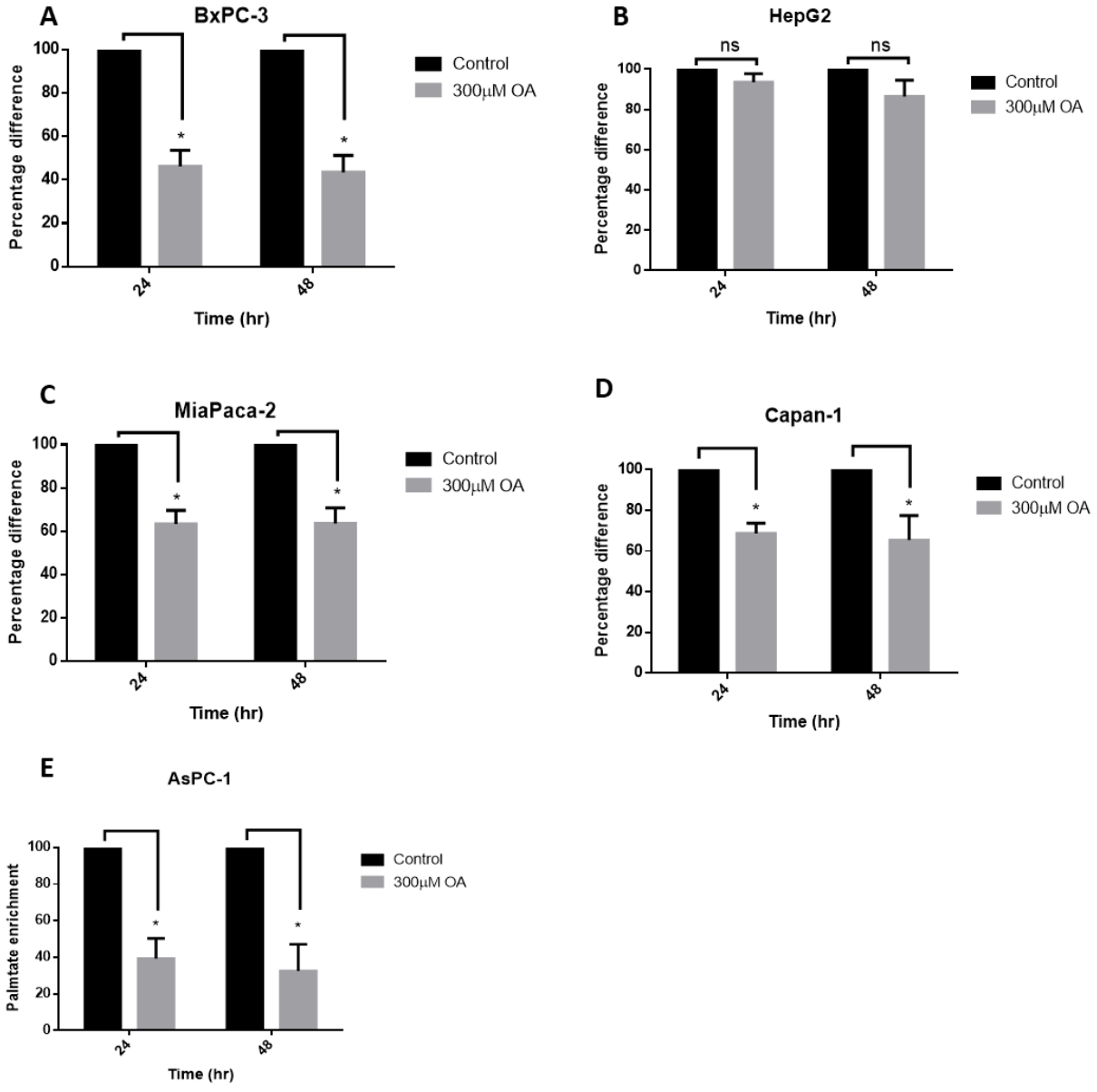

Figure 5.5 – [U-13C] glucose derived PA.
The above panel of graphs demonstrates the percentage change of M+2 label derived from [U-13C] glucose to palmitate over a 24 and 48 hour period. No significant changes were shown in HepG2 cells at 24 hours, however all other cell lines show significant changes ($p<0.0001$) (BxPC-3 n=4, AsPC-1 n=5, Capan-1 n=3, MiaPaca-2 n=4 and HepG2 n=4). The data has been normalized based on the control for each experimental run, on the day of collection (*) statistically significant, (ns) no significance.

5.3.3 Glutamine derived DNL

As pancreatic cancer cells reduce the incorporation of glucose derived carbon to palmitate, when cultured with exogenous OA, the ability of glutamine to do the same was also examined. AsPC-1 and Capan-1 cells were included as this enables comparison of data from more cell lines with different KRAS status. Cells were cultured with [5-^{13}C] glutamine for a 48 hour period, which can be used to determine the contribution of the anaplerotic pathway of the TCA cycle towards DNL (See section 5.3.2). Figure 5.6 shows that BxPC-3 cells had an increase of M+1 label of ~25%, however a ~50% drop was seen for M+2. MiaPaca-2 and HepG2 cells showed no significant changes in M+1 enrichment, and only demonstrated a decrease in glutamine contribution to PA (M+2) ranging between 10-20%.

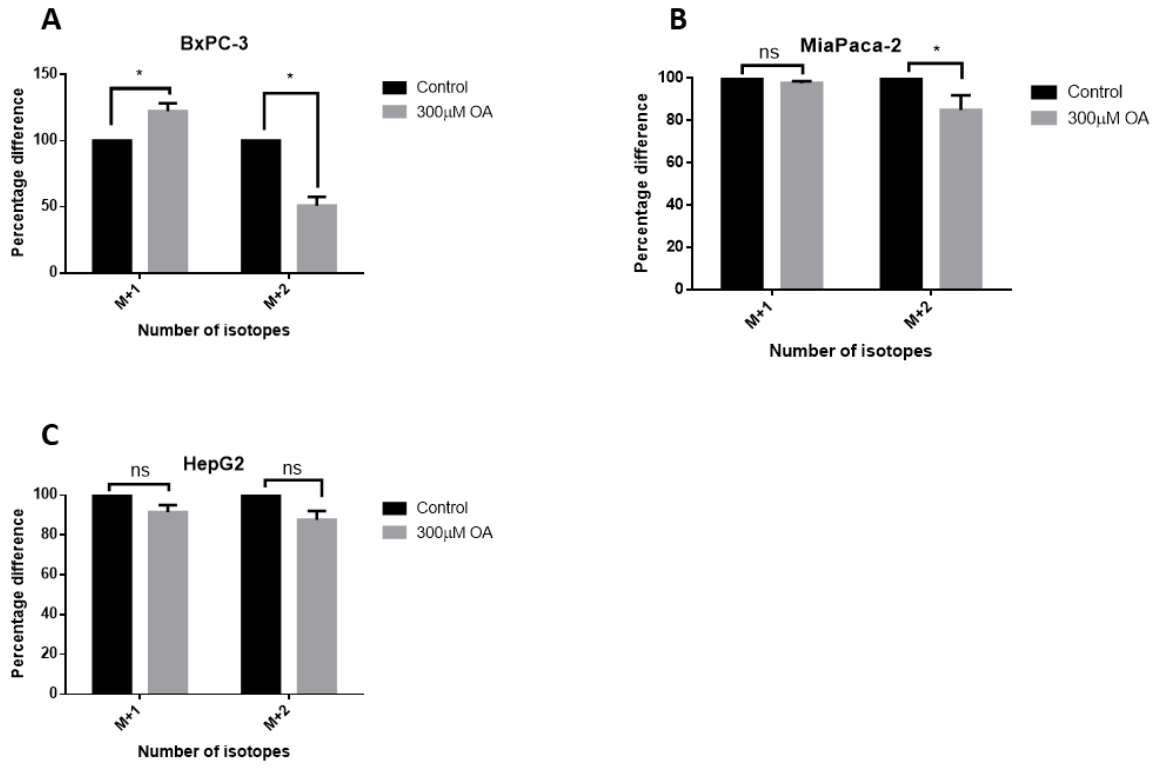

Figure 5.6 – [5-13C] glutamine derived PA. The above panel of graphs demonstrates the percentage change of M+1 and M+2 label derived from [5-13C] glutamine to palmitate over a 48 hour period (n=3). BxPC-3 cells demonstrate significant changes ($p<0.0001$), MiaPaca-2 cells show a significant difference at M+2 labelling only ($p<0.01$) and HepG2 cells show significant difference for both M+1 and M+2 ($p<0.0001$). The data has been normalized based on the control for each experimental run, on the day of collection (*) statistically significant, (ns) no significance.

5.4 Discussion

Following Warburg's discovery in the 1920s, that cancer cells demonstrate high rates of glucose uptake and perform glucose fermentation independent of oxygen availability, Medes, established that cancer cells readily convert glucose or acetate into lipids, at a similar rate to the liver (Medes *et al*., 1953). Although Medes' study concluded that cancer cells would still require lipids from the host which were provided from the extracellular environment, Ookhtens provided evidence indicating that tumour cells can produce almost all their cellular FAs through DNL. Decades later, fatty acid synthase (FAS) was identified as tumour antigen OA-519 in an aggressive breast cancer and multiple studies have now concluded the importance of FA synthesis in cancer cell growth (Kuhajda *et al*., 1994; Santos and Schulze, 2012).

This study demonstrates changes in DNL via the addition of (a neutral FA) OA in pancreatic cancer cell line. It is also noteworthy that the effects shown here are induced only by the addition of OA at a concentration similar to that found in plasma. In order to investigate the effects of OA on DNL the expression levels of FAS (EC 2.3.1.85) and ACC (EC 6.4.12) were examined upon addition of OA by Western blotting. FAS is a complex multifunctional enzyme consisting of two identical monomers (~270kDa) and has six catalytic activities. While the FAS monomer contains all active domains required for palmitate synthesis, only the dimer form of the synthase is functional. Furthermore, biochemical and small-angle neutron-scattering analysis have revealed that the dimer form of the enzyme has the monomers arranged in a head-to-tail manner, thus giving rise to two palmitate generating centres (Chirala and Wakil, 2004). Fatty Acid Synthase catalyses the synthesis of saturated FAs such as myristate, palmitate and stearate by

using the substrates acetyl-CoA, malonyl-CoA and NADPH (Chakravarty *et al*., 2004). ACC catalyses the rate-limiting reaction of long chain FA biosynthesis by producing the fatty acid synthesis substrate malonyl-CoA. ACC activity is tightly regulated by reversible phosphorylation. Eight different phosphorylation sites have been identified on ACC which are serine residues 23, 25, 29, 77, 79, 95, 1200, 1215. The two known protein kinases which have been identified to inhibit ACC activity by phosphorylation are cAMP-dependent protein kinase and AMPK (Ha *et al*., 1994).

BxPC-3 and Capan-1 cells demonstrated OA induced growth inhibition, whereas AsPC-1, MiaPaca-2 and HepG2 cells were unaffected. In order to provide an understanding of the effects of OA on lipid metabolism in these cell lines the first approach adopted was to measure the expression levels of the two major lipogenic enzymes. ACC, which is generally considered the rate-determining step of the lipogenic pathway (Natali *et al*., 2007), was shown to be expressed at significantly lower levels in BxPC-3 cells (15-fold) compared to MiaPaca-2 and HepG2 cells (at baseline or after addition of OA). This would imply that the latter two cell lines have a lipogenic phenotype compared to BxPC-3 cells. Furthermore, the doubling rate of MiaPaca-2 cells is 40 hours, whereas BxPC-3 ranges from 48-60 hours, therefore it is expected that MiaPaca-2 cells will have a higher lipogenic rate in order to meet their lipid requirements (Deer *et al*., 2010). Upon addition of OA, MiaPaca-2 cells showed a significant decrease in ACC expression (1.5-fold). The downregulation of ACC by OA is in agreement with the data published by (Natali *et al*., 2007), in glial cells. Their study demonstrated that of the several FAs used (OA, PA and myristate), only OA was capable of reducing ACC expression. This could suggest that MiaPaca-2 cells were

able to downregulate ACC expression in order to maintain lipid content at a homeostatic level, thus avoiding lipotoxicity. In addition, HepG2 cells showed no changes in both FAS and ACC expression upon addition of OA. This can be explained by the known prominent lipogenic phenotype of liver cells, and their high capacity for lipid storage (Bechmann *et al*., 2012). Finally, BxPC-3 cells showed no changes in expression of either enzyme, although levels of ACC were very low. However, since addition of OA induces growth inhibition in this cell line, this may imply that BxPC-3 cells are unable to sense changes in metabolite concentrations and subsequently rewire metabolic pathways as efficiently as MiaPaca-2 cells in order to not undergo lipotoxicity. Subsequently, this may imply they are metabolically less flexible when dealing with an exogenous lipid supply.

Inhibition of DNL which results in cell death is typically induced by targeting FAS or ACC using either pharmacological inhibitors or siRNA mediated knockdown (Flavin *et al*., 2010). However, the specific cause of cell death remains unclear. It has been speculated that cell death is related to end product starvation (lack of palmitate) or to a build-up of biochemical precursors (malonyl-CoA). Although initial studies suggested elevated levels of malonyl-CoA were toxic to the cell (Pizer *et al*., 2000), later studies challenged this hypothesis as inhibition of ACC was as equally effective in inducing cancer cell death (Brusselmans *et al*., 2005). This was also found to be true for inhibiting ATP citrate lyase (Hatzivassiliou *et al*., 2005b). Furthermore, it has been demonstrated that carnitine palmitoyltransferase-1 inhibition, caspase mediated apoptosis, reduced levels of phospho-Akt, inhibition of Bcl-2 and Mcl-1, production of ROS, mitochondrial impairment, ceramide production, ER stress, inhibition of mTOR

and autophagy as possible up stream events related to the induction of cell death (Flavin *et al*., 2010). Establishing the exact mechanisms or the drivers of these effects will provide novel approaches to drug therapy beyond those relating to just inhibiting the enzymes themselves.

Traditional methods of interrogating metabolic pathways depended on quantitative methods, i.e. measuring changes in enzyme concentration or the increase and decrease in concentrations of substrates or products. As shown in Figure 5.4, FAS levels remained constant upon addition of OA and only MiaPaca-2 cells showed a drop in ACC content. This would have led to the assumption that DNL is only affected in MiaPaca-2 cells via ACC downregulation. However, by using stable isotopes and monitoring changes in fluxes from one carbon source (glucose or glutamine) to another (palmitate) changes in DNL may be indicated even though enzyme concentrations remain unaffected,

By culturing cells with 50% [U-13C] glucose and measuring ^{13}C carbon on palmitate, changes in the contribution of glucose derived carbon to palmitate can be measured. BxPC-3 and AsPC-1 cells showed a ~50-60% drop in M+2 carbon contribution and MiaPaca-2 and Capan-1 cells showed a decrease of ~30-40%. This indicates that all 4 pancreatic cell lines downregulate carbon contribution from glucose to palmitate upon addition of OA. Moreover, HepG2 cells did not show any changes at 24 or 48 hours, thus suggesting that HepG2 cells continue to utilize biosynthetic carbon from glucose to fuel DNL even when supplied with lipid.

HepG2 cells are known to have high levels of basal lipogenic activity and increased lipid storage capacity. This is due to the liver being a major lipogenic tissue (Bechmann

et al., 2012). Therefore, it is expected that an exogenous influx of lipid would not significantly influence DNL. The liver is the hub of lipid metabolism in the body, hepatocytes are able to undergo lipid uptake, esterification, oxidation and secretion (Gluchowski *et al*., 2017). During the fed state, the liver stores excess carbohydrates as lipids, via DNL. FAs in the liver can be converted to TG and cholesterol esters to be secreted as very low-density lipoprotein particles. Adipose triglyceride lipase (ATGL) is also expressed in the liver, albeit at lower levels compared to adipose tissue, and it is thought to be one of the main regulators of beta oxidation, which ensures lipid homeostasis and the prevention of lipotoxicity (Lehner *et al*., 2012). Other lipases such as patatin-like phospholipase domain-containing protein 3 (PNPLA3) which are localized in LDs and share 50% homology with ATGL are also thought to facilitate lipolysis and regulate lipid homeostasis (Reid *et al*., 2008, Wu *et al*., 2011). Therefore, it can be speculated that due to the robust metabolic phenotype of hepatocytes, DNL is resistant to the exogenous supply of lipid due to their elevated and inherent capacity to store, oxidise, export or utilize excess fat.

In contrast to HepG2 cells, the four pancreatic cancer cell lines demonstrated a percentage drop of glucose derived carbon into palmitate, ranging between 30-60%. As shown in Chapter 4, negligible quantities of TG were detected in BxPC-3 and MiaPaca-2 cells compared to HepG2 cells at baseline. Therefore, it is shown that under optimal growth media conditions, basal lipid levels in the pancreatic cell lines are minimal when compared to HepG2 cells. BxPC-3 cells which are KRAS wild type, undergo growth arrest followed by a reduction in proliferation as shown in Chapter 4, and additionally downregulate DNL. MiaPaca-2, ASPC-1 and Capan-1 cells, which are

KRAS mutant cell lines, also downregulate DNL, although cell proliferation is unaffected in MiaPaca-2 and AsPC-1 cells (less acute changes in proliferation are noted in Capan-1 cells compared to BxPC-3 cells). The difference in the proliferative phenotype observed in BxPC-3 cells as compared to AsPC-1 and MiaPaca-2 therefore does not appear to be related to the cells ability to regulate DNL as fueled through glucose.

The drop noted in both ACC expression and glucose contribution to DNL in MiaPaca-2 cells was unexpected, as cell proliferation (Chapter 4) appeared to be unaffected. Metallo *et al*., (2012) have produced data, to show A549 (adenocarcinomic human alveolar basal epithelial) cells when cultured under hypoxia, cease to utilize glucose as the main carbon contributor to DNL and switch to utilization of glutamine (Metallo *et al*., 2011). Since MiaPaca-2 cells demonstrated a drop in both ACC and glucose derived lipogenesis, it was hypothesized that glutamine could have contributed towards DNL thus explaining why no changes in MiaPaca-2 cell proliferation were noted. Similarly, it could be proposed that BxPC3 cells would not be able to utilize glutamine and would therefore show a decrease in proliferation. However, this would be highly unlikely as it is known that many cancer cells including pancreatic cancer cells are sensitive to glutamine starvation (Wise and Thompson, 2010). This was confirmed as there appeared to be an increase in label incorporation into palmitate, no changes were noted for M+1 glutamine derived label being incorporated into palmitate for MiaPaca-2 and HepG2 cells (Figure 5.6). These results show a general dependence on glutamine metabolism irrespective of the addition of OA under normoxic conditions.

Furthermore, the increased M+1 enrichment on PA derived from [5-13C] glutamine in BxPC-3 cells may indicate a salvage mechanism attempting to restore DNL or provide carbon to fuel/restore processes which have become dysregulated by the supplementation of OA. However, changes in M+2 enrichment is more difficult to interpret. These could be due to processes such as conversion of labelled glutamine to oxaloacetate, lactate or pyruvate which may result in re-cycling. This could have major effects on the enrichment of acetyl-CoA causing the reduction in enrichment of specific isotopomers (Jones, 2014). Therefore, no clear conclusions can be drawn regarding glutamine M+2 derived PA synthesis, and experiments are required.

Fatty acid synthesis relies on NADPH as a reducing agent, which can be provided from various sources including the PPP (Chakravarthy *et al*., 2005). In pancreatic cancer cell lines, it has been demonstrated that mutant KRAS drives glucose uptake and its diversion into the non-oxidative arm of the PPP generating ribose 5-phosphate which is used in nucleic acid biosynthesis. This finding was unexpected since this metabolic reprogramming bypasses the oxidative NADPH generating arm of the PPP, suggesting the existence of alternative sources for NADPH production (Lyssiotis *et al*., 2013). Studies have indicated that cytosolic aspartate aminotransferase GOT1 is crucial in maintaining redox control and pancreatic cell proliferation where GOT1 functions upstream of the malic enzyme (ME1) which is necessary for NADPH generation (Lyssiotis *et al*., 2013). Knock down of either GOT1 or ME1 increased the oxidized to reduced NADPH, thus indicating that this pathway was the major source of NADPH generation in KRAS+ pancreatic cancer (Yuan et al., 2012). BxPC-3 cells however, being KRAS wild type, depend on the oxidative arm of the PPP for generating NADPH.

NADP+ becomes reduced by oxidizing glucose, (especially under normoxic conditions), subsequently donating a reducing equivalent to palmitate to fuel DNL.

Results demonstrating that the addition of OA causes a reduction in the incorporation of glucose derived carbon into palmitate, in all pancreatic cell lines may suggest downregulation of glucose uptake in response to the influx of lipid. Subsequently, in cells depending on the oxidative arm of the PPP for generating NADPH, as in BxPC-3 cells, NADPH generation would be expected to decrease. For cells which are dependent for generating NADPH through sources other than the PPP, the down regulation of glucose uptake may not be as critical in relation to NADPH production.

Like most energy producing molecules such as ATP, the pool of NADP+/NADPH in cells is small relative to its flux through pathways that require the cofactor (Pollak *et al*., 2007b). Significantly, the overall biosynthetic demand for NADPH is >80% of the cytosolic pool, with the majority being used in fatty acid synthesis (Fan *et al*., 2014). Therefore, the interconversion between the oxidized and reduced states must be coupled across all reactions involving this cofactor (Pollak *et al*., 2007a).

Due to the inability of pancreatic cells to utilize exogenous lipid as efficiently as HepG2 cells, they may be required to downregulate DNL. A reduction in DNL would reduce the activity of one of the major NADPH generating systems in the cell, as well as causing an imbalance between the coupling of the oxidative arm of the PPP and DNL. This could result in an increase in cytosolic NADPH which would provide advantages such as increased capability to combat ROS. However, cells relying on the oxidative arm of the PPP to fuel nucleotide synthesis will become less capable of oxidizing glucose to

fuel the PPP. This could ultimately result in a decreased production of nucleic acids, growth arrest and cell death. This hypothesis will be further examined in Chapter 6.

Chapter 6 – DNL induced metabolic vulnerabilities through re-distributing NADPH

6.1 Introduction

Proliferating cells are required to replicate cellular contents such as nucleotides, amino acids and lipids. Palmitic acid (PA) synthesis requires 7 molecules of ATP, 16 carbons from 8 molecules of acetyl-CoA, and 28 electrons from 14 molecules of NADPH. Furthermore, the production of a 16-carbon FA such as PA, requires 7 glucose molecules to produce the required amount of NAPDH. In contrast, 1 glucose molecule, produces 5-times the amount of necessary ATP (Carta et al., 2017). This high asymmetry can only be balanced by reducing the amount of glucose molecules committed to acetyl-CoA and ATP generation. If the total amount of glucose consumed was utilized for ATP generation, it would perturb the ATP/ADP ratio and subsequently impair the flux of glycolytic intermediates, reducing the synthesis of acetyl-CoA and NADPH, which are necessary for macromolecular synthesis (Vander Heiden *et al*., 2009).

Cytosolic NADPH is primarily generated via the oxidative arm of the PPP (Vander Heiden *et al*., 2011). Other sources of NADPH include the enzymes isocitrate dehydrogenase, malic enzyme (ME), and methylene tetrahydrofolate dehydrogenase (Pollak *et al*., 2007b). Different isoforms of these enzymes catalyse identical reactions in the mitochondria and cytosol and can therefore be responsible for the potential

transfer of reducing equivalents between these compartments. For example, the reductive carboxylation of α-ketoglutarate to isocitrate by IDH2 utilises mitochondrial NADPH, where citrate/isocitrate can then be exported to the cytosol when it can be oxidised by IDH1, thus producing cytosolic NADPH. The reverse cycle is also possible, giving rise to mitochondrial NADPH (Lewis *et al*., 2014).

NADPH has therefore, taken the focus away from ATP, as being the rate limiting cofactor responsible for cancer cell growth, due to its vital role in the biosynthesis of lipids and deoxynucleotides (Jeon *et al*., 2012). Furthermore, and of importance, is that NADPH is also a substrate for multiple antioxidant enzymes that convert oxidized glutathione (GSSG) into reduced glutathione (GSH) the primary antioxidant defense system in the cell (Meitzler *et al*., 2014; Diehn *et al*., 2009).

Glucose fuels both glycolysis and the PPP. Nonlabile hydrogen atoms on glucose carbons 1 and 3 are transferred to NADPH via the oxidative PPP enzymes G6PD and 6PGD. Therefore [3-^{2}H] glucose can be used to label NADPH with deuterium. By using GC-MS and examining palmitate labelling it was established that labelled NADPH from the PPP accounts for 12-20% of lipogenic NADPH as used for palmitate synthesis in lung cancer cell lines A549 and H1299 (Lewis *et al*., 2014).

The pool size of NADPH in cells is low relative to its flux through pathways which utilise this cofactor (Pollak *et al*., 2007b). Therefore, interconversion between the two states (oxidised and reduced) must be tightly coupled across all reactions and assessing overall concentration may prove uninformative when examining NADPH changes in a particular pathway (Figure 6.1) (Lewis *et al*., 2014).

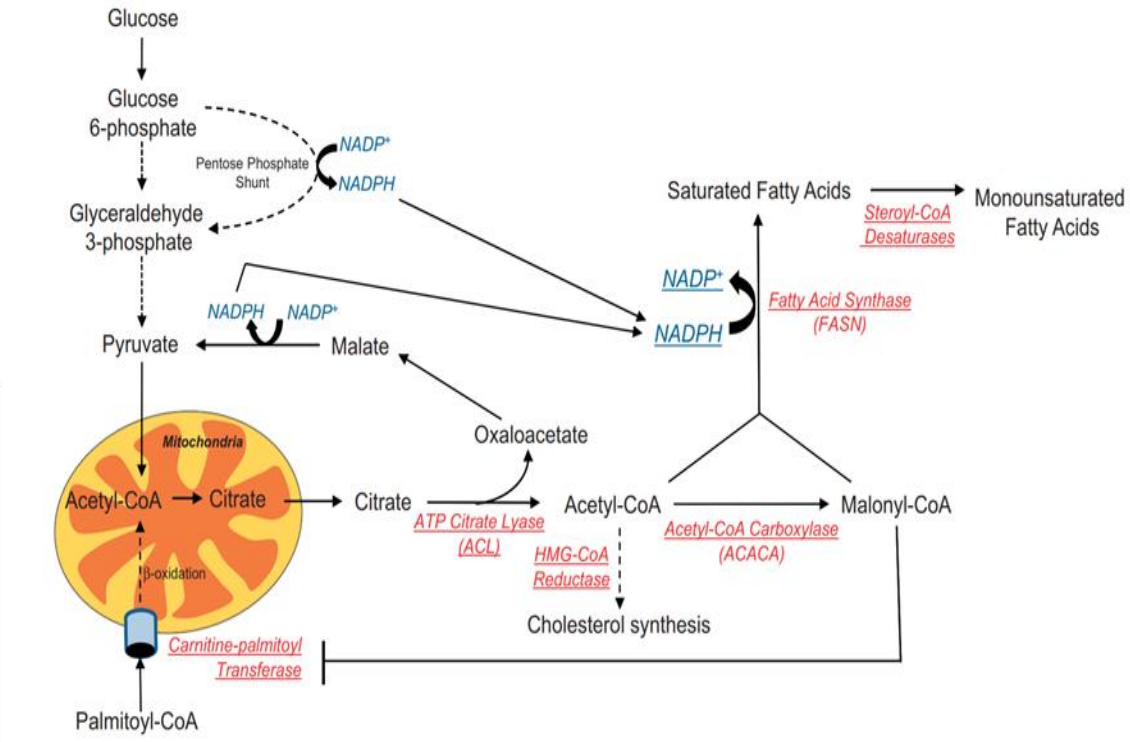

Figure 6.1 – Lipid metabolism.
The above schematic illustrates the conversion of metabolic intermediates into FFAs and phospholipids. Reducing equivalents which are produced by the PPP in the form of NADPH are later consumed by DNL for the synthesis of palmitate (Image adapted from Schug *et al*., 2012).

This study has shown that when cultured with exogenous OA, BxPC-3 and MiaPaca-2 cells reduce glucose incorporation into palmitate, but only BxPC-3 cells show signs of cell death. Therefore, it was hypothesized that DNL could also be used as a major sink for the NADPH oxidizing pathway in BxPC-3 cells. Since the production of NADP+ fuels the PPP by oxidizing G6P to 6PG, and is subsequently used for nucleotide synthesis, inhibition of NADPH oxidation may result in proliferating cells lacking nucleotides and therefore unable to undergo DNA replication (Figure 6.2). Consequently, inhibition of the PPP may result in decreased cell proliferation and eventually cell death, due to a lack of nucleotides. Therefore, the addition of exogenous OA, may be perturbing

metabolic homeostasis, resembling cell starvation, when cells are being cultured with a surplus of lipid nutrients.

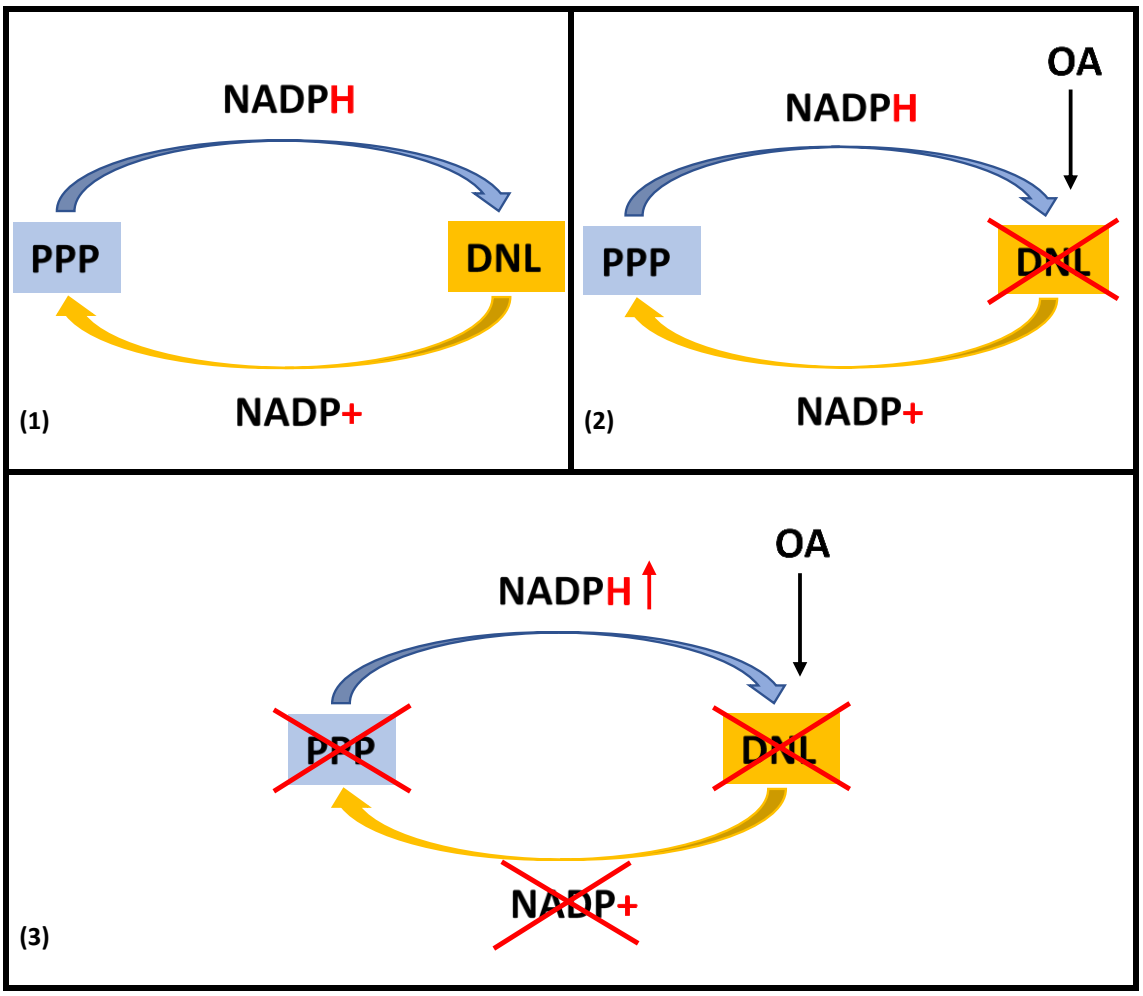

Figure 6.2 – OA mediated disruption of redox balance.
The above panel of images illustrates the proposed mechanism of OA induced inhibition of cell proliferation. Box 1 demonstrates optimal conditions, where crosstalk between the PPP and DNL occurs, each reducing and oxidizing NADPH and thus maintaining redox balance. Box 2 shows upon addition of OA, DNL downregulation on the addition of OA. Consequently, as shown in box 3, by downregulating DNL, NADPH is not oxidized to NADP+ which will then cause an inhibition of the PPP and a buildup of NADPH.

This chapter will utilize a method developed by Lewis *et al*., (2014) to examine whether the addition of OA causes significant changes in the transfer of electrons from glucose to palmitate, via NADPH. Furthermore, changes in NADP+/NADPH ratio and G6PD activity will also be examined upon addition of OA, to provide insight regarding the crosstalk between DNL and the PPP.

As demonstrated by (Lewis *et al*., 2014) and (Schug *et al*., 2012) the link between the PPP and DNL is crucial. Since MiaPaca-2 cells are KRAS positive, and utilize the non-oxidative arm of the PPP, it may be that they rely on alternative sources for NADPH generation such as the ME1, which BxPC-3 cells cannot utilise.

Furthermore, since NADPH is tightly linked with ROS detoxification (by reducing GSH), it can be hypothesised that the higher quantities of NADPH available to the cell result in a higher capacity to combat ROS. Therefore, a preliminary investigation on the effects of H_2O_2 on cell growth along with supplementation with OA will be undertaken. Moreover, AMPK has been shown to control NADPH consumption and production via the regulation of DNL and β-oxidation respectively, under oxidative stress (Hardie *et al*., 2012; Jeon *et al*., 2012; Mihaylova and Shaw, 2011; Diradourian *et al*., 2005). Beta-oxidation has been shown to support cancer cell metabolism by oxidising reduced fatty acids to generate ATP and through the production of NADPH. For each pair of carbons in a fatty acid, complete oxidation also results to in the production of 14 molecules of ATP (Yao et al., 2018). Furthermore, each cycle of β-oxidation generates acetyl-CoA, which then enters the TCA cycle. The increased contribution of acetyl-CoA to the TCA cycle, increases the production of citrate which may be metabolised towards DNL, or alternatively be metabolised via IDH1 or ME1 for NADPH production (Pike *et al*., 2011).

Since MiaPaca-2 cells rely on ME1 and IDH1 for NADPH generation, they may also depend on or have a higher capacity for upregulating β-oxidation compared to BxPC-3 cells. Therefore, the effects of the irreversible CPT1 inhibitor etomoxir on cell growth, along with changes in the expression levels of two major enzymes involved in β-oxidation, very long-chain specific acyl-CoA dehydrogenase (ACADVL) and acyl-Coenzyme A dehydrogenase, C-4 to C-12 straight chain (ACADM) will also be examined.

6.2 – Material and Methods

6.2.1 Oleic acid mediated effects on G6PD activity (PPP)

BxPC-3, MiaPaca-2 and HepG2 cells were cultured in 6-well plates until achieving ~30% confluency. Two experimental models were used for this experiment, a single and a refed model. During the single fed model, cells were treated with and without media supplemented with 300μM OA over a 48 hour period before being lysed according to the manufacturer's instructions. For the refed model, cells were treated with fresh media after 24 hours, following removal of old media. G6PD activity was measured by a colourimetric assay following the manufacturer's instructions (AbCam, UK). Briefly, G6PD converts G6P to gluconolactone. The assay uses an alternative substrate, which upon oxidation converts a colourless probe to a coloured product absorbance OD 450nm. The colour intensity is proportional to G6PD activity. Statistical analysis was performed using a two-way ANOVA.

6.2.2 The effects of re-feeding BxPC-3 cells with oleic acid supplemented media on cell growth

BxPC-3 cells were seeded into 6-well plates until achieving ~20% confluency. Cells were treated with fresh media and 300μM OA supplemented media over a 48 hour period. The control wells (media only and media supplemented with 300μM OA) were left over a 5-day period. Refed cells were treated at 48 hours with fresh media with or without OA (discarding old media). Cells were incubated for a further 72 hour period.

Cell growth in terms of confluency was measured using the IncuCyte Zoom real time imaging systems (EssenBioscience, UK).

6.2.3 NADP+/NADPH assay

BxPC-3, MiaPaca-2 and HepG2 cells were cultured in 6-well plates until achieving ~30 confluency. Two experimental models were used for this experiment, a single and a refed model. During the single fed model, cells were treated with and without media supplemented with 300μM OA over a 48 hour period before being lysed according to the manufacturer's instructions. For the refed model, cells were treated with fresh media after 24 hours, following removal of old media. The NADP+/NADPH ratio was then determined following the manufacturer's protocol (SigmaAldrich, UK). Briefly, samples were split into two aliquots with the first aliquot heated to 60^{o}C to decompose NADP+. A cycling reaction was performed on the second aliquot to convert all NADP+ to NADPH. The NADPH developer was then added for 2 hours and absorbance was measured at OD 450nm. The ratio of NADP/NADPH was determined by using the following formula: ($NADP_{total}$ – NADPH)/NADPH. Statistical analysis was performed using a two-way ANOVA.

6.2.4 NADPH labelling via [3-^{2}H] glucose

BxPC-3, MiaPaca-2 and HepG2 cells were cultured in 6-well plates until achieving ~30 confluency. Cells were then treated with media containing 100% [3-^{2}H] glucose along with or without 300μM OA for a 48 hour period. Cells were then washed twice with PBS

and were collected by trypsinisation. The Folch lipid extraction procedure as described in section 2.4 was then applied. Statistical analysis was performed using a two-way ANOVA. This method had been previously applied by Lewis et al., (2014) and was shown to be a valid strategy for measuring glucose derived hydrogen contribution to palmitate via NADP(H) labelling.

When culturing cells with [3-2H] glucose, glucose is metabolized to G6P. During glycolysis, G6PD, converts G6P into 6PG. Furthermore, during the conversion of 6PG to Ru5P via 6PGD, NADP+ oxidises 6PG and is reduced into NADPH, which is a reaction of the PPP. The deuterated NADPH (since cells are cultured with [3-2H] glucose) is then donated to PA synthesis, which can be detected via GC-MS (Figure 6.3) (Lewis et al., 2014).

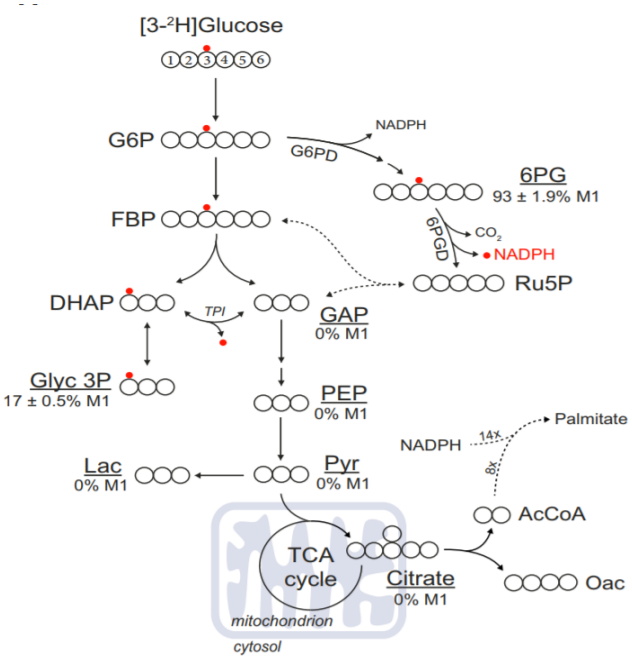

Figure 6.3 – [3-^{2}H] glucose generates labelled cytosolic NADPH.
The above schematic demonstrates the metabolic pathway in which [3-^{2}H] glucose is metabolised via glycolysis into generating labelled NADPH (Lewis *et al*., 2014).

6.2.5 Hydrogen peroxide and oleic acid mediated effects on cell growth

BxPC-3, MiaPaca-2 and HepG2 cells were cultured in 6-well plates until achieving ~20% confluency. BxPC-3, MiaPaca-2 and HepG2 cells were then treated with 25, 12.5 and 50μM H_2O_2 and 25, 12.5 and 50μM H_2O_2 along with 300μM OA over a 5-day period. The H_2O_2 concentrations had been selected based on a preliminary charcterisation of cell growth when cultured under 6.25, 12.5, 25, 50, 100 and 200μM H_2O_2 over a 5 day period and demonstrated ~50% reduction in cell growth. Cell growth in terms of confluency was measured using the IncuCyte Zoom real time imaging systems (EssenBioscience, UK).

6.2.6 Etomoxir mediated effects on cell growth

BxPC-3, MiaPaca-2 and HepG2 cells were cultured in 6-well plates until achieving ~20% confluency. BxPC-3, MiaPaca-2 and HepG2 cells were treated with 0.2, 0.4, 0.6, 0.8 and 1mM etomoxir over a 5-day period. Multiple concentrations were trialed in order to identify which concentration reduced proliferation by approximately 50%. The concentrations tested were in agreement with (Vincourt et al., 2011).

Cells were then treated using 0.2mM etomoxir alone and 0.2mM etomoxir with 300μM OA over a 5-day period. Cell growth in terms of confluency was measured using the IncuCyte Zoom real time imaging systems (EssenBioscience, UK).

6.2.7 Etomoxir and oleic acid mediated effects on ACADVL and ACADM expression

BxPC-3, MiaPaca-2 and HepG2 cells were cultured in 6-well plates until achieving ~30% confluency. Cells were treated with (and without) 0.2mM etomoxir, 300μM OA and 0.2mM etomoxir with 300μM OA over a 48 hour period and were compared to the control (media treated only cells). The effects on ACADM and ACADVL expression were examined by Western blotting (Chapter 2, Section 2.2). Further information regarding the antibodies used is shown in Table 6.1.

Table 6.1 – ACADM and ACADVL antibodies
Antibodies used for β-oxidation western blot.

ACADM and ACADVL Antibodies					
Antibody	**Species**	**Concentration**	**Product code**	**Vendor**	**Application**
ACADM	Rabbit	1:1000	ab92461	AbCam	Primary
ACADVL	Rabbit	1:1000	ab188872	AbCam	Primary
β-actin	Mouse	1:1000	sc-517582	Santacruz	Primary
IRDye 680 anti-rabbit	Donkey	1:10000	926-68073	LI-Cor	Secondary
IRDye 680 anti-mouse	Goat	1:10000	925-68070	Li-Cor	Secondary

6.2.8 Examining oleic acid mediated effects on ACADVL via immunoprecipitation

Immunoprecipitation was performed to detect native ACADVL protein in lysates from OA treated and untreated cells. Briefly, MiaPaca-2 cells were cultured in 6-well plates until achieving ~30% confluency. Cells were treated with 300μM OA over a 48-hour period. The culture media was then discarded, and cells washed twice with ice-cold PBS. Lysis buffer (RIPA buffer plus 1:100 protease inhibitors; 200μl) was then added to the cells which were left to incubate for 20 minutes on ice. The ACADVL antibody was then incubated with 1mL of MiaPaca-2 pooled cell lysate (1:40) overnight at 4ºC, at a rotation speed of 14 rpm. The antibody bound lysates were next incubated with 50μL of pre-washed sheep anti-rabbit IgG Dynabeads for 1 hour at 4ºC, with rotation at 14 rpm. The immunocomplexes were captured on a DynaMag™-2 for 2 minutes, supernatants were aspirated, and the samples were washed 3 times with PBS. The

complexes were then eluted by mixing beads with LDS sample buffer (25% NuPAGE LDS buffer [4x], 10% reducing agent [10x] and 65% distilled water; Invitrogen, UK), and heated to 75ºC for 10 minutes before being analysed by SDS-PAGE. The samples were processed on an NuPAGE 4-12% 1mm thick gradient gel and ran using MES running buffer for 40 minutes at 200V (ThermoFisher, UK). The gel was then examined using the Odyssey Li-Cor Infra-red imaging system (Li-Cor Biotechnology, UK).

6.3 Results

6.3.1 Oleic acid mediated effects on G6PD activity

Glucose-6-phosphate dehydrogenase (G6PD) catalyzes the conversion of G6P to 6-phosphoglucono-δ-lactone, the first and rate limiting step of the PPP. NADP+ activates G6PD via competitive binding with NADPH, stabilising G6PD and preventing the p53-G6PD interaction (Jiang et al., 2011). G6PD regulates the PPP which produces R5P for nucleotide generation and NADPH for reductive biosynthesis and ROS detoxification (Jiang et al., 2014). BxPC-3, MiaPaca-2 and HepG2 cells were treated with OA over a 48-hour period. BxPC-3 cells demonstrated a significant reduction ($p<0.01$) (Figure 6.4) in G6PD activity. MiaPaca-2 and HepG2 cells showed no statistically significant changes. Moreover, cells were refed at 24 hours with fresh control (no OA) and OA supplemented media, BxPC-3 and MiaPaca-2 cells demonstrated an increased ~2-fold higher rate of enzyme activity at 48 hours; however, no significant changes in control and OA treated cells was shown. HepG2 cells showed a statistically significant decrease in enzyme activity upon addition of OA ($p<0.01$) (Figure 6.4).

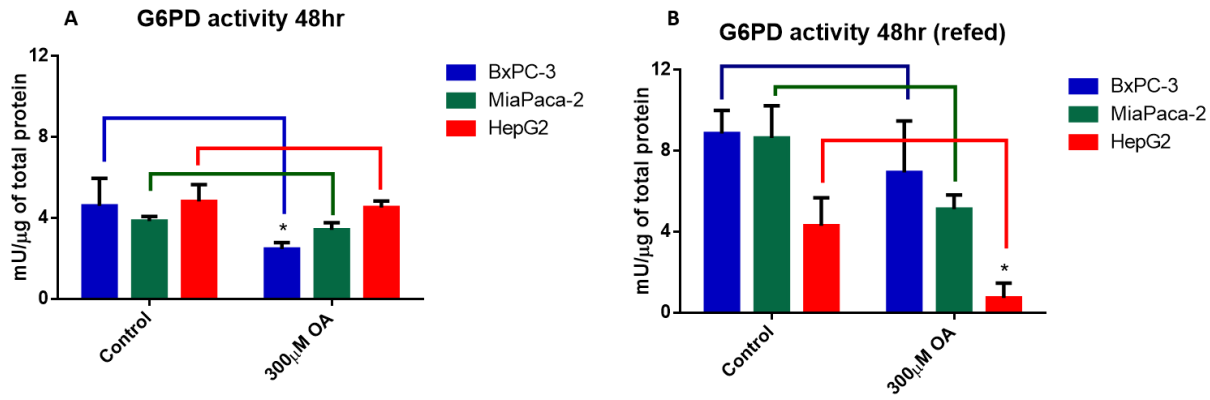

Figure 6.4 – OA mediate changes in G6PD activity
Graph **(A)** G6PD activity following 48 hours incubation in media with and without OA. **(B)** G6PD activity following a 48-hour incubation in media with and without OA after media had been refreshed at 24 hours (n=3). (*) statistical significance. ($p<0.01$) vs control of cell type.

6.3.2 Double dosing oleic mediated effects on BxPC-3 cell growth – a pilot study

Since BxPC-3 cells, when refed with fresh media supplemented with OA restored G6PD activity, it was hypothesized that cell proliferation would also be restored. Therefore, a preliminary experiment was conducted using BxPC-3 cells since they demonstrated the highest reduction in cell proliferation upon treatment with OA. BxPC-3 cells were cultured with and without OA over a 48 hour period and were refed using control (no OA) and OA supplemented media, to determine the effects on cell proliferation (Figure 6.5). The data suggests that refeeding OA treated cells using control media results in immediate recovery at 48 hours. Additionally, refeeding OA treated cells with fresh media supplemented with OA, causes an initial 24 hour delay, followed by full recovery of cell proliferation.

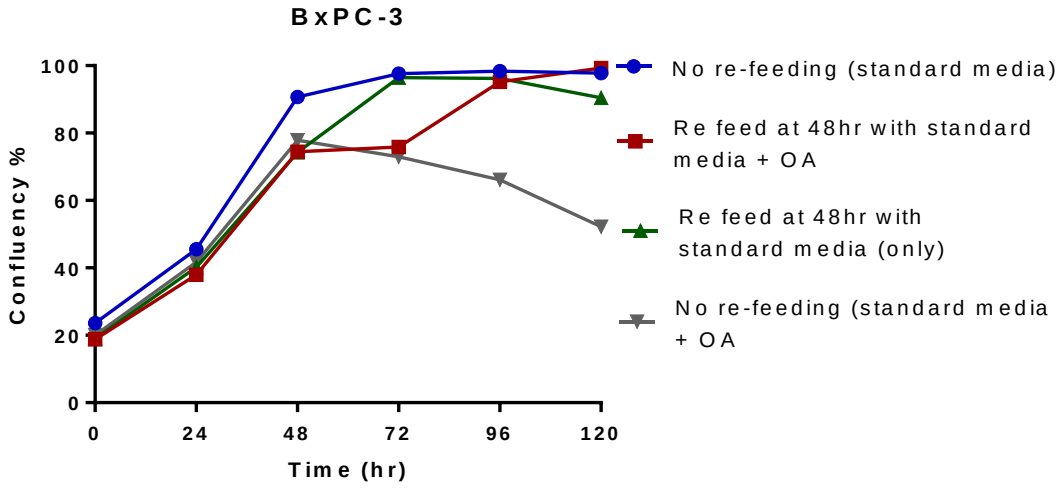

Figure 6.5 – OA mediated effects on BxPC-3 cell growth
The graph demonstrates OA treated cells when refed at 48 hours with control and OA supplemented media respectively, both show complete restoration of the proliferative profile, whilst demonstrating a 24 hour delay in cells treated with OA supplemented media only (n=1).

6.3.3 Oleic acid mediated effects on NADP+/NADPH ratio

Since the addition of OA reduces cell proliferation, causes growth arrest in G0/G1 phase, downregulates glucose derived carbon contribution towards PA synthesis and downregulates G6PD activity in BxPC-3 cells (Figures 4.2, 4.5, 5.5, 6.4) it was hypothesised that OA supplementation would also cause a decrease in the NADP+/NADPH ratio. Therefore, the NADP+/NADPH ratio was measured in BxPC-3, MiaPaca-2 and HepG2 cells over a 48 hour period in both a single fed and a 24 hour re-fed model. HepG2 cells showed a statistically significant increase in NADPH, as a decrease in the NADP+/NADPH ratio ($p<0.05$) was demonstrated when receiving a single feed over a 48 hour period. However, BxPC-3 and MiaPaca-2 cells demonstrated no changes in the NADP+/NADPH ratio following treatment with OA

(Figure 6.6A). Furthermore, when cells were refed at 24 hours with control or OA supplemented media, (Figure 6.6B), both BxPC-3 and MiaPaca-2 NADP+/NADPH ratios remained unchanged (control re-fed vs OA re-fed). Refed MiaPaca-2 demonstrated a 2-fold increase in NADPH ($p<0.01$); whereas HepG2 cells demonstrated a 3-fold increase in NADP+ ($p<0.0001$) compared to single fed MiaPaca-2 and HepG2 cells. Furthermore, upon re feeding with OA, HepG2 cells increased NADPH significantly ($p<0.0001$), whereas no changes were seen in BxPC-3 and MiaPaca-2 cells (Figure 6.6B).

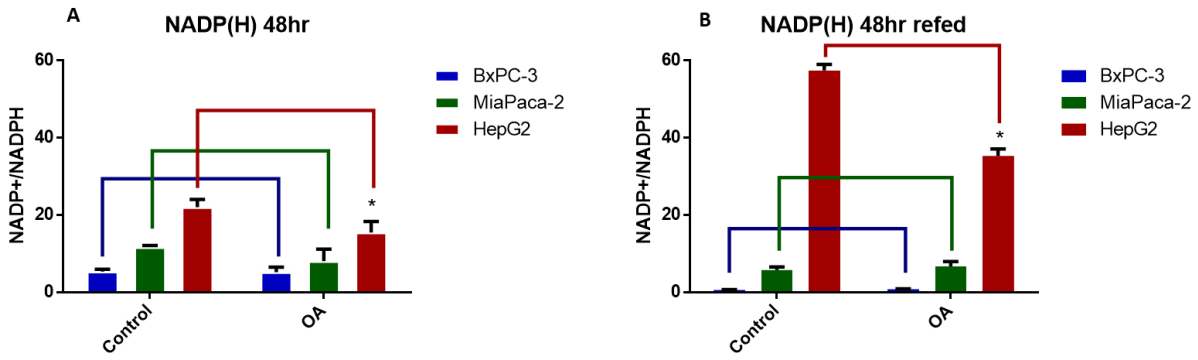

Figure 6.6 – OA mediated alterations in the NADP+/NADPH ratio
Graph **(A)** demonstrates the changes in the NADP+/NADPH ratio during treatment with and without 300μM OA over a 48 hour period. Graph **(B)** demonstrates the changes in the NADP+/NADPH ratio during treatment with and without 300μM OA at 0 and 24 hours (n=3). Figure 6.6A (*) $p<0.05$, HepG2 OA vs control. Figure 6.6B (*) $p<0.0001$ HepG2 OA vs control.

6.3.4 NADPH labeling via [3-^{2}H] glucose and utilization by DNL

In order to demonstrate the interconnectivity between the PPP and DNL, BxPC-3, MiaPaca-2 and HepG2 cells were cultured with [3-^{2}H] glucose over a 48 hour period.

Furthermore, the effect of OA on reductive biosynthesis, i.e. the transfer of electrons from glucose to PA via NADPH (in the form of ^{2}H) was also measured. BxPC-3 cells demonstrated ~20% ($p<0.01$) reduction in M+1 enrichment but no significant changes in M+2 PA labeling. Unexpectedly, MiaPaca-2 which do not undergo oxidative PPP showed a larger reduction of ~20 and 35% for M+1 ($p<0.01$) and M+2 ($p<0.0001$) PA labeling. HepG2 cells, demonstrated no significant changes in M+1 enrichment and ~20% decrease ($p<0.001$) in M+2 enrichment (Figure 6.7).

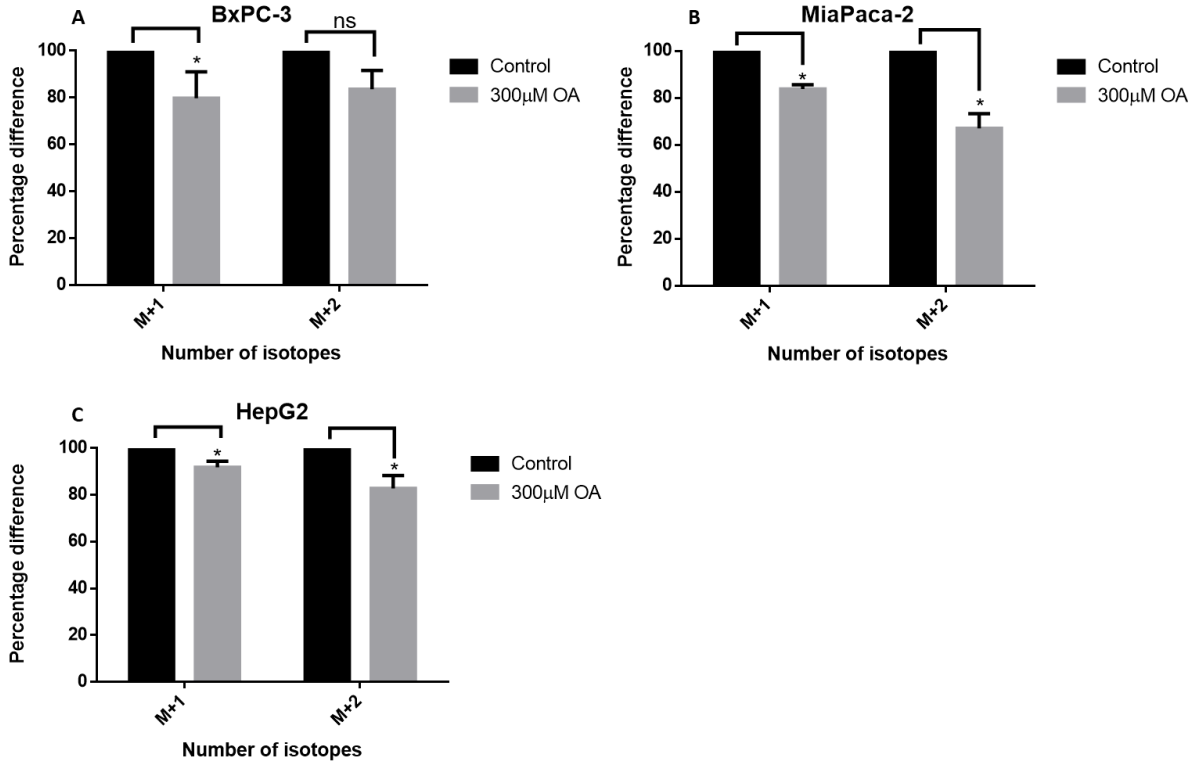

Figure 6.7 – [3-^{2}H] glucose derived DNL.
The above panel of graphs demonstrates the percentage change of M+1 and M+2 label in BxPC-3 and MiaPaca-2 and HepG2 cells derived from [3-^{2}H] glucose to palmitate over a 48 hour period (n=3), (*) statistical significance, (ns) no significance. The data was normalized based to the control for each experimental run on the day of acquisition.

6.3.5 Hydrogen peroxide and oleic acid supplementation mediated effects on cell growth – a pilot study.

Figure 6.2. demonstrates the hypothesis that exogenous OA causes an upregulation of NADPH by downregulating DNL and the PPP (Figures 5.5 and 6.4). NADPH is known to exert a role in reductive biosynthesis as well as ROS detoxification. Therefore, a preliminary study examining whether OA could ameliorate the toxic effects caused by H_2O_2 was conducted using BxPC-3, MiaPaca-2 and HepG2 cells. This experiment also provided preliminary information related to cell specific H_2O_2 tolerance when determining the dosages of H_2O_2 to use for this study. Prior to treating cells with H_2O_2, cells were cultured under 6.25, 12.5, 25, 50, 100 and 200μM H_2O_2, in order to identify the concentration by which cell growth reduced ~50%. BxPC-3 cells were able to tolerate 25μM (double the amount) of H_2O_2 compared to MiaPaca-2 cells (12.5μM H_2O_2), whereas HepG2 cells were cultured using 100μM of H_2O_2.

Figure 6.8A suggests a synergistic effect between H_2O_2 and OA causing further cell death in BxPC-3. In contrast, MiaPaca-2 and HepG2 cells demonstrate a minor rescue effect when cultured with both H_2O_2 and OA (Figure 6.8B and C). Replicate data is necessary to confirm these findings.

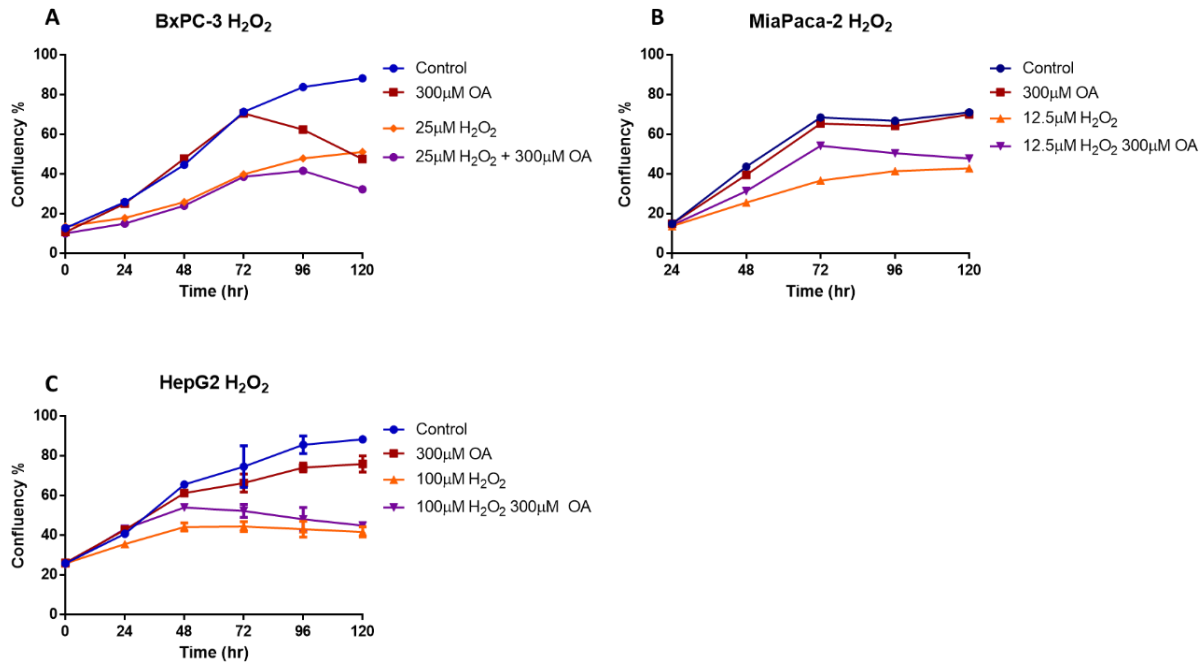

Figure 6.8 – H_2O_2 and OA mediated effects on cell growth
Graph **(A)** BxPC-3 cells cultured with both H_2O_2 and OA suggests a synergistic effect causing further cell death at 72 hours (n=1). Graphs **(B)** and **(C)** indicate that MiaPaca-2 and HepG2 cells, when cultured with both H_2O_2 and OA show a minor rescue effect by the addition of OA (n=1, n=2 respectively).

6.3.6 Association of NADPH generation and β-oxidation through Etomoxir mediated effects on cell growth

The CPT1 inhibitor etomoxir, was trialed at 0, 0.2, 0.4, 0.6, 0.8 and 1mM over a 5-day period, in order to identify the concentration for which cell growth is reduced by approximately 50% for each cell line (Figure 6.9). Results demonstrated that cells were sensitive to concentrations above 0.2mM, which caused growth arrest. Furthermore, HepG2 cells showed the highest level of sensitivity when treated with Etomoxir.

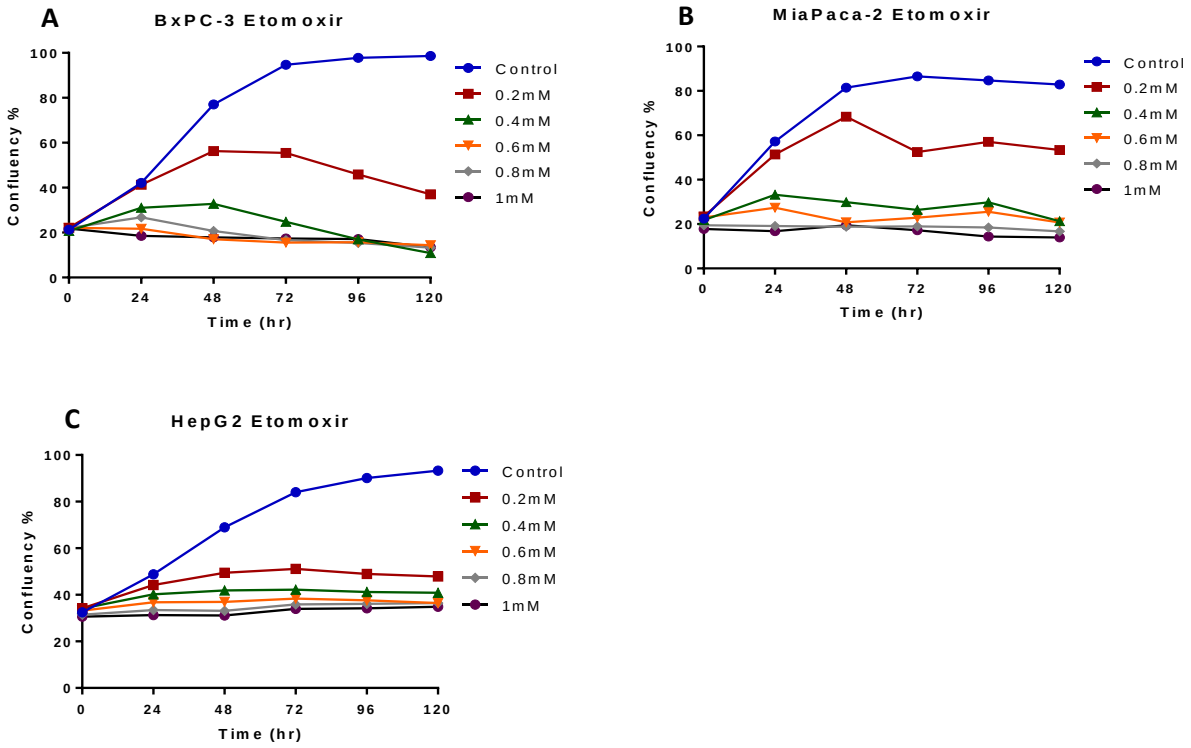

6.9 – Etomoxir mediated effects on cell growth

The above graphs demonstrate the effect of Etomoxir treated cells when treated with 0, 0.2, 0.4, 0.6, 0.8 and 1mM etomoxir. Concentrations above 0.2mM resulted in complete growth arrest (n=1).

6.3.7 Etomoxir and OA mediated effects on cell growth

BxPC-3, MiaPaca-2 and HepG2 cells were cultured using 0.2mM etomoxir and 300µM OA, to determine whether OA would be able to rescue the etomoxir induced growth arrest. The data demonstrates that addition of OA in etomoxir treated cells, produces the same growth profile as OA only treated cells for all cell lines (Figure 6.10).

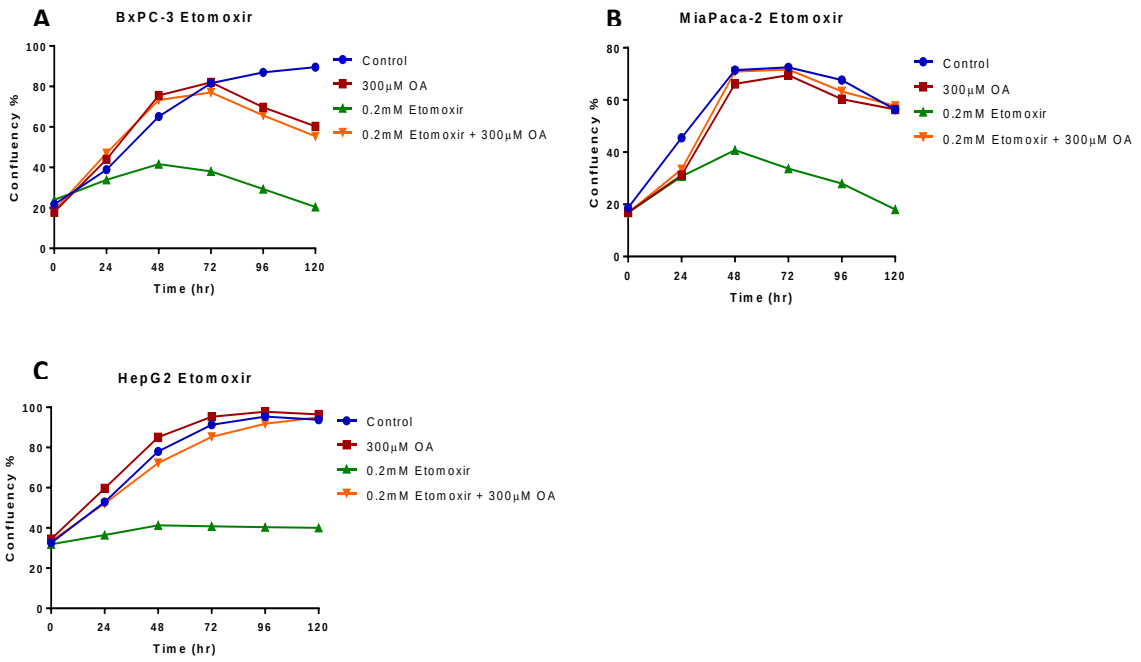

Figure 6.10 – Etomoxir and OA mediated effects on cell growth.
BxPC-3, MiaPaca-2 and HepG2 cells were treated with OA, etomoxir and etomoxir + OA. The data demonstrates that addition of OA to etomoxir treated cells restores cell growth to the exact proliferative phenotype of OA only treated cells (n=1).

6.3.8 Etomoxir and OA mediated effects on ACADVL and ACADM expression

In order to further characterise the effect of OA on β-oxidation, changes in the expression levels of ACADVL and ACADM were examined via Western blotting. This section focused on comparing BxPC-3 and MiaPaca-2 cells (n=3) whereas HepG2 cells were only examined qualitatively (n=1). Figures 6.12 and 6.13 demonstrate that MiaPaca-2 cells express both β-oxidation enzymes (ACADVL and ACADM) at ~2.5 and 2-fold higher concentration compared to BxPC-3 cells ($p<0.0001$). Furthermore, the ACADVL band migrates several kDa further in OA (and OA + etomoxir treated cells), compared to control (and etomoxir treated only) cells. This was evident in all three cell lines at both 24 and 48 hours of treatment (Figure 6.10).

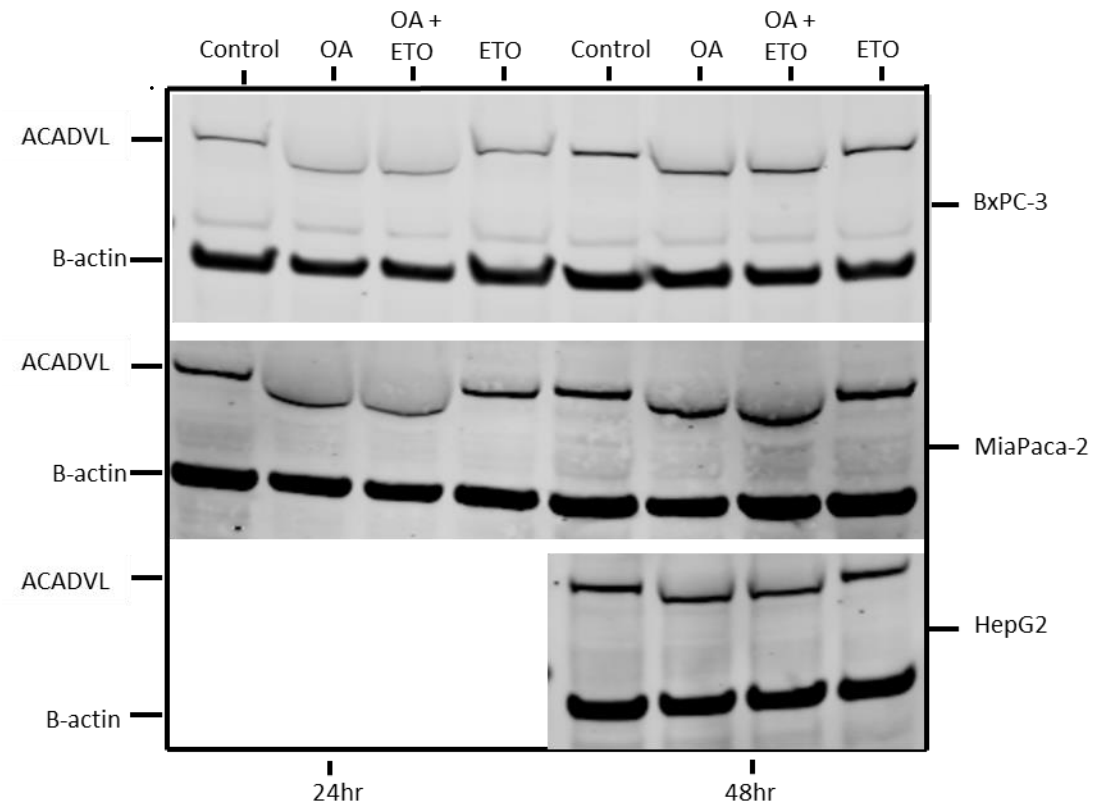

Figure 6.11 – Etomoxir and OA mediated effects on ACADVL expression
BxPC-3, MiaPaca-2 and HepG2 cells treated with OA, etomoxir and etomoxir + OA. The data demonstrates that addition of OA along with OA and etomoxir causes a shift in the detection of the ACADVL band at both 24 and 48 hours (BxPC-3 n=3, MiaPaca-2 n=3, HepG2 n=1).

Densitometry analysis revealed no changes in BxPC-3 cells upon addition of OA, however MiaPaca-2 cells demonstrated a significant drop ($p<0.0001$) in ACADVL expression (Figure 6.11).

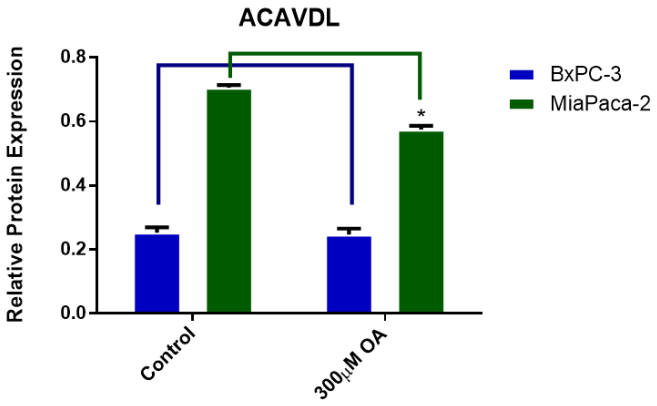

Figure 6.12 – OA mediated effects on ACADVL expression
BxPC-3 express ~3-fold lower quantities of ACADVL compared to MiaPaca-2 cells. Furthermore, no changes are noted in BxPC-3 cells upon addition of OA compared to MiaPaca-2 cells which demonstrate a statistically significant reduction in ACADVL expression (n=3) statistically significant (*) ($p<0.0001$).

Changes in the expression levels of ACADM, upon addition of OA were also investigated. BxPC-3 and MiaPaca-2 cells showed no statistically significant changes upon addition of OA (Figure 6.13).

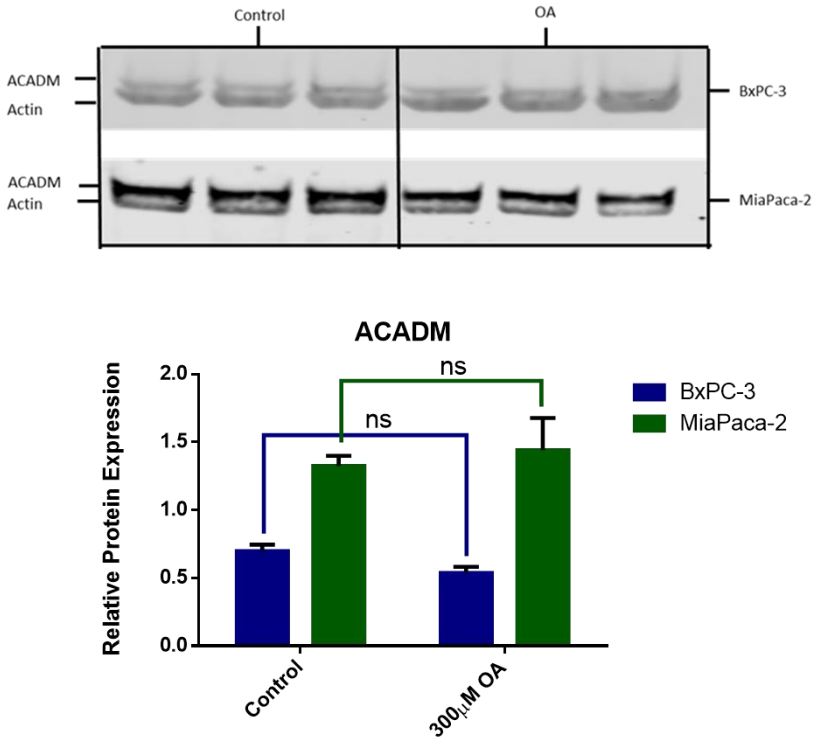

Figure 6.13 – OA mediated effects on ACADM expression
MiaPaca-2 cells express ~2-fold higher quantities of ACADM compared to BxPC-3 cells (when comparing both control and treated cells respectively). Furthermore, no changes were noted in ACADM expression in BxPC-3 and MiaPaca-2 cells upon addition of OA (n=3), not significant (ns).

6.3.9 Oleic acid mediated effects on ACADVL investigated via Immunoprecipitation

An immunoprecipitation (IP) experiment was performed in order to investigate the shift in migration that was demonstrated ACADVL in OA treated cells (Figures 6.11). Since MiaPaca-2 cells demonstrated significantly higher quantities of ACADVL compared to BxPC-3 cells, preliminary data was only produced using MiaPaca-2 cells. Figure 6.14 demonstrates that IP was able to successfully isolate the ACADVL enzyme whereas the ACADVL band was absent in OA treated cells (see Appendix 1 Figure 1.2).

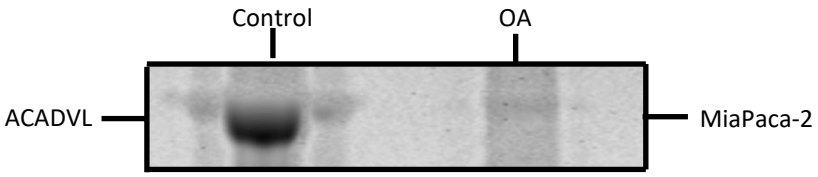

Figure 6.14 – OA mediated effects on ACADVL.
IP analysis revealed that OA treated cells are negative for ACADVL.

6.4 Discussion

The PPP and DNL are processes which should no longer be thought as independent metabolic pathways, but as two tightly interconnected pathways, which are mutually dependent. The PPP exerts a critical role in nucleotide synthesis and NADPH production through the oxidation of glucose and subsequently the reduction of NADP+ to NADPH. Furthermore, DNL utilizes NADPH to reduce fatty acid acyl chains, thus enabling FA synthesis and by extend oxidizing NADPH to NADP+. The interconnection between the two pathways, through the interconversion between NADP+ and NADPH is a tightly coupled mechanism, necessary to maintain reductive biosynthesis and redox homeostasis (Lewis *et al*., 2014). In order to examine changes in the PPP via the addition of OA, G6PD activity was measured. BxPC-3 cells treated over a 48 hour period demonstrated ~50% reduction in G6PD activity ($p<0.01$), whereas HepG2 and MiaPaca-2 cell activity remained unchanged. The data is in agreement with the hypothesis stating, “a reduction in DNL will reduce NADP+ availability and subsequently reduce PPP flux”. Moreover, upon refeeding at 24 hours with control media, BxPC-3 and MiaPaca-2 cells demonstrated a 2-fold increase in G6PD activity, without displaying any statistically significant changes when refed with OA supplemented media.

Oleic acid has been shown to cause changes in cell proliferation, DNL and the PPP in BxPC-3 cells, whereas MiaPaca-2 only demonstrate changes in DNL. Therefore, due to the interconnection between the PPP and DNL it was hypothesized that OA would influence the ratio of the NADP+/NADPH. However, Figure 6.6 demonstrates that the

hypothesis is true only for HepG2 cells and no significant changes were shown in BxPC-3 and MiaPaca-2 cells. Moreover, upon refeeding cells at 24 hours HepG2 cells showed a 3-fold increase in NADPH compared to control cells and ~30% increase in NADPH when refed with OA supplemented media.

The NADP+/NADPH assay demonstrated that NADP+ is available in higher quantities to NADPH, with HepG2 cells demonstrating the highest NADP+/NADPH ratio. Moreover, HepG2 cells are known to be highly lipogenic (Nelson *et al*., 2017) and due to the liver's metabolically active phenotype, HepG2 cells have been described as a metabolically flexible cell line (Amoêdo *et al*., 2013). Therefore, although addition of OA may cause an increase in NADPH (Figure 6.6), the default higher levels of NADP+ may be able to compensate for the NADP+/NADPH imbalance and allow the PPP to proceed without causing any disruptions. However, no statistically significant changes were shown upon addition of OA to BxPC-3 and MiaPaca-2 cells. The NADP+/NADPH assay measures total cell NADP+/NADPH; therefore, due to contamination of cytosolic and mitochondrial NADP+/NADP the assay's sensitivity may have been impacted. In order to accurately examine changes in the NADP/NADPH ratio, compartment specific (i.e. cytosolic/mitochondrial) quantification of NADP/NADPH may need to be performed.

In order to demonstrate the interconnectivity between the PPP and DNL a method developed by Lewis *et al* (2014) using [3-^{2}H] glucose had been deployed. NADP+ is reduced to NADPH during oxidation of [3-^{2}H] glucose via the PPP which is then used to reduce acyl chains during DNL (Lewis *et al*., 2014). This approach can be used to provide insights into compartment-specific redox reactions. It has been previously

established using lung cancer cell lines H1299 and A549, that lipogenic NADPH obtained via [3-^{2}H] glucose accounts for ~15-20% of the total NADPH used for PA synthesis (Lewis *et al*., 2014). H1299 and A549 cells are KRAS WT, and therefore provided a good model for calculating NADPH contribution to DNL via the PPP (since they both rely on the oxidative arm of the PPP). BxPC-3, MiaPaca-2 and HepG2 cells demonstrated a reduction in ^{2}H incorporation into PA varying between ~10-35% when treated with OA. This was also apparent in KRAS positive MiaPaca-2 cells which utilize the non-oxidative arm of the PPP (Lyssiotis *et al*., 2013). Therefore, the data suggests that MiaPaca-2 cells generate a portion of their NADPH via the oxidative arm of the PPP, whilst retaining the metabolic flexibility to switch to the non-oxidative arm when required.

Although depletion of NADP+ to NADPH may cause growth arrest (BxPC-3) an increase in NADPH may provide increased capacity to combat ROS. MiaPaca-2 cells display a mesenchymal phenotype due to poor differentiation, faster doubling rates, a high metastatic potential and are KRAS positive when compared to BxPC-3 cells which demonstrate an epithelial phenotype. Interestingly, BxPC-3 cells were able to tolerate double the concentration of H_2O_2 (25μM) compared to MiaPaca-2 cells (12.5μM). Although a KRAS mutation provides the cell with multiple proliferative/survival advantages, i.e. growth under hypoxic conditions, which is essential for pancreatic cancers as they are by nature hypoxic, it may also inadvertently result in weaknesses. The data demonstrates that BxPC-3 cells are sensitive to changes in lipid metabolism compared to MiaPaca-2 cells; however, since they are able to tolerate double the concentration of H_2O_2, this may indicate stronger antioxidant protection mechanisms.

Since KRAS positive cells utilise the non-oxidative arm of the PPP, they are dependent on the non-canonical pathway for generating NADPH, which requires upregulation of GLUT1 and depends on the anaplerotic pathway of glutamine and ME1 (Lyssiotis *et al*., 2013). Although rerouting metabolic pathways must meet the biosynthetic and redox demands to sustain cell survival and proliferation under hypoxic conditions; NADPH generation may be less efficient which subsequently renders the cell less capable to combat ROS. However, by reducing DNL which is possible for all cell lines investigated, a higher portion of the NADPH pool can be utilized for neutralizing ROS.

The aforementioned hypothesis is supported by Nelson *et al* (2014) demonstrating that inhibition of hepatic DNL enhances tumourigenesis by increasing antioxidant defense (Nelson *et al*., 2017). Hepatic DNL was inhibited by knocking out ACC in mice treated with the hepatocellular carcinogen diethylnitrosamine. Mice lacking ACC, demonstrated a 2-fold increase in tumour incidence and tumour proliferation compared to controls. Moreover, a 25% increase in NADPH was shown which subsequently reduced GSSH to GSH, enhancing antioxidant defense mechanisms (Nelson *et al*., 2017).

Moreover, considering the hypothesis that OA causes decrease in the NADP+/NADPH ratio due to a down regulation of DNL, it was further hypothesised that addition of OA may increase the rate of β-oxidation; therefore, increasing NADPH levels. Figure 4.4B demonstrates that OA treated MiaPaca-2 cells are able to reduce TG to baseline levels in 96 hours, compared to BxPC-3 cells. Beta-oxidation prevents cell lipotoxiticy by maintaining homeostatic lipid levels when overloaded with lipid (Samudio *et al*., 2010). Each cycle of β-oxidation generates one molecule of acetyl-CoA, which enters the TCA

cycle. Increased fueling of the TCA cycle gives rise to citrate, which is then exported into the cytosol and is metabolised either by ME1 or IDH1. Both pathways give rise to NADPH (Pike *et al*., 2011). Therefore, it is expected that OA treated cells will have a higher capacity to neutralise ROS due to the increased levels of NADPH. Figure 6.8 demonstrates that a synergistic effect is shown in BxPC-3 cells when treated with both OA and H_2O_2 causing further cell death, whereas MiaPaca-2 and HepG2 cells show increased proliferation in OA and H_2O_2 treated cells compared to H_2O_2 treated cells alone. The OA appearing to have an antioxidant effect.

Due to the different genetic phenotypes (KRAS) of BxPC-3 and MiaPaca-2 cells, it was anticipated that they would demonstrate varying levels and dependencies on β-oxidation. The CPT1 blocker etomoxir (which blocks CPT1), was trialed at different concentrations to identify which concentrations inhibited cell growth by ~50% and the degree to which cells were dependent on β-oxidation. All three cell lines were shown to inhibit cell growth at concentrations >2mM, indicating that all the cells required β-oxidation. Furthermore, the effects of culturing cells with both etomoxir and OA were examined. Interestingly, upon addition of OA to etomoxir treated cells, the etomoxir induced growth phenotype was fully replaced by the OA only treated phenotype. This suggests that etomoxir was unable to effectively block CPT1 in the presence of OA or that the effects of blocking CPT1 become inconsequential with the addition of OA. Previous studies have reported that OA incubation in myotubes resulted in a 3.7-fold increase in CPT1 expression (Henique *et al*., 2010). Increased levels of CPT1 may render etomoxir ineffective, as β-oxidation would be restored. Further investigation via either RT-PCR or Western blotting, examining CPT1 expression would provide further

information on this mechanism. Alternatively, this may also suggest an intricate nutrient sensing gene inducing mechanism which is able to override the effect of the inhibitor.

Furthermore, the effects of OA and etomoxir on β-oxidation were further examined by measuring changes in expression levels of ACADM and ACADVL (by Western blot), two enzymes located in the mitochondria involved in the oxidation of medium and long chained FA chains respectively (Gregersen *et al*., 2001). Western blot analysis revealed that MiaPaca-2 cells, contained 3 and 2-fold higher quantities of ACADVL and ACADM than BxPC-3 cells respectively. No statistically significant changes were noted for either cell line regarding the expression of ACADM upon treatment with OA.

A decrease in ACADVL expression occurred upon addition of OA in MiaPaca-2 cells. This may indicate that MiaPaca-2 cells are able to respond to the influx of lipid more efficiently than BxPC-3 cells. Since DNL is downregulated upon treatment with OA, by reducing ACADVL expression, MiaPaca-2 cells also reduce lipid oxidation, which may suggest that the exogenous lipid is being utilized not only for bioenergetic and redox purposes, but also for biosynthesis. This hypothesis requires further investigation.

When refeeding cells with fresh media (with and without OA), the NADP/NADPH ratio and G6PD activity had increased. This would suggest that if cell growth was reduced due to the addition of OA, refeeding the cells with fresh media with and without OA, may restore cell proliferation. Indeed, as suggested by Figure 6.5, cells treated with fresh control media restore growth immediately, whereas OA treated cells demonstrated a 24 hour delay, before also restoring cell proliferation. In order for this phenomenon to be explained, further experiments such as investigating nutrient specific gene expression responses must be performed.

An unexpected phenomenon was observed during examination of ACADVL expression upon addition of OA via Western blotting. The ACADVL band migrated several kDa further compared to the control band, in MiaPaca-2, BxPC-3 and HepG2 cells. In order to further characterise this result immunoprecipitation (IP) analysis was performed. IP successfully isolated the control ACADVL protein; however, OA treated cells appeared to be negative. Antibodies which are suitable for IP are able to bind to an epitope which is present under native conditions, whilst the protein retains its tertiary structure. However, antibodies which are typically suitable only for Western blot, can only bind to the epitope during reduced conditions once the protein is linearized. Two possible explanations may account for the antibody not binding to the native protein when incubated with OA.

Firstly, it can be hypothesised that OA treatment induces increased lipidation of the ACADVL protein. As in the case of the autophagy protein LC3, it exists in two states, a lipidated (LC3-II) and non-lipidated (LC3-I) form. LC3-II although a larger protein (due to increased lipidation), has a higher molecular weight, and is therefore detected above LC3-I. However, LC3-II shows faster electrophoretic mobility in SDS-PAGE gels, due to increased hydrophobicity (Dancourt and Melia, 2014). Perhaps this may also be the case of ACADVL upon treatment with OA. Increased lipidation may increase ACADVL's electrophoretic mobility to change when detected by Western blot. Additionally, OA may have masked the antibody binding sites, thus presenting a physical barrier for the ACADVL antibody to bind its target epitope. It must be noted that this effect was not noted with any of the other proteins when incubated with OA and analysed by Western blotting.

Alternatively, OA may be inducing the expression of an ACADVL splice variant. Although the epitope is present in both variants, the splice variant may have a different tertiary structure with the epitope being internalized. Therefore, the epitope would only be accessible to the antibody when linearized for detection via Western blotting. Indeed, by searching the ENSEMBL database, it was revealed there are 39 transcripts for the ACADVL gene, eight of which are predicted to encode a protein. There are 4 transcripts for which the coding sequence is complete, 3 of which are predicted protein coding and 1 predicted to undergo nonsense-mediated decay. These variants were predicted using Expasy and a shift between two of these variants was found to be consistent with the size difference demonstrated by Western blot analysis. The difference in size of the three variants 203, 205 and 202 was 70.4, 72.3 and 68.1kDa.

The transcripts 203 and 202 differ in terms of domains by the inclusion of an intrinsically disordered region in the N' domain of the 203 protein that is absent in the 202 protein. The protein encoded by the 205 variants also has two intrinsically disordered domains at the N', but interestingly it has a signal peptide and is predicted to be a non-cytoplasmic protein, either secreted or possibly transmembrane (Phobius predicted analysis). Further investigation of the potential ACADVL variants using RT-PCR is necessary, in order to determine both their presence and expression levels.

The aim of Chapter 6 was to demonstrate the interconnection between the PPP and DNL and furthermore, to provide evidence that OA causes an increase in NADPH which results in downregulation of the PPP due to the unavailability of NADP+. Although the interconnectivity between the two pathways was demonstrated by culturing cells using [3-^{2}H] glucose, the NADP+/NADPH assay was only able to

conceptually demonstrate that OA causes a change in the NADP+/NADPH ratio in HepG2 cells. Since the assay measured total NADP+/NADPH, it was unable to provide data supporting this hypothesis for BxPC-3 and MiaPaca-2 cells. Although, additional supporting data was obtained such as decreased G6PD activity upon treatment with OA, it is essential that NADP+ and NADPH are quantitatively measured in a compartmentalized manner. Future studies can deploy a method developed by Lewis *et al* (2014) using liquid chromatography mass spectrometry to measure NADP+/NADPH.

In order to further characterize whether OA exerts an antioxidant role by increasing NADPH levels, in addition to completing the necessary replicates for Figure 6.8, the GSH/GSSG ratio must be examined. Oxidized glutathione (GSSG) is reduced by G6PD generated NADPH to GSH. GSH is responsible for neutralizing ROS and maintaining a reduced intracellular environment (Berg et al., 2007).

Finally, in addition to examining OA mediated changes in β-oxidation by measuring changes in ACADVL and ACADM expression levels further investigation remains necessary. Future studies can utilise radioactive palmitate in control and OA treated cells to directly measure changes in β-oxidation. Oxidation of ^{14}C-labelled palmitate via β-oxidation generates acetyl-CoA, which is further oxidised to CO_2 via the TCA cycle. By measuring the amount of CO_2 generated using scintillation counting, a more comprehensive understanding can be obtained regarding baseline levels and changes in the rate of β-oxidation (Huynh et al., 2014).

Chapter 7 – General Discussion

It is now well established that metabolic reprogramming is one of the defining characteristics of carcinogenesis, enabling the cell to meet its bioenergetic and biosynthetic demands. Most cancer cells have been shown to exhibit a high dependence towards lipids, which is expected as they are an energy rich source, as well as precursors for the biosynthesis of cell membranes and mediators of signaling processes (Beloribi-Djefaflia *et al*., 2016). Furthermore, cancer cells upregulate DNL in order to meet their high lipid requirements, even in cases where they are located in areas with high levels of exogenous lipid. For example, tumours have been shown to form metastasis or grow in close proximity to adipose tissue (breast cancer), which is an important source of fatty acids but still upregulate DNL (Kinlaw *et al*., 2016).

Data from Ehrlich ascites (an undifferentiated carcinoma) suggests that cancer cells synthesize >93% of their triacylglycerides *de novo*, irrespective of being able to utilize FAs that can be obtained exogenously (Ookhtens *et al*., 1984, Menendez and Lupu, 2007). This apparent contradiction has been the motivation behind this study. Targeting features of lipid metabolism and DNL pathways have been viewed as promising targets for anti-cancer therapies. This thesis has focused on examining how manipulating the lipid environment through supplementation with oleic acid (OA), may differentially alter the metabolism and subsequent proliferation of a panel of pancreatic cancer cell lines, which possess different levels of metastatic potential as well as differentiation. This can provide new insights to the changes in metabolism involved in specific cell lines and their dependencies on lipids.

Initially, a panel of pancreatic cancer cell lines, including HepG2 liver cells which is used as a comparative cell line and SH-SY5Y (positive control for Twist) were profiled to determine EMT status as well as glucose dependency for both proliferation and DNL. The data demonstrated that BxPC-3 and MiaPaca-2 cells were the most epithelial and mesenchymal pancreatic cells lines respectively. Furthermore, BxPC-3 cells showed higher levels of glucose dependency when compared to MiaPaca-2 cells. This was indicated by BxPC-3 cells being unable to proliferate under low glucose concentrations, whereas MiaPaca-2 cells demonstrated glucose concentration dependent growth, supporting higher rates of growth under reduced glucose conditions. This phenomenon was also apparent in MiaPaca-2 and HepG2 cells in relation to DNL. These cell lines demonstrated glucose concentration dependent changes in palmitate enrichment, whereas AsPC-1, BxPC-3 and Capan-1 cells, showed similar levels of palmitate enrichment, irrespective of glucose concentration. This is indicative of nutrient sensing mechanisms and a potential target to examine would be ChREBP. ChREBP expression and activity has been shown to be influenced by cellular levels of nutrients and has been described as a master regulator of glycolytic and lipogenic enzymes (Hatzivassiliou *et al*., 2005a). Therefore, multiple metabolic phenotypes may result depending on baseline ChREBP expression levels (Tong *et al*., 2009).

Cell growth in relation to confluence was assessed, with BxPC-3 and Capan-1 cells showing a reduction in growth post 48 hours upon the addition of OA, whereas AsPC-1, MiaPaca-2 and HepG2 cells remained unaffected when supplemented with OA. The effects of supplementation with OA on cell growth was assessed using the IncuCyte real-time imaging system. BxPC-3 and Capan-1 cells showed a reduction in growth,

post 48 hours, upon the addition of 300μM OA, whereas AsPC-1, MiaPaca-2 and HepG2 cell growth was unaffected. Furthermore, CFSE staining and cell cycle distribution was also examined to monitor effects on cell proliferation. Confirmatory results with CFSE staining at 48 hours demonstrated a 14% reduction in BxPC-3 cell proliferation when compared to MiaPaca-2 and HepG2 cells which remained unaffected when cell lines were supplemented with OA. Furthermore, only 50% of cells were able to re-enter S-phase in OA treated compared to untreated BxPC-3 cells, whereas MiaPaca-2 cells demonstrated a 2.8 and 2.3-fold increase in both S and G2/M phase respectively when supplemented with OA. Therefore, three independent experimental approaches demonstrate that BxPC-3 proliferation decreases upon addition of OA.

Cell cycle arrest at S-Phase and induction of apoptosis has been reported in various pancreatic cancer cell lines. These effects can be induced by the addition of specialized lipids such as sphingolipids (Yamada *et al*., 1997) and polyunsaturated fatty acids such as eicosapentaenoic acid which have been shown to have potent effects on cell growth at low concentrations (50μM) (Lai *et al*., 1996). The aforementioned study showed that these effects in MiaPaca-2 cells were consistent with two other unnamed pancreatic cell lines, suggesting a common cytotoxic mechanism of action which may be involved with the production of prostaglandins. The present study suggests the effects mediated by OA are dependent on the phenotype of the cell line under investigation. Studies in a panel of breast and gastric cancer cell lines, which were incubated with 400μM OA for a period of up to 72 hours showed that OA promoted cell proliferation in high metastatic cancer cells but had an inhibitory effect in low metastatic cancer cells,

providing evidence that cancer cells can show specific adaptations to different aspects of lipid metabolism. The study suggested that this was mediated by the activation of AMPK which enabled cellular plasticity by enhancing β-oxidation (Li *et al*., 2014). To account for these differences, it was first decided to demonstrate that all cells could take up the lipids at similar rates. Forty-eight-hour exposure to OA demonstrated similar increases in intracellular TG levels in all cell lines. However, following 96 hours BxPC-3 cells still retained a significant amount TG; whereas, MiaPaca-2 cells had significantly reduced TG concentrations to basal levels. This result may indicate that MiaPaca-2 cells are able to utilize their TG stores in comparison to BxPC-3 cells. This can be achieved by utilizing lipids to either provide energy (β-oxidation) or, building blocks for biosynthesis. Chapter 6 demonstrates that β-oxidation enzymes ACADVL and ACADM were expressed at 2-3-fold higher quantities in MiaPaca-2 compared to BxPC-3 cells which suggests that BxPC-3 cells are less able to utilise β-oxidation pathways. This could explain why higher levels of TG were detected in BxPC-3 compared to MiaPaca-2 cells.

In addition, data also suggested that supplementation with OA induced apoptosis in BxPC-3 cells, as measured by annexin V staining. Although this result needs to be confirmed with an alternative method, the data suggests that BxPC-3 cell death is mediated via apoptosis.

Cells were then characterized in terms of their autophagic flux by examining LC3-II accumulation. Preliminary results indicate that the metabolic phenotype of BxPC-3 cells is more dependent on self-catabolic processes mediated via autophagy for the intracellular acquisition of nutrients compared to MiaPaca-2 and HepG2 cells, even

when cultured under standard conditions. This implies the control mechanisms for TG store lipolysis may differ between pancreatic cancer cell lines. If BxPC3 cells are more dependent on the autophagic control of lipolysis, this may have implications for the utilization of TG (lipophagy) under conditions of stress or nutrient depletion. Similar concentrations of the fatty acids used in this study have been shown to suppress autophagic turnover in B-cells (Las *et al*., 2011). This may limit the utilization of lipids and provide an explanation for the retention of TG.

BxPC-3 and MiaPaca-2 cells stored negligible basal TG levels. Increasing intracellular TG concentration would result in lipotoxicity (Liu and Czaja, 2013), if the cell was not able to restore basal TG concentrations. Therefore, by downregulating lipid synthesis the cell may be attempting to prevent lipotoxicity.

Furthermore, since MiaPaca-2 cells are KRAS positive, they utilise the oxidative arm of the PPP to synthesise NADPH via the anaplerotic pathway which utilises glutamine and depends on citrate metabolism via IDH1 and ME1 (Lyssiotis *et al*., 2013). As β-oxidation generates acetyl-CoA which fuels the TCA cycle, thus increasing the export of citrate, it is anticipated that MiaPaca-2 cells will have higher quantities of β-oxidation enzymes in order to generate NADPH, and be able to utilize stored TG levels to fuel β-oxidation more efficiently than BxPC-3 cells.

In order to provide further insight into the mechanisms that cause reduced proliferation upon addition of OA in BxPC-3 cells and not MiaPaca-2 cells, changes in DNL were examined. The expression of FAS and ACC the enzymes which catalyse the synthesis of saturated FAs and malonyl-CoA respectively, were examined by Western blotting. ACC which is considered the rate-determining step of the lipogenic pathway was

expressed at 15-fold higher quantities in MiaPaca-2 and HepG2 cells when compared to BxPC-3 cells. Upon addition of OA, MiaPaca-2 cells were able to downregulate ACC expression which is in agreement with published data (Natali *et al*., 2007). The study showed that decreased DNL in glial cells was manifested by an 80% reduction in ACC expression but no changes in FAS activity. A decrease in DNL was induced by the addition of 100μM OA. This indicates that MiaPaca-2 cells are more capable in modulating their lipid content to homeostatic levels, thus preventing lipotoxicity.

DNL was also interrogated by use of stable isotopes to monitor changes in carbon fluxes from glucose and glutamine substrates towards palmitate synthesis. BxPC-3 and AsPC-1 cells demonstrated ~50-60% drop in enrichment derived from ^{13}C glucose. MiaPaca-2 and Capan-1 cells showed a decrease of ~30-40%, whereas HepG2 cells were unaffected. As indicated by the data relating to TG content, HepG2 cells have a high capacity for lipid storage, as well as being a major lipogenic tissue (Bechmann *et al*., 2012). It is therefore anticipated that an exogenous lipid influx would not necessarily influence DNL. Interestingly, the data demonstrates that all pancreatic cancer cell lines irrespective of their genomic profile decreased glucose derived carbon contribution by 30-60%, implying they were able to regulate metabolic pathways involved in directing glucose to acetyl-CoA. BxPC-3 and MiaPaca-2 cells store negligible basal levels of TG. Perturbing this system by acutely increasing intracellular TG concentration would result in lipotoxicity (Liu and Czaja, 2013; Quiroga and Lehner, 2012), unless TG levels returned to baseline concentrations. Therefore, by downregulating lipid synthesis the cell may be attempting to prevent lipotoxicity.

Furthermore, changes in the contribution of glutamine derived carbon towards palmitate synthesis was assessed upon addition of OA. MiaPaca-2 cells demonstrated no changes in enrichment of the M+1 label. However, BxPC-3 cells appeared to increase glutamine contribution by ~30%. This is suggestive of an increase in the anaplerotic pathway, and an increase in citrate export from the TCA cycle. An increase of citrate export would potentially increase carbon contribution towards DNL (as supplied by glutamine but reduced via glucose for this cell line). However, it will also increase IDH1 and ME1 metabolism, thus increasing NADPH generation. This may account for the increased stored TG as well as an attempt by BxPC-3 cells to increase levels of NADPH but inadvertently also increasing intracellular substrates for lipid synthesis (citrate) or acetyl-CoA.

BxPC-3, MiaPaca-2 and HepG2 cells were also shown to reduce ^{2}H contribution to palmitate upon addition of OA by ~10-35%. Under basal conditions, the cell contains higher concentrations of NADP+ to NADPH. However, as the addition of OA causes a reduction in NADPH oxidation, it may cause an imbalance in the NADP+/NADPH ratio.

Upon examination of the NADP+/NADPH ratio, only HepG2 cells demonstrated an increase in NADPH. Evidence supporting the hypothesis that OA will downregulate DNL and increase NADPH was only demonstrated in HepG2 cells, which have a high NADP+/NADPH ratio and could therefore tolerate a shift in ratio not detrimental to cell growth. Furthermore, a 50% reduction of G6PD activity was noted in BxPC-3 cells upon addition of OA, whereas MiaPaca-2 and HepG2 cells were unaffected. Therefore, the data suggests that reducing the rate of DNL may also reduce the rate of the PPP in BxPC3 cells, but not in MiaPaca-2 or HepG2 cells. Interestingly, refeeding the cells at

24 hours with both fresh and OA supplemented media, demonstrated a 2-fold increase in G6PD activity, with no significant changes being found between control and OA treated cells. This would suggest reversibility; indeed, preliminary data supports this statement as growth was restored.

In order to provide supporting evidence regarding the hypothesis that downregulation of DNL via exogenously supplied OA causes an increase in NADPH concentration, cell proliferation was monitored upon treatment with OA and OA/H_2O_2 treated cells. Interestingly, although BxPC-3 cells resemble an epithelial like phenotype, compared to MiaPaca-2 cells (mesenchymal), they were found to be able to tolerate twice the amount of H_2O_2 as MiaPaca-2 cells. BxPC-3 cells depend on the oxidative arm of the PPP to generate NADPH, and MiaPaca-2 cells are dependent on citrate metabolism via IDH1 and ME1, which further implies that the oxidative arm of the PPP is more efficient in generating NADPH. Furthermore, a synergistic effect was noted whereby the addition of OA and H_2O_2 caused further decreases in BxPC3 cell proliferation.

Finally, indirect changes in β-oxidation and its influence on generating NADPH were examined upon addition of OA. Interestingly, cells treated with both etomoxir (an inhibitor of CPT1) and OA demonstrated full recovery and reverted to the OA only treated growth phenotype. This suggests, that CPT1 expression could be increased upon treatment with OA, and that etomoxir is unable to block β-oxidation effectively at the concentration used (0.2mM) as determined in this study.

Collectively, this study has provided a novel understanding in metabolite driven expression profiles between genetically diverse cell lines. It has demonstrated that cell death via apoptosis can be induced in cells by the addition of a neutral fatty acid.

Furthermore, until recently DNL has only been able to be manipulated via small molecule inhibitors or siRNA methods. This study demonstrates that DNL can be manipulated by the addition of a neutral FA provided exogenously at physiological concentrations in cancer cells.

This study provides insight to how lipid metabolism is interconnected with nucleotide synthesis and that these two processes are mutually dependent. This is in agreement with published data, demonstrating that the rate limiting step for cancer cell growth is not a lack of energy in the form of ATP, but maintaining the optimal balance of NADP+/NADPH (Lewis et al., 2014; Fan et al., 2014). Perturbing the NADP+/NADPH balance can cause a disruption in anabolic processes which will have detrimental effects on cancer cell survival.

A KRAS positive tumour will be able to utilise the non-oxidative arm of the PPP, which will enhance its proliferative capacity compared to KRAS WT BxPC-3 cells. DNL and the PPP are less likely to be as interdependent, as NADPH is produced via ME1 and IDH1 metabolism and not the PPP. Moreover, the increased capacity for undergoing β-oxidation for ATP and subsequently NADPH production by increasing the fuelling of the TCA cycle provides further advantages and reduces the likelihood of lipotoxcity. However, BxPC-3 cells which depend mostly on the PPP for NADPH generation, will have a higher capacity to generate NADPH and to combat ROS more effectively.

In conclusion, further experiments are required for characterising the molecular networks which regulate these metabolic processes. Specifically, changes in the expression levels of regulatory proteins such as ChERBP and AMPK must be investigated, to provide insight as to how cells can sense nutrient concentration levels

and regulate anabolic processes. Moreover, TG in media must be quantified before, after and during incubation with OA. This will determine whether the cells are able to secrete excess intracellular lipid to prevent cytotoxicity. Capan-1 cells, although being KRAS positive, demonstrated similar metabolic weaknesses as KRAS wild type BxPC-3 cells. Further research must be conducted in order to characterise this result. Moreover, upon refeeding at 24 hours, G6PD activity is restored, as well as cell proliferation. The same should be performed in cells cultured with [U-^{13}C] glucose to verify whether DNL can also be restored. Transcriptomic analysis upon addition of OA and on cells receiving a second dose of OA would greatly enhance our understanding of the molecular networks which regulate such metabolic pathways. Investigating changes in expression of the CPT1 protein upon addition of OA would also help explain as to why cells treated with both etomoxir and OA revert to an OA only treated phenotype. Furthermore, ACADVL expression and whether a potential splice variant is induced, or the protein is subjected to increased lipidation upon addition of OA must be further examined. Additionally, compartment specific quantification of NADP+/NADPH, will determine the extent to which OA perturbs the NADP+/NADPH balance. Finally, metabolomic analysis via computational algorithms mapping isotopic fluxes between various pathways whilst determining rates of metabolic pathways will provide more advanced clarification than that described by measures of changes in isotopic enrichment.

Data in relation to providing a descriptive analysis of the enrichment of single substrate was provided. This project did not however incorporate any data into computational flux models which provide the basis for information related to the changes in a given

metabolic network. This would need to be incorporated into any future studies and can be obtained by monitoring the labelling patterns obtained from substrates and combining this data with information related to the metabolic network stoichiometry and atom transition matrices (reaction networks). Future studies would need to incorporate the use of computational tools such as Metran software (available from the University of Delaware; Antoniewicz Lab) or INCA software (Vanderbilt University; Young Lab) which enable flux analysis. A recent paper has highlighted a clear need for guidelines that encourage good practice when considering experiments with flux analysis (Crown and Antoniewicz, 2013; Crown and Antoniewicz, 2013). The authors provided a check list for researchers to enhance the quality of published work with minimum information requirements for data related to the experimental design, the metabolic network under consideration, incorporation of growth rate data, providing clear descriptions of isotopomer distributions, descriptions of flux software packages used, measurement of goodness-of-fit data and a description of how confidence intervals were determined for the data obtained.

Appendix 1

Table 1.1 – Multiple comparison test for BxPC-3 cells

A two-way ANOVA was used to statistically analyse the dose response curves shown in figure 2 for BxPC-3 cells.

Two-way ANOVA for BxPC-3 cells

0hr

Test	Mean Diff.	95% CI of diff.	Significance
Control vs. 37.5µM	1.285	-7.952 to 10.52	No
Control vs. 75µM	2.183	-7.054 to 11.42	No
Control vs. 150µM	2.115	-7.122 to 11.35	No
Control vs. 300µM	2.449	-6.788 to 11.69	No
Control vs. 600µM	4.231	-5.006 to 13.47	No
37.5µM vs. 75µM	0.8978	-8.977 to 10.77	No
37.5µM vs. 150µM	0.8303	-9.044 to 10.70	No
37.5µM vs. 300µM	1.164	-8.710 to 11.04	No
37.5µM vs. 600µM	2.946	-6.928 to 12.82	No
75µM vs. 150µM	-0.06749	-9.942 to 9.807	No
75µM vs. 300µM	0.2663	-9.608 to 10.14	No
75µM vs. 600µM	2.048	-7.826 to 11.92	No
150µM vs. 300µM	0.3338	-9.541 to 10.21	No
150µM vs. 600µM	2.116	-7.759 to 11.99	No
300µM vs. 600µM	1.782	-8.093 to 11.66	No

24hr

Test	Mean Diff.	95% CI of diff.	Significance
Control vs. 37.5µM	5.19	-4.047 to 14.43	No
Control vs. 75µM	6.829	-2.408 to 16.07	No
Control vs. 150µM	5.224	-4.013 to 14.46	No
Control vs. 300µM	6.19	-3.047 to 15.43	No
Control vs. 600µM	10.52	1.279 to 19.75	Yes
37.5µM vs. 75µM	1.639	-8.236 to 11.51	No
37.5µM vs. 150µM	0.0334	-9.841 to 9.908	No
37.5µM vs. 300µM	0.9997	-8.875 to 10.87	No
37.5µM vs. 600µM	5.326	-4.549 to 15.20	No
75µM vs. 150µM	-1.605	-11.48 to 8.269	No
75µM vs. 300µM	-0.6391	-10.51 to 9.235	No
75µM vs. 600µM	3.687	-6.188 to 13.56	No
150µM vs. 300µM	0.9663	-8.908 to 10.84	No
150µM vs. 600µM	5.292	-4.582 to 15.17	No
300µM vs. 600µM	4.326	-5.549 to 14.20	No

48hr

Test	Mean Diff.	95% CI of diff.	Significance
Control vs. 37.5µM	6.349	-2.888 to 15.59	No
Control vs. 75µM	9.035	-0.2018 to 18.27	No
Control vs. 150µM	6.81	-2.427 to 16.05	No
Control vs. 300µM	9.329	0.09204 to 18.57	Yes
Control vs. 600µM	22	12.76 to 31.23	Yes
37.5µM vs. 75µM	2.686	-7.188 to 12.56	No
37.5µM vs. 150µM	0.4608	-9.414 to 10.34	No
37.5µM vs. 300µM	2.98	-6.894 to 12.85	No
37.5µM vs. 600µM	15.65	5.773 to 25.52	Yes
75µM vs. 150µM	-2.225	-12.10 to 7.649	No
75µM vs. 300µM	0.2938	-9.581 to 10.17	No
75µM vs. 600µM	12.96	3.087 to 22.84	Yes
150µM vs. 300µM	2.519	-7.355 to 12.39	No
150µM vs. 600µM	15.19	5.313 to 25.06	Yes
300µM vs. 600µM	12.67	2.793 to 22.54	Yes

72hr

Test	Mean Diff.	95% CI of diff.	Significance
Control vs. 37.5µM	1.422	-7.814 to 10.66	No
Control vs. 75µM	3.255	-5.982 to 12.49	No
Control vs. 150µM	5.171	-4.066 to 14.41	No
Control vs. 300µM	11.36	2.121 to 20.59	Yes
Control vs. 600µM	21.48	12.24 to 30.72	Yes
37.5µM vs. 75µM	1.832	-8.042 to 11.71	No
37.5µM vs. 150µM	3.749	-6.126 to 13.62	No
37.5µM vs. 300µM	9.936	0.06135 to 19.81	Yes
37.5µM vs. 600µM	20.06	10.18 to 29.93	Yes
75µM vs. 150µM	1.916	-7.958 to 11.79	No
75µM vs. 300µM	8.103	-1.771 to 17.98	No
75µM vs. 600µM	18.22	8.350 to 28.10	Yes
150µM vs. 300µM	6.187	-3.687 to 16.06	No
150µM vs. 600µM	16.31	6.433 to 26.18	Yes
300µM vs. 600µM	10.12	0.2461 to 20.00	Yes

96hr

Test	Mean Diff.	95% CI of diff.	Significance
Control vs. 37.5µM	0.5684	-8.668 to 9.805	No
Control vs. 75µM	2.049	-7.187 to 11.29	No
Control vs. 150µM	6.521	-2.716 to 15.76	No
Control vs. 300µM	15.6	6.366 to 24.84	Yes
Control vs. 600µM	24.54	15.30 to 33.77	Yes
37.5µM vs. 75µM	1.481	-8.394 to 11.36	No
37.5µM vs. 150µM	5.953	-3.922 to 15.83	No
37.5µM vs. 300µM	15.03	5.160 to 24.91	Yes
37.5µM vs. 600µM	23.97	14.09 to 33.84	Yes
75µM vs. 150µM	4.472	-5.403 to 14.35	No
75µM vs. 300µM	13.55	3.679 to 23.43	Yes
75µM vs. 600µM	22.49	12.61 to 32.36	Yes
150µM vs. 300µM	9.081	-0.7930 to 18.96	No
150µM vs. 600µM	18.01	8.140 to 27.89	Yes
300µM vs. 600µM	8.933	-0.9411 to 18.81	No

120hr

Test	Mean Diff.	95% CI of diff.	Significance
Control vs. 37.5µM	0.2849	-8.952 to 9.522	No
Control vs. 75µM	1.479	-7.757 to 10.72	No
Control vs. 150µM	10.04	0.7991 to 19.27	Yes
Control vs. 300µM	23.72	14.48 to 32.95	Yes
Control vs. 600µM	35.83	26.59 to 45.07	Yes
37.5µM vs. 75µM	1.194	-8.680 to 11.07	No
37.5µM vs. 150µM	9.751	-0.1235 to 19.63	No
37.5µM vs. 300µM	23.43	13.56 to 33.30	Yes
37.5µM vs. 600µM	35.54	25.67 to 45.42	Yes
75µM vs. 150µM	8.556	-1.318 to 18.43	No
75µM vs. 300µM	22.24	12.36 to 32.11	Yes
75µM vs. 600µM	34.35	24.48 to 44.22	Yes
150µM vs. 300µM	13.68	3.805 to 23.55	Yes
150µM vs. 600µM	25.79	15.92 to 35.67	Yes
300µM vs. 600µM	12.11	2.240 to 21.99	Yes

Table 1.2 – Multiple comparisons test for MiaPaca-2 cells

A two-way ANOVA was used to statistically analyse the dose response curves shown in figure 2 for MiaPaca-2 cells.

Two-way ANOVA for MiaPaca-2 cells

0hr

Test	Mean Diff.	95% CI of diff.	Significance
Control vs. 37.5µM	-0.5484	-7.044 to 5.947	No
Control vs. 75µM	0.2363	-6.259 to 6.732	No
Control vs. 150µM	0.1186	-6.377 to 6.614	No
Control vs. 300µM	-0.2623	-6.758 to 6.233	No
Control vs. 600µM	0.639	-5.857 to 7.135	No
37.5µM vs. 75µM	0.7848	-5.711 to 7.281	No
37.5µM vs. 150µM	0.667	-5.829 to 7.163	No
37.5µM vs. 300µM	0.2861	-6.210 to 6.782	No
37.5µM vs. 600µM	1.187	-5.308 to 7.683	No
75µM vs. 150µM	-0.1177	-6.614 to 6.378	No
75µM vs. 300µM	-0.4986	-6.994 to 5.997	No
75µM vs. 600µM	0.4026	-6.093 to 6.898	No
150µM vs. 300µM	-0.3809	-6.877 to 6.115	No
150µM vs. 600µM	0.5204	-5.975 to 7.016	No
300µM vs. 600µM	0.9013	-5.595 to 7.397	No

24hr

Test	Mean Diff.	95% CI of diff.	Significance
Control vs. 37.5µM	-0.6145	-7.110 to 5.881	No
Control vs. 75µM	1.693	-4.803 to 8.188	No
Control vs. 150µM	1.887	-4.609 to 8.383	No
Control vs. 300µM	1	-5.495 to 7.496	No
Control vs. 600µM	4.501	-1.995 to 11.00	No
37.5µM vs. 75µM	2.307	-4.189 to 8.803	No
37.5µM vs. 150µM	2.502	-3.994 to 8.998	No
37.5µM vs. 300µM	1.615	-4.881 to 8.111	No
37.5µM vs. 600µM	5.115	-1.380 to 11.61	No
75µM vs. 150µM	0.1946	-6.301 to 6.690	No
75µM vs. 300µM	-0.6922	-7.188 to 5.804	No
75µM vs. 600µM	2.808	-3.688 to 9.304	No
150µM vs. 300µM	-0.8868	-7.383 to 5.609	No
150µM vs. 600µM	2.614	-3.882 to 9.109	No
300µM vs. 600µM	3.5	-2.995 to 9.996	No

48hr

Test	Mean Diff.	95% CI of diff.	Significance
Control vs. 37.5µM	-1.812	-8.308 to 4.684	No
Control vs. 75µM	1.01	-5.485 to 7.506	No
Control vs. 150µM	-0.8804	-7.376 to 5.615	No
Control vs. 300µM	-1.133	-7.629 to 5.363	No
Control vs. 600µM	5.313	-1.183 to 11.81	No
37.5µM vs. 75µM	2.822	-3.673 to 9.318	No
37.5µM vs. 150µM	0.9316	-5.564 to 7.427	No
37.5µM vs. 300µM	0.679	-5.817 to 7.175	No
37.5µM vs. 600µM	7.125	0.6289 to 13.62	Yes
75µM vs. 150µM	-1.891	-8.387 to 4.605	No
75µM vs. 300µM	-2.143	-8.639 to 4.352	No
75µM vs. 600µM	4.302	-2.194 to 10.80	No
150µM vs. 300µM	-0.2526	-6.748 to 6.243	No
150µM vs. 600µM	6.193	-0.3027 to 12.69	No
300µM vs. 600µM	6.446	-0.05009 to 12.94	No

72hr

Test	Mean Diff.	95% CI of diff.	Significance
Control vs. 37.5µM	1.48	-5.016 to 7.976	No
Control vs. 75µM	3.614	-2.882 to 10.11	No
Control vs. 150µM	2.698	-3.798 to 9.194	No
Control vs. 300µM	2.49	-4.005 to 8.986	No
Control vs. 600µM	5.446	-1.050 to 11.94	No
37.5µM vs. 75µM	2.134	-4.362 to 8.630	No
37.5µM vs. 150µM	1.218	-5.277 to 7.714	No
37.5µM vs. 300µM	1.011	-5.485 to 7.506	No
37.5µM vs. 600µM	3.966	-2.530 to 10.46	No
75µM vs. 150µM	-0.9158	-7.412 to 5.580	No
75µM vs. 300µM	-1.124	-7.619 to 5.372	No
75µM vs. 600µM	1.832	-4.664 to 8.327	No
150µM vs. 300µM	-0.2078	-6.704 to 6.288	No
150µM vs. 600µM	2.747	-3.748 to 9.243	No
300µM vs. 600µM	2.955	-3.541 to 9.451	No

96hr

Test	Mean Diff.	95% CI of diff.	Significance
Control vs. 37.5µM	-0.996	-7.492 to 5.500	No
Control vs. 75µM	-2.709	-9.205 to 3.787	No
Control vs. 150µM	-5.905	-12.40 to 0.5908	No
Control vs. 300µM	-6.966	-13.46 to -0.4704	Yes
Control vs. 600µM	0.6514	-5.844 to 7.147	No
37.5µM vs. 75µM	-1.713	-8.209 to 4.783	No
37.5µM vs. 150µM	-4.909	-11.40 to 1.587	No
37.5µM vs. 300µM	-5.97	-12.47 to 0.5257	No
37.5µM vs. 600µM	1.647	-4.848 to 8.143	No
75µM vs. 150µM	-3.196	-9.692 to 3.300	No
75µM vs. 300µM	-4.257	-10.75 to 2.239	No
75µM vs. 600µM	3.361	-3.135 to 9.856	No
150µM vs. 300µM	-1.061	-7.557 to 5.435	No
150µM vs. 600µM	6.556	0.06063 to 13.05	Yes
300µM vs. 600µM	7.618	1.122 to 14.11	Yes

120hr

Test	Mean Diff.	95% CI of diff.	Significance
Control vs. 37.5µM	-3.038	-9.534 to 3.457	No
Control vs. 75µM	-7.516	-14.01 to -1.020	Yes
Control vs. 150µM	-11.17	-17.67 to -4.674	Yes
Control vs. 300µM	-12.23	-18.72 to -5.730	Yes
Control vs. 600µM	0.3396	-6.156 to 6.835	No
37.5µM vs. 75µM	-4.477	-10.97 to 2.019	No
37.5µM vs. 150µM	-8.132	-14.63 to -1.636	Yes
37.5µM vs. 300µM	-9.187	-15.68 to -2.692	Yes
37.5µM vs. 600µM	3.378	-3.118 to 9.874	No
75µM vs. 150µM	-3.655	-10.15 to 2.841	No
75µM vs. 300µM	-4.71	-11.21 to 1.786	No
75µM vs. 600µM	7.855	1.359 to 14.35	Yes
150µM vs. 300µM	-1.055	-7.551 to 5.440	No
150µM vs. 600µM	11.51	5.014 to 18.01	Yes
300µM vs. 600µM	12.57	6.069 to 19.06	Yes

Table 1.3 – Multiple comparison test for HepG2 cells

A two-way ANOVA was used to statistically analyse the dose response curves shown in figure 2 for HepG2 cells

Two-way ANOVA for HepG2 cells

0hr

Test	Mean Diff.	95% CI of diff.	Significance
Control vs. 37.5µM	-0.407	-8.375 to 7.561	No
Control vs. 75µM	-0.605	-8.573 to 7.363	No
Control vs. 150µM	-0.7383	-8.706 to 7.229	No
Control vs. 300µM	-1.262	-9.230 to 6.706	No
Control vs. 600µM	-0.8415	-8.809 to 7.126	No
37.5µM vs. 75µM	-0.198	-8.166 to 7.770	No
37.5µM vs. 150µM	-0.3313	-8.299 to 7.636	No
37.5µM vs. 300µM	-0.8552	-8.823 to 7.112	No
37.5µM vs. 600µM	-0.4346	-8.402 to 7.533	No
75µM vs. 150µM	-0.1333	-8.101 to 7.834	No
75µM vs. 300µM	-0.6572	-8.625 to 7.311	No
75µM vs. 600µM	-0.2366	-8.204 to 7.731	No
150µM vs. 300µM	-0.5239	-8.492 to 7.444	No
150µM vs. 600µM	-0.1033	-8.071 to 7.864	No
300µM vs. 600µM	0.4206	-7.547 to 8.388	No

24hr

Test	Mean Diff.	95% CI of diff.	Significance
Control vs. 37.5µM	-1.528	-9.496 to 6.440	No
Control vs. 75µM	-1.856	-9.823 to 6.112	No
Control vs. 150µM	-2.704	-10.67 to 5.264	No
Control vs. 300µM	-4.715	-12.68 to 3.253	No
Control vs. 600µM	-5.965	-13.93 to 2.003	No
37.5µM vs. 75µM	-0.3275	-8.295 to 7.640	No
37.5µM vs. 150µM	-1.176	-9.143 to 6.792	No
37.5µM vs. 300µM	-3.187	-11.15 to 4.781	No
37.5µM vs. 600µM	-4.437	-12.40 to 3.531	No
75µM vs. 150µM	-0.8482	-8.816 to 7.120	No
75µM vs. 300µM	-2.859	-10.83 to 5.108	No
75µM vs. 600µM	-4.109	-12.08 to 3.858	No
150µM vs. 300µM	-2.011	-9.979 to 5.956	No
150µM vs. 600µM	-3.261	-11.23 to 4.707	No
300µM vs. 600µM	-1.25	-9.218 to 6.718	No

48hr

Test	Mean Diff.	95% CI of diff.	Significance
Control vs. 37.5µM	-2.826	-10.79 to 5.142	No
Control vs. 75µM	-5.074	-13.04 to 2.894	No
Control vs. 150µM	-5.875	-13.84 to 2.093	No
Control vs. 300µM	-11.41	-19.37 to -3.439	Yes
Control vs. 600µM	-14.3	-22.27 to -6.333	Yes
37.5µM vs. 75µM	-2.248	-10.22 to 5.720	No
37.5µM vs. 150µM	-3.049	-11.02 to 4.919	No
37.5µM vs. 300µM	-8.58	-16.55 to -0.6127	Yes
37.5µM vs. 600µM	-11.48	-19.44 to -3.507	Yes
75µM vs. 150µM	-0.8009	-8.769 to 7.167	No
75µM vs. 300µM	-6.333	-14.30 to 1.635	No
75µM vs. 600µM	-9.227	-17.20 to -1.260	Yes
150µM vs. 300µM	-5.532	-13.50 to 2.436	No
150µM vs. 600µM	-8.426	-16.39 to -0.4587	Yes
300µM vs. 600µM	-2.895	-10.86 to 5.073	No

72hr

Test	Mean Diff.	95% CI of diff.	Significance
Control vs. 37.5µM	-6.006	-13.97 to 1.962	No
Control vs. 75µM	-10.37	-18.34 to -2.406	Yes
Control vs. 150µM	-9.31	-17.28 to -1.342	Yes
Control vs. 300µM	-14.44	-22.40 to -6.469	Yes
Control vs. 600µM	-14.64	-22.61 to -6.674	Yes
37.5µM vs. 75µM	-4.368	-12.34 to 3.600	No
37.5µM vs. 150µM	-3.304	-11.27 to 4.664	No
37.5µM vs. 300µM	-8.431	-16.40 to -0.4630	Yes
37.5µM vs. 600µM	-8.636	-16.60 to -0.6684	Yes
75µM vs. 150µM	1.064	-6.904 to 9.032	No
75µM vs. 300µM	-4.063	-12.03 to 3.905	No
75µM vs. 600µM	-4.268	-12.24 to 3.699	No
150µM vs. 300µM	-5.127	-13.09 to 2.841	No
150µM vs. 600µM	-5.332	-13.30 to 2.635	No
300µM vs. 600µM	-0.2054	-8.173 to 7.762	No

96hr

Test	Mean Diff.	95% CI of diff.	Significance
Control vs. 37.5µM	-4.367	-12.33 to 3.601	No
Control vs. 75µM	-8.678	-16.65 to -0.7102	Yes
Control vs. 150µM	-6.98	-14.95 to 0.9880	No
Control vs. 300µM	-11.05	-19.02 to -3.087	Yes
Control vs. 600µM	-10.59	-18.56 to -2.623	Yes
37.5µM vs. 75µM	-4.311	-12.28 to 3.657	No
37.5µM vs. 150µM	-2.613	-10.58 to 5.355	No
37.5µM vs. 300µM	-6.688	-14.66 to 1.280	No
37.5µM vs. 600µM	-6.224	-14.19 to 1.744	No
75µM vs. 150µM	1.698	-6.269 to 9.666	No
75µM vs. 300µM	-2.377	-10.34 to 5.591	No
75µM vs. 600µM	-1.913	-9.880 to 6.055	No
150µM vs. 300µM	-4.075	-12.04 to 3.893	No
150µM vs. 600µM	-3.611	-11.58 to 4.357	No
300µM vs. 600µM	0.4641	-7.504 to 8.432	No

120hr

Test	Mean Diff.	95% CI of diff.	Significance
Control vs. 37.5µM	-2.562	-10.53 to 5.405	No
Control vs. 75µM	-7.027	-14.99 to 0.9406	No
Control vs. 150µM	-5.009	-12.98 to 2.959	No
Control vs. 300µM	-8.733	-16.70 to -0.7657	Yes
Control vs. 600µM	-7.995	-15.96 to -0.02727	Yes
37.5µM vs. 75µM	-4.465	-12.43 to 3.503	No
37.5µM vs. 150µM	-2.447	-10.41 to 5.521	No
37.5µM vs. 300µM	-6.171	-14.14 to 1.796	No
37.5µM vs. 600µM	-5.433	-13.40 to 2.535	No
75µM vs. 150µM	2.018	-5.950 to 9.986	No
75µM vs. 300µM	-1.706	-9.674 to 6.261	No
75µM vs. 600µM	-0.9679	-8.936 to 7.000	No
150µM vs. 300µM	-3.724	-11.69 to 4.243	No
150µM vs. 600µM	-2.986	-10.95 to 4.982	No
300µM vs. 600µM	0.7385	-7.229 to 8.706	No

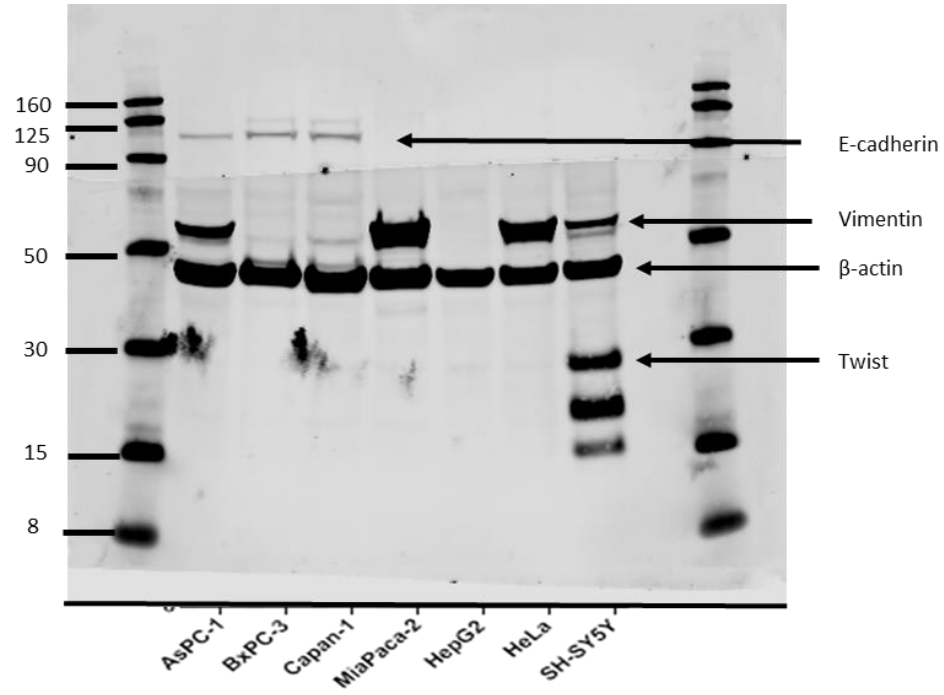

Figure 1.1 – Examination of EMT status
Expression of EMT markers by Western blotting, demonstrating the molecular weight ladder (kDa), the EMT markers E-cadherin, Vimentin and Twist in AsPC-1, BxPC-3, Capan-1, MiaPaca-2, HepG2, HeLa and SH-SY5Y cells.

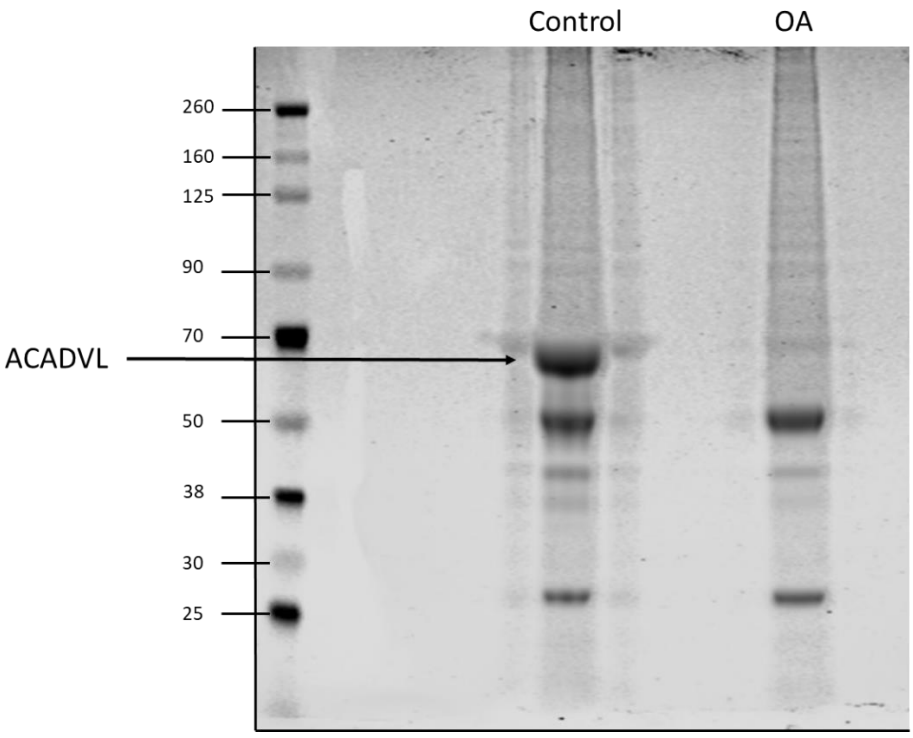

Figure 1.2 – OA mediated effects on ACADVL
IP analysis revealed that OA treated cells are negative for ACADVL in MiaPaca-2 cells.

References

ABDELMAGID, S. A., CLARKE, S. E., NIELSEN, D. E., BADAWI, A., EL-SOHEMY, A., MUTCH, D. M. & MA, D. W. 2015. Comprehensive profiling of plasma fatty acid concentrations in young healthy Canadian adults. *PLoS One,* 10**,** e0116195.

AFTAB, O., NAZIR, M., FRYKNAS, M., HAMMERLING, U., LARSSON, R. & GUSTAFSSON, M. G. 2014. Label free high throughput screening for apoptosis inducing chemicals using time-lapse microscopy signal processing. *Apoptosis,* 19**,** 1411-8.

AGMON, E. & STOCKWELL, B. R. 2017. Lipid homeostasis and regulated cell death. *Curr Opin Chem Biol,* 39**,** 83-89.

AHN, J. H., KIM, M. H., KWON, H. J., CHOI, S. Y. & KWON, H. Y. 2013. Protective Effects of Oleic Acid Against Palmitic Acid-Induced Apoptosis in Pancreatic AR42J Cells and Its Mechanisms. *Korean J Physiol Pharmacol,* 17**,** 43-50.

AIRLEY, R. E., MCHUGH, P., EVANS, A. R., HARRIS, B., WINCHESTER, L., BUFFA, F. M., AL-TAMEEMI, W., LEEK, R. & HARRIS, A. L. 2014. Role of carbohydrate response element-binding protein (ChREBP) in generating an aerobic metabolic phenotype and in breast cancer progression. *British Journal of Cancer,* 110**,** 715-723.

ALBERTS, B. 2008. *Molecular biology of the cell,* New York, Garland Science.

ALTENBERG, B. & GREULICH, K. O. 2004. Genes of glycolysis are ubiquitously overexpressed in 24 cancer classes. *Genomics,* 84**,** 1014-20.

ALTMAN, B. J., STINE, Z. E. & DANG, C. V. 2016. From Krebs to clinic: glutamine metabolism to cancer therapy. *Nature Reviews Cancer,* 16**,** 619.

AMOÊDO, NÍVEA D., VALENCIA, JUAN P., RODRIGUES, MARIANA F., GALINA, A. & RUMJANEK, FRANKLIN D. 2013. How does the metabolism of tumour cells differ from that of normal cells. *Bioscience Reports,* 33**,** e00080.

ANASTASIOU, D. & CANTLEY, L. C. 2012. Breathless cancer cells get fat on glutamine. *Cell Res,* 22**,** 443-6.

ARTYMOVICH, K. & APPLEDORN, D. M. 2015. A multiplexed method for kinetic measurements of apoptosis and proliferation using live-content imaging. *Methods Mol Biol,* 1219**,** 35-42.

BAENKE, F., PECK, B., MIESS, H. & SCHULZE, A. 2013. Hooked on fat: the role of lipid synthesis in cancer metabolism and tumour development. *Dis Model Mech,* 6**,** 1353-63.

BANKO, M. R., ALLEN, J. J., SCHAFFER, B. E., WILKER, E. W., TSOU, P., WHITE, J. L., VILLEN, J., WANG, B., KIM, S. R., SAKAMOTO, K., GYGI, S. P., CANTLEY, L. C., YAFFE, M. B., SHOKAT, K. M. & BRUNET, A. 2011. Chemical genetic screen for AMPKalpha2 substrates uncovers a network of proteins involved in mitosis. *Mol Cell,* 44**,** 878-92.

BECHMANN, L. P., HANNIVOORT, R. A., GERKEN, G., HOTAMISLIGIL, G. S., TRAUNER, M. & CANBAY, A. 2012. The interaction of hepatic lipid and glucose metabolism in liver diseases. *J Hepatol,* 56**,** 952-64.

BECKER, A. E., HERNANDEZ, Y. G., FRUCHT, H. & LUCAS, A. L. 2014. Pancreatic ductal adenocarcinoma: risk factors, screening, and early detection. *World J Gastroenterol,* 20**,** 11182-98.

BEGUN, J. & XAVIER, R. J. 2013. Autophagy at the crossroads of metabolism and cellular defense. *Curr Opin Gastroenterol,* 29**,** 588-96.

BELORIBI-DJEFAFLIA, S., VASSEUR, S. & GUILLAUMOND, F. 2016. Lipid metabolic reprogramming in cancer cells. *Oncogenesis,* 5**,** e189.

BENSAAD, K., FAVARO, E., LEWIS, C. A., PECK, B., LORD, S., COLLINS, J. M., PINNICK, K. E., WIGFIELD, S., BUFFA, F. M., LI, J. L., ZHANG, Q., WAKELAM, M. J. O., KARPE, F., SCHULZE, A. & HARRIS, A. L. 2014. Fatty acid uptake and lipid storage induced by HIF-1alpha contribute to cell growth and survival after hypoxia-reoxygenation. *Cell Rep,* 9**,** 349-365.

BERG, J. M., TYMOCZKO, J. L., STRYER, L. & STRYER, L. 2007. *Biochemistry,* New York, W.H. Freeman.

BHUTIA, Y. D., BABU, E., RAMACHANDRAN, S. & GANAPATHY, V. 2015. Amino Acid transporters in cancer and their relevance to "glutamine addiction": novel targets for the design of a new class of anticancer drugs. *Cancer Res,* 75**,** 1782-8.

BIANKIN, A. V., WADDELL, N., KASSAHN, K. S., GINGRAS, M. C., MUTHUSWAMY, L. B., JOHNS, A. L., MILLER, D. K., WILSON, P. J., PATCH, A. M., WU, J., CHANG, D. K., COWLEY, M. J., GARDINER, B. B., SONG, S., HARLIWONG, I., IDRISOGLU, S., NOURSE, C., NOURBAKHSH, E., MANNING, S., WANI, S., GONGORA, M., PAJIC, M., SCARLETT, C. J., GILL, A. J., PINHO, A. V., ROOMAN, I., ANDERSON, M., HOLMES, O., LEONARD, C., TAYLOR, D., WOOD, S., XU, Q., NONES, K., FINK, J. L., CHRIST, A., BRUXNER, T., CLOONAN, N., KOLLE, G., NEWELL, F., PINESE, M., MEAD, R. S., HUMPHRIS, J. L., KAPLAN, W., JONES, M. D., COLVIN, E. K., NAGRIAL, A. M., HUMPHREY, E. S., CHOU, A., CHIN, V. T., CHANTRILL, L. A., MAWSON, A., SAMRA, J. S., KENCH, J. G., LOVELL, J. A., DALY, R. J., MERRETT, N. D., TOON, C., EPARI, K., NGUYEN, N. Q., BARBOUR, A., ZEPS, N., AUSTRALIAN PANCREATIC CANCER GENOME, I., KAKKAR, N., ZHAO, F., WU, Y. Q., WANG, M., MUZNY, D. M., FISHER, W. E., BRUNICARDI, F. C., HODGES, S. E., REID, J. G., DRUMMOND, J., CHANG, K., HAN, Y., LEWIS, L. R., DINH, H., BUHAY, C. J., BECK, T., TIMMS, L., SAM, M., BEGLEY, K., BROWN, A., PAI, D., PANCHAL, A., BUCHNER, N., DE BORJA, R., DENROCHE, R. E., YUNG, C. K., SERRA, S., ONETTO, N., MUKHOPADHYAY, D., TSAO, M. S., SHAW, P. A., PETERSEN, G. M., GALLINGER, S., HRUBAN, R. H., MAITRA, A., IACOBUZIO-DONAHUE, C. A., SCHULICK, R. D., WOLFGANG, C. L., et al. 2012. Pancreatic cancer genomes reveal aberrations in axon guidance pathway genes. *Nature,* 491**,** 399-405.

BOROS, L. G., LEE, P. W., BRANDES, J. L., CASCANTE, M., MUSCARELLA, P., SCHIRMER, W. J., MELVIN, W. S. & ELLISON, E. C. 1998. Nonoxidative pentose phosphate pathways and their direct role in ribose synthesis in tumors: is cancer a disease of cellular glucose metabolism? *Med Hypotheses,* 50**,** 55-9.

BOROS, L. G., TORDAY, J. S., LIM, S., BASSILIAN, S., CASCANTE, M. & LEE, W. N. 2000. Transforming growth factor beta2 promotes glucose carbon

incorporation into nucleic acid ribose through the nonoxidative pentose cycle in lung epithelial carcinoma cells. *Cancer Res,* 60**,** 1183-5.
BOYA, P., REGGIORI, F. & CODOGNO, P. 2013. Emerging regulation and functions of autophagy. *Nat Cell Biol,* 15**,** 713-20.
BRUSSELMANS, K., DE SCHRIJVER, E., VERHOEVEN, G. & SWINNEN, J. V. 2005. RNA interference-mediated silencing of the acetyl-CoA-carboxylase-alpha gene induces growth inhibition and apoptosis of prostate cancer cells. *Cancer Res,* 65**,** 6719-25.
CAI, L., SUTTER, B. M., LI, B. & TU, B. P. 2011. Acetyl-CoA induces cell growth and proliferation by promoting the acetylation of histones at growth genes. *Mol Cell,* 42**,** 426-37.
CAMPBELL, S. L., KHOSRAVI-FAR, R., ROSSMAN, K. L., CLARK, G. J. & DER, C. J. 1998. Increasing complexity of Ras signaling. *Oncogene,* 17**,** 1395-413.
CANTLEY, L. C. 2002. The phosphoinositide 3-kinase pathway. *Science,* 296**,** 1655-7.
CARMONA-FONTAINE, C., BUCCI, V., AKKARI, L., DEFORET, M., JOYCE, J. A. & XAVIER, J. B. 2013. Emergence of spatial structure in the tumor microenvironment due to the Warburg effect. *Proc Natl Acad Sci U S A,* 110**,** 19402-7.
CARRACEDO, A., CANTLEY, L. C. & PANDOLFI, P. P. 2013. Cancer metabolism: fatty acid oxidation in the limelight. *Nat Rev Cancer,* 13**,** 227-32.
CARTA, G., MURRU, E., BANNI, S. & MANCA, C. 2017. Palmitic Acid: Physiological Role, Metabolism and Nutritional Implications. *Front Physiol,* 8**,** 902.
CHAJES, V., CAMBOT, M., MOREAU, K., LENOIR, G. M. & JOULIN, V. 2006. Acetyl-CoA carboxylase alpha is essential to breast cancer cell survival. *Cancer Res,* 66**,** 5287-94.
CHAKRAVARTHY, M. V., PAN, Z., ZHU, Y., TORDJMAN, K., SCHNEIDER, J. G., COLEMAN, T., TURK, J. & SEMENKOVICH, C. F. 2005. "New" hepatic fat activates PPARalpha to maintain glucose, lipid, and cholesterol homeostasis. *Cell Metab,* 1**,** 309-22.
CHAKRAVARTY, B., GU, Z., CHIRALA, S. S., WAKIL, S. J. & QUIOCHO, F. A. 2004. Human fatty acid synthase: structure and substrate selectivity of the thioesterase domain. *Proc Natl Acad Sci U S A,* 101**,** 15567-72.
CHANDEL, N. S., BUDINGER, G. R., CHOE, S. H. & SCHUMACKER, P. T. 1997. Cellular respiration during hypoxia. Role of cytochrome oxidase as the oxygen sensor in hepatocytes. *J Biol Chem,* 272**,** 18808-16.
CHIRALA, S. S. & WAKIL, S. J. 2004. Structure and function of animal fatty acid synthase. *Lipids,* 39**,** 1045-53.
COCCO, L., GILMOUR, R. S., OGNIBENE, A., LETCHER, A. J., MANZOLI, F. A. & IRVINE, R. F. 1987. Synthesis of polyphosphoinositides in nuclei of Friend cells. Evidence for polyphosphoinositide metabolism inside the nucleus which changes with cell differentiation. *Biochem J,* 248**,** 765-70.
COLEMAN, W. B. & TSONGALIS, G. J. 2009. *Molecular pathology : the molecular basis of human disease,* Burlington, Mass., Academic Press.
COMMISSO, C., DAVIDSON, S. M., SOYDANER-AZELOGLU, R. G., PARKER, S. J., KAMPHORST, J. J., HACKETT, S., GRABOCKA, E., NOFAL, M., DREBIN, J. A., THOMPSON, C. B., RABINOWITZ, J. D., METALLO, C. M., VANDER

HEIDEN, M. G. & BAR-SAGI, D. 2013. Macropinocytosis of protein is an amino acid supply route in Ras-transformed cells. *Nature,* 497**,** 633-7.
CORRADETTI, M. N. & GUAN, K. L. 2006. Upstream of the mammalian target of rapamycin: do all roads pass through mTOR? *Oncogene,* 25**,** 6347-60.
CROWN, S. B. & ANTONIEWICZ, M. R. 2013. Publishing 13C metabolic flux analysis studies: a review and future perspectives. *Metab Eng,* 20**,** 42-8.
CZAJA, M. J. 2016. Function of Autophagy in Nonalcoholic Fatty Liver Disease. *Dig Dis Sci,* 61**,** 1304-13.
DAEMEN, A., PETERSON, D., SAHU, N., MCCORD, R., DU, X., LIU, B., KOWANETZ, K., HONG, R., MOFFAT, J., GAO, M., BOUDREAU, A., MROUE, R., CORSON, L., O'BRIEN, T., QING, J., SAMPATH, D., MERCHANT, M., YAUCH, R., MANNING, G., SETTLEMAN, J., HATZIVASSILIOU, G. & EVANGELISTA, M. 2015. Metabolite profiling stratifies pancreatic ductal adenocarcinomas into subtypes with distinct sensitivities to metabolic inhibitors. *Proc Natl Acad Sci U S A,* 112**,** E4410-7.
DANG, L., JIN, S. & SU, S. M. 2010. IDH mutations in glioma and acute myeloid leukemia. *Trends Mol Med,* 16**,** 387-97.
DANIELS, V. W., SMANS, K., ROYAUX, I., CHYPRE, M., SWINNEN, J. V. & ZAIDI, N. 2014. Cancer cells differentially activate and thrive on de novo lipid synthesis pathways in a low-lipid environment. *PLoS One,* 9**,** e106913.
DEBERARDINIS, R. J., MANCUSO, A., DAIKHIN, E., NISSIM, I., YUDKOFF, M., WEHRLI, S. & THOMPSON, C. B. 2007. Beyond aerobic glycolysis: transformed cells can engage in glutamine metabolism that exceeds the requirement for protein and nucleotide synthesis. *Proc Natl Acad Sci U S A,* 104**,** 19345-50.
DEBRUYNE, D. N., BHATNAGAR, N., SHARMA, B., LUTHER, W., MOORE, N. F., CHEUNG, N. K., GRAY, N. S. & GEORGE, R. E. 2016. ALK inhibitor resistance in ALK(F1174L)-driven neuroblastoma is associated with AXL activation and induction of EMT. *Oncogene,* 35**,** 3681-91.
DEER, E. L., GONZALEZ-HERNANDEZ, J., COURSEN, J. D., SHEA, J. E., NGATIA, J., SCAIFE, C. L., FIRPO, M. A. & MULVIHILL, S. J. 2010. Phenotype and genotype of pancreatic cancer cell lines. *Pancreas,* 39**,** 425-35.
DESHPANDE, A., SICINSKI, P. & HINDS, P. W. 2005. Cyclins and cdks in development and cancer: a perspective. *Oncogene,* 24**,** 2909-15.
DIEHN, M., CHO, R. W., LOBO, N. A., KALISKY, T., DORIE, M. J., KULP, A. N., QIAN, D., LAM, J. S., AILLES, L. E., WONG, M., JOSHUA, B., KAPLAN, M. J., WAPNIR, I., DIRBAS, F. M., SOMLO, G., GARBEROGLIO, C., PAZ, B., SHEN, J., LAU, S. K., QUAKE, S. R., BROWN, J. M., WEISSMAN, I. L. & CLARKE, M. F. 2009. Association of reactive oxygen species levels and radioresistance in cancer stem cells. *Nature,* 458**,** 780-3.
DIRADOURIAN, C., GIRARD, J. & PEGORIER, J. P. 2005. Phosphorylation of PPARs: from molecular characterization to physiological relevance. *Biochimie,* 87**,** 33-8.
DONG, C., YUAN, T., WU, Y., WANG, Y., FAN, T. W., MIRIYALA, S., LIN, Y., YAO, J., SHI, J., KANG, T., LORKIEWICZ, P., ST CLAIR, D., HUNG, M. C., EVERS, B. M. & ZHOU, B. P. 2013. Loss of FBP1 by Snail-mediated repression provides metabolic advantages in basal-like breast cancer. *Cancer Cell,* 23**,** 316-31.

EAGLE, H. 1955. The growth requirements of two mammalian cell lines in tissue culture. *Trans Assoc Am Physicians,* 68**,** 78-81.

EILERS, M. & EISENMAN, R. N. 2008. Myc's broad reach. *Genes Dev,* 22**,** 2755-66.

ENG, C. H., WANG, Z., TKACH, D., TORAL-BARZA, L., UGWONALI, S., LIU, S., FITZGERALD, S. L., GEORGE, E., FRIAS, E., COCHRAN, N., DE JESUS, R., MCALLISTER, G., HOFFMAN, G. R., BRAY, K., LEMON, L., LUCAS, J., FANTIN, V. R., ABRAHAM, R. T., MURPHY, L. O. & NYFELER, B. 2016. Macroautophagy is dispensable for growth of KRAS mutant tumors and chloroquine efficacy. *Proceedings of the National Academy of Sciences of the United States of America,* 113**,** 182-187.

FALCON, S. C., HUDSON, C. S., HUANG, Y., MORTIMORE, M., GOLEC, J. M., CHARLTON, P. A., WEBER, P. & SUNDARAM, H. 2013. A non-catalytic role of choline kinase alpha is important in promoting cancer cell survival. *Oncogenesis,* 2**,** e38.

FAN, J., YE, J., KAMPHORST, J. J., SHLOMI, T., THOMPSON, C. B. & RABINOWITZ, J. D. 2014. Quantitative flux analysis reveals folate-dependent NADPH production. *Nature,* 510**,** 298-302.

FAUBERT, B., BOILY, G., IZREIG, S., GRISS, T., SAMBORSKA, B., DONG, Z., DUPUY, F., CHAMBERS, C., FUERTH, B. J., VIOLLET, B., MAMER, O. A., AVIZONIS, D., DEBERARDINIS, R. J., SIEGEL, P. M. & JONES, R. G. 2013. AMPK is a negative regulator of the Warburg effect and suppresses tumor growth in vivo. *Cell Metab,* 17**,** 113-24.

FLAVIN, R., PELUSO, S., NGUYEN, P. L. & LODA, M. 2010. Fatty acid synthase as a potential therapeutic target in cancer. *Future Oncol,* 6**,** 551-62.

FOLCH, J., LEES, M. & SLOANE STANLEY, G. H. 1957. A simple method for the isolation and purification of total lipides from animal tissues. *J Biol Chem,* 226**,** 497-509.

FREED-PASTOR, W. A., MIZUNO, H., ZHAO, X., LANGEROD, A., MOON, S. H., RODRIGUEZ-BARRUECO, R., BARSOTTI, A., CHICAS, A., LI, W., POLOTSKAIA, A., BISSELL, M. J., OSBORNE, T. F., TIAN, B., LOWE, S. W., SILVA, J. M., BORRESEN-DALE, A. L., LEVINE, A. J., BARGONETTI, J. & PRIVES, C. 2012. Mutant p53 disrupts mammary tissue architecture via the mevalonate pathway. *Cell,* 148**,** 244-58.

GARRETT, W. S. 2015. Cancer and the microbiota. *Science,* 348**,** 80-6.

GLUCHOWSKI, N. L., BECUWE, M., WALTHER, T. C. & FARESE, R. V., JR. 2017. Lipid droplets and liver disease: from basic biology to clinical implications. *Nat Rev Gastroenterol Hepatol,* 14**,** 343-355.

GOTTFRIED, E., KUNZ-SCHUGHART, L. A., EBNER, S., MUELLER-KLIESER, W., HOVES, S., ANDREESEN, R., MACKENSEN, A. & KREUTZ, M. 2006. Tumor-derived lactic acid modulates dendritic cell activation and antigen expression. *Blood,* 107**,** 2013-21.

GREGERSEN, N., ANDRESEN, B. S., CORYDON, M. J., CORYDON, T. J., OLSEN, R. K., BOLUND, L. & BROSS, P. 2001. Mutation analysis in mitochondrial fatty acid oxidation defects: Exemplified by acyl-CoA dehydrogenase deficiencies, with special focus on genotype-phenotype relationship. *Hum Mutat,* 18**,** 169-89.

GUILLAUMOND, F., LECA, J., OLIVARES, O., LAVAUT, M. N., VIDAL, N., BERTHEZENE, P., DUSETTI, N. J., LONCLE, C., CALVO, E., TURRINI, O., IOVANNA, J. L., TOMASINI, R. & VASSEUR, S. 2013. Strengthened glycolysis under hypoxia supports tumor symbiosis and hexosamine biosynthesis in pancreatic adenocarcinoma. *Proc Natl Acad Sci U S A,* 110**,** 3919-24.

HA, J., DANIEL, S., BROYLES, S. S. & KIM, K. H. 1994. Critical phosphorylation sites for acetyl-CoA carboxylase activity. *J Biol Chem,* 269**,** 22162-8.

HAN, L., MA, Q., LI, J., LIU, H., LI, W., MA, G., XU, Q., ZHOU, S. & WU, E. 2011. High glucose promotes pancreatic cancer cell proliferation via the induction of EGF expression and transactivation of EGFR. *PLoS One,* 6**,** e27074.

HANAHAN, D. & COUSSENS, L. M. 2012. Accessories to the crime: functions of cells recruited to the tumor microenvironment. *Cancer Cell,* 21**,** 309-22.

HANAHAN, D. & WEINBERG, R. A. 2011. Hallmarks of cancer: the next generation. *Cell,* 144**,** 646-74.

HARDIE, D. G., ROSS, F. A. & HAWLEY, S. A. 2012. AMPK: a nutrient and energy sensor that maintains energy homeostasis. *Nat Rev Mol Cell Biol,* 13**,** 251-62.

HARDY, S., LANGELIER, Y. & PRENTKI, M. 2000. Oleate activates phosphatidylinositol 3-kinase and promotes proliferation and reduces apoptosis of MDA-MB-231 breast cancer cells, whereas palmitate has opposite effects. *Cancer Res,* 60**,** 6353-8.

HARRIS, A. L. 2002. Hypoxia--a key regulatory factor in tumour growth. *Nat Rev Cancer,* 2**,** 38-47.

HATZIVASSILIOU, E. G., TSICHRITZIS, T. & MOSIALOS, G. 2005a. Induction of apoptosis by rewiring the signal transduction of Epstein-Barr virus oncoprotein LMP1 toward caspase activation. *J Virol,* 79**,** 5215-9.

HATZIVASSILIOU, G., ZHAO, F., BAUER, D. E., ANDREADIS, C., SHAW, A. N., DHANAK, D., HINGORANI, S. R., TUVESON, D. A. & THOMPSON, C. B. 2005b. ATP citrate lyase inhibition can suppress tumor cell growth. *Cancer Cell,* 8**,** 311-21.

HEDESKOV, C. J. 1968. Early effects of phytohaemagglutinin on glucose metabolism of normal human lymphocytes. *Biochem J,* 110**,** 373-80.

HENIQUE, C., MANSOURI, A., FUMEY, G., LENOIR, V., GIRARD, J., BOUILLAUD, F., PRIP-BUUS, C. & COHEN, I. 2010. Increased mitochondrial fatty acid oxidation is sufficient to protect skeletal muscle cells from palmitate-induced apoptosis. *J Biol Chem,* 285**,** 36818-27.

HEZEL, A. F., KIMMELMAN, A. C., STANGER, B. Z., BARDEESY, N. & DEPINHO, R. A. 2006. Genetics and biology of pancreatic ductal adenocarcinoma. *Genes Dev,* 20**,** 1218-49.

HEZEL, M. E. V., NIEUWLAND, R., BRUGGEN, R. V. & JUFFERMANS, N. P. 2017. The Ability of Extracellular Vesicles to Induce a Pro-Inflammatory Host Response. *Int J Mol Sci,* 18.

HOTZ, B., ARNDT, M., DULLAT, S., BHARGAVA, S., BUHR, H. J. & HOTZ, H. G. 2007. Epithelial to mesenchymal transition: expression of the regulators snail, slug, and twist in pancreatic cancer. *Clin Cancer Res,* 13**,** 4769-76.

HUYNH, F. K., GREEN, M. F., KOVES, T. R. & HIRSCHEY, M. D. 2014. Measurement of fatty acid oxidation rates in animal tissues and cell lines. *Methods Enzymol,* 542**,** 391-405.

INOKI, K. & GUAN, K. L. 2006. Complexity of the TOR signaling network. *Trends Cell Biol,* 16**,** 206-12.

JEON, S. M., CHANDEL, N. S. & HAY, N. 2012. AMPK regulates NADPH homeostasis to promote tumour cell survival during energy stress. *Nature,* 485**,** 661-5.

JIANG, P., DU, W., WANG, X., MANCUSO, A., GAO, X., WU, M. & YANG, X. 2011. p53 regulates biosynthesis through direct inactivation of glucose-6-phosphate dehydrogenase. *Nat Cell Biol,* 13**,** 310-6.

JIANG, P., DU, W. & WU, M. 2014. Regulation of the pentose phosphate pathway in cancer. *Protein Cell,* 5**,** 592-602.

JIYONG, J., TIANCHA, H., HUIQIN, W. & JINGFEN, J. 2013. Effect of gastric versus post-pyloric feeding on the incidence of pneumonia in critically ill patients: observations from traditional and Bayesian random-effects meta-analysis. *Clin Nutr,* 32**,** 8-15.

JONES, J. G. 2014. Identifying Sources of Hepatic Lipogenic Acetyl-CoA Using Stable Isotope Tracers and NMR. *Advances in Radiology,* 2014**,** 9.

JU, Y. S., ALEXANDROV, L. B., GERSTUNG, M., MARTINCORENA, I., NIK-ZAINAL, S., RAMAKRISHNA, M., DAVIES, H. R., PAPAEMMANUIL, E., GUNDEM, G., SHLIEN, A., BOLLI, N., BEHJATI, S., TARPEY, P. S., NANGALIA, J., MASSIE, C. E., BUTLER, A. P., TEAGUE, J. W., VASSILIOU, G. S., GREEN, A. R., DU, M. Q., UNNIKRISHNAN, A., PIMANDA, J. E., TEH, B. T., MUNSHI, N., GREAVES, M., VYAS, P., EL-NAGGAR, A. K., SANTARIUS, T., COLLINS, V. P., GRUNDY, R., TAYLOR, J. A., HAYES, D. N., MALKIN, D., GROUP, I. B. C., GROUP, I. C. M. D., GROUP, I. P. C., FOSTER, C. S., WARREN, A. Y., WHITAKER, H. C., BREWER, D., EELES, R., COOPER, C., NEAL, D., VISAKORPI, T., ISAACS, W. B., BOVA, G. S., FLANAGAN, A. M., FUTREAL, P. A., LYNCH, A. G., CHINNERY, P. F., MCDERMOTT, U., STRATTON, M. R. & CAMPBELL, P. J. 2014. Origins and functional consequences of somatic mitochondrial DNA mutations in human cancer. *Elife,* 3.

JUNG, C. H., RO, S. H., CAO, J., OTTO, N. M. & KIM, D. H. 2010. mTOR regulation of autophagy. *FEBS Lett,* 584**,** 1287-95.

KALLURI, R. & WEINBERG, R. A. 2009. The basics of epithelial-mesenchymal transition. *J Clin Invest,* 119**,** 1420-8.

KAMPHORST, J. J., CROSS, J. R., FAN, J., DE STANCHINA, E., MATHEW, R., WHITE, E. P., THOMPSON, C. B. & RABINOWITZ, J. D. 2013. Hypoxic and Ras-transformed cells support growth by scavenging unsaturated fatty acids from lysophospholipids. *Proc Natl Acad Sci U S A,* 110**,** 8882-7.

KARNEVI, E., SAID, K., ANDERSSON, R. & ROSENDAHL, A. H. 2013. Metformin-mediated growth inhibition involves suppression of the IGF-I receptor signalling pathway in human pancreatic cancer cells. *BMC Cancer,* 13**,** 235.

KARRETH, F. & TUVESON, D. A. 2004. Twist induces an epithelial-mesenchymal transition to facilitate tumor metastasis. *Cancer Biol Ther,* 3**,** 1058-9.

KATADA, S., IMHOF, A. & SASSONE-CORSI, P. 2012. Connecting threads: epigenetics and metabolism. *Cell,* 148**,** 24-8.

KINLAW, W. B., BAURES, P. W., LUPIEN, L. E., DAVIS, W. L. & KUEMMERLE, N. B. 2016. Fatty Acids and Breast Cancer: Make Them on Site or Have Them Delivered. *J Cell Physiol,* 231**,** 2128-41.

KLIMSTRA, D. S. & LONGNECKER, D. S. 1994. K-ras mutations in pancreatic ductal proliferative lesions. *Am J Pathol,* 145**,** 1547-50.

KNUDSON, A. G. 1993. Antioncogenes and human cancer. *Proc Natl Acad Sci U S A,* 90**,** 10914-21.

KOIZUME, S. & MIYAGI, Y. 2016. Lipid Droplets: A Key Cellular Organelle Associated with Cancer Cell Survival under Normoxia and Hypoxia. *Int J Mol Sci,* 17.

KOMATSU, M., WAGURI, S., UENO, T., IWATA, J., MURATA, S., TANIDA, I., EZAKI, J., MIZUSHIMA, N., OHSUMI, Y., UCHIYAMA, Y., KOMINAMI, E., TANAKA, K. & CHIBA, T. 2005. Impairment of starvation-induced and constitutive autophagy in Atg7-deficient mice. *J Cell Biol,* 169**,** 425-34.

KRAJCOVIC, M., KRISHNA, S., AKKARI, L., JOYCE, J. A. & OVERHOLTZER, M. 2013. mTOR regulates phagosome and entotic vacuole fission. *Mol Biol Cell,* 24**,** 3736-45.

KRAUSE, M., PARK, M., ZHANG, J. M., YUAN, J., HARFE, B., XU, S. Q., GREENWALD, I., COLE, M., PATERSON, B. & FIRE, A. 1997. A C. elegans E/Daughterless bHLH protein marks neuronal but not striated muscle development. *Development,* 124**,** 2179-89.

KUERSCHNER, L., MOESSINGER, C. & THIELE, C. 2008. Imaging of lipid biosynthesis: how a neutral lipid enters lipid droplets. *Traffic,* 9**,** 338-52.

KUHAJDA, F. P., JENNER, K., WOOD, F. D., HENNIGAR, R. A., JACOBS, L. B., DICK, J. D. & PASTERNACK, G. R. 1994. Fatty acid synthesis: a potential selective target for antineoplastic therapy. *Proc Natl Acad Sci U S A,* 91**,** 6379-83.

KWOK, W. K., LING, M. T., LEE, T. W., LAU, T. C., ZHOU, C., ZHANG, X., CHUA, C. W., CHAN, K. W., CHAN, F. L., GLACKIN, C., WONG, Y. C. & WANG, X. 2005. Up-regulation of TWIST in prostate cancer and its implication as a therapeutic target. *Cancer Res,* 65**,** 5153-62.

LAI, P. B., ROSS, J. A., FEARON, K. C., ANDERSON, J. D. & CARTER, D. C. 1996. Cell cycle arrest and induction of apoptosis in pancreatic cancer cells exposed to eicosapentaenoic acid in vitro. *Br J Cancer,* 74**,** 1375-83.

LAS, G., SERADA, S. B., WIKSTROM, J. D., TWIG, G. & SHIRIHAI, O. S. 2011. Fatty acids suppress autophagic turnover in beta-cells. *J Biol Chem,* 286**,** 42534-44.

LEHNER, R., LIAN, J. & QUIROGA, A. D. 2012. Lumenal lipid metabolism: implications for lipoprotein assembly. *Arterioscler Thromb Vasc Biol,* 32**,** 1087-93.

LEHNINGER, A. L., NELSON, D. L. & COX, M. M. 1993. *Principles of biochemistry,* New York, NY, Worth Publishers.

LEWIS, C. A., PARKER, S. J., FISKE, B. P., MCCLOSKEY, D., GUI, D. Y., GREEN, C. R., VOKES, N. I., FEIST, A. M., VANDER HEIDEN, M. G. & METALLO, C. M. 2014. Tracing compartmentalized NADPH metabolism in the cytosol and mitochondria of mammalian cells. *Mol Cell,* 55**,** 253-63.

LI, J. & ZHOU, B. P. 2011. Activation of β-catenin and Akt pathways by Twist are critical for the maintenance of EMT associated cancer stem cell-like characters. *BMC Cancer,* 11**,** 49-49.

LI, S., ZHOU, T., LI, C., DAI, Z., CHE, D., YAO, Y., LI, L., MA, J., YANG, X. & GAO, G. 2014. High Metastaticgastric and Breast Cancer Cells Consume Oleic Acid in an AMPK Dependent Manner. *PLOS ONE,* 9**,** e97330.

LIN, C.-C., CHENG, T.-L., TSAI, W.-H., TSAI, H.-J., HU, K.-H., CHANG, H.-C., YEH, C.-W., CHEN, Y.-C., LIAO, C.-C. & CHANG, W.-T. 2012. Loss of the respiratory enzyme citrate synthase directly links the Warburg effect to tumor malignancy. *Scientific reports,* 2**,** 785-785.

LIU, K. & CZAJA, M. J. 2013. Regulation of lipid stores and metabolism by lipophagy. *Cell Death Differ,* 20**,** 3-11.

LUNT, S. Y. & VANDER HEIDEN, M. G. 2011. Aerobic glycolysis: meeting the metabolic requirements of cell proliferation. *Annu Rev Cell Dev Biol,* 27**,** 441-64.

LUPU, R. & MENENDEZ, J. A. 2006. Pharmacological inhibitors of Fatty Acid Synthase (FASN)--catalyzed endogenous fatty acid biogenesis: a new family of anti-cancer agents? *Curr Pharm Biotechnol,* 7**,** 483-93.

LYSSIOTIS, C. A., SON, J., CANTLEY, L. C. & KIMMELMAN, A. C. 2013. Pancreatic cancers rely on a novel glutamine metabolism pathway to maintain redox balance. *Cell Cycle,* 12**,** 1987-8.

MAKOHON-MOORE, A. & IACOBUZIO-DONAHUE, C. A. 2016. Pancreatic cancer biology and genetics from an evolutionary perspective. *Nat Rev Cancer,* 16**,** 553-65.

MATSUO, N., SHIRAHA, H., FUJIKAWA, T., TAKAOKA, N., UEDA, N., TANAKA, S., NISHINA, S., NAKANISHI, Y., UEMURA, M., TAKAKI, A., NAKAMURA, S., KOBAYASHI, Y., NOUSO, K., YAGI, T. & YAMAMOTO, K. 2009. Twist expression promotes migration and invasion in hepatocellular carcinoma. *BMC Cancer,* 9**,** 240.

MEDES, G., SPIRTES, M. A. & WEINHOUSE, S. 1953. The estimation of fatty acid synthesis in rat liver slices. *J Biol Chem,* 205**,** 401-8.

MEITZLER, J. L., ANTONY, S., WU, Y., JUHASZ, A., LIU, H., JIANG, G., LU, J., ROY, K. & DOROSHOW, J. H. 2014. NADPH oxidases: a perspective on reactive oxygen species production in tumor biology. *Antioxid Redox Signal,* 20**,** 2873-89.

MENDEZ, M. G., KOJIMA, S. & GOLDMAN, R. D. 2010. Vimentin induces changes in cell shape, motility, and adhesion during the epithelial to mesenchymal transition. *FASEB J,* 24**,** 1838-51.

MENENDEZ, J. A. & LUPU, R. 2007. Fatty acid synthase and the lipogenic phenotype in cancer pathogenesis. *Nat Rev Cancer,* 7**,** 763-77.

MENENDEZ, J. A., VAZQUEZ-MARTIN, A., ROPERO, S., COLOMER, R. & LUPU, R. 2006. HER2 (erbB-2)-targeted effects of the omega-3 polyunsaturated fatty acid, alpha-linolenic acid (ALA; 18:3n-3), in breast cancer cells: the "fat features" of the "Mediterranean diet" as an "anti-HER2 cocktail". *Clin Transl Oncol,* 8**,** 812-20.

METALLO, C. M. 2012. Expanding the reach of cancer metabolomics. *Cancer Prev Res (Phila),* 5**,** 1337-40.

METALLO, C. M., GAMEIRO, P. A., BELL, E. L., MATTAINI, K. R., YANG, J., HILLER, K., JEWELL, C. M., JOHNSON, Z. R., IRVINE, D. J., GUARENTE, L., KELLEHER, J. K., VANDER HEIDEN, M. G., ILIOPOULOS, O. &

STEPHANOPOULOS, G. 2011. Reductive glutamine metabolism by IDH1 mediates lipogenesis under hypoxia. *Nature,* 481**,** 380-4.
METALLO, C. M. & VANDER HEIDEN, M. G. 2013. Understanding metabolic regulation and its influence on cell physiology. *Mol Cell,* 49**,** 388-98.
MICALIZZI, D. S., FARABAUGH, S. M. & FORD, H. L. 2010. Epithelial-mesenchymal transition in cancer: parallels between normal development and tumor progression. *J Mammary Gland Biol Neoplasia,* 15**,** 117-34.
MIHAYLOVA, M. M. & SHAW, R. J. 2011. The AMPK signalling pathway coordinates cell growth, autophagy and metabolism. *Nat Cell Biol,* 13**,** 1016-23.
MIZUSHIMA, N., LEVINE, B., CUERVO, A. M. & KLIONSKY, D. J. 2008. Autophagy fights disease through cellular self-digestion. *Nature,* 451**,** 1069-75.
MORENO-SANCHEZ, R., RODRIGUEZ-ENRIQUEZ, S., MARIN-HERNANDEZ, A. & SAAVEDRA, E. 2007. Energy metabolism in tumor cells. *FEBS J,* 274**,** 1393-418.
MORRY, J., NGAMCHERDTRAKUL, W. & YANTASEE, W. 2017. Oxidative stress in cancer and fibrosis: Opportunity for therapeutic intervention with antioxidant compounds, enzymes, and nanoparticles. *Redox Biol,* 11**,** 240-253.
MUNYON, W. H. & MERCHANT, D. J. 1959. The relation between glucose utilization, lactic acid production and utilization and the growth cycle of L strain fibroblasts. *Exp Cell Res,* 17**,** 490-8.
NATALI, F., SICULELLA, L., SALVATI, S. & GNONI, G. V. 2007. Oleic acid is a potent inhibitor of fatty acid and cholesterol synthesis in C6 glioma cells. *J Lipid Res,* 48**,** 1966-75.
NELSON, M. E., LAHIRI, S., CHOW, J. D., BYRNE, F. L., HARGETT, S. R., BREEN, D. S., OLZOMER, E. M., WU, L. E., COONEY, G. J., TURNER, N., JAMES, D. E., SLACK-DAVIS, J. K., LACKNER, C., CALDWELL, S. H. & HOEHN, K. L. 2017. Inhibition of hepatic lipogenesis enhances liver tumorigenesis by increasing antioxidant defence and promoting cell survival. *Nat Commun,* 8**,** 14689.
NEMECZ, M., CONSTANTIN, A., DUMITRESCU, M., ALEXANDRU, N., FILIPPI, A., TANKO, G. & GEORGESCU, A. 2018. The Distinct Effects of Palmitic and Oleic Acid on Pancreatic Beta Cell Function: The Elucidation of Associated Mechanisms and Effector Molecules. *Front Pharmacol,* 9**,** 1554.
NICKLIN, P., BERGMAN, P., ZHANG, B., TRIANTAFELLOW, E., WANG, H., NYFELER, B., YANG, H., HILD, M., KUNG, C., WILSON, C., MYER, V. E., MACKEIGAN, J. P., PORTER, J. A., WANG, Y. K., CANTLEY, L. C., FINAN, P. M. & MURPHY, L. O. 2009. Bidirectional transport of amino acids regulates mTOR and autophagy. *Cell,* 136**,** 521-34.
NIEMAN, K. M., KENNY, H. A., PENICKA, C. V., LADANYI, A., BUELL-GUTBROD, R., ZILLHARDT, M. R., ROMERO, I. L., CAREY, M. S., MILLS, G. B., HOTAMISLIGIL, G. S., YAMADA, S. D., PETER, M. E., GWIN, K. & LENGYEL, E. 2011. Adipocytes promote ovarian cancer metastasis and provide energy for rapid tumor growth. *Nat Med,* 17**,** 1498-503.
O'REILLY, E. M., LEE, J. W., ZALUPSKI, M., CAPANU, M., PARK, J., GOLAN, T., TAHOVER, E., LOWERY, M. A., CHOU, J. F., SAHAI, V., BRENNER, R., KINDLER, H. L., YU, K. H., ZERVOUDAKIS, A., VEMURI, S., STADLER, Z. K.,

DO, R. K. G., DHANI, N., CHEN, A. P. & KELSEN, D. P. 2020. Randomized, Multicenter, Phase II Trial of Gemcitabine and Cisplatin With or Without Veliparib in Patients With Pancreas Adenocarcinoma and a Germline BRCA/PALB2 Mutation. *J Clin Oncol***,** JCO1902931.

OLLILA, S. & MAKELA, T. P. 2011. The tumor suppressor kinase LKB1: lessons from mouse models. *J Mol Cell Biol,* 3**,** 330-40.

ONDER, T. T., GUPTA, P. B., MANI, S. A., YANG, J., LANDER, E. S. & WEINBERG, R. A. 2008. Loss of E-cadherin promotes metastasis via multiple downstream transcriptional pathways. *Cancer Res,* 68**,** 3645-54.

OOKHTENS, M., KANNAN, R., LYON, I. & BAKER, N. 1984. Liver and adipose tissue contributions to newly formed fatty acids in an ascites tumor. *Am J Physiol,* 247**,** R146-53.

PATRA, S. K. 2008. Dissecting lipid raft facilitated cell signaling pathways in cancer. *Biochim Biophys Acta,* 1785**,** 182-206.

PAVLOVA, N. N. & THOMPSON, C. B. 2016. The Emerging Hallmarks of Cancer Metabolism. *Cell Metab,* 23**,** 27-47.

PIKE, L. S., SMIFT, A. L., CROTEAU, N. J., FERRICK, D. A. & WU, M. 2011. Inhibition of fatty acid oxidation by etomoxir impairs NADPH production and increases reactive oxygen species resulting in ATP depletion and cell death in human glioblastoma cells. *Biochim Biophys Acta,* 1807**,** 726-34.

PIZER, E. S., THUPARI, J., HAN, W. F., PINN, M. L., CHREST, F. J., FREHYWOT, G. L., TOWNSEND, C. A. & KUHAJDA, F. P. 2000. Malonyl-coenzyme-A is a potential mediator of cytotoxicity induced by fatty-acid synthase inhibition in human breast cancer cells and xenografts. *Cancer Res,* 60**,** 213-8.

POLLAK, N., DOLLE, C. & ZIEGLER, M. 2007a. The power to reduce: pyridine nucleotides--small molecules with a multitude of functions. *Biochem J,* 402**,** 205-18.

POLLAK, N., NIERE, M. & ZIEGLER, M. 2007b. NAD kinase levels control the NADPH concentration in human cells. *J Biol Chem,* 282**,** 33562-71.

PORSTMANN, T., GRIFFITHS, B., CHUNG, Y. L., DELPUECH, O., GRIFFITHS, J. R., DOWNWARD, J. & SCHULZE, A. 2005. PKB/Akt induces transcription of enzymes involved in cholesterol and fatty acid biosynthesis via activation of SREBP. *Oncogene,* 24**,** 6465-81.

POTTER, V. R. 1958. The biochemical approach to the cancer problem. *Fed Proc,* 17**,** 691-7.

QUIROGA, A. D. & LEHNER, R. 2012. Liver triacylglycerol lipases. *Biochim Biophys Acta,* 1821**,** 762-9.

RACHAGANI, S., SENAPATI, S., CHAKRABORTY, S., PONNUSAMY, M. P., KUMAR, S., SMITH, L. M., JAIN, M. & BATRA, S. K. 2011. Activated KrasG(1)(2)D is associated with invasion and metastasis of pancreatic cancer cells through inhibition of E-cadherin. *Br J Cancer,* 104**,** 1038-48.

REID, B. N., ABLES, G. P., OTLIVANCHIK, O. A., SCHOISWOHL, G., ZECHNER, R., BLANER, W. S., GOLDBERG, I. J., SCHWABE, R. F., CHUA, S. C., JR. & HUANG, L. S. 2008. Hepatic overexpression of hormone-sensitive lipase and adipose triglyceride lipase promotes fatty acid oxidation, stimulates direct

release of free fatty acids, and ameliorates steatosis. *J Biol Chem,* 283**,** 13087-99.
REILING, J. H. & SABATINI, D. M. 2006. Stress and mTORture signaling. *Oncogene,* 25**,** 6373-83.
RICOULT, S. J., YECIES, J. L., BEN-SAHRA, I. & MANNING, B. D. 2016. Oncogenic PI3K and K-Ras stimulate de novo lipid synthesis through mTORC1 and SREBP. *Oncogene,* 35**,** 1250-60.
ROHRIG, F. & SCHULZE, A. 2016. The multifaceted roles of fatty acid synthesis in cancer. *Nat Rev Cancer,* 16**,** 732-749.
ROLLAND, J. F., HENQUIN, J. C. & GILON, P. 2002. Feedback control of the ATP-sensitive K(+) current by cytosolic Ca(2+) contributes to oscillations of the membrane potential in pancreatic beta-cells. *Diabetes,* 51**,** 376-84.
ROSENBLATT, J., CHINKES, D., WOLFE, M. & WOLFE, R. R. 1992. Stable isotope tracer analysis by GC-MS, including quantification of isotopomer effects. *Am J Physiol,* 263**,** E584-96.
RUI, L. 2014. Energy metabolism in the liver. *Compr Physiol,* 4**,** 177-97.
RUSTIN, P. 2002. Mitochondria, from cell death to proliferation. *Nat Genet,* 30**,** 352-3.
SAMUDIO, I., HARMANCEY, R., FIEGL, M., KANTARJIAN, H., KONOPLEVA, M., KORCHIN, B., KALUARACHCHI, K., BORNMANN, W., DUVVURI, S., TAEGTMEYER, H. & ANDREEFF, M. 2010. Pharmacologic inhibition of fatty acid oxidation sensitizes human leukemia cells to apoptosis induction. *J Clin Invest,* 120**,** 142-56.
SAMUELS, Y. & ERICSON, K. 2006. Oncogenic PI3K and its role in cancer. *Curr Opin Oncol,* 18**,** 77-82.
SÁNCHEZ-MARTÍNEZ, R., CRUZ-GIL, S., DE CEDRÓN, M. G., ÁLVAREZ-FERNÁNDEZ, M., VARGAS, T., MOLINA, S., GARCÍA, B., HERRANZ, J., MORENO-RUBIO, J., REGLERO, G., PÉREZ-MORENO, M., FELIU, J., MALUMBRES, M. & DE MOLINA, A. R. 2015. A link between lipid metabolism and epithelial-mesenchymal transition provides a target for colon cancer therapy. *Oncotarget,* 6**,** 38719-38736.
SANTOS, C. R. & SCHULZE, A. 2012. Lipid metabolism in cancer. *FEBS J,* 279**,** 2610-23.
SATOH, T., UEHARA, Y. & KAZIRO, Y. 1992. Inhibition of interleukin 3 and granulocyte-macrophage colony-stimulating factor stimulated increase of active ras.GTP by herbimycin A, a specific inhibitor of tyrosine kinases. *J Biol Chem,* 267**,** 2537-41.
SCHLAEPFER, I. R., RIDER, L., RODRIGUES, L. U., GIJON, M. A., PAC, C. T., ROMERO, L., CIMIC, A., SIRINTRAPUN, S. J., GLODE, L. M., ECKEL, R. H. & CRAMER, S. D. 2014. Lipid catabolism via CPT1 as a therapeutic target for prostate cancer. *Mol Cancer Ther,* 13**,** 2361-71.
SCHUG, Z. T., FREZZA, C., GALBRAITH, L. C. & GOTTLIEB, E. 2012. The music of lipids: how lipid composition orchestrates cellular behaviour. *Acta Oncol,* 51**,** 301-10.
SHYH-CHANG, N., LOCASALE, J. W., LYSSIOTIS, C. A., ZHENG, Y., TEO, R. Y., RATANASIRINTRAWOOT, S., ZHANG, J., ONDER, T., UNTERNAEHRER, J. J., ZHU, H., ASARA, J. M., DALEY, G. Q. & CANTLEY, L. C. 2013. Influence of

threonine metabolism on S-adenosylmethionine and histone methylation. *Science,* 339**,** 222-6.
SINGH, R. & CUERVO, A. M. 2012. Lipophagy: connecting autophagy and lipid metabolism. *Int J Cell Biol,* 2012**,** 282041.
SINGH, R., KAUSHIK, S., WANG, Y., XIANG, Y., NOVAK, I., KOMATSU, M., TANAKA, K., CUERVO, A. M. & CZAJA, M. J. 2009. Autophagy regulates lipid metabolism. *Nature,* 458**,** 1131-5.
SON, J., LYSSIOTIS, C. A., YING, H., WANG, X., HUA, S., LIGORIO, M., PERERA, R. M., FERRONE, C. R., MULLARKY, E., SHYH-CHANG, N., KANG, Y., FLEMING, J. B., BARDEESY, N., ASARA, J. M., HAIGIS, M. C., DEPINHO, R. A., CANTLEY, L. C. & KIMMELMAN, A. C. 2013. Glutamine supports pancreatic cancer growth through a KRAS-regulated metabolic pathway. *Nature,* 496**,** 101-5.
STADLER, S. C. & ALLIS, C. D. 2012. Linking epithelial-to-mesenchymal-transition and epigenetic modifications. *Semin Cancer Biol,* 22**,** 404-10.
STRACHAN, T., READ, A. P. & STRACHAN, T. 2011. *Human molecular genetics,* New York, Garland Science.
TANIDA, I., MINEMATSU-IKEGUCHI, N., UENO, T. & KOMINAMI, E. 2005. Lysosomal turnover, but not a cellular level, of endogenous LC3 is a marker for autophagy. *Autophagy,* 1**,** 84-91.
THOMPSON, C. B. 2009. Metabolic enzymes as oncogenes or tumor suppressors. *N Engl J Med,* 360**,** 813-5.
TIBBETTS, A. S. & APPLING, D. R. 2010. Compartmentalization of Mammalian folate-mediated one-carbon metabolism. *Annu Rev Nutr,* 30**,** 57-81.
TONG, X., ZHAO, F., MANCUSO, A., GRUBER, J. J. & THOMPSON, C. B. 2009. The glucose-responsive transcription factor ChREBP contributes to glucose-dependent anabolic synthesis and cell proliferation. *Proceedings of the National Academy of Sciences of the United States of America,* 106**,** 21660-21665.
TOWBIN, B. D., GONZALEZ-AGUILERA, C., SACK, R., GAIDATZIS, D., KALCK, V., MEISTER, P., ASKJAER, P. & GASSER, S. M. 2012. Step-wise methylation of histone H3K9 positions heterochromatin at the nuclear periphery. *Cell,* 150**,** 934-47.
VACANTI, N. M., DIVAKARUNI, A. S., GREEN, C. R., PARKER, S. J., HENRY, R. R., CIARALDI, T. P., MURPHY, A. N. & METALLO, C. M. 2014. Regulation of substrate utilization by the mitochondrial pyruvate carrier. *Mol Cell,* 56**,** 425-35.
VANDER HEIDEN, M. G., CANTLEY, L. C. & THOMPSON, C. B. 2009. Understanding the Warburg effect: the metabolic requirements of cell proliferation. *Science,* 324**,** 1029-33.
VANDER HEIDEN, M. G., LUNT, S. Y., DAYTON, T. L., FISKE, B. P., ISRAELSEN, W. J., MATTAINI, K. R., VOKES, N. I., STEPHANOPOULOS, G., CANTLEY, L. C., METALLO, C. M. & LOCASALE, J. W. 2011. Metabolic pathway alterations that support cell proliferation. *Cold Spring Harb Symp Quant Biol,* 76**,** 325-34.
VENTURA, R., MORDEC, K., WASZCZUK, J., WANG, Z., LAI, J., FRIDLIB, M., BUCKLEY, D., KEMBLE, G. & HEUER, T. S. 2015. Inhibition of de novo Palmitate Synthesis by Fatty Acid Synthase Induces Apoptosis in Tumor Cells

by Remodeling Cell Membranes, Inhibiting Signaling Pathways, and Reprogramming Gene Expression. *EBioMedicine,* 2**,** 808-24.

VICKERS, A. E. 2009. Characterization of hepatic mitochondrial injury induced by fatty acid oxidation inhibitors. *Toxicol Pathol,* 37**,** 78-88.

VINCOURT, V., ESCRIOU, V., LARGEAU, C., BESSODES, M., SCHERMAN, D., CHAUMEIL, J. C. & DUMORTIER, G. 2011. Altered HepG2 cell models using etomoxir versus tert-butylhydroperoxide. *Cell Biol Toxicol,* 27**,** 363-70.

WADDELL, N., PAJIC, M., PATCH, A. M., CHANG, D. K., KASSAHN, K. S., BAILEY, P., JOHNS, A. L., MILLER, D., NONES, K., QUEK, K., QUINN, M. C., ROBERTSON, A. J., FADLULLAH, M. Z., BRUXNER, T. J., CHRIST, A. N., HARLIWONG, I., IDRISOGLU, S., MANNING, S., NOURSE, C., NOURBAKHSH, E., WANI, S., WILSON, P. J., MARKHAM, E., CLOONAN, N., ANDERSON, M. J., FINK, J. L., HOLMES, O., KAZAKOFF, S. H., LEONARD, C., NEWELL, F., POUDEL, B., SONG, S., TAYLOR, D., WADDELL, N., WOOD, S., XU, Q., WU, J., PINESE, M., COWLEY, M. J., LEE, H. C., JONES, M. D., NAGRIAL, A. M., HUMPHRIS, J., CHANTRILL, L. A., CHIN, V., STEINMANN, A. M., MAWSON, A., HUMPHREY, E. S., COLVIN, E. K., CHOU, A., SCARLETT, C. J., PINHO, A. V., GIRY-LATERRIERE, M., ROOMAN, I., SAMRA, J. S., KENCH, J. G., PETTITT, J. A., MERRETT, N. D., TOON, C., EPARI, K., NGUYEN, N. Q., BARBOUR, A., ZEPS, N., JAMIESON, N. B., GRAHAM, J. S., NICLOU, S. P., BJERKVIG, R., GRUTZMANN, R., AUST, D., HRUBAN, R. H., MAITRA, A., IACOBUZIO-DONAHUE, C. A., WOLFGANG, C. L., MORGAN, R. A., LAWLOR, R. T., CORBO, V., BASSI, C., FALCONI, M., ZAMBONI, G., TORTORA, G., TEMPERO, M. A., AUSTRALIAN PANCREATIC CANCER GENOME, I., GILL, A. J., ESHLEMAN, J. R., PILARSKY, C., SCARPA, A., MUSGROVE, E. A., PEARSON, J. V., BIANKIN, A. V. & GRIMMOND, S. M. 2015. Whole genomes redefine the mutational landscape of pancreatic cancer. *Nature,* 518**,** 495-501.

WAHLSTROM, T. & HENRIKSSON, M. A. 2015. Impact of MYC in regulation of tumor cell metabolism. *Biochim Biophys Acta,* 1849**,** 563-9.

WANG, R., DILLON, C. P., SHI, L. Z., MILASTA, S., CARTER, R., FINKELSTEIN, D., MCCORMICK, L. L., FITZGERALD, P., CHI, H., MUNGER, J. & GREEN, D. R. 2011. The transcription factor Myc controls metabolic reprogramming upon T lymphocyte activation. *Immunity,* 35**,** 871-82.

WARBURG, O. 1956. On respiratory impairment in cancer cells. *Science,* 124**,** 269-70.

WEINBERG, R. A. 2007. *The biology of cancer,* New York, Garland Science.

WIEMAN, H. L., WOFFORD, J. A. & RATHMELL, J. C. 2007. Cytokine stimulation promotes glucose uptake via phosphatidylinositol-3 kinase/Akt regulation of Glut1 activity and trafficking. *Mol Biol Cell,* 18**,** 1437-46.

WISE, D. R., DEBERARDINIS, R. J., MANCUSO, A., SAYED, N., ZHANG, X. Y., PFEIFFER, H. K., NISSIM, I., DAIKHIN, E., YUDKOFF, M., MCMAHON, S. B. & THOMPSON, C. B. 2008. Myc regulates a transcriptional program that stimulates mitochondrial glutaminolysis and leads to glutamine addiction. *Proc Natl Acad Sci U S A,* 105**,** 18782-7.

WISE, D. R. & THOMPSON, C. B. 2010. Glutamine addiction: a new therapeutic target in cancer. *Trends Biochem Sci,* 35**,** 427-33.

WISE, D. R., WARD, P. S., SHAY, J. E., CROSS, J. R., GRUBER, J. J., SACHDEVA, U. M., PLATT, J. M., DEMATTEO, R. G., SIMON, M. C. & THOMPSON, C. B. 2011. Hypoxia promotes isocitrate dehydrogenase-dependent carboxylation of alpha-ketoglutarate to citrate to support cell growth and viability. *Proc Natl Acad Sci U S A,* 108**,** 19611-6.

WU, J. W., WANG, S. P., ALVAREZ, F., CASAVANT, S., GAUTHIER, N., ABED, L., SONI, K. G., YANG, G. & MITCHELL, G. A. 2011. Deficiency of liver adipose triglyceride lipase in mice causes progressive hepatic steatosis. *Hepatology,* 54**,** 122-32.

WU, Y. T., TAN, H. L., SHUI, G., BAUVY, C., HUANG, Q., WENK, M. R., ONG, C. N., CODOGNO, P. & SHEN, H. M. 2010. Dual role of 3-methyladenine in modulation of autophagy via different temporal patterns of inhibition on class I and III phosphoinositide 3-kinase. *J Biol Chem,* 285**,** 10850-61.

XU, X. D., SHAO, S. X., JIANG, H. P., CAO, Y. W., WANG, Y. H., YANG, X. C., WANG, Y. L., WANG, X. S. & NIU, H. T. 2015. Warburg effect or reverse Warburg effect? A review of cancer metabolism. *Oncol Res Treat,* 38**,** 117-22.

YACHIDA, S., JONES, S., BOZIC, I., ANTAL, T., LEARY, R., FU, B., KAMIYAMA, M., HRUBAN, R. H., ESHLEMAN, J. R., NOWAK, M. A., VELCULESCU, V. E., KINZLER, K. W., VOGELSTEIN, B. & IACOBUZIO-DONAHUE, C. A. 2010. Distant metastasis occurs late during the genetic evolution of pancreatic cancer. *Nature,* 467**,** 1114-7.

YAMADA, T., OKAJIMA, F., OHWADA, S. & KONDO, Y. 1997. Growth inhibition of human pancreatic cancer cells by sphingosylphosphorylcholine and influence of culture conditions. *Cell Mol Life Sci,* 53**,** 435-41.

YAMASHITA, N., TOKUNAGA, E., INOUE, Y., TANAKA, K., NAKASHIMA, Y., ANDO, K., OGAKI, K., SAEKI, H., OKI, E. & MAEHARA, Y. 2015. Clinical significance of co-expression of E-cadherin and vimentin in invasive breast cancer. *Journal of Clinical Oncology,* 33**,** e22013-e22013.

YANG, L., HOU, Y., YUAN, J., TANG, S., ZHANG, H., ZHU, Q., DU, Y. E., ZHOU, M., WEN, S., XU, L., TANG, X., CUI, X. & LIU, M. 2015. Twist promotes reprogramming of glucose metabolism in breast cancer cells through PI3K/AKT and p53 signaling pathways. *Oncotarget,* 6**,** 25755-69.

YAO, C. H., LIU, G. Y., WANG, R., MOON, S. H., GROSS, R. W. & PATTI, G. J. 2018. Identifying off-target effects of etomoxir reveals that carnitine palmitoyltransferase I is essential for cancer cell proliferation independent of beta-oxidation. *PLoS Biol,* 16**,** e2003782.

YING, H., KIMMELMAN, A. C., LYSSIOTIS, C. A., HUA, S., CHU, G. C., FLETCHER-SANANIKONE, E., LOCASALE, J. W., SON, J., ZHANG, H., COLOFF, J. L., YAN, H., WANG, W., CHEN, S., VIALE, A., ZHENG, H., PAIK, J. H., LIM, C., GUIMARAES, A. R., MARTIN, E. S., CHANG, J., HEZEL, A. F., PERRY, S. R., HU, J., GAN, B., XIAO, Y., ASARA, J. M., WEISSLEDER, R., WANG, Y. A., CHIN, L., CANTLEY, L. C. & DEPINHO, R. A. 2012. Oncogenic Kras maintains pancreatic tumors through regulation of anabolic glucose metabolism. *Cell,* 149**,** 656-70.

YU, Q., ZHANG, K., WANG, X., LIU, X. & ZHANG, Z. 2010. Expression of transcription factors snail, slug, and twist in human bladder carcinoma. *J Exp Clin Cancer Res,* 29**,** 119.

YUAN, M., BREITKOPF, S. B., YANG, X. & ASARA, J. M. 2012. A positive/negative ion-switching, targeted mass spectrometry-based metabolomics platform for bodily fluids, cells, and fresh and fixed tissue. *Nat Protoc,* 7**,** 872-81.

YUN, J., RAGO, C., CHEONG, I., PAGLIARINI, R., ANGENENDT, P., RAJAGOPALAN, H., SCHMIDT, K., WILLSON, J. K., MARKOWITZ, S., ZHOU, S., DIAZ, L. A., JR., VELCULESCU, V. E., LENGAUER, C., KINZLER, K. W., VOGELSTEIN, B. & PAPADOPOULOS, N. 2009. Glucose deprivation contributes to the development of KRAS pathway mutations in tumor cells. *Science,* 325**,** 1555-9.

ZACK, T. I., SCHUMACHER, S. E., CARTER, S. L., CHERNIACK, A. D., SAKSENA, G., TABAK, B., LAWRENCE, M. S., ZHSNG, C. Z., WALA, J., MERMEL, C. H., SOUGNEZ, C., GABRIEL, S. B., HERNANDEZ, B., SHEN, H., LAIRD, P. W., GETZ, G., MEYERSON, M. & BEROUKHIM, R. 2013. Pan-cancer patterns of somatic copy number alteration. *Nat Genet,* 45**,** 1134-40.

ZAUGG, K., YAO, Y., REILLY, P. T., KANNAN, K., KIARASH, R., MASON, J., HUANG, P., SAWYER, S. K., FUERTH, B., FAUBERT, B., KALLIOMAKI, T., ELIA, A., LUO, X., NADEEM, V., BUNGARD, D., YALAVARTHI, S., GROWNEY, J. D., WAKEHAM, A., MOOLANI, Y., SILVESTER, J., TEN, A. Y., BAKKER, W., TSUCHIHARA, K., BERGER, S. L., HILL, R. P., JONES, R. G., TSAO, M., ROBINSON, M. O., THOMPSON, C. B., PAN, G. & MAK, T. W. 2011. Carnitine palmitoyltransferase 1C promotes cell survival and tumor growth under conditions of metabolic stress. *Genes Dev,* 25**,** 1041-51.

ZECHNER, R. & MADEO, F. 2009. Cell biology: Another way to get rid of fat. *Nature,* 458**,** 1118-9.

ZHU, Y., SCHWARZ, S., AHLEMEYER, B., GRZESCHIK, S., KLUMPP, S. & KRIEGLSTEIN, J. 2005. Oleic acid causes apoptosis and dephosphorylates Bad. *Neurochem Int,* 46**,** 127-35.

ZU, X. L. & GUPPY, M. 2004. Cancer metabolism: facts, fantasy, and fiction. *Biochem Biophys Res Commun,* 313**,** 459-65.

ZWEEMER, A. J. M., FRENCH, C. B., MESFIN, J., GORDONOV, S., MEYER, A. S. & LAUFFENBURGER, D. A. 2017. Apoptotic Bodies Elicit Gas6-Mediated Migration of AXL-Expressing Tumor Cells. *Mol Cancer Res,* 15**,** 1656-1666.